DE-EXCITATION PROCESS OF HIGHLY EXCITED DEFORMED NUCLEI

Thesis submitted for

the degree of

Doctor of Philosophy

by

Kazushige Maeda

Department of Physics,

Osaka University,

July, 1980

CONTENTS

Abstract

Pre-equilibrium-equilibrium (PEQ-EQ) de-excitation process for (α, xn γ) and (α, xn yp γ) reactions induced by 50 $\sim$ 120 MeV α-particles were studied. The complex reaction mechanisms were investigated by measuring rotational γ-rays which are characteristic of the reaction channels (residual nuclei), and decay protons and neutrons in singles and various coincidence with protons and discrete γ-rays were shown to be very useful for studying the experimental evidences of the PEQ process. They were found in the reaction channels with small neutron multiplicities x, the average neutron energy $<E_n>$, fast and slow components of the neutron energy spectra, and finite values of the A_1 coefficient in the high energy components of the neutron angular distributions. These features much depends on the way to excite the PEQ phase. Proton energy spectra of each reaction channel were found to have double peaks, especially in the small x channels. The high energy narrow peaks correspond to the high energy proton emission at the first doorway state. Medium and low energy broad peaks correspond to the high energy neutron emission at the PEQ phase. The present data were analyzed in terms of an exciton model for multi-particle emission process. The multiplicity distributions and decay particle spectra were well reproduced with the initial exciton numbers of (5, 1) and (6, 2). Comparing between the experiments and the calculations, the PEQ fractions and the entry lines to the EQ stage were deduced, and found to be constant for each reaction channel.

I. INTRODUCTION

1-1. Mechanism of (particle, xn yp γ) Reaction

Mechanisms of fusion-like (particle, xn yp γ) reactions induced by medium energy projectiles with several tens of MeV/nucleon are of current interest in view of a pre-equilibrium (PEQ)- equilibrium (EQ) de-excitation process.[1] The mechanism of fusion like reactions induced by relatively low energy projectiles ($\lesssim$ 10 MeV/nucleon) is considered to be a statistical process. Decay particles (mostly neutrons in medium and heavy nuclei) following these low energy reactions are evaporated from the compound nuclei in the EQ phase. As the projectile energy increases beyond the nuclear Fermi energy of 20 $\sim$ 30 MeV/nucleon, particle emissions at the PEQ stage become important because of the large widths of particle escape channels at the first few doorway stages of the de-excitation process in the PEQ phase.[2-4] With increasing projectile energy, the collision probability of the projectile nucleons with the target nucleons increases and the multiple scattering process for these reactions becomes dominant in the PEQ stage of the reaction. As the projectile energy increases beyond 50 MeV/nucleon, quasi-free scatterings become to take the major part of the first stage of the reaction process.[5]

It is assumed that the incident nucleons interact

initially with the target nucleus through the nucleon-nucleon interaction forming the first doorway of the reaction process. Then the reaction process may be approximately classified by the following two types of mechanisms. One is a direct reaction channel (e. q. stripping, pick up, inelastic, projectile break up and so on). This tends to leave the resiudal nucleus in discrete states at low excitation energies. Another process is a fusion like reaction channel, in which a highly excited nucleus in a continuous energy region is formed. The de-excitation process of the latter nucleus is interesting from a view point of the PEQ-EQ mechanism.[6] In the fusion like reaction, a particle-hole pair is created by the first interaction between the projectile and the target. These excited particles and holes are called excitons.[7] A series of exciton-exciton collisions, namely a nuclear cascade[8], is initiated. During the cascade, the number of exciton increases step by step (state spreading). One or a few high energy particles may escape (PEQ particle emission) through the cascade process. If the number of excitons increases beyond $20 \sim 30$ in the cascade process for the medium heavy nuclei, no escape is feasible at the PEQ stage and the residual nuclei is likely to be equilibriated. The equilibrium (compound) nucleus cools down statistically by evaporating low energy particles (mostly neutrons), finally followed by the γ de-excitation process. A schematical description of

this process is shown in fig. 1-1. The present work is focused on the PEQ de-excitation process following highly excited nuclei (50 ∿ 120 MeV) produced by α-particle induced reactions.

1-2. Reaction Models

There are many different approaches to understand these processes described above. They are the intra-nuclear cascade model (INC)[9-12], the quasi-free scattering model (QFS)[13, 14], and the exciton model[7, 14-16]. These models have been described well the various experimental data. The INC model deals with successive two body collisions between the nucleons in the excited nucleus. The trajectory of the colliding nucleons is simply treated classically. The nucleons lose their energies by escaping from the boundary of the nucleus. The deformation effects (diffraction and deflection at the nuclear boundary) were also taken into account in the several calculations.[10] This model predicts energy and angular distributions of the emitted nucleons. These predictions are in good agreement with the experimental data for nuclear reactions induced by high energy projectiles beyond 100 MeV/nucleon. But an application of this model to the lower excitation energy region[18, 19] yielded inconsistent results

with experiments for both energy and angular distributions.[20] Futhermore, the INC model can hardly treat reaction processes with complex projectiles and outgoing complex particle emissions. In order to improve the INC model, the QFS model[13] has been proposed. This model describes the intra-nuclear nucleon-nucleon and cluster-nucleon scattering kinematics. The decay rates of the particles to continuum states are calculated from phase space and penetrability considerations[13]. As well as the INC model, the QFS model has not been able to reproduce the experimental data in the lower excitation energy region ($\lesssim$ 100 MeV)[21]. The PEQ exciton model proposed by J. J. Griffin[7] describes the nuclear states in terms of exciton numbers $m = p + h$ with total excitation energy E, where p and h are the number of excited particles and holes, respectively. An excited state with exciton number m has some unbound particles which may escape to continuum states. Therefore the excited nucleus decays partly by emitting these particles and partly by spreading to more complicated states. Cline and Blann[23] combined this model with the master equation approach of Harp, Miller and Berne (HMB model)[22]. It has been generalized as a hybrid model by Blann.[24, 25] The refinement and improvement of the model has also been done by E. Gadioli et al.[26]. Blann has developed the model by taking into account a geometry-dependent hybrid model (GDH)[24]. Recently, the exciton model has been extended to

calculate the angular distributions of emitted particles.[27-31] Recent reviews on these subjects are given by Blann[14, 32] and Gadioli[33]. On the other hand, an approach with the multi-step direct reaction theory (MSDR) was proposed by T. Tamura et al.[34]. They analyzed (p, p')[34] and (p, α)[35] reactions successfully, and recently analyzing powers in the continuum region of the (p, p') reaction[36] have also been analyzed using the MSDR method.

1-3. Investigation of (particle, xn yp γ) Process by Decay Particle-γ Coincidence Method

It is important to investigate fast and slow neutrons following (particle, xn yp γ) reactions as a function of the neutron multiplicity x in order to investigate the de-excitation process through the PEQ and EQ phases of the reaction. Here the neutron multiplicity x can be identified by requiring a coincidence with discrete γ-rays characteristic of the final reaction channels. Previously, Ejiri et al.[3] made a detailed study of the ^{165}Ho(p, xn γ)Er reaction at E_p = 60 MeV, and found the properties of the neutrons emitted at the PEQ stage. Since the projectile used was 60 MeV protons, the neutron multiplicity x was limited to $x = 2 \sim 6$ and the angular momentum involved was small. Sakai et al.[37]

has extended the previous (p, xn γ) reaction induced by 60 MeV protons to the (α, xn γ) reaction induced by 120 MeV α-particles, where the range of the neutron multiplicity was much larger and the angular momentum involved was also much larger. They studied characteristic behavior of emitted neutrons through the PEQ and EQ stages as a function of the neutron multiplicity x in a wide range of the neutron multiplicity $x = 4 \sim 11$.

The (particle, xn γ) reaction mechanism has also been studied by singles γ-ray and coincidence γ-γ measurements. Recently γ-ray multiplicities for (α, xn γ) reactions and the median spin value of the ground state rotational band have been found to saturate as the projectile energy increases well beyond the threshold energy.[38-41] This suggests that a considerable fraction of input angular momentum is carried away by the PEQ neutrons. The energy, angular and multiplicity distributions of decay neutrons were analyzed in terms of the effective energy parameter (quasi-temperature) and active exciton particles (local mass).

The de-excitation properties following the heavy ion induced reaction also have been investigated by several authors[41-44]. The neutron coincidence experiments for the ^{165}Tm(^{14}N, xn γ) reaction at $E(^{14}N) = 130$ MeV showed that the neutrons came mostly from the EQ stage[42], and γ-ray spectra following the ^{169}Tm(^{14}N, xn yp γ) reaction at $E(^{14}N) =$

210 MeV showed that some fast particles were emitted at the PEQ stage[43]. Westenberg et al.[44] found some PEQ neutron in the n-γ coincidence measurement for the ^{158}Gd(^{12}C, xn γ) reaction at E(^{12}C) = 152 MeV.

1-4. Purpose of the Present Work

The present subject is the PEQ process for nucleon emissions following highly excited nuclei in the 50 $\sim$ 120 MeV excitation region produced by α-particle bombardments on medium heavy nuclei. This energy region is very interesting because the PEQ and EQ processes co-exist and the phase transition from the PEQ to the EQ stage is expected. From the experimental point of view, the complex reaction mechanisms can be studied by measuring the cascade γ-rays which are used to identify the final reaction channels and by observing the energy spectra of emitted particles from the de-exciting nuclei. The emitted particles are measured by singles and/or coincidence with the cascade γ-rays.

In order to perform these experiments, decay particles and γ-rays following the $^{162,\ 164}$Dy(α, xn γ) reaction at E_α = 50, 70, 90 and 120 MeV, the ^{158}Ho(α, xn yp γ) reaction at E_α = 109 and 120 MeV, and the ^{158}Gd(α, xn γ) reaction at E_α = 70 MeV were investigated. As the residual nuclei

following these reactions are well known rotors the neutron multiplicities (reaction channels) can be easily obtained from well defined rotational γ-rays. The yields of the residual nuclei can be obtained from the yields of the rotational transitions of $4^+ \rightarrow 2^+$ and/or $2^+ \rightarrow 0^+$ which accumulate most of the de-excitation flows. Several investigators[37-44] carried out the γ-ray multiplicity measurements using the deformed nuclei with same reason as mentioned above. These results are available to be compared with the present measurements.

The present work aims at the following:

(1) To study experimental evidences for the PEQ process, neutron multiplicity distributions, mean neutron energy and angular momentum transfer were investigated.

(2) To study dynamic properties of the PEQ process, the data obtained in the present work were analyzed with a simple two phase (PEQ-EQ phase) model and a de-excitation model based on the exciton model. The PEQ process is shown to depend strongly on the projectiles and the reactions used to excite the PEQ phase. The analyses give the quasi-temperatures of the nucleus at the PEQ and the EQ phases the effective number of the excitons, the effective collision probabilities and the critical energy of the PEQ de-excitation.

The experimental instruments and apparatuses are discribed in chap. II. In chap. III, the experimental procedures and the obtained experimental results are presented. The following quantities were obtained; the cross sections of each reaction channel, the neutron multiplicity distributions, the mean neutron energies, the quasi-temperatures of the PEQ and the EQ stages, and the differential and angle integrated decay particle cross sections both for singles and coincidence measurements. In chap. IV, the experimental results are analyzed in terms of the exciton model for multi-particle emission process and the simple two phase approximation. The results of the present work are discussed and concluded in chaps. V and VI, respectively.

II. EXPERIMENTAL INSTRUMENTS AND APPARATUSES

2-1. General Descriptions

PEQ and EQ processes of the (α, xn yp γ) reactions on deformed nuclei were studied by investigating neutron multiplicity distributions, and energy and angular distributions of decay neutrons and protons. Incident α-particles of energies between 50 and 120 MeV were provided by the 230 cm AVF cyclotron[45] at RCNP (Research Center for Nuclear Physics), Osaka University. The enriched $^{162,\ 164}$Dy targets were prepared by depositing of oxide powder onto thin mylar films (30 μm in thickness). Self-supporting metalic foils of natural holmium and enriched gadrinium were obtained by rolling for ^{165}Ho and ^{158}Gd targets. The thickness and the enrichment of these targets are tabulated in table I.

Neutron multiplicity distributions for (α, xn yp γ) reactions were obtained from singles γ-ray spectra for the reactions of $^{162,\ 164}$Dy(α, xn γ)$^{166-X,\ 168-X}$Er at E_α = 50, 70, 90 and 120 MeV, ^{165}Ho(α, p xn γ)$^{168-X}$Er at E_α = 110 and 120 MeV, and ^{158}Gd(α, xn γ)$^{162-X}$Dy at E_α = 70 MeV. The singles γ-ray spectra were measured at lab. angle θ_ℓ = 125 deg. with respect to the beam axis by a 1.4 cc pure Ge detector (LEPS) with energy resolution ΔE = 1 keV for 511 keV γ-rays. Absolute yields of the reaction residues were estimated from cascade

rotational γ-transitions by refering to the branching ratios observed in previous in-beam works[46-60].

The neutron multiplicity distribution for the ^{165}Ho(α, p xn γ) $^{168-x}$Er reaction at E_α = 110 MeV for the particular proton energy was achieved by coincidence measurements of discrete γ-rays with decay protons. Angular and energy distributions of decay protons were measured at lab. angles of θ_p= 25, 40 and 125 deg. with respect to the beam axis. A counter telescope system was used for the proton detection. It consists of a ΔE counter of silicon surface barrior detector (300 μm in thickness) and an E counter of NaI(Tl) scintillation counter (31.75 mm diameter × 31.75 mm thick and/or 25.4 mm diameter × 125 mm thick). In the coincidence measurements, discrete γ-rays were detected by a large volume (55cc) pure Ge detector (GAMMA-X) at θ_ℓ= 130 deg. with respect to the beam axis.

Angular and energy correlations between decay protons and neutrons following the reaction mentioned above (^{165}Ho (α, xn yp γ) at E_α = 110 MeV) were measured both in the reaction plane and the out of this plane. Protons were measured at the fixed angle of θ_ℓ= 30 deg. with respect to the beam axis. The neutrons were detected by an NE213 liquid scintillator (127 mm diameter × 127 mm thick) which was placed at a distance of 120 cm from the target. The neutrons were separated from γ-rays with a pulse-shape analysis metod[61]. Moreover, a 2 cm lead absorber was placed in front of the

neutron counter to reduce the γ-ray background. The small absorption effect due to the lead absorber was corrected for by measuring the neutron spectra with and without the lead absorber.

The neutron-γ coincidence measurement was carried out by using the $^{158}Gd(\alpha, xn\ \gamma)$ reaction at $E_\alpha = 70$ MeV. The neutron spectra were obtained by requiring coincidence with discrete γ-rays which are characteristic of each reaction channel ($x = 4 \sim 6$). The neutrons were detected by an NE213 liquid scintillator (127 mm diameter × 76.2 mm thick) with n - γ discrimination. The neutron detector was placed at 48 cm from the target. A larger solid angle could be obtained than that in the p-n coincidence experiment. In order to reduce the accidental coincidence owing to a large background of the γ-ray sprectrum, such large solid angle is essential for this work. The neutron angular distributions were measured at $\theta_\ell = 35$, 70, 110 and 145 deg. with respect to the beam axis. The discrete γ-rays were detected at $\theta_\ell = 90$ deg. with respect to the beam axis using GAMMA-X. It was placed at a distance of 9.6 cm from the target.

The neutron energy spectra were obtained by means of a TOF (time of flight) technique. The energy resolution ($\Delta E = 1$ MeV for 5 MeV neutrons) for a typical flight path ($\ell = 120$ cm) is sufficient to select high energy neutrons for the angular distribution measurements and to give rough shapes of

the continuous energy spectra characteristic of the PEQ and EQ processes. The absolute efficiency of the NE213 scintillators presently used was calculated by a Monte Carlo calculation code provided by K. Shin[62]. The calculated detection efficiency with the lower discrimination for the experiment was compared with the experimental values[63], and a reasonable consistency was obtained.

Background neutrons due to lead shields and other surroundings to the neutron spectra were examined and found to be negligibly small in the present coincidence experiments.

The counting rates of all the detectors were kept constant so that the dead time correction was nealy constant over the runs.

All the experimental informations were accumulated onto the magnetic tapes in an event-by-event mode. The raw data processor[64] controlled by PDP 11/40 computer was used for data takings. After the experiments, off-line analyses were performed. Data tapes were editted using the central computer TOSBAC 5600.

A typical experimental arrangement of the detectors is shown in fig. 2-1, and a schematical diagram of the experimental flow is illustrated in fig. 2-2.

In the following sections, we describe in details the apparatuses, the detectors and the data taking system used for these measurements.

2-2. Beam Course

The F beam course in the RCNP is aimed for inbeam photon, electron and particle (PEP) spectroscopy. The profile is shown in fig. 2-3.

Alpha beams from the RCNP AVF cyclotron are analyzed in energy by an analyzing magnet and deflected by a switching magnet. They are focussed on a defining slit after the swiching magnet. Then, they refocussed on the first target port (F) in F beam course by means of two sets of quadrupole magnets. The target port F is used for the measurements of γ-rays, charged particles and neutrons. The beams are refocussed by an another set of quadrupole magnets on the second target port (F'). A steering magnet is used to correct the beam discrepancy from the center of the second target. In this target port, an electron spectrometer called AGNES is placed. Finally, the beams are stoped by the beam dumper made of Ta. In order to decrease the room backgrounds of stray neutrons and γ-rays, the beam dumper is shielded with paraffin, iron and lead blocks. This beam dumper is also used as a Faraday cup in order to measure the beam current.

A typical size of the beam spot for α-particles is about 1.5 mmϕ at the first target position (F), when the beam current is a few nA.

There are no beam defining slits inside the beam duct in

the experimental room in order to avoid background γ-rays and neutrons from them. There are seven graphite buffers with apertures of 8 ∿ 30 mm diameter are placed inside the beam duct and the exit of the target chamber. They are used to reject the stray beam and to avoid the activation of the beam duct and the target chamber.

The beam duct and the target chambers were evacuated using three turbomolecular pumps and two sets of liquid nitrogen traps placed up- and down-stream of the target chambers. The pressure in the first target chamber was typically 1×10^{-5} torr.

2-3. Target Chamber and Goniometer

The target chamber installed on the F target port is illustrated in fig. 2-4. This chamber was designed for measurements of γ-rays, neutrons and charged particles outside the chamber. It has two arms for charged particle counters. They can be rotated manually for measuring angular distributions in the reaction plane (θ direction). The chamber with particle counters can be rotated itself about the beam axis (φ direction) automatically using a stepping moter. Several kinds of angular correlation measurements (n - n, n - γ, p - n, p - γ, and γ - γ etc.) can be carried out by rotating charged particle counters

in the θ - ϕ plane, and γ-ray and neutron counters in the horizontal plane.

The side wall of the chamber is made of stainless steel with 3 mm thickness. It has wide opening windows which are vacuum sealded with a thin mylar film (25 μm in thickness) for measuring angular distributions in a wide angular range of $-150 \sim 150$ deg..

Absorption of γ-rays and neutrons due to the mylar window may be neglected for energetic charged particles of the present interest. The energy loss of a charged particle through the mylar film is about 300 keV for 10 MeV proton. The cap of the chamber was made of Al (5 mm in thickness) in order to reduce absorption of neutrons when the chamber was rotated around the beam axis. The absorption due to the Al cap was estimated less than 5 per cent for fast neutrons.

The goniometer which is installed at the F target port has four turn tables. Two of them can be rotated automatically by using stepping motors. They are used for γ-ray detectors (Ge(Li), LEPS and GAMMA-X). One of the other two turn tables are used for a NaI(Tl) scintillation counter, which is used to measure continuous γ-rays, and another has an extended plate on which an NE213 liquid scintillation counter can be set. The neutron time of flight measurements were carried out using this extended plate. It can be rotated on the rail around the target to measure the angular distributions

of neutrons. The length of neutron flight path is adjustable from 20 cm to 120 cm.

2-4. Detectors

A. Charged particle counter

Energies of charged particles were measured by a counter telescope consisting of a Si surface barrier SSD and a NaI(Tl) scintillation counter.

The Si surface barrier SSD with 450 mm^2 detection area and 300 μm thickness was used for the energy loss counter (ΔE). The lower limits of energy ranges for any charged particle are determined by the ΔE counter. In the case of this detector, they were 6.5 MeV for protons and 25.0 MeV for alpha particles. The NaI(Tl) scintillation counters were used for the E counter. Two types of NaI(Tl) counters were used. One is 25.4 mm diameter × 25.4 mm length with 50 μm Al window (OYO-KOKEN), and another is 31.75 mm diameter × 31.75 mm length with 25 μm Al window (HARSHOW). Both counters can detect up to 80 MeV protons. The typical energy resolutions of these NaI(Tl) counters are 2.0 MeV FWHM (OYO-KOKEN); and 1.0 MeV FWHM (HARSHOW) for 120 MeV alpha particles. Ordinary, the latter detector (HARSHOW) was used because of its better resolution,

wider detection area and thinner window than the former (OYO-KOKEN). Photo-productions in the NaI(Tl) counters caused by the present high energy charged particles ($\sim$ 100 MeV) are much larger than that in the ordinary use, so a breeder circuit for the photo-multiplier (R580, HAMAMATSU) was changed to obtain stable out-put gain. The resistances of the breeder were converted to about one tenth value of the ordinary ones. Fig. 2-5 shows the circuit of the breeder.

The pulse hight responses of the NaI(Tl) scintillator for charged particles deviate from linearity over an energy range of several tens of MeV[65]. In order to determine the energy dependence of this non-linearity for the NaI(Tl) crystal presently used, the pulse height responses of the elastic scattered protons and α-particles were measured. The energies of these particles were determined with detection angles and absorbers. Fig. 2-6 shows the pulse height responce of the crystal of 31.75 mm diameter $\times$ 31.75 mm thickness to higher energy protons.

This counter telescope was mounted on a brass case, in order to reduce noises caused by light etc.. A slit system to determine the solid angle of the charged particle detection was fixed to this brass case. A typical solid angle of this counter telescope for coincidence measurements was as large as 60 msr. The mounting of the counter telescope system is shown in fig. 2-7. Fig. 2-8 shows a typical particle

identification spectrum obtained by the present counter telescope system.

B. Liquid scintillation detector

Neutron was detected by an NE213 liquid scintillation detector. A time of flight (TOF) technique was employed to determine the kinetic energy of neutrons. The NE213 liquid scintillator has a good detection efficiency for fast neutrons, and is suitable for pulse shape discrimination analysis between neutrons and γ-rays. The pulse height response and the detection efficiency of the scintillator for fast neutrons have been studied by many authors[66-69]. The pulse height response of the NE213 scintillator is an important quantity to estimate the absolute detection efficiency. It varies with the size and form of the scintillator.

The liquid scintillator detects fast neutrons through recoiling protons. The recoiling protons make continuous pulse height response distributions corresponding to their kinetic energy. This property depends on the angular distributions of the recoiling protons with respect to the momentum direction of the incident neutrons. The amount of secondary scatterings of the neutrons affects the pulse height response function, and depends on the scintillator geometry. The measurement of the pulse height response function was made

with the use of a pulse shape discriminator to reject the γ-ray events. The γ-rays are detected in the liquid scintillator through the compton electron scatterings. The decay time of the fluorescent light output of the NE213 scintillator consists of two time components[70]. One is a fast component (2-4 ns) due to the low ionization density produced mainly by γ-ray events, another is a slow component (10-30 ns) due to higher ionization density produced mainly by neutron events. This property is used to distinguish the events of neutrons form that of γ-rays. We used a pulse shape discriminator (Model 2160, CAMBERRA) in order to perform this problem. A pulse shape discrimination spectrum is shown in fig. 2-9-a and the neutron energy dependence of the pulse shape discrimination is shown in fig. 2-9-b. Measured response functions for various energy neutrons are shown in fig. 2-10. The detection efficiency is critically dependent on the bias setting at low light output side because of a sudden steep character at this region. This character may cause a serious error to the low energy neutron ($\sim$ 5 MeV) detection efficiency. At the higher light output region above $E_e = 2.0$ MeV, the efficiency changes just slowly with the bias setting because of its relatively flat character. We should take care of these natures of the used scintillation detectors to calculate the absolute detection efficiencies of the fast neutrons. A Monte Calro calculation was used to estimate the neutron

detection efficiency. We calculated the detection efficiency for the used scintillator with a Monte Calro calculation code provided by K. Shin[62]. The calculated detection efficiency with a certain threshold is compared with experimental value[64]. Fig. 2-11 shows the results of the calculation for neutron detection efficiency (lower distribution level E_e = 800 keV).

The energy calibration of the time of flight was carried out with the maximum of the light output. The light output is proportional to about 3/2 powers of the energy of protons. This relation between the light output and the proton energy for the NE213 scintillator was measured by V. V. Verbinski et al.[69]. The light output calibration of the NE213 scintillator is usually carried out by measuring the compton edge of γ-rays; $^{56}Co(E_e = 3017, 2365$ and 1027 keV), $^{88}Y(E_e = 1632$ keV) and $^{22}Na(E_e = 1062$ and 341 keV). The light output for higher energy electrons were extraporated. The calibration curve and experimental points obtained with monoenergitic neutrons following $^{7}Li(p, n)^{8}Be^{*}$ reactions are shown in fig. 2-12. The time and energy calibration for neutrons are shown in fig. 2-13. The neutron flight time was measured with time differences between the neutron signals from the scintillator and the RF signals from the cyclotron for neutron singles

---

*) Proton beams were provided by the AVF cyclotron at the Cyclotron Radio-isotope Center, Tohoku University.

and neutron-γ coincidence experiments. In the case of charged particle-neutron coincidence measurements, the neutron flight time was measured with the time differences between the neutron signals and the charged particle signals from the ΔE counter (Si surface barrier SSD). Fig. 2-14 shows the time spectrum of neutrons for the latter case.

In order to reduce the backgrounds (stray neutrons and γ-rays), paraffin blocks, lead plates (30 mm thickness) and brass plate (5 mm thickness) at the side of the scintillator, and lead plates (20 mm thickness) and brass plate (5 mm thickness) in front of it were used for shields. The absorption of the neutrons of the front shield was measured. Fig. 2-15 shows the effects of the front shield and the total neutron detection efficiency. The neutron background was estimated from the yields of neutrons with a blank target. A typical neutron time structure is shown in fig. 2-16.

All the informations; The pulse height spectra, the time of flight spectra and the pulse shape discrimination spectra, were recorded in an event by event mode by use of the Raw Data Processor. After the experiment, off line analyses were performed.

C. Gamma detectors

Highly excited nuclei have many decaying channels. The

γ-ray spectra are much complicated because of many decaying channels. These complicated spectra were precisely measured by a 1.4 cc high purity Ge detector in a singles mode. This detector called LEPS (Low Energy Photon Spectrometer) has the higher energy resolution than a ordinary large volume Ge(Li) detector. The energy resolution is 1 keV for 511 keV γ-rays. In order to avoid the ambiguity of the dead time correction, the counting rate was always kept as 700 counts/sec. In front of LEPS, a brass plate (1 mm thickness) was placed to reduce the x-rays from the target. Photo-peak energies were determined within 0.2 keV by using LEPS. It was very powerful to identify the γ-rays from the final nuclei accurately. We could determine precise distributions of the residual nuclei (neutron multiplicity distributions).

In the times of coincidence experiments (n - γ and p - γ), a large volume Ge(Li) detector (60 cc) and a Ge(pure) detector (55 cc one called GAMMA-X) were used in order to improve the coincidence efficiency. The energy resolutions of these detectors were about 2.0 keV for ^{60}Co 1332 keV γ-rays. The counting rate had also to be nearly constant to keep the counting condition to be stable.[1] These detectors were shielded by lead blocks (50 mm thickness) to reduce background γ-rays. A copper plate (1 mm thickness) was inserted between the lead shields and an Al cap of the Ge detector to absorb the x-rays from the lead sheild. In front of the detector, a copper or

a brass absorber (3 mm thickness) was set to reduce the x-rays and low energy γ-rays coming from the target.

The absolute efficiencies of these Ge(pure) and Ge(Li) detectors were measured every time after experiment by an calibrated RI source set at the target position. The counting rate and electronics were maintained as the same condition as the inbeam experiments. The typical examples of absolute efficiency curves obtained for GAMMA-X and LEPS are shown in figs. 2-17-a and 2-17-b.

2-4. Data Taking System

The electronic circuit used are mostly NIM module circuits. The typical block diagram is shown in fig. 2-18. They are composed three parts. One is the coincidence circuit block. Conventional fast-slow coincidence modes were used. The signals through these circuits were processed by the raw data processor. And they were written onto the magnetic tape which is controlled by the PDP 11/40 computer. The second part is the circuit for measurements of the singles γ-ray spectra. The signals from LEPS or Ge(Li) are accumulated in the multi-channel analyzers (CAMBERRA 8100, 8700 or SCORPIO). The third part is the on-line monitor circuit for the coincidence measurements.

After on-line data taking, off line analyses were performed. Data tapes were sorted by various modes (projection, digital gate and two dimension etc.) using the central computor TOSBAC 5600.

III. EXPERIMENTAL PROCEDURES AND RESULTS

Table II summarized types of the reaction studied. It lists the target nuclei, energies of incident α-particles, initial fused nuclei and their excitation energies, modes of experiments, and laboratory angles of observations are tabulated.

3-1. Neutron Multiplicity

A systematic study of the de-excitation process for the fusion like (α, xn yp γ) reactions in an energy range of 50∿120 MeV is important from a view point of the PEQ neutron emission. When a medium heavy nuclei is excited by the α-particle bombardment, a small number of fast neutrons are expected to be emitted through the PEQ process. A part of these neutrons which is emitted at the first doorway state take away large excitation energy. After one or two these neutron emissions, the residual nucleus transits to the EQ phase at the excitation energy of 25∿40 MeV. The equilibriated nucleus cools down by a several number of neutrons proportional to the excitation energy. Thus the neutron multiplicity x is much smaller than the statistical model prediction for the fast neutron emissions at the first stage of the PEQ process.

On the other hand, after several state spreadings at the PEQ stage of the de-excitation process, relatively low energy neutrons are also expected to be emitted through the PEQ phase. The phase transition from the PEQ stage to the EQ stage occurs at higher excitation energy of $35 \sim 50$ MeV. This process corresponds to the large neutron multiplicity. Thus the neutron multiplicity distribution is sensitive to the first stage neutron emission at the PEQ phase. The neutron multiplicity in a wide range can be measured experimentally by observing discrete γ-rays characteristic of the residual nuclei.

The discrete γ-rays were measured in coincidence with protons for the (α, p xn γ) reaction in order to study correlations between the neutron multiplicity, and energy and angular distributions of decay protons. Almost the decay protons without low energy part are considered to be emitted from the PEQ stage. They leave the residual nuclei at the PEQ stage. Characteristic properties of the PEQ stage such as the exciton number and the excitation energy of the residual nucleus should be reflected upon the kinetic energies and the angular distributions of first emitted protons. As mentioned above the neutron multiplicity is sensitive to the PEQ properties. Therefore the neutron multiplicity distributions in coincidence with protons are expected to be sensitive to the exciton number and the excitation energy at the proton

emission.

A. Neutron multiplicities for the (α, xn yp γ) reactions

i) Procedure of neutron multiplicity measurement

We measured neutron multiplicity for the reactions of $^{162,\ 164}$Dy(α, xn γ)$^{166-x}$Er at E_α = 50, 70, 90 and 120 MeV, ^{165}Ho(α, p xn γ)$^{168-x}$Er at E_α = 110 and 120 MeV, and ^{158}Gd(α, xn γ)$^{162-x}$Dy at E_α = 70 MeV by means of singles γ-ray measurements. The thickness and form of the bombarded targets are listed in table I. The singles γ-ray spectra were obtained by use of LEPS (Ge(pure) detector) at 125 deg. with respect to the beam axis. A typical singles γ-ray spectrum following the ^{164}Dy(α, xn γ) reaction at E_α = 120 MeV is shown in fig. 3-1.

Cross sections for each reaction channel with neutron multiplicity x were obtained from the detailed γ-ray spectra. Total cross sections $\sigma(x)$ are estimated from the absolute yields of discrete γ-rays characteristic of the xn reaction channels. For the even-even isotopes, the $\sigma(x)$ are approximately given by the yields of the ground band $4^+ \rightarrow 2^+ \rightarrow 0^+$ transitions. The cross section of the $2^+ \rightarrow 0^+$ γ-transition may be assumed to stand for the cross section of the reaction channel, and the yield of the $4^+ \rightarrow 2^+$ γ-transition for the 80

per cent of total yield of the reaction channel. The $\sigma(x)$ for odd-A isotopes were estimated from the intensity ratios of the γ-rays along the yrast, yrare and other possible bands observed in refs. 41-59. In the case of each odd-A Er isotope, the γ-ray yields of the yrast $\frac{21^+}{2} \rightarrow \frac{17^+}{2} \rightarrow \frac{13^+}{2}$ transitions and yrare $\frac{19^+}{2} \rightarrow \frac{15^+}{2} \rightarrow \frac{11^+}{2}$ transitions were used. The total yields for the feedings of each reaction channel were obtained by summing up the intensities of the transitions with correction for the electron conversion. Small corrections ($\tilde{}$ 10 per cent) for the anisotropic distribution of the γ-rays have been made by use of the stretched E2 transitions. A phenomenological $A_2P_2(\cos\theta)$ term[68] for the stretched E2 transitions was used.

ii) Results

The total cross sections for the $^{162,\ 164}$Dy(α, xn γ) reactions at E_α = 50, 70, 90 and 120 MeV are plotted in fig. 3-2 as a function of the kinetic energy sum E_T of the decay neutrons. The E_T is defined as

$$E_T = \sum_{n=1}^{x} E_n, \qquad (3\text{-}1)$$

where x is the number of neutrons emitted, namely neutron multiplicity. The sum E_T is equivalent to the energy excess above the reaction threshold, and it is simply related to the

neutron multiplicity x as follows.

$$E_T = E^* - x\langle B_n \rangle - E_\gamma, \qquad (3\text{-}2)$$

where E^* is the initial excitation energy, $\langle B_n \rangle$ is the average neutron binding energy and E_γ is the excitation energy removed by γ-rays. We assumed a constant value of $E_\gamma = 9.0$ MeV for all residual nuclei. A prominent feature is that the cross sections for small number x of emitted neutrons with large E_T are much larger than those expected from a simple calculation within the compound nucleus model. Thus most of the cross section at large E_T (small x) may be due to the PEQ process. This feature gets more pronounced with the increasing projectile energy. In fig. 3-3, the cross sections for the reactions of ^{165}Ho(α, p xn γ) and ^{164}Dy(α, xn γ) at $E_\alpha = 120$ MeV are presented as a function of the neutron multiplicity. The sum of the cross sections for the (α, p xn) reaction is rather flat as a function of the neutron multiplicity x.

B. Neutron multiplicity in coincidence with protons following the ^{165}Ho(α, p xn γ) reaction at $E_\alpha = 109$ MeV

i) Procedure of neutron multiplicity measurement gated by energy and angle of decay protons

In order to obtain the neutron multiplicity distributions in coincidence with protons. We studied the ^{165}Ho(α, p xn γ) $^{168-x}$Er reaction by means of the proton-γ coincidence measurement. A 5.5 mg/cm^2 metallic ^{165}Ho target was irradiated by 109 MeV α-particles. Two sets of counter telescope were used to detect charged particles. They were observed at lab. angles of 25, 40 and 129 deg. with respect to beam axis. Discrete γ-ray were detected by GAMMA-X (Ge(pure) detector) at 130 deg. to the beam axis.

Cross sections of each reaction channel $\frac{d^2\sigma_x}{dE_p d\Omega_p}$ were obtained from the γ-ray spectra gated by five proton energy intervals at each detection angle. As described in the previous section, each rotational γ-transition observed in the gated spectra was used to estimate the absolute values of $\frac{d^2\sigma_x}{dE_p d\Omega_p}$.

ii) Result

The observed neutron multiplicity distributions are shown in fig. 3-4. The neutron multiplicity distributions gated with forward low energy protons are similar to those for the (α, xn γ) reactions, namely the cross sections with small neutron multiplicity x is so large as to be expected from the EQ calculation. The residual nucleus is thought to be left at the high excitation with small number of excitons after forward low energy proton emissions. The forward high energy

proton emissions give only the reaction channels with small neutron multiplicity. When these proton emission occur, the residual nucleus transits rapidly to the EQ phase. The characteristic properties of the PEQ process can not be observed. On the other hand, the multiplicity distribution gated by backward protons is close to what was expected by the evaporation process indicating large number of excitons after the proton emission.

3-2. Energy Spectra of Decaying Neutrons and Protons

It is important to investigate fast and slow neutrons following the de-exciting nucleus at the PEQ and the EQ phases. Energy and angular distributions of these neutrons give direct informations about the PEQ de-excitation process, namely the PEQ neutrons can be easily distringuished from the EQ neutrons which indicate a typical evaporative energy distributions as $\propto E \exp(-\frac{E}{kT_e})$, where kT_e is the nuclear temperature of the equilibriated nucleus, and a isotropic angular distribution. On the other hand, protons following the de-exciting nucleus considered to be mostly emitted at the PEQ phase since the evaporation of protons is suppressed by the Coulomb barrier of the compound system. Although a part of protons and fast neutrons can be emitted through a single collision with

protons and neutrons from the PEQ stage are ejected after multi-collisions (state spreadings) with nucleons in the compound system. In order to investigate these complicated process, energy and angular correlations between protons and neutrons were measured. The PEQ neutrons should give the informations about the excitons and excitation energy at the proton emitted states. Proton energy spectra for each reaction channel can be obtained by requiring the coincidence with the discrete γ-ray which is characteristic of each reaction channel. They can be related to the excitation and the excitons of the residual nucleus at the proton emission.

Recently very detailed measurements of the γ-ray multiplicity distributions for (α, xn γ) reactions have been carried out by using the multiple NaI counter system by M. A. J. de Voigt et al.[40]. The measured multiplicities and γ-ray energies were used to locate the γ-ray entry lines in the final nucleus after neutron emission in the excitation-energy versus spin plane. In that work tests on the conservation of angular momentum could only be made by using neutron data obtained with other reactions.

We carried out the n - γ coincidence measurement to correlate the previous γ-ray multiplicity and the present neutron data for one and the same reaction. This will serve as a more stringent test on the conservation of energy and angular momentum in the reaction and to construct a consistent

picture of the decay in terms of competing equilibrium and pre-equilibrium processes. For this purpose the $^{158}Gd(\alpha, xn\ \gamma)^{162-x}Dy$ reaction was chosen with x = 4, 5 and 6 at bombarding energy of $E_x = 70$ MeV. The γ-ray data taken at the Groningen cyclotron a Ge(Li) - 16 NaI detectors multiplicity filter indicated that the (α, 6n) reaction led to predominently compound-nucleus formations whereas significant PEQ effects seemed to be present in the (α, 4n) reaction, with the (α, 5n) exit channel acting as an intermediate phase. The deduced entry lines[40] are used in the present work to obtain the average energy and angular momentum release by the quasi-continuum and discrete γ-ray cascades.

A. Neutron energy spectra following the $^{165}Ho(\alpha, xn\ yp)$ reaction at $E_\alpha = 110$ MeV

i) Procedure of neutron measurements

Both singles and proton gated neutron energy spectra were obtained from the $^{165}Ho(\alpha, xn\ yp)$ reaction at $E_\alpha = 109$ MeV. The energy of neutrons were determined by means of TOF method. The flight path was L = 120 cm. Neutrons were detected by an NE213 liquid scintillation counter which has a good neutron detection efficiency and character of n - γ discrimination. The energy range of neutrons which was determined with the

flight path and the beam cycle of the cyclotron was between 1.2 and 30 MeV.

Angular distributions and correlations with decay protons which were detected by a counter telescope system at fixed angle $\theta_p = 30$ deg. were measured at $\theta_h = -69.2$, -53.8, -20.3, 23.9, 33.6, 53.8, 63.2, 108.6 and 139.1 deg.

ii) Result

Differential neutron spectra at lab. angles $\theta_h = 20.3$ and 139.1 deg. are shown in fig. 3-5. The neutron energy spectra at the forward angles show large high energy tailes, and those at backward angles show a typical evaporation pattern. The former and the latter may correspond to the PEQ and the EQ neutron-emissions[1-6], respectively.

The differential cross sections $\frac{d^2\sigma}{dEd\Omega}$ in the center of mass (C. M.) frame were integrated over C. M. angles using the following equation;

$$\frac{d\sigma}{dE} = \int \frac{d^2\sigma}{dEd\Omega} d\Omega = 2\pi \int_0^{\pi} \frac{d^2\sigma}{dEd\Omega} \sin\theta d\theta. \qquad (3\text{-}3)$$

The integration was carried out by means of a spline function which can connect the experimental value smoothly. Fig. 3-6 shows the angle integrated neutron spectrum. The errors in this spectrum were mostly due to the TOF resolution which

consisted of the time resolutions of the cyclotron beam bunch and the detector length relative to the length of the flight-path. Stray neutrons (room background), which were carefully surveyed, were estimated less than 5 per cent of the total neutron yield. In fig. 3-6, there is a large high energy tail considered as due to the PEQ neutron emission. Deviations from a statistical estimation for any physical quantity in the present energy region may be connected to it. The PEQ neutrons account for about ten per cent of total yields of the neutrons. An energy integration of the angle integrated neutron cross section can be obtained from the following equation;

$$\sigma_n = \int_0^{E_{max}} \frac{d\sigma}{dE} dE \simeq \langle M_n \rangle \sigma_\Omega, \qquad (3\text{-}4)$$

where $\langle M_n \rangle$ is the mean value of the neutron multiplicity and σ_Ω is the total reaction cross section accompanied with neutron emissions. The mean neutron multiplicity $\langle M_n \rangle \simeq 7.5$ is obtained from the observed neutron multiplicity. Inserting this value into eq. 3-4, we get the total reaction cross section $\sigma_\Omega \simeq 1.63$ b. It agress with the cross section obtained from the singles γ-ray spectra.

The neutron momentum distributions deduced from the angular distributions in coincidence with protons for three energy bins are shown in fig. 3-7. The relative yields are

plotted as contour lines of each one half value. The shaded portions in the fig. 3-7 represent the coincident proton momenta, and the lozenges are the momentum of the incident α-particles. It is approximately seen that there are conspicuous forward peakings of high momentum tails of neutrons. On the other hand, neutrons with low momentum (< 5 MeV in energy) indicate isotropic angular distributions. Angular correlations between the PEQ protons and neutrons could not be found in the present experiment, because of the lack of higher momentum (> 30 MeV in energy) neutron detection. Fig. 3-8 presents mean energies of the neutrons $\langle E_n \rangle$ at each detection angle in three proton energy bins. It is seen that $\langle E_n \rangle$ gated by the proton energy of $\geq$ 50 MeV, is nearly constant at all the detection angles. However, $\langle E_n \rangle$ gated by lower energy protons indicate large forward peakings. The ratios of high (> 5 MeV) and low energy (< 5 MeV) neutron cross sections in three proton bins are presented in fig. 3-9. The angular behavior is very simillar to that of the mean neutron energy.

B. Exclusive proton spectra for each reaction channel of the ^{165}Ho(α, p xn γ) reaction at E_α = 109 MeV

i) Procedure of the measurement

The same procedure as the measurement of neutron multiplicity distribution in coincidence with protons described in sec. 3-1-B were employed. Here the proton energy spectra at each detection angle were gated by the discrete γ-rays characteristic of the reaction channels with neutron multiplicity range $x = 2 \sim 8$.

ii) Result

The proton energy spectra obtained from the proton-γ coincidence measurements in the neutron multiplicity range $x = 2 \sim 8$ are presented in fig. 3-10-a for even mass isotopes and in fig. 3-1-b for odd mass isotopes at lab. angles θ_p = 25 and 129 deg. The proton energy spectra consist of high energy part and low energy tail. The high energy part corresponds to the EQ neutron emission. As shown in sec. 3-1-b, the high energy proton emissions leave the residual nucleus at the low excitation region with a small exciton number. In these nuclei, more particle emissions are not feasible, so the residual nucleus transit rapidly to the EQ phase where additional de-excitation proceeds by emitting the evaporative neutrons and γ-rays. On the other hand, the low energy part corresponds to the PEQ neutron emission. These protons are considered to be secondly emitted after the more energetic neutron emission at the first doorway state.

The forward proton spectra for the (α, p 2n γ) and (α, p 3n γ) reactions seem to have even two peaks, namely the high energy narrow peak and the medium energy broad peak. The high energy peaks in these reactions leave the residual nuclei at low excitation energy (< 50 MeV) where the EQ process becomes to be dominant. For the higher excitation energy (> 50 MeV) of the residual nucleus after the proton emission, the PEQ process is important as same as the first doorway state. Thus, the medium energy broad peak may correspond to the PEQ emission of neutrons. These double peaking charactor in both (α, p 2n) and (α, p 3n) reactions indicate the phase transition between the PEQ and the EQ phases.

C. Neutron energy spectra following the $^{158}Gd(\alpha, xn\ \gamma)^{162-x}Dy$ reaction at $E_\alpha = 70$ MeV

i) Procedure of neutron measurement

The energies and angular momenta released by the emitted neutrons were obtained in the present work for each specified exit channel from neutron TOF spectra and angular distributions. The exit channels were specified by observed discrete γ-ray transitions in a Ge(Li) detector. A check on the γ-ray multiplicities was made from one additional NaI(Tl) detector, which also enabled us to observe triple coincidences between the

Ge(Li), NaI(Tl) and NE213 neutron detectors. Because of the poor statistics in the latter correlations the main conclusions on the physics will be based on the double Ge(Li) - NE213 correlations.

The 70 MeV α-particle beam was obtained from the RCNP AVF cyclotron. The target was self-supporting and isotopically enriched to 99.0 % ^{158}Gd with a thickness of 2.6 mg/cm. A 55 cm Ge detector was placed at D = 9.6 cm from the target at θ = 90° with respect to the beam direction. Low-energy γ-rays were attenuated by a 1 mm brass absorber. A 10.4 cm diameter × 10.4 cm long NaI(Tl) detector was positioned at D = 25 cm and θ = 145°. A lead collimetor and a 3 mm brass absorber were used to flatten as much as possible the response function with a low-energy cut-off at 150 keV. The neutrons were detected by means of a 12.7 cm diameter × 7.6 cm NE213 liquid scintillator. They were separated from γ-rays by means of pulse-shape discrimination. Their energies were obtained from the time-of-flight over a distance of 48 cm. Angular distributions for those neutrons were measured at angles of θ_n = 35°, 70°, 110° and 145°.

ii) Result

The γ-ray spectra obtained in coincidence with neutrons at lab. angle of θ_n = 35 deg. for three energy intervals are

shown in fig. 3-11. It is clearly seen that in coincidence with low energy neutrons enhances the (α, 6n) exit channel and high energy neutrons the (α, 4n) channel. The neutron energy spectra for the three exit channels measured at four angles are presented in fig. 3-12. As shown in the fig. 3-12, the shape of the neutron spectra depends much on both the exit channel with neutron multiplicity x and the angles of observation. The low energy neutron may be due to the EQ process which shows on the neutron spectrum a characteristic evaporation pattern. Such shape is dominantly seen in the reaction channel with large neutron multiplicity. On the other hand the high energy ones may be due to the PEQ process, being dominant in the reaction channel with small neutron multiplicity. These results indicate that the fast neutron emissions at the PEQ stage of the de-excitation process also gets important in the 70 MeV α-particle induced reaction.

IV. ANALYSES

4-1. A De-excitation Model

A. A general consideration

Present calculations were designed to describe multi-particle emission processes of highly excited nuclei ($\sim$ 100 MeV). Based on the exciton model[15, 71-73], we employ the decay rates for particle emission and exciton-exciton interaction reported in previous works[74-76]. The Monte Carlo method, which was developed for the calculation of the nuclear evaporation process by Dostrovsky et al.[77], was used to evaluate complex reaction processes. Gadioli et al. applied the Monte Carlo method for the exciton model calculation of the PEQ - EQ de-excitation process.[78]

In the frame work of the exciton model, the de-excitation process can be described by the Pauli master-equation which is given by[15]

$$\frac{d}{dt}P_n(t) = \sum_m [P_m(t)W_{m\to n} - W_{n\to m}P_n(t)], \qquad (4\text{-}1)$$

where the $P_m(t)$ is the occupation probability of the m-exciton state (m is the sum of the excited particles and holes) at time t, the $W_{m\to n} = W_{n\to m}$ is a mean value of the square of the

transition matrix element. The master equation (4-1) describes a gain and a loss of occupation probabilities. It can be solved by a diagonalization of the kernel with following initial condition as

$$P_m(0) = \delta_{m\,m_0}. \tag{4-2}$$

We require the condition that the solutions of eq. (4-1) has to approach finally to the equilibrium values;

$$\lim_{t\to\infty} P_m(t) = P_m(\infty) = \frac{\rho_m}{\sum\limits_{\substack{m=m_0 \\ \Delta m=2}}^{2n} \rho_m}, \tag{4-3}$$

where level density ρ_m is given in Appendix. The mean number of the exciton is given as $\bar{n} = \sqrt{2gE^*}$[15], where g is the single particle level density. The differential cross section of the particle b for the reaction is given by

$$\frac{d\sigma^b}{d\varepsilon} = \alpha \sum_{\substack{m=m_0 \\ \Delta m=2}}^{2\bar{n}} W_m^b(\varepsilon) \int_0^{T_{eq}} P_m(t')dt' + \left(\frac{d\sigma^b}{d\varepsilon}\right)_{evaporation}. \tag{4-4}$$

Here, α is proportional to the square of the mean transition matrix element of the residual interaction $|M|^2$, while W_m^b is the average decay rate from the m-exciton state to a channel where the particle b has kinetic energy ε, and T_{eq} is the

equilibration time. The time integration of $P_m(t)$ is interpreted with a physical assumption as a sum of the emission probabilities[15, 27] at the m-exciton state between the time 0 and T_{eq}. Therefore, the integration can be rewritten as

$$\sum_{m}^{2\bar{n}} \int_{0}^{T_{eq}} P_m(t)dt \propto \sum_{\substack{m \\ \Delta m=2}}^{2\bar{n}} \frac{\Gamma_c^m}{\Gamma_c^m+\Gamma_s^m} = \sum_{\substack{m \\ \Delta m=2}}^{2\bar{n}} \tau_m, \tag{4-5}$$

where Γ_c^m and Γ_s^m are the escape and the spreading widths at m-exciton state, respectively. Eq. (4-4) becomes

$$\frac{d\sigma^b}{d\varepsilon} = \bar{\sigma}_b(\varepsilon) \sum_{\substack{m=m_0 \\ \Delta m=2}}^{2\bar{n}} \tau_m W_m^b(\varepsilon) + \left(\frac{d\sigma^b}{d\varepsilon}\right)_{evaporation}, \tag{4-6}$$

where $\bar{\sigma}_b$ is the inverse reaction cross section, and is obtained from the continuum theory[79] as

$$\bar{\sigma}_n(\varepsilon_n) = \lambda R^2 C_n (1 + \beta/\varepsilon_n) A^{\frac{2}{3}}, \tag{4-7-a}$$

where

$$C_n = 0.76 + 2.2\ A^{-\frac{1}{3}}, \tag{4-7-b}$$

and

$$\beta = (2.12A^{-\frac{2}{3}} - 0.05)C_n, \qquad (4\text{-}7\text{-}c)$$

for neutrons. And for charged particle j, as well

$$\bar{\sigma}_j(\varepsilon_j) = (1 + C_m)(1 - k_n V_{cj}/\varepsilon_j)\lambda R^2, \qquad (4\text{-}7\text{-}d)$$

where

$$V_{cj} = \frac{z_j Z}{R + 1.2}. \qquad (4\text{-}7\text{-}e)$$

Here, $R = 1.3A^{\frac{1}{3}}$ is the nuclear radius and V_{cj} the height of the Coulomb barrier, while c_n, β, c_j and k_j are the parameters determined by an empirical table listed in table III.

The escape width Γ_c^m for m-exciton state is defined as

$$\Gamma_c^m = \hbar \sum_m \int_0^{E-B_b} W_m^b(\varepsilon)d\varepsilon, \qquad (4\text{-}8)$$

where B_b is the binding energy and $W_m^b(\varepsilon)d\varepsilon$ is the probability per unit time for the emission of particle b with kinetic energy between ε and $\varepsilon + d\varepsilon$. It is given as

$$W_m^b(\varepsilon)d\varepsilon = \gamma_m^b \bar{\sigma}_b \varepsilon[\rho(i)/\rho(f)]d\varepsilon. \qquad (4\text{-}9)$$

Here, γ_m^b is the function of the spin of the particle b, reduced mass and the exciton number, and $\bar{\sigma}_b$ is the mean

inverse cross section, and $\rho(i)$ and $\rho(f)$ are initial and final state densities, respectively. The spreading width Γ_s^m is defined[73] as

$$\Gamma_s^m = 2\pi \sum_n |M_{mn}|^2 \rho_{m\to n}, \tag{4-10}$$

where M_{mn} is the transition matrix element from n- to m-exciton state. The matrix element M_{mn} vanishes unless $m = n \pm 2$ because of the assumption of a two body interaction, and the $|\overline{M_{mn}}|^2$ can be assumed as $|\overline{M_{mn}}|^2 = |\overline{M_{mn}}|^2 = |\overline{M}|^2$. The $\rho_{m\to n}$ is the effective level density of the n-exciton state which can be reached from a m-exciton state.

In the case of multi-particle emissions at the PEQ phase, eqs. (4-4) and (4-6) should be added term of a secondary, thirdly part and so on. The secondary part is given as

$$\frac{d\sigma^{b''}}{d\varepsilon} = \alpha \sum_{\Delta m=2}^{2\bar{n}} W_m^b \sum_{\substack{m'=m_0 \\ \Delta m'=2}}^{m} W_{m'}^b \int_0^{T_{eq}} p_{m'}(t')dt'$$

$$= \bar{\sigma}^b(\varepsilon) \sum_{\Delta m=2}^{2\bar{n}} W_m^b \sum_{\substack{m'=m_0 \\ \Delta m'=2}}^{m} W_{m'}^b \tau_{m'}. \tag{4-11}$$

The cascading properties of the PEQ - EQ de-excitation was followed by the Monte Carlo method using random numbers instead of the summations in eqs. (4-6) and (4-11). At the

beginning of the calculations, for each particle considered and each set of (p, h) values, the decay rates into the continuum have been numerically evaluated. The values of the maxima and of the integral over the emitted particle energy are calculated and that of integral over the exciton-exciton interaction decay rates are calculated and tabulated.

The extraction of a sequence of random numbers allows to choose one particular next reaction channel, where a possible kinetic energy is determined by the reaction Q-value and the Coulomb barrier for a particle emission, and next state is defined for both the escape and the spreading channel. The calculation end of the PEQ cascade is determined as the exciton number $m \geq \sqrt{2g_A E^*}$. Then the PEQ cascade transitions to the EQ cascade. When the nucleus de-excite to the neutron threshold energy, the calculation is stopped and the next cascade is started.

The detailed formulations of the present multi-step calculation are described by deviding the de-excitation process into the PEQ and the EQ stages.

B. Numerical results

In order to carry out the calculations, quantities like the level density g_A, average two body matrix elements $|\overline{M}|^2$ and so on, must be given numerically. For this porpose,

expressions of the exciton model was employed.[73] In the followings, the expressions are briefly described.

The state density for the m(=p+h)-exciton state is written in terms of the equi-distance Fermi gas model[74] as follows.

$$\rho(E,\ p,\ h) = g_A(g_A E - A_{ph})^{m-1}/p!h!(m-1)!, \qquad (4\text{-}12)$$

where A_{ph} is a correction factor due to the first order Pauli exclusion principle[73], and is given as

$$A_{ph} = (p^2 + h^2 + p - 3h)/4g_A . \qquad (4\text{-}13)$$

The level density g_A in eq. (4-12) is given by the single nuclear value,

$$g_A = \frac{3A}{4\pi^2}, \qquad (4\text{-}14)$$

the g_A in eq. (4-13) is given by $g_A = 6a/\pi^2$, where a is an ordinary level density parameter given as $a = A/a_0$ ($a_0 = 8 \sim 15$).

The effective level densities $\rho_{m\to m+2}$ used for calculating the spreading width are

$$\rho_{m\to m+2} = \frac{g_A}{2(m+1)} (g_A E - C_{p+1\,h+1})^2 \qquad (4\text{-}15)$$

$$\rho_{m\to m-2} = g_A ph(m-2), \tag{4-16}$$

where $C_{ph} = (p^2 + h^2)/2$ is the correction due to the Pauli exclusion principle. The matrix element $|\overline{M}|^2$ is assumed to be independent of m. It is

$$|\overline{M}|^2 \simeq \frac{h}{g_A(g_A E)^2}\,\lambda(E), \tag{4-17}$$

where $\lambda(E)$ is the effective nuclear collision probability in the nucleus. Kikuchi and Kawai[80] were obtained by using a simple Fermi gas model,

$$\lambda(E) = (1.6\times 10^{21} - 6.0\times 10^{18}E)E\ [\mathrm{sec}^{-1}]. \tag{4-18}$$

Some authors[81-83] have used reduced probabilities $\lambda(E)/C$, were $C = 3 \sim 5$. Reduction factor C reproduce experimental data for the PEQ process. Alternatively, one may use a factor K for $|\overline{M}|^2$ as

$$|\overline{M}|^2 = \frac{K}{A^3}\,\frac{1 - 0.375\times 10^{-2}E}{E}, \tag{4-17'}$$

The reduction factor $C = 4.8$[23] corresponds to the value $K = 1450\ \mathrm{MeV}^3$.[27]

First the ratios $\Gamma_c^m/(\Gamma_c^m + \Gamma_s^m)$ are plotted in fig. 4-1 as a function of the excitation energy and the exciton numbers

in the case of $^{166}Er^*$ system. It is seen in the figure that there is a critical energy E_c for the PEQ particle emission around the excitation energy $E^* \simeq 40$ MeV. As the initial excitation energy exceeds $E_c = 40$ MeV, features of the PEQ process get apparent. Therefore a highly excited nucleus with excitation energy of about 100 MeV firstly decay by emitting one or two high energy particles down to about 40 MeV and then the residual cascading nucleus quickly transit from the PEQ phase to the EQ phase. In fig. 4-2, entry lines of each reaction channel to the EQ stage is shown as a function of the excitation energy for the $^{166}Er^*$ system. Where the initial exciton number $(p_0, h_0) = (5, 1)$ was used. The energies of the phase transition seems to be independent of the initial excitation energy.

Fig. 4-3 gives the ratios $f_p = n_p/(n_p + n_e)$ and $f_e = n_e(n_p + n_e)$, where n_p and n_e represent the numbers of neutron emitted at the PEQ and the EQ phases, respectively, as a function of the order of the cascades for the $^{166}Er^*$ system with the initial excitation energy $E^* = 120$ MeV and the initial exciton number $(p_0, h_0) = (5, 1)$. The maximum of the PEQ fraction lyes at the initial cascade, and then the PEQ fraction decays exponentially as successive cascades. After several cascades, the EQ fraction increases rapidly and the de-excitation process reaches the statistical equilibrium.

The calculated neutron spectra following the $^{164}Dy(\alpha, xn\ yp)^{168-x}Er$ reaction with initial excitation energy $E^* = 90$

MeV are presented in figs. 4-4 and 4-5. In fig. 4-4, the total neutron spectrum is decomposed to each reaction channel with neutron multiplicity x ($x = 3 \sim 8$). The neutron spectra with low multiplicity x seem to have three components which are the evaporative low energy part, medium energy broad part and high energy confined peak. It is difficult to reproduce these shapes with simple Maxwellian distributions $E \cdot \exp(-\frac{T}{kT})$, where kT is a quasi-temperature of the nucleus. On the other hand, in fig. 4-5, the total neutron spectrum is decomposed to the neutron emitted firstly, secondly and so on. We are able to fit the individual spectrum with the Maxwellian distributions with two quasi-temperatures, namely, the PEQ and the EQ temperatures.

C. Comparison with experiments

Using the procedure just mentioned, the neutron multiplicity distributions and the energy spectra of decay particles were calculated. In order to reproduce the experiments, the initial exciton number (p_0, h_0) and the reduction factor C for the average two body matrix element $|\overline{M}|^2$ (see eqs. (4-17) and (4-17')) were treated as free parameters. The initial exciton number is an important parameter to determine the spectrum shapes. With low energy α-particle incidence ($\gtrsim$ 50 MeV) either a(4-0) or a(5-1) configuration has been used. For

above 50 MeV α-particle induced reactions (5, 1) or (6, 2) configurations give over all fits to the experiments. Note that for proton and deuteron induced reactions give the best fits with (2-1) and (3-1) configurations, respectively.[84] The reduction factor for the average two body transition matrix element determines the relative rates between the particle decays and the state spreadings which determine the PEQ decay fraction. A value of 1.5 gives good fits for the present data.

In figs. 4-6-a ∿ 4-6-c, comparisons between the experimental and calculated neutron multiplicity distributions for the reactions of α-particle incidence upon $^{162,\ 164}$Dy, ^{165}Ho and ^{158}Gd are shown, where dotted lines represent the present calculations. Full lines are the results of Sakai et al.[8] using the two phase analysis. Used initial exciton numbers were $(p_0,\ h_0) = (5,\ 1)$ at $E_\alpha = 50$, 70 and 90 MeV, and $(p_0,\ h_0) = (6,\ 2)$ at $E_\alpha = 120$ MeV. In all cases, the reduction factor $C = 1.5$ for two body matrix element was used. On the whole, the calculations reproduced the experiments. Only in the case of 120 MeV α-incidence, the cross sections with small x are somewhat under estimated. This is presumably the same treatments as lower excitation energy region ($\lesssim$ 90 MeV) are not suitable for these high excitation region. We should consider carefully the contributions from outside of the statistical process as the direct reaction process.

The cross section with neutron emission for each reaction channel is written as follows;

$$\sigma^{n}(x) = [\sigma_{p}^{n}(x) + \sigma_{e}^{n}(x)], \tag{4-19}$$

where $\sigma_{p}^{n}(x)$ and $\sigma_{e}^{n}(x)$ are angle and energy integrated neutron cross sections of the xn reaction channel through the PEQ and the EQ processes, respectively. The respective numbers of the PEQ and the EQ neutrons are given as

$$n_{p}(x) = \sigma_{p}^{n}(x)/\sigma(x), \tag{4-20}$$

and

$$n_{e}(x) = \sigma_{e}^{n}(x)/\sigma(x),$$

where

$$n_{p}(x) + n_{e}(x) = x.$$

A PEQ fraction $f_{p}(x)$ for each reaction channel is defined as

$$f_{p}(x) = \frac{n_{p}(x)}{x} = \frac{\sigma_{p}^{n}(x)}{\sigma^{n}(x)}, \tag{4-21}$$

and the total PEQ fraction f_{p} is

$$f_p = \frac{\sum_x n_p(x)}{\sum_x [n_p(x) + n_e(x)]}, \qquad (4\text{-}21')$$

where $\sigma^n = x^\sigma(x)$ and $\sigma_p^n = \sigma_p^n(x)$. Estimations for the $f_p(x)$ and f_p were carried out comparing the experiments and the calculations. In fig. 4-7, the $f_p(x)$ is plotted as a function of neutron multiplicity x, and fig. 4-8 the f_p as a function of the initial excitation energy.

Only the experimental angle-integrated energy spectra were compared with the calculation, because the exciton model which does not contain the angular momentum informations has been developed and is reasonably successful in predicting angle-integrated particle energy spectra. Figs. 3-6 and 4-9 show the comparisons between the exciton model and Maxwellian distributions, and the angle integrated neutron and proton spectrum following the ^{165}Ho(α, xn yp) reaction at $E_\alpha = 109$ MeV. Full lines represent the exciton model. The experimental neutron spectrum does not reflect the first stage contribution because of the lack of higher energy component. (> 30 MeV). However the PEQ contributions which are not able to be represented with Maxwellian distributions (dotted lines) of the neutron spectrum are reasonably reproduced. The calculated proton spectrum which is consisted of almost the PEQ fraction because of the Coulomb barrier suppression is slightly over-estimated in the medium energy region (∿ 30 MeV). The first and the

second stage contributions may be small in the calculation. The larger reduction factor C = 2.0 gives better result.

Angle integrated neutron spectra following the $^{158}Gd(\alpha, xn)$ at $E_\alpha = 70$ MeV for each reaction channel ($x = 4 \sim 6$) are shown in fig. 4-10. The same parameters used in the calculation of the neutron-multiplicity distribution presented in fig. 4-6-b were employed. The calculations give good fits for neutron spectra of the (α, 6n) and the (α, 4n) reaction channels. In the (α, 5n) channel the calculation slightly over-estimate for the PEQ emission. However, in order to check the prediction, higher energy neutrons ($\gtrsim$ 15 MeV) should be observed. In this case, the Maxwellian distributions with quasi-temperatures of the PEQ and the EQ stage, $kT_e = 1.0$ MeV and $kT_p = 6.0$ MeV, $kT_e = 1.0$ MeV and $kT_p = 4.0$ MeV, and $kT_e = 0.9$ MeV and $kT_p = 2.2$ MeV for 6n, 5n and 4n reaction channel, respectively.

4-2. Two Phase Analysis

In order to obtain an essence of the PEQ - EQ de-excitation process, a simple two phase model accoring to ref. 3 is employed for an analysis of the average neutron energies, angular momenta emitted and neutron multiplicity distributions. An analytical formula is used to represent the energy spectra of the i - th emitted nucleon;

$$f_i(E_i) = CE_i \exp(-E_i/kT_i). \qquad (4\text{-}22)$$

This reproduces well the observed data and is also in accord with calculations based on the exciton model[85] and the model described in sec. 4-1.

The observed spectrum is decomposed into two components, thus a fit is performed in which two parameters T_i, are obtained, one for neutrons emitted at equilibrium state with $E_n^p = 2kT_p$ and another for those emitted at an equilibrium stage $E_n^e = 2kT_e$. Here the kT_e is the nuclear temperature at the equilibrium phase, and kT_p may be called the quasi-temperature for convenience at the PEQ phase, although the temperature can not be defined at the PEQ stage.

The results of such fittings for the neutron spectra with the corresponding temperature kT_i for the two components are indicated in fig. 3-5 following the ^{165}Ho + 110 MeV α-particle reaction at $\theta_n = 20.3$ and 140 deg.

The neutron spectra for the ^{158}Gd(α, xn) reactions at $E_\alpha = 70$ MeV at the four angles (25, 40, 110 and 140 deg.) were fitted to correct for angular distribution effects. The average numbers of neutrons <n> emitted in the PEQ and the EQ stages are presented in table VI. The average quasi-temperatures of the two stages are expressed in terms of the average kinetic energies $\langle E_n \rangle$ which are also given in table VI. These data allow us to check the energy conservation in the reaction

which is expressed in the values for the incoming and outgoing energies E_{in} and E_{out}, respectively. For this we obtained the total γ-ray energy release E_γ from the average excitation energy of the entry state given in ref. 40. The reported average γ-ray multiplicities agreed within the experimental errors with those obtained from Ge-NaI coincidences. They vary between 10 and 12 for all exit channels including the discrete transitions.

The angular distributions, which should contain information on the angular momenta released by the neutrons, are given in fig. 4-11. The EQ process gives the neutrons distributed symmetric with respect to 90 deg. in the Center of Mass system. Since the asymmetry through the transformation to the lab. system is only a couple of per cent, one would expect almost symmetric distribution in the laboratory system for equilibrium neutrons. However, all exit channels show pronounced forward peaking which is a clear indication of the occurance of PEQ neutron emission even in the (α, 6n) channel. The asymmetry of the angular distribution can be experssed by the A_i coefficient of the Legendre polynomial expansions $\Sigma_i A_i P_i(\cos\theta_n)$. The results of such expansions are also given in fig. 4-11, and yield for (α, 4n), (α, 5n) and (α, 6n) exit channels the asymmetry coefficients $A_i = 0.34 \pm 0.08$, 0.17 ± 0.07 and 0.09 ± 0.04, respectively. The angular momentum removed by the PEQ emitted neutrons can be estimated[8] as;

$$\ell_n^p = 2/9\, n^p A_i^p \bar{p} R/h, \qquad (4\text{-}23)$$

where R is the nuclear radius (calculated with $r_0 = 1.35$ fm). $\bar{p}$ is the average momentum and A_i^p the expansion coefficient for the PEQ neutrons. This coefficient is related to the observed one by $A_i = n^p A_i^p / x$ with x being the total number of the emitted neutrons. Here, we assumed only the PEQ neutron contribution to be asymmetry. $\bar{p}$ is obtained form $\langle E_n^p \rangle$ given in table VI. The angular momentum released by neutrons emitted in the EQ phase is estimated on the basis of a spin dependent level density calculation.[2] The final results and angular momentum balance are presented in table V.

V. DISCUSSIONS

5-1. Energy and Angular Momentum Balance of the PEQ-EQ Process

The energy balance of the fusion like (particle, xn γ) reactions is discussed by using the average neutron energies $\langle E_n \rangle$. They are obtained from the neutron multiplicity distributions using following eqs.

$$\langle E_n(x) \rangle = (E^* - E_\gamma)/x - \langle B_n \rangle \qquad (5\text{-}1)$$

and

$$E_n = \frac{\sum_x \sigma(x)\{(E^* - E_\gamma)/x - \langle B_n \rangle}{\sum_x \sigma(x)}, \qquad (5\text{-}2)$$

where E^* is the excitation energy, $\langle B_n \rangle$ is the average value of the neutron binding energy, E_γ is the energy removed by γ-rays, and the $\sigma(x)$ is the cross section of the xn reaction channel. The values of $\langle E_n \rangle$ which were deduced from the present (α, xn γ) reactions at E_γ = 50, 70, 90 and 120 MeV as a function of $(E^* - E_\gamma)$ are shown in fig. 5-1-a, where open circles represent the (α, xn γ) reactions. An example of the quantitative energy balance decomposed to the E_n^p, E_n^e and E_γ for ^{158}Gd(α, xn γ) reaction at E_α = 70 MeV is shown in fig. 5-2. The E_n^p and E_n^e were obtained from the present $\langle E_n \rangle$, $\langle E_n(x) \rangle$ and f_p values as

$$\langle E_n(x) \rangle = E_n^p(x) \cdot f_p(x) + E_n^e(x) \cdot f_e(x), \qquad (5\text{-}3)$$

where

$$E_n^e(x) \simeq \frac{4}{3} \sqrt{(E^* - E)/a}$$
$$= 2kT_e \qquad (5\text{-}4)$$

where kT_e is the nuclear temperature of the EQ phase and a is the ordinary level density parameter. The E_γ, which is the energy removed by γ-rays, was estimated by several investigators [3,37-40]. As shown in figs. 4-1 and 4-2, there are critical energy E_c of the PEQ de-excitation process for each reaction channel. The E_c values of small x channels are lower than those of large x channels. A high energy neutron emission at the first doorway state leaves a lower excited nucleus with a small number of excitons. The residual excited nucleus rapidly reaches to the PEQ limit ($m \geq 2\sqrt{2gE^*}$) after emission of a few fast neutrons.
(≃10 MeV) neutron emission occurs at the first doorway, a relatively highly excited nucleus may be left with a small exciton number as well as initial exciton number. Until the nucleus reaches to the PEQ limit, several neutron emissions can be allowed. The latter process should need more complex decay process and larger time than the former.

The angular momentum of these reactions can also be decomposed to three parts as $\ell = \ell_n^p + \ell_n^e + \ell_\gamma$, where ℓ_n^p and ℓ_n^e are the angular momenta removed by the PEQ and EQ neutrons, respectively, and ℓ_γ by the γ-rays. Previously M. J. A. de Voigt et al[40] obtained the ℓ_γ of each reaction from a γ-γ coincidence measurement for the ^{158}Gd(α, xn γ) $^{162-x}$Dy reaction at E_α = 70 MeV. They have deduced energy-spin entry lines for quasi-continuum γ-ray cascade of the (α, 4n) and (α, 6n) reaction channels. In the present n-γ

coincidence work, angular momenta carried away by the PEQ and the EQ neutrons were evaluated for the same reaction. These values, listed in table V, does show quantitatively an important role of the PEQ neutrons for the angular momentum changes. The obtained values ℓ_n^p/neutron increase with decreasing the neutron multiplicity. They are 1.2, 1.0 and 0.6 $\hbar$. As these values are propotional to $\sqrt{\overline{E}_n^x} \propto \overline{p}_n^x$, where $\overline{E}_n^x$ and $\overline{p}_n^x$ are mean values of decay the neutron energy and momentum for each exit channel, respectively, the PEQ neutrons may be emitted at a rocated region of the nucleus, namely nuclear surface. Angular momenta ℓ_n^e/neutron are 0.4∿0.5 $\hbar$ for all exit channels. The neutrons from the equilibriated nucleus are mostly s and p waves. Thus, a schematical angular momentum balances, in consistent with the energy balances of the PEQ-EQ process, can be illustrated as fig. 5-2 for each exit channel.

The comparisons of the $\langle E_n \rangle$ between present light ion results and (H.I., xn γ) reactions whose energy/nucleon are generally smaller (≃15 MeV/nucleon). is quite interesting The compound nucleus ^{170}Yb excited by ^{12}C ions to an energy of 132 MeV (11 MeV/nucleon) was reported to de-excite first by 0.6 and 1.8 fast neutrons in the 8n and 10n exit channels[87], respectively. The average neutron kinetic energies $\langle E_n \rangle$ for ^{12}C induced reaction is considerably higher and the fraction of fast neutrons emitted at the PEQ phase is about a factor of two lower than that of proton

or α-particle induced reactions. However, one has to realize that in (H.I., xn) reactions with $E_{H.I.} \simeq 10$ MeV/ nucleon angular momentum limitations play an important role. Particularly for the reactions of angular momenta greater than than a critical value, imcomplete fusion processes remove significant amounts of the excitation energy and angular momentum which has also been observed through the measurements of emitted charged fragments.[87-89)]

The average values $\langle E_n(x) \rangle$ of neutrons for (p, xn)[8)], (α, xn), (^{12}C, xn)[42,87)], (^{14}N, xn)[42)] and (^{20}Ne, xn)[42,87)] reactions are shown in figs. 5-1-a and -b, where the average neutron energies are plotted as functions of E^* and $(E^*-30)/A_i^{1/3}$ The experimental values, however, increase much more than the $2kT_e$ with increasing the excitation energy. The $\langle E_n \rangle$ is expressed phenomenologically as $\langle E_n \rangle_{exp} \simeq (1.8 + 0.1(E^* - 30)/ A_i^{1/3}$ MeV, where A_i is the projectile mass. The number of the PEQ neutrons increases with the increasing projectile energy and with the decreasing projectile mass. This is because the escape width increases as the excitation energy with excitons introduced at the first stage of the doorway increases, and heavy ion introduced reactions whose initial exciton number are much larger than light ion induced reactions should rapidly reach to the PEQ limit. Note that the dependence on the projectile mass as well as initial exciton number is really characteristic of the PEQ process.

5-2. Decay Particle Spectra

Neutrons follwing the (α, p xn) reactions also classified into the PEQ and the EQ process. Fig. 5-4 shows the angle integrated neutron spectra following the ^{165}Ho(α, p xn) reaction at E_α = 109 MeV. These spectra were obtaind in coincidence with protons detected at a lab. angle θ_p = 30 deg. The neutron spectra gated by three proton energy intervals are well reproduced by both the two phase approximations and the exciton model for malti-particle emission process calculations. As shown in fig. 3-8, the angular dependence of the average neutron energy $\langle E_n \rangle$ in coincidence with high energy protons (E_p>50 MeV) is nearly constant value ($\langle E_n \rangle$ = 2.5∿3.0 MeV) which is expected from the statistical model. Thus, these protons should be emitted at the first PEQ stage with large kinetic energies. The residual nuclei after these emissions decay to the PEQ limit without more particle emissions at the PEQ stage. On the other hand, the $\langle E_n \rangle$ with lower energy protons ($E_p \leq$ 50 MeV) indicate foward peakings which are characteristic feature of the PEQ process. The some neutron fractions should be emitted at the PEQ stage after the forward proton emission.

Proton energy spectra for given neutron multiplicity x for the (α, p xn γ) reaction are presented in figs.3-10-a and 3-10-b. The present exciton model calculations for angle integrated proton spectra of each reaction channel are

shown in fig. 5-5. The conspicuous two peak charactors of the spectrum shape can be reproduced. According to the calculation, the protons which compose the high energy peak are first emitted at the PEQ stage but the medium energy protons are not emitted only at the first stage but also at the second stage after one or two neutron emissions. On the other hand, the identification of the reaction channel (α, p 4n γ) defines the energy sum $E_p + \Sigma E_n \simeq 70$ MeV. Thus the high energy peak at $E_p \simeq 50$ MeV corresponds to the low energy EQ neutrons and the broad peak at $E_p \simeq 30$ MeV corresponds to the PEQ neutrons. The average neutron energy $\langle E_n \rangle$ for given proton energy, namely for given excitation energy at the high energy proton gate, decreases as proton angle increases. Finally they approach to the EQ value of $2kT_e$ (fig. 3-5). The dependence of the proton angle of the (α, p xn) reaction is characteristic of the PEQ process. This feature can quantitively be explained by the number of exciton particles at the PEQ stage. The protons emitted at larger angles leaves more exciton particles than at smaller angles. The average number of exciton particles after a proton emission is plotted in fig. 5-6 by reffering to the relation between $\langle E_n \rangle$ and the projectile mass.

5-3. Calculation of the Exciton Model for Multi-particle Emission process

The exciton model has been considered the first stage distributions of the de-exciting particles. This approach can be applied only to the low initial excitation region ($\leq$40 MeV), where less than one PEQ decay is possible. In order to apply the exciton model to more energetic reactions, multi-particle emissions should be considered. The multi-step calculation of the exciton model improved the medium and low energy parts of the decay particle spectra.

The two body matrix element, which is obtained by analyzing the experimental data by use of the present model, has a week energy dependence up to energies of $\sim$100 MeV, and is smaller than the value expected on the basis of calculations based on the Fermi gas model and the use of free nucleon-nuleon cross sections. We used the reduction factor C = 1.5. This value means that the real nucleus may be more transparent than the nuclear matter. It seems that the PEQ process proceeds in the rather low nucleon density region, namely nuclear surface. In the ordinary exciton models, C = 3$\sim$5 have been used for the reduction factor. These values correspond to the enhancement of the PEQ fraction, which may correct the under-estimation because of the single step calculation at the PEQ stage, and give an over-estimation in the multi-step calculation.

The two phase approximation has reproduced various experimental data. As shown in fig. 4-9, the i-th emitted (i = 1, 2, 3, ·····n) neutron spectra can be approximated with a Maxwellian distribution. However, it is seen that the total PEQ neutrons are not able to be described with one quasi-temperature. These are more lower energy fractions of the PEQ neutrons than the Maxwellian fits. The neutron spectra for individual reaction channel seem to have three energy region in the exciton model calculation. One is a evaporation region. It is completely same pattern as the Maxwellian shape. Second part is medium energy region which has a rather flat pattern and third part has a narrow peaking, especially in the reaction channels with small neutron multiplicities. It is difficult to be described with a simple Maxwellian shape. In these energy regions the two phase approximation may be over-simplification. In order to deduce the essence of the PEQ-EQ process, the two phase model should be treated carefully.

VI. SUMMARY

The PEQ-EQ de-excitation process with α-particle induced reactions in an energy range of E_α= 50∿120 MeV were studied by measuring the detailed γ-rays, and decay protons and neutrons with singles and various coincidence modes. The experimental results were compared with the calculations in terms of an exciton model for multi-particle emission process and a simple two phase approximation. Energy and angular momentum balances of the PEQ-EQ de-excitation process were discussed. The results and the concluding remarks are summarized as follows:

1) Measurements of neutrons in coincidence with charged particles and discrete γ-rays are shown to be very useful for studying the PEQ-EQ de-excitation process in the (particle, xn yp γ) reactions.

2) Experimental evidences of the PEQ process are found in the reaction channel with small neutron multiplicity x, and the average neutron energy $\langle E_n \rangle >> 2kT_e$ which is the nuclear temperature of the equilibriated nucleus, fast and slow components of the neutron energy spectra, the finite value of the A_1coefficient of the $P_1(\cos\theta)$ term in the neutron angular distribution, the large angular momenta removed by the fast neutrons, and the good spin alignment of the residual nucleus. These features depend much on the way to excite the PEQ phase, namely

on both the reaction type and the projectile.

3) The proton energy spectra of each reaction channel were studied with the ^{165}Ho(α, p xn γ) reaction at E_α = 109 MeV. We found that the proton spectra with small number of neutron multiplicities (x = 2∿5) seem to have double peaks, namely high energy narrow, and medium and low energy broad peaks. The high energy peak corresponds to the energetic proton emission at the first stage of the PEQ process being followed by evaporation of the several neutrons. The medium and low energy broad peak corresponds to the case where the fast proton as well as some fast neutrons are emitted at the PEQ stage. Some neutrons may evaporate after these fast particles. We can conclude that the first stage emissions of the PEQ particles determine the successive cascade process and the final exit channel.

4) The exciton model calculation for multi-particle emission process was applied for the present analysis. The neutron multiplicity distributions and the energy spectra of decay particles were well reproduced with the initial exciton numbers of (5, 1) for the incident α-particle energies of E_α = 50, 70, and 90 MeV, and with (6, 2) for E_α = 120 MeV. Comparing the experimental results with the calculations, The PEQ fractions and the entry lines to the EQ stage were deduced. The PEQ fractions

and entry lines to the EQ stages are roughly constant for various reaction channels in a wide range of the initial excitation energy.

5) Effective collision probabilities in the excited nuclei were estimated from the comparisons between the various experiments and the present exciton model calculations. They agree with the expection of another model and calculations for the first doorway state, and smaller than the estimation for the nuclear matter.

6) The simple two phase approximation is considered to be a good approximation to describe characteristic features of the PEQ-EQ de-excitation process. However, it is difficult to reproduce the whole of the decay particle spectra, especially high energy part (> 40 MeV) which contributes little to the total cross sections.

7) Properties of the PEQ process can be well studied by observing the multiplicities of decay neutrons, the proton and neutron energy and angular distributions, and γ-rays. The PEQ phase is characterized by the excitation energy and the exciton particles. The number of exciton particles at the first doorway state depends on the projectile mass for the (particle, xn yp γ) reaction, and on the detection angles of the PEQ particles.

8) In the present energy resion, it is not nessesary to seriously consider the effect of the angular momentum transfers in order to estimate the energy balance of the α-particle induced reactions. In the case of the H. I. induced reactions the angular momentum transfers are much larger than the α-particle incidences. It is considered that the effects of the angular momenta to the PEQ de-excitation may be clearly investigated with the H. I. induced reactions.

Acknowledgement

The author would like to acknowledge the continuing guidance and warm encouradgement of Professor H. Ejiri during the course of this work. The author is much indebted to Drs. K. Okada, H. Sakai and T. Shibata for valuable discussions and criticism. The author is also indebted to Prof. A. Shimizu, Drs. M. Sasao and T. Motobayashi for their excellent collaborations and valuable discussions. The author would like acknowledge the excellent ideas and discussions of Prof. M. J. A. de Voigt. Many thanks are also due to Drs. Y. Nagai and S. Nakayama, and Messrs. T. Kishimoto, H. Suzuki, Y. Masakawa and staffs of the OULNS and the RCNP for kind help and discussions.

APPENDIX

Multi-step Calculation for De-excitation Process

In order to carry out the calculation of the de-excitation process at the PEQ and EQ stages, decay rates for various competing processes have to be determined. An exciton model and a statistical model were employed for the calculation for the PEQ and the EQ stages, respectively.

A. Pre-equilibrium decay

In the case of the PEQ decay process, a concrete expression of an escape probability W_m^b for a particle b which is decaying from m-exciton state, has to be required to calculate an escape width. Applying the exciton model, eq. (4-9) becomes

$$W_m^b = \frac{2s_b+1}{\pi^2\hbar^3}\,\mu_b\varepsilon\bar{\sigma}R_b(p,h)p_b!\,\frac{\rho(E-\varepsilon-B_b,p-p_b,h)}{\rho(E,p,h)}\,, \qquad \text{(A-1)}$$

where subscript b denotes the escaping particle with spin s_b, reduced mass μ_b, and binding energy B_b obtained from the Mayer and Swiatesky mass formula,[92] and $\rho(E, p, h)$ and $\rho(E-\varepsilon-B_b, p-p_b, h)$ are the initial and the final level densities with the exciton numbers $m(=p+h)$ and $m-p_b(=(p-p_b)+h)$, respectively, in which p_b is the number of the out-going particles. The extra two factors of $R_b(p, h)$ and $p_b!$ are empirical adjustment parameters being incorporated into the model in order to obtain reasonable values of complex particle emission rates.

The function $R_b(p, h)$ gives a formation probability of a complex particle which consists of p_b nucleons. A right combination of protons and neutrons to form the out-going particle was taken into account for $R_b(p, h)$. The latter additional factor $p_b!$ is an empirical variable introduced by C. K. Cline.[71] However, it can not be derived from a microscopic reversibility.[72,73] This factor causes too many high energy particles, especially for α-particles.[71,72] We introduced a factor G_b instead of $p_b!$. The factor of G_b should describe internal structure effects of the out-going particle. In the case of a structureless particle such as a proton or a neutron, G_b should be unity. In the present calculation, G_b was treated as a free parameter in order to obtain an analytical expression for the decay probability W_m^b. So, making use of this approximation, eq. (A-1) becomes

$$W_m^b = \frac{2s_b+1}{\pi^2\hbar^3}\mu_b\varepsilon\bar{\sigma}R_b(p,h)G_b\frac{\rho(E-\varepsilon-B_b,\ p-p_b,\ h)}{\rho(E,p,h)} \qquad (A\text{-}1')$$

The complex particle formation factor $R_b(p, h)$ was given by C. K. Cline.[71] It is expressed as

$$R_b(p,h)=\sum_{i=0}^{p-p_b}\left[\frac{(p-p_a)!}{i!(p-p_a-i)!}\left(\frac{Z}{A}\right)^i\left(\frac{N}{A}\right)^{p-p_a-i}\right]\left[\frac{(\pi_a+i)!}{\pi_b!(\pi_a+i-\pi_b)!}\right. \qquad (A\text{-}2)$$

$$\left.\times\frac{(p-p_a-i)!}{\nu_b!(p-\pi_a-i-\nu_b)!}\right]\Big/\frac{p!}{p_b!(p-p_b)!}\ ,$$

where π and ν are numbers of protons and neutrons, respectively, and p is the number of nucleons ($=\pi+\nu$). Subscripts a and b denote the projectile and the ejectile, respectively. We can get the expression of $R_b(p, h)$ for protons, neutrons, deuterons and α-particles:

$$R_p(p,h)=(\frac{N}{A})^{p-p_a}\frac{\pi_a}{p}+\sum_{i=1}^{p-p_a}W_i(p_a)\frac{\pi_a+i}{p}, \tag{A-3}$$

$$R_n(p,h)=(\frac{N}{A})^{p-p_a}\frac{p-\pi_a}{p}+\sum_{i=1}^{p-p_a}W_i(p_a)\frac{p-\pi_a-i}{p}, \tag{A-4}$$

$$R_d(p,h)=2(\frac{N}{A})^{p-p_a}\frac{\pi_a(p-\pi_a)}{p(p-1)}+\sum_{i=1}^{p-p_a}2W_i(p_a)\frac{(\pi_a+i)(p-\pi_a-i)}{p(p-1)} \tag{A-5}$$

and

$$R_\alpha(p,h)=6(\frac{N}{A})^{p-p_a}\frac{\pi_a(\pi_a-1)(p-\pi_a)(p-\pi_a-1)}{p(p-1)(p-2)(p-3)}+\sum_{i=1}^{p-p_a}[6W_i(p_a)$$

$$\times\frac{(\pi_a+i)(\pi_a+i-1)(p-\pi_a-i)(p-\pi_a-i-1)}{p(p-1)(p-2)(p-3)}], \tag{A-6}$$

where

$$W_i(p_a)=\frac{(p-p_a)!}{i!(p-p_a-i)!}(\frac{Z}{A})^i(\frac{N}{A})^{p-p_a-i}. \tag{A-7}$$

An equi-distance Fermi gas model was employed for the calculation of state densities. For the m(=p+h) exciton state, the state density is given in eq. (4-12). Using these expressions, concrete forms of the escape probabilities per unit time and unit energy can be given for protons, neutrons, deuterons and α-particles as

$$W_m^p = \frac{2M_p R^2}{\pi\hbar^3} R_p(p,h)\left(\frac{A-1}{A}\right)^{m-1} \frac{p(m-1)}{g_A} (\varepsilon - V_{cp}) \times \frac{(E-B_p-V_{cp}-A_{p-1\ h}-(\varepsilon-V_{cp}))^{m-2}}{(E-A_{ph})^{m-1}}, \quad \text{(A-8)}$$

$$W_m^n = \frac{2M_n R^2}{\pi\hbar^3} R_n(p,h)\left(\frac{A-1}{A}\right)^{m-1} \frac{p(m-1)}{g_A} \varepsilon \frac{(E-B_n-A_{p-1\ h}-\varepsilon)^{m-2}}{(E-A_{ph})^{m-1}}, \quad \text{(A-9)}$$

$$W_m^d = \frac{3M_d R^2}{\pi\hbar^3} R_d(p,h)\left(\frac{A-1}{A}\right)^{m-2} \frac{p(p-1)(m-1)(m-2)}{g_A^2} (\varepsilon - V_{cd}) \times \frac{(E-B_d-V_{cd}-A_{p-2\ h}-(\varepsilon-V_{cd}))^{m-3}}{(E-A_{ph})^{m-1}} \quad \text{(A-10)}$$

and

$$W_m^\alpha = \frac{M_\alpha R^2}{\pi\hbar^3} R_\alpha(p,h)\left(\frac{A-1}{A}\right)^{m-4} \frac{p(p-1)(p-2)(p-3)(m-1)(m-2)(m-3)(m-4)}{g_A} \times (\varepsilon - V_{c\alpha}) \frac{(E-B_\alpha-V_{c\alpha}-A_{p-4\ h}-(\varepsilon-V_{c\alpha}))^{m-5}}{(E-A_{ph})^{m-1}}. \quad \text{(A-11)}$$

In order to simplify the calculation, using normalized escape probabilities $W_m^{a'}$ were used. They are defined as $W_m^{a'}$ max = 1.0. Using this definition, eqs. (A-8)~(A-11) are rewritten as

$$W_m^{p'} = \frac{(m-1)^{m-1}}{(m-2)^{m-2}} (\varepsilon - V_{cp}) \frac{(E-B_p-A_{p-1\ h}-V_{cp}-(\varepsilon-V_{cp}))^{m-2}}{(E-B_p-A_{p-1\ h}-V_{cp})^{m-1}}, \quad \text{(A-8')}$$

$$W_m^{n'} = \frac{(m-1)^{m-1}}{(m-2)^{m-2}} \varepsilon \frac{(E-B_n-A_{p-1\ h}-\varepsilon)^{m-2}}{(E-B_n-A_{p-1\ h})^{m-1}}, \quad \text{(A-9')}$$

$$W_m^{d'} = \frac{(m-2)^{m-2}}{(m-3)^{m-3}} (\varepsilon - V_{cd}) \frac{(E-B_d-A_{p-2\ h}-V_{cd}-(\varepsilon-V_{cd}))^{m-3}}{(E-B_d-A_{p-2\ h}-V_{cd})^{m-2}} \qquad \text{(A-10')}$$

and

$$W_m^{\alpha'} = \frac{(m-4)^{m-4}}{(m-5)^{m-5}} (\varepsilon - V_c) \frac{(E-B_\alpha-A_{p-4\ h}-V_{c\alpha}-(\varepsilon-V_{c\alpha}))^{m-5}}{(E-B_\alpha-A_{p-4\ h}-V_{c\alpha})^{m-4}} , \qquad \text{(A-11')}$$

respectively.

Following the general definition of the escape width given by eq. (4-8), integrations of eqs. (A-9)~(A-11) gives the total escape widths for protons, neutrons, deuterons and α-particles, respectively. The integrations can be carried out analytically to be

$$\Gamma_p = \frac{M_p R^2}{\pi \hbar^2} R_p(p,h) \frac{E-A_{ph}}{g_A} \left(\frac{A-1}{A}\right) \frac{p}{m} \left(\frac{E-B_p-V_{cp}-A_{p-1\ h}}{E-A_{ph}}\right)^m , \qquad \text{(A-12)}$$

$$\Gamma_p = \frac{M_n R^2}{\pi \hbar^2} R_n(p,h) \frac{E-A_{ph}}{g_A} \left(\frac{A-1}{A}\right)^{m-1} \frac{p}{m} \left(\frac{E-B_n-A_{p-1\ h}}{E-A_{ph}}\right)^m , \qquad \text{(A-13)}$$

$$\Gamma_d = \frac{3M_d R^2}{\pi \hbar^2} R_d(p,h) \frac{p(p-1)}{g_A} \left(\frac{A-1}{A}\right)^{m-2} \left(\frac{E-B_d-A_{p-2\ h}}{E-A_{ph}}\right)^{m-2} \qquad \text{(A-14)}$$

and

$$\Gamma_\alpha = \frac{M_\alpha R^2}{2\pi \hbar^2} R_\alpha(p,h) \frac{p(p-1)(p-2)(p-3)(m-1)(m-2)}{g_A^4 (E-A_{ph})^2}$$

$$\times \left(\frac{E-B_\alpha-V_{c\alpha}-A_{p-4\ h}}{E-A_{ph}}\right)^{m-3} \qquad \text{(A-15)}$$

In the exciton model, the de-excitation proceeds through exciton-exciton scatterings. Only when a change of the exciton

number occurs, the excited state spreads to the next continuum state. In this process, each intermediate state may be formed by the creation of a particle-hole pair ($\Delta p = \Delta h = +1$) or the annihilation of it ($\Delta p = \Delta h = -1$). Transition rates given in eq. (4-10) of the spreading process can be estimated, based on a first order time dependent perturbation theory.[75,76] The respective spreading widths of Γ_+ ($\Delta p = \Delta h = +1$) and Γ_- ($\Delta p = \Delta h = -1$) are written as

$$\Gamma_+ (E,p,h) = \pi |M|^2 \frac{g_A}{p+h+1} (g_A E - C_{p+1\ h+1})^2 \qquad (A-16)$$

and

$$\Gamma_-(E,p,h) = \pi |M|^2 g_A\ ph(p+h-2)\ , \qquad (A-17)$$

where $C_{ph} = (p^2+h^2)/2$ is the correction due to the Pauli exclusion principle and $|M|$ which is given in eq. (4-17') is the average two body transition matrix-element. The average two body matrix element $|\overline{M}|^2$ was treated as the only free parameter. We adopted the value of $|\overline{M}|^2$ which reproduce neutron multiplicity distributions.

B. Equilibrium Decay

In the present calculation the de-excitation process of the EQ stage was followed essentially in the same way as the Monte Carlo calculation developed by Dostrovsky et al.[77]. In their calculation, eq. (4-9) was given as

$$W^a(\varepsilon)d\varepsilon = \frac{2s_a+1}{\pi^2\hbar^3}\,\mu_a\,\bar{\sigma}\varepsilon\,\frac{\rho(f)}{\rho(i)}\,d\varepsilon\,, \qquad \text{(A-18)}$$

where s_a and μ_a are the spin and the reduced mass of the particle a, respectively, and $\bar{\sigma}$ is the cross section for the inverse reaction, and $\rho(i)$ and $\rho(f)$ are the level densities of the initial and final states with their respective excitation energies. $\bar{\sigma}$ was obtained from eqs. (4-7-a)~(4-7-e). The simplest and most widely used formulation for the level density with the excitation energy E was given by Weisskopff[79] for complete degenerate Fermi gas, and is written as

$$\rho(E) = C \cdot \exp\{2\sqrt{a(E-\delta)}\} \qquad \text{(A-19)}$$

In more refined treatments the factor C should be a function of the excitation energy E. However, in order to get an analytical integration of eq. (A-22), the variation of C with E was neglected. This simplification may cause a small effect to the results because of the dominant exponential term.

The level density parameter a has a slight dependence on the neutron excess as follows for light particles,

$$\begin{aligned} a_p &= a(1+1.3\theta/A)^2, \\ a_n &= a(1-1.3\theta/A)^2, \\ a_d &= a(1-0.5\theta/A)^2 \\ &\text{and} \\ a_\alpha &= a(1-1.5\theta/A)^2, \end{aligned} \qquad \text{(A-20)}$$

where $\theta=(N-Z)/A$, and a is the level density parameter. In eq. (A-19), δ denotes a correction to the level density for an even-odd effect arising from the ground state energy displacement caused by a nucleon pairing.[93] The values of δ can be evaluated from the pairing energies for neutrons and protons.

Using eqs. (A-18)~(A-24), the following equation was obtained for the neutron emissions.

$$W_n(\varepsilon_n) = \frac{2s_n+1}{\pi^2\hbar^3}\mu_n R_0^2 A_n^{2/3}\exp\{-\sqrt{a(E-\delta)}\}\varepsilon_n\left(1+\frac{\beta}{\varepsilon}\right)$$

$$\times \exp\{2\sqrt{a_n(E-Q_n-\delta_n-\varepsilon}\}\, d\varepsilon\ , \qquad \text{(A-21)}$$

where Q_n is the neutron binding energy, and it is assumed that the maximum available energy for the evaporation process is $(\varepsilon_n)max=E-Q_n-\delta_n$. The decay probability of a charged particle j is

$$W_j(\varepsilon_j) = \frac{2s_j+1}{\pi^2\hbar^3}\mu_j R_0^2 A_n^{2/3}\exp\{-2\sqrt{a(E-\delta)}\}\varepsilon_n(1+c_j)(\varepsilon-k_j V_{cj})$$

$$\times \exp\{2\sqrt{a_j(E-Q_j-\delta_j-\varepsilon)}\}d\varepsilon\ . \qquad \text{(A-22)}$$

The escape widths may be obtained by integration of eqs. (A-19) and (A-20). The total neutron escape width is

$$\Gamma_n = \hbar\int_0^{E-Q_n-\delta_n} W_n(\varepsilon_n)d\varepsilon_n\ , \qquad \text{(A-23)}$$

and the total escape width of a charged particle j is

$$\Gamma_j = \hbar \int_{k_j V_{cj}}^{E-Q_j-\delta_j} W_j(\varepsilon_j)d\varepsilon_j \quad . \qquad \text{(A-24)}$$

These integrations yield for neutrons as

$$\Gamma_j = \frac{2s_n+1}{2\pi\hbar^2}\mu_n\gamma_a^2 A^{\frac{2}{3}}\frac{\alpha}{a_n^2}\exp\{-2\sqrt{a_a(E-\delta_a)}\}$$

$$\times \{a_nR_n[2\exp\{2\sqrt{a_nR_n}\}+1]-(3-2a_n\beta)$$

$$\times (a_n\beta)^{-\frac{3}{2}}\exp\{2\sqrt{a_nR_n}\}-\tfrac{1}{2}(3-2a_n\beta)[1-\exp\{2\sqrt{a_nR_n}\}]\} \ , \qquad \text{(A-23')}$$

and for charged particles as

$$\Gamma_j = \frac{2s_j+1}{2\pi\hbar^2}\mu_j\gamma_0^2 A_j^{\frac{2}{3}}\frac{(1+C_j)}{a_j^2}\exp\{-2\sqrt{a_0(E-\delta_0)}\}$$

$$\times \{a_jR_j[2\exp\{2\sqrt{a_jR_j}\}+1]-3\sqrt{a_jR_j}$$

$$\times \exp\{2\sqrt{a_jR_j}\}-\frac{3}{2}[1-\exp\{2\sqrt{a_jR_j}\}]\} \qquad \text{(A-24')}$$

with

$$R_n = E - Q_n - \delta_n \qquad \text{(A-25)}$$

and

$$R_j = E - Q_j - k_jV_{cj} - \delta_j \qquad \text{(A-26)}$$

As R_n and R_j mean the maximum possible values of kinetic energies of emitted neutrons and charged particles, respectively. In our case, exponential terms are always $\exp[2(a_nR_n)^{\frac{1}{2}}]>>1$ and

$\exp[2(a_j R_j)^{\frac{1}{2}}] >> 1$. Therefore, eqs. (A-23') and (A-24') can be simplified as

$$\Gamma_n \simeq \frac{2s_n+1}{2\pi\hbar^2}\,\mu_n\gamma_0^2\,A^{\frac{2}{3}}\exp\{-2\sqrt{a_0(E-\delta_0)}\}$$

$$\times \frac{\alpha}{a_n^2}\exp\{2\sqrt{a_n R_n}\}\{2a_n R_n-(\tfrac{3}{2}-a_n\beta)[2\sqrt{a_n R_n}-1]\}, \qquad \text{(A-23")}$$

and

$$\Gamma_j \simeq \frac{2s_j+1}{2\pi\hbar^2}\,\mu_j\gamma_0^2\,A^{\frac{2}{3}}\exp\{-2\sqrt{a_0(E-\delta_0)}\}$$

$$\times \frac{1+C_j}{a_j^2}\exp\{2\sqrt{2(a_j R_j)}\}\{2a_j R_j-\tfrac{3}{2}[2\sqrt{a_j R_j}-1]\}\ . \qquad \text{(A-24)}$$

It is to be noted that the maximum excitation energy has to be limited so as not to overflow in the calculation because of the positive exponential term to be a very large value for a highly excited nucleus. The schematical procedure of the calculation is shown in fig. A-1.

References

1) H. Feshbach, Rev. Mod. Phys. 46 (1974) 1.

2) H. Ejiri, T. Shibata, T. Itahashi, Y. Nagai, H. Sakai, S. Nakayama, T. Kishimoto, K. Maeda and H. Hoshi, J. Phys. Soc. Japan Suppl., 44 (1978) 655.

3) H. Ejiri, et al., Nucl. Phys. A305 (1978) 167.

4) H. Ejiri, Proc. Int. Workshop on Nuclear Reaction Models of Continuum Spectra of Light ions, Bad-Honnef, West Germany, 1978.

5) G. Roos and N. S. Wall, Phys. Rev. 140 (1965) 1237; ibid. Phys. Rev. 150 (1966) 811.

6) H. Ejiri, Colloque Franco-Japonais on Nucl., Gif sur Yvette, Oct. 1979.

7) J. J. Griffin, Phys. Rev. Lett. 17 (1966) 478.

8) H. Sakai, Thesis, Osaka Univ.

9) M. L. Goldberger, Phys. Rev. 74 (1948) 1289.

10) N. Metropolis et al., Phys. Rev. 110 (1958) 185; ibid., 110 (1958) 204.

11) H. W. Bertini, Phys. Rev. 131 (1963) 1801.

12) K. Chen et al., Phys. Rev. C4 (1971) 2234.

13) A. Mignerey, M. Blann and W. Scobel, Nucl. Phys. A273 (1976) 125.

14) M. Blann, Ann. Rev. Nucl. Science, 25 (1975) 123.

15) D. Agassi, H. A. Weidenmüller and G. Mantzouranis, Phys. Rep. 22 (1975) 145.

16) M. Blann, A. Mignerey and W. Scobel, Nucleonika, 21 (1976) 335.

18) H. Hofman and P. Siemens, Phys. Lett. 58B (1975) 417.

19) W. Nörenberg, Phys. Lett. 58B (1974) 289.

20) W. Nörenberg, Z. Phys. A274 (1975) 241.

21) G. D. Harp, J. M. Miller and B. J. Berne, Phys. Rev. 165 (1968) 1166; ibid. Phys. Rev. C3 (1971) 1847.

22) C. K. Cline and M. Blann, Nucl. Phys. A172 (1971) 225.

23) M. Blann, Phys. Rev. Lett. 27 (1971) 337; ibid. 28 (1972) 757.

24) M. Blann. Lecture Notes in Phys., Vol 22 (Springer Veriag, Berlin 1973).

25) E. Gadioli, E. Gadioli-Erba and P. G. Sona, Nucl. Phys. A217 (1973) 570.

26) M. Machner, Phys. Lett. 86B (1979) 129.

27) G. Mantzouranis, H. A. Weidenmüller and D. Agassi, Z. Phys. A276 (1976) 145.

28) S. Yoshida, Proc. IPCR Symposium, (1977) 359.

29) J. M. Akkermans, Phys. Lett. 82B (1978) 20.

30) M. Blann and A. Mignerey, Nucl. Phys. A186 (1972) 245.

31) P. Mädler and R. Reif, Nucl. Phys. A337 (1980) 445

32) M. Blann, Nukleonika 21 (1975) 335.

33) E. Godioli and E. Godioli Erba, Nucl. Instr. Method 146 (1977) 335.

34) T. Tamura, T. Udagawa, D. H. Feng and K.-K. Kan, Phys. Lett. 66B (1977) 109.

35) T. Tamura and T. Udagawa, Phys. Lett. 71B (1977) 273.

36) H. Sakai et al. to be published.

37) H. Sakai et al., Phys. Rev. C20 (1979) 464.

38) Y. Nakai, T. Shibata, H. Sakai, T. Kishimoto and H. Ejiri, J. Phys. Soc. Japan 46 (1979) 1025.

39) M. Ogawa, P. Kleinheiz, S. Lunakah, O. W. Schult, and M. Fenzl, Z. Phys. A284 (1978) 271.

40) W. J. Ockels, M. J. A. de Voigt and Z. Sujkcuski, Phys. Lett. 48B (1978) 4.
M. A. J. de Voigt, W. J. Ockels, Z. Sujkowski, A. Zglinski and J. Mooibroek, Nucl. Phys., A323 (1979) 317.

41) D. G. Sarantites, L. Westenberg, R. A. Dayras, M. L. Halbert, D. C. Hansley, and J. H. Barker, Phys. Rev. C17 (1978) 601; ibid., C18 (1978) 774.

42) H. Suzuki et al., private communication.

43) H. Ejiri et al., private communication.

44) L. Westenberg, D. G. Sarantites, D. C. Hensley, R. A. Dayras, M. L. Halbert, and J. H. Barker, Phys. Rev. C18 (1978) 796.

45) M. Kondo et al., Proc. 7th Int. Conf. Cycl., 1975.

46) F. M. Lanzafame and M. Blann, Nucl. Phys. A142 (1970) 545.

47) M. Blann and F. M. Lanzafame, Nucl. Phys. A142 (1970) 559.

48) S. A. Hjorth, H. Ryde, K. A. Hargemann, G. Løvhøiden, and J. C. Waddington, Nucl. Phys. A144 (1970) 513.

49) J. Boutet, and J. P. Torres, Nucl. Phys. A175 (1971) 167.

50) R. M. Lieder, H. Beuscher, W. F. Davidson, J. John, J. H. Probst, and C. Mayer-Bröke, Z. Phys. 257 (1972) 147.

51) A. Johnson, H. Ryde and S. A. Hojrth, Nucl. Phys. A179 (1972) 753.

52) E. Grosse, F. S. Stephans and R. M. Diamond, Phys. Rev. Lett. 31 (1973) 840.

53) H. Ryde, S. A. Hjorth, D. Barneoud, A. Johnson, G. B. Hargemann and B. Herskind, Nucl. Phys. A207 (1973) 513.

54) K. Krien, R. A. Naumann, J. O. Rasmussen and I. Rezanka, Nucl. Phys. A209 (1973) 572.

55) W. Andejtscheff, P. Manfrass, H. Prade, K. D. Schilling, G. Winter, H. Fuia, R. Ion-Mihai, A. B. Khalikulov, V. A. Morozov, N. Z. Marupov and T. M. Muminov, Nucl. Phys. A220 (1974) 438.

56) M. V. Banaschik, C. Günter, H. Hübel and A. C. Rester, Nucl. Phys. A222 (1974) 459.

57) W. Andrejtscheff, P. Manfrass, K. D. Schilling and W. Seidel, Nucl. Phys. A225 (1974) 300.

58) R. Broda, M. Ishihara, B. Herskind, H. Deschler, S. Ogaza and H. Ryde, Nucl. Phys. A248 (1976) 356.

59) R. Janssens, Y. El-Masri, J. M. Ferte, C. Michel, J. Steyaert, and J. Vervier, Nucl. Phys. A283 (1977) 493.

60) O. C. Kistner, A. W. Sunyar, and E. der Mateosian, Phys. Rev. C17 (1978) 1417.

61) P. Sperr, H. Spieler, and M. R. Maier, Nucl. Instr. and Meth. 116 (1974) 55.

62) K. Shin, private communication.

63) V. V. Verbinski, J. C. Courtney, and N. Betz, Nucl. Instr. and Meth. 52 (1969) 181.

64) I. Katayama and H. Ogata, PCNP Annual Report 1976 153.

65) R. H. Loveberg, Phys. Rev. 84 (1951) 853.

66) R. Batchelor, W. B. Gilboy, J. B. Parker, and J. H. Towle, Nucl. Instr. and Meth. 13 (1961) 70.

M. Drosg, Nucl. Instr. and Meth. 105 (1972) 573.

67) M. M. Abd-Razaek and J. H. Thorngate, Nucl. Instr. and Meth. 141 (1977) 477.

68) H. W. Bzofk and C. E. Andeson, Rev. of Sient. Instr. 31 (1960) 1063.

69) V. V. Verbinski et al., Nucl. Instr. and Meth. 65 (1968) 8

70) R. A. Wingard et al., Nucl. Instr. and Meth. 95 (1971) 141; ibid, 98 (1972) 525.

71) C. K. Cline, Nucl. Phys., A193 (1972) 417.

72) I. Ribanski and P. Oblozinsky, Phys. Lett., 45B (1973) 318.

73) C. Kalbach, Z. Phys., A283 (1977) 401.

74) T. Ericson, Adv. In Phys., 9 (1960) 425.

75) F. C. Williams Jr., Phys. Lett., 31B (1970) 184.

76) P. Oblozinsky, I. Ribansky and E. Betak, Nucl. Phys. A226 (1974) 347.

77) I. Dostrovsky, Z. Frankel and L. Winsberg, Phys. Rev., 118 (1960) 781; ibid., 116 (1959) 683.

78) E. Gadioli, E. Gadioli Erba and J. J. Hogan, Phys. Rev. C16 (1977) 1404.

79) J. Blatt and V. F. Wiesskopf, Theoretical Nuclear Physics, John Wiley & Sons, Inc., New York, 1952.

80) K. Kikuchi and K. Kawai, Nuclear matter and Nuclear Interaction, North Holland Publishing Co., Amsterdam, 1968.

81) E. Gadioli et al., Phys. Lett. 65B (1976) 311.

82) M. Blann, Phys. Lett., 67B (1977) 145.

83) J. Ginocchio and M. Blann, Phys. Lett. 68B (1977) 405.

84) J. R. Wu, C. C. Chang and H. D. Hogan, Phys. Rev., C19 (1979) 370; ibid., C19 (1979) 659; ibid. C19 (1979) 698.

85) H. Sakai et al., Proc. IPCR Symposium, (1977) 400.

86) D. L. Hills, J. D. Garret, O. Christensen, B. Fernandez, G. B. Hargemann, B. Herskind, B. B. Back and F. Folkmann, to be published.

87) D. G. Sarantites, J. H. Baker, M. L. Halbert, D. C. Hensley, R. A. Dayras, E. Eichler and N. R. Johnson, Phys. Rev. C14 (1976) 2138; ibid., C17 (1978) 774.

88) K. Wilcrinski, E. H. de Marchei van Voorthuysen, J. van Papfa, R. H. Siemssen and J. Wilcrynski, Phys. Rev., Lett. 42 (1979) 1599.

89) T. Inamura, M. Ishihara, T. Fukuda, T. Shimoda and H. Hiruta, Phys. Lett. 68B (1977) 51.

90) C. F. Williamson, S. M. Ferguson, B. J. Shepherd and I. Halpern, Phys. Rev. 174 (1968) 1544.

91) S. Ferguson, H. Ejiri and I. Halpern, Nucl. Phys., A188 (1972) 1; H. Ejiri and I. Halpern, Bull. Amer. Phys. Soc. 13 (1968) 700.

92) W. D. Myers and W. J. Swiatecki, Nucl. Phys. 81 (1966) 1.

93) M. El-Nadi and M. Wafik, Nucl. Phys. 9 (1958) 22

94) P. O. Tjøm et al., Phys. Rev. Lett. 33 (1974) 593; G. B. Hargemann et. al., Nucl. Phys. A245 (1975) 166.

95) E. der Mateosian, O. C. Kistner and A. W. Sunyar, Phys. Rev. Lett. 33 (1975) 99; J. O. Newton et al., Phys. Rev. Lett. 34 (1974) 99.

96) J. O. Newton et al., Phys. Rev. Lett. 38 (1977) 810

Table I

Target	Target Isotopic Enrichmrnt (%)	Thickness (mg/cm^2)	Target Form
^{162}Dy	95.0	4.0	depositing oxide powder onto thin mylar(30 μm)
^{164}Dy	98.4	3.3	depositing oxide powder onto thin mylar(30 μm)
^{165}Ho	100.0	5.48	metallic foil
^{158}Gd	99.0	2.6	metallic foil

Table III

Parameters in the calculation for charged particle inverse cross section.

Z	k_p	c_p	k_α	c_α
10	0.42	0.50	0.58	0.10
20	0.58	0.28	0.82	0.10
30	0.68	0.20	0.91	0.10
50	0.77	0.15	0.97	0.08
$\geq$70	0.80	0.10	0.98	0.06

In the table, p and α mean proton and α-particle,respectively. It turned out that, at all values of Z, $c_d=c_p/2$ and $k_d=k_p+0.06$. Similarly, it is assumed that $c_t=c_p/3$ and $k_t=k_p+0.12$, and that $c_{^3He}=4c_\alpha/3$ and $k_{^3He}=k_\alpha-0.06$, where subscripts d and t denote deutron and triton, respectively.

Table II

Target	Energy of Projectile (MeV)	Initial Compound System	Initial Excitation Energy	Mode of Experiment	Obseved Angle(deg.)
^{162}Dy	120	^{166}Er	116.6	single γ-ray	125(LEPS)
	110		106.8		
	90		87.3		
	70		67.8		
	50		48.3		
^{164}Dy	120	^{168}Er	116.3	single γ-ray	125(LEPS)
	110		106.5		
	90		87.0		
	70		67.8		
	50		48.0		
^{165}Ho	110	^{169}Tm	106.2	single γ-ray	125(LEPS)
				proton-γ coincidence	130(GAMMA-X)
					25,40,125(counter telescope)
				proton-neutron coincidence	30(counter telescope)
					20.3,23.9,33.6,53.8,63.2,69.2
					108.6,139.1,-69.2,-53.8,-20.3
					(NE213)
^{158}Gd	70	^{162}Dy	68.2	neutron-γ coincidence	130(GAMMA-X)
					35,70,110,140(NE213)

Table VI

Energy blance analyzed with two phase approximation in the ^{158}Gd(α, xn) reaction at E_α= 70 MeV.

	$\langle n^e \rangle$	$\langle E_n^e \rangle$	$\langle n^p \rangle$	$\langle E_e^p \rangle$	E_n	E_γ	E_{out} b)	E_{in} c)
α, 4n	2.3	2.0	1.7	12.0	24.3	12.1	36.4	38.3
α, 5n	3.7	2.0	1.3	8.0	17.8	10.0	27.8	29.2
α, 6n	5.0	1.8	1.0	4.4	10.4	11.1	21.5	22.2
error(%)	±20	±15	±20	±15	±20	±10	±25	±1

a) All energies are given in MeV. Far meaning of the simbols, see text. b) $E_{out} = E_n + E_\gamma$ with $E_n = \langle n^2 \rangle \langle E_n \rangle + \langle n^p \rangle \langle E_n^p \rangle$ and E_γ is the average energy release of the quasi-continuum and discrete γ-ray cascades[86]. c) $E_n = E_{CM} - E_b$ where E_{CM} stands for the excitation energy of the compound nucleus and E_b for the binding energy of the x neutrons in the nucleus.

Table V

Angular momentum balance analyzed with two phase approximation in the ^{158}Gd(α, xn) reaction at E_α= 70 MeV

	ℓ_n^e	ℓ_n^p	ℓ_n^{tot}	$\bar{\ell}_\gamma$	$\bar{\ell}_{out}$	$\bar{\ell}_{in}$
α, 4n	1.0	2.0	3.0	17.2	20.2	
α, 5n	1.7	1.2	2.9	15.8	18.6	21.0
α, 6n	2.4	0.6	3.0	16.2	19.2	
error(%)	±15	±15	±15	±15	±15	

Estimated average input angular momentum from the calculation with computer code ALICE.[24]

Figure Captions.

1-1. Schematic picture of the particle-hole door-ways for the PEQ and EQ processes.

2-1. Typical counter arrangement for charged particles, neutrons and γ-rays.

2-2. A schematic view of a typical arrangement for the particle-γ correlations.

2-3. F-beam transport system in the M experimental room at RCNP.

2-4. Target chamber for various coincidence measurements for in- and out of the reaction plane.

2-5. Breeder circuit diagram for charged particle measurements with $1\frac{1}{2}$" photomultipliyer (R580).

2-6. Pulse height response of the NaI(Tl) crystal (31.75 mm ϕ × 31.75 mm) for various energy protons.

2-7. Mounting of the Si + NaI(Tl) counter telescope system.

2-8. Typical particle identification spectrum following the ^{165}Ho + 110 MeV α reaction.

2-9. a) Neutron-γpulse shape discrimination spectrum. b) Neutron-γ pulse shape discrimination spectra for ten different neutron energies selected by the neutron-TOF. For a) and b) the ^{165}Ho + 110 MeV α reaction was used.

2-10. a) Pulse hight response of NE213 (5"ϕ × 3") scintillator for monoenergetic neutrons following ^{7}Li(p,n)^{7}Be reactions. b) An example of the comparison between the experimental neutron response function and a Monte Carlo calculation (full line)[62].

2-11. Neutron detection efficiency of a 125 mm diameter × 125 mm NE213 scintillator. Closed circles are the results of Monte Carlo calculation.[62]

2-12. Neutron energy vs. electron energy for an NE213 scintillator. Open circles represent experimental results for the monenergetic neutrons. Full line is the calibration taken from ref.63.

2-13. Time and energy calibration of neutrons with the ^{165}Ho + 110 MeV α reaction.

2-14. Time spectrum of neutrons and γ-rays in the case of neutron-charged particle coincidence experiments with the ^{165}Ho + α-particle reaction. Large and small dots represent the discriminated spectra for neutrons and γ-rays, respectively.

2-15. Effects of the front shields with lead(20 mm) and brass (5 mm). Closed circles represent the attenuation due to the shields. Full and dotted line are the neutron detection efficiencies with and without the shields, respectively.

2-16. Background of the time spectrum measured with ^{165}Ho target and without target.

2-17. Typical example of absolute efficiency curve for γ-rays. a) GAMMA-X, b) LEPS.

2-18. Block diagram of electronics in the case of neutron-charged particle coincidence experiment. Simbols mean NIM modules; PA(Pre-Amp.), SA(Spectroscopic-Amp.), TFA(Timing-Filter-Amp.), TSCA(Timing-Single-Channel-Analyzer) CFD(Constant-Fraction-Disc.), GDG(Gate & Delay-Generater), LGS(Linear-Gate & Streacher), DA(Delay-Amp.), PI(Particle-Identifier), PSA(Pulse-Shape-Analyzer).

3-1. Typical singles γ-ray spectrum following ^{164}Dy + 120 MeV α-particle reaction.

3-2. Total reaction cross section for each reaction channel of the reaction ^{162,164}Dy + α-particle at E_α = 50, 70, 90 and 120 MeV. Open circles are experimental results deduced from singles γ-ray spectra, and plotted as a function of the energy sum E_T (see text).

3-3. Total reaction cross sections for each reaction channel following the ^{164}Dy and ^{165}Ho + 120 MeV α-particle reactions.

3-4. Neutron multiplicity distributions of ^{165}Ho + 110 MeV α-particle reaction, which gated with five energy bins of the protons at lab. angles θ_p = 25, 40 and 129 deg..

3-5. Differential neutron spectra following ^{165}Ho + 110 MeV α reaction at lab. angles θ_n = 20.3 and 140 deg..

3-6. Angle integrated neutron spectra following ^{165}Ho + 110 MeV α reaction.

3-7. Neutron momentum distributions in coincidence with protons for three energy bins following ^{165}Ho + 110 MeV α reaction. Solid lines describe each half yeld.

3-8. Cross section ratios of high-(>5 MeV) and low-energy (<5 MeV) neutrons in three proton energy bins.

3-9. Mean energies of neutrons at each detection angle in three proton energy bins.

3-10. a) Proton spectra following the ^{165}Ho(α, xn yp γ) reaction at E_α = 109 MeV in a neutron multiplicity range x = 2-8 at θ_p = 25 deg.. b) at θ_p = 129 deg..

3-11. Four γ-ray spectra obtained from the $^{158}Gd(\alpha, xn\ \gamma)$ reaction at E_α = 70 MeV in coincidence with neutrons in the energy intervals (from top to bottom) of 1.2 - 3.1 MeV, 3.1 - 9.5 MeV and 9.5 - 30 MeV. The peaks corresponding to the main transitions in $^{156,157,158}Dy$.

3-12. Neutron energy spectra for the three exit channels measured at four angles for the $^{158}Gd(\alpha, xn)$ reaction at E_α = 70 MeV.

4-1. Ratio Γ_c / Γ_{tot} vs. excitation energy and exciton number for $^{166}Er^*$ system, where Γ_c and Γ_{tot} represent particle and total decay width.

4-2. Entry lines of each reaction channel to the EQ stage as a function of the excitation energy for the $^{168}Er^*$ system. Dotted line denotes the mean value of the entry energy.

4-3. Ratios f_p and f_e as a function of the order of the cascades, where f_p and f_e are the PEQ and the EQ fractions, respectively, defined in text.

4-4. Neutron spectra following $^{164}Dy(\alpha, p\ xn)$ reaction at E_α = 90 MeV decomposed to each reaction channel (x = 3~8).

4-5. Neutron spectra following $^{164}Dy(\alpha, p\ xn)$ reaction at E_α = 90 MeV de composed to order of emissions.

4-6. a) Comparisons between experimental and calculated neutron multiplicity distributions for the ^{162,164}Dy (α, xn) reactions at E_α = 50, 70, 90 and 120 MeV. Closed and open circles represent ^{162}Dy and ^{164}Dy target, respectively. The calculations are dotted line. b) ^{165}Ho(α, p xn) reaction at E = 120 MeV. c) ^{158}Gd(α, xn) reaction at E_α = 70 MeV.

4-7. PEQ fraction $f_p(x)$ for each reaction channel defined in eq. (4-21) vs. neutron multiplicity x in the ^{162,164}Dy(α, xn) reactions at E_α = 50, 70, 90 and 120 MeV. Each point is deduced from the comparison between the experiments and calculations.

4-8. Total PEQ fraction f_p vs. initial excitation energy for the ^{162,164}Dy(α, xn) reaction at E = 50, 70, 90 and 120 MeV.

4-9. Angle integrated proton spectrum following the ^{165}Ho (α, xn yp) reaction, where solid line represent the calculation.

4-10. Angle integrated neutron spectra following the ^{158}Gd (α, xn) reaction at E_α = 70 MeV gated by characteristic γ-rays of the reaction channel (x = 4~6), where closed circles represent experiments, and solid and dotted lines are the exciton model calculation and Maxwellian distributions $kT \cdot \exp(-E/kT)$.

4-11. Angular distributions of the PEQ and the EQ neutrons in coincidence with characteristic γ-rays of the (α, 6n), (α, 5n) and (α, 4n) reaction channel for the ^{158}Gd(α, xn) reaction at E_α = 70 MeV. Closed and open circles denote the neutron cross sections of the EQ and PEQ processes, respectively.

5-1. a) Average neutron energy for (p, xn), (α, xn), (^{12}C, xn)^{44,87}), (^{20}Ne, xn) and (^{40}Ar, xn)^{87}) reactions vs. initial excitation energies. b) vs. $(E^*-30)/A_i^{1/3}$, where E^* is the initial excitation energy and A_i is the projectile mass number.

5-2. Schematic de-excitation energy balance of the α-particle induced reaction at E_α =70 MeV.

5-3. Schematic angular momentum balance of the α-particle induced reaction at E_α = 70 MeV.

5-4. Angle integrated neutron spectra following the ^{165}Ho (α, xn yp) reaction at E_α = 109 MeV. Neutrons were measured in coincidence with protons detected at θ_1 = 30 deg.. Full and dotted lines are the exciton model calculations and fittings with two approximation, respectively.

5-5. Exciton model calculations for the angle integrated proton spectra of each reaction channel following the ^{165}Ho(α, p xn) reaction at E_α = 109 MeV.

5-6. Average neutron energies and exciton particle number of the PEQ phase for the ^{165}Ho(α, p xn) reaction at E_α = 109 MeV.

A-1. Flow diagram of the exciton model calculation for multi-particle emissions.

Program List; Computer Code for the exciton model calculation for multi-particle emissions.

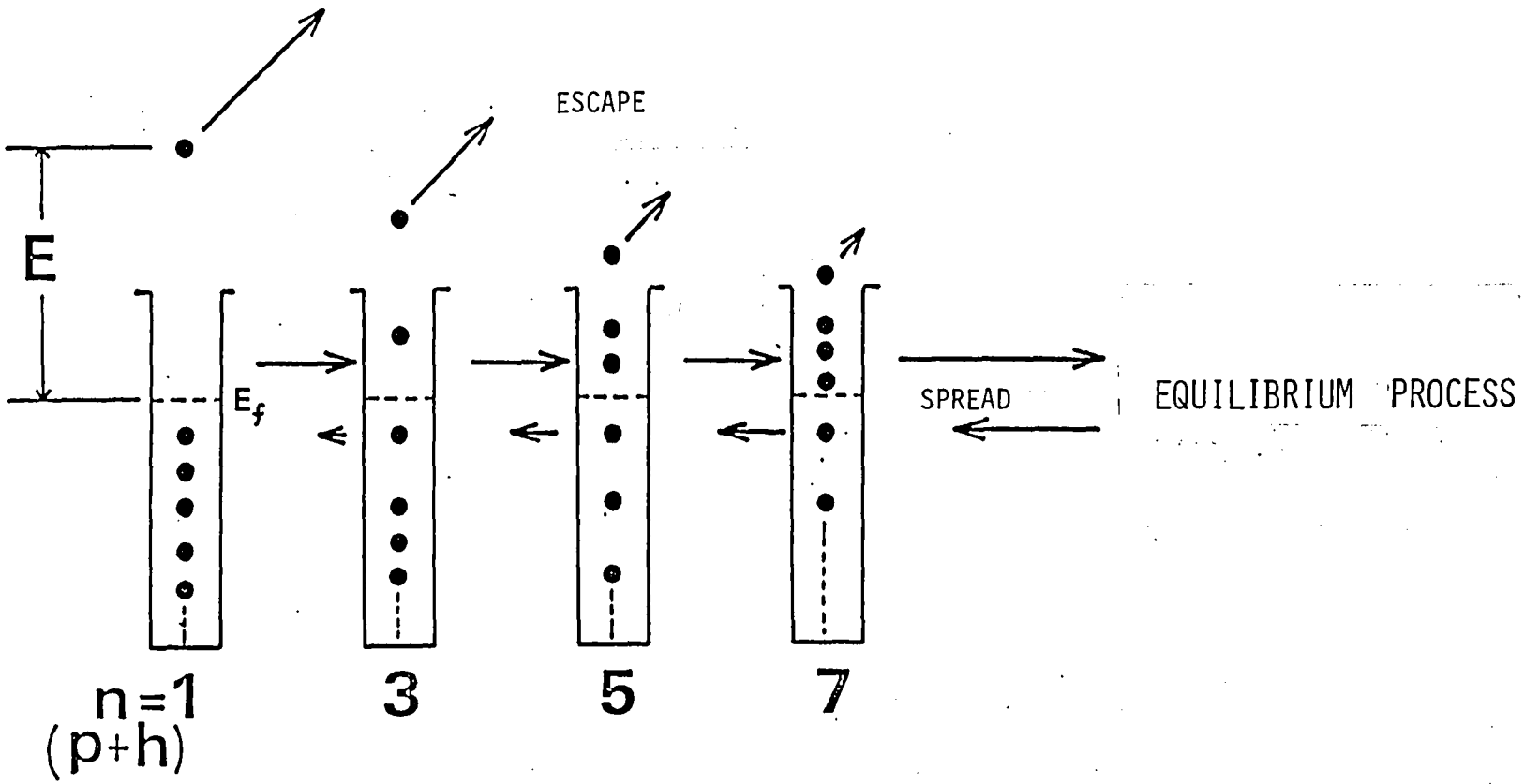
ESCAPE
E
E_f
SPREAD
EQUILIBRIUM PROCESS
n=1
(p+h)
3
5
7
PRE-EQUILIBRIUM PROCESS

Fig. 1-1

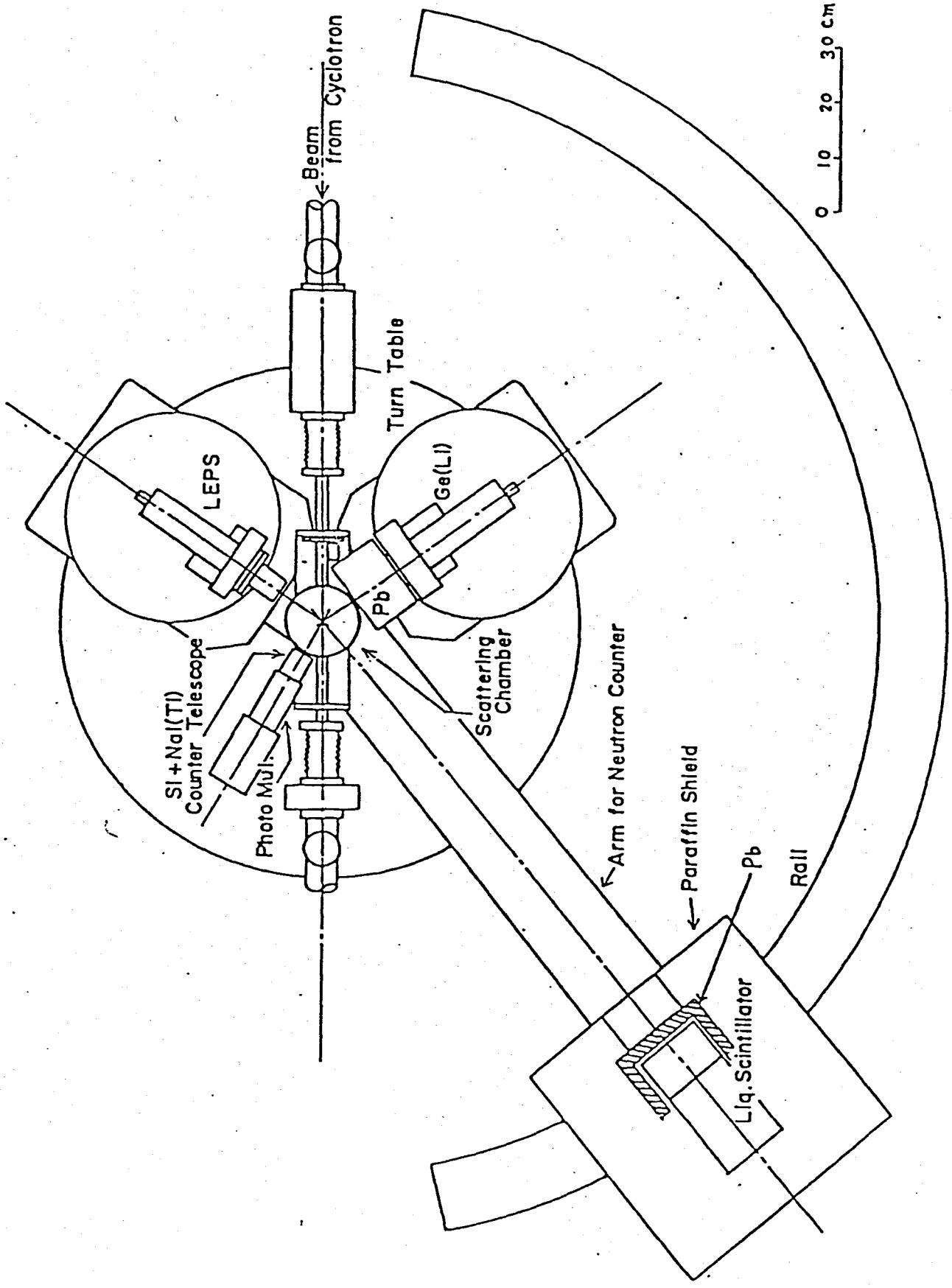
Beam from Cyclotron
Turn Table
LEPS
Ge(Li)
Pb
Si+NaI(Tl) Counter Telescope
Photo Mul.
Scattering Chamber
Arm for Neutron Counter
Paraffin Shield
Pb
Rail
Liq. Scintillator
0 10 20 30 cm

Fig. 2-1

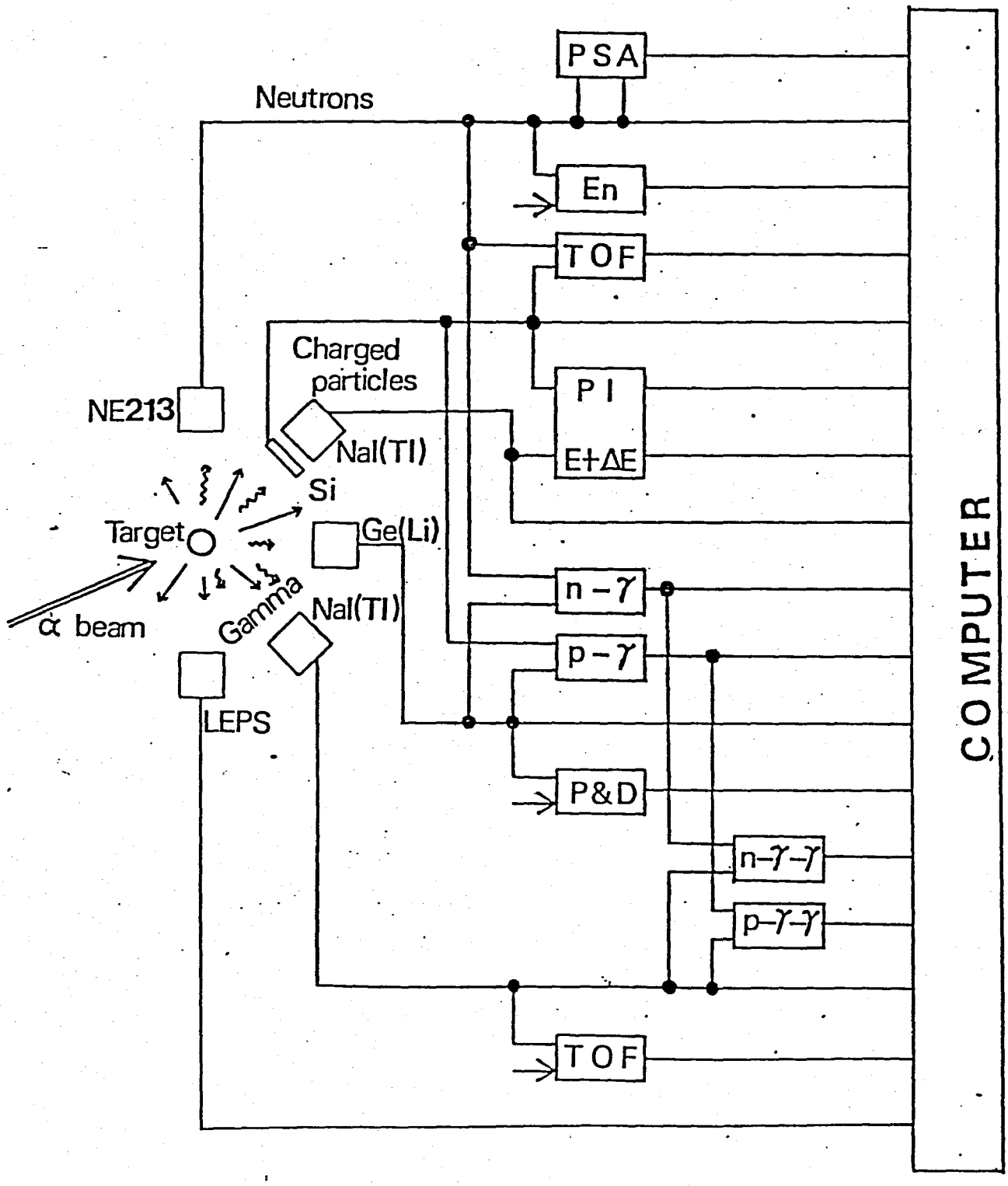
PSA
Neutrons
En
TOF
Charged
particles
PI
E+ΔE
NE213
NaI(TI)
Si
Target
Ge(Li)
n-γ
α beam
Gamma
NaI(TI)
p-γ
LEPS
P&D
n-γ-γ
p-γ-γ
TOF
COMPUTER

Fig. 2-2

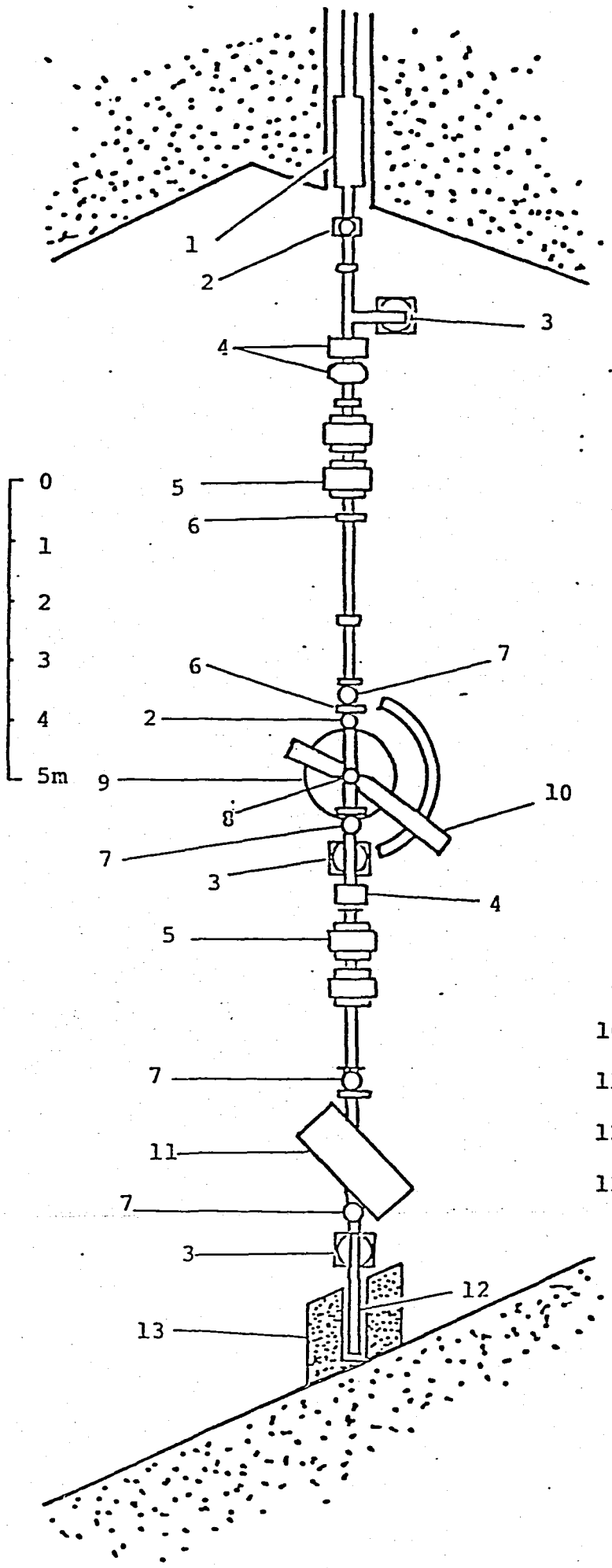

1 rotary shutter
2 beam viewer
3 terbo molecular pump(250 l/s)
4 steering magnet
5 magnetic Q doublet
6 gate valve
7 liq. N_2 trap
8 target chamber
9 goniometer
10 TOF plate
11 AGNES
12 Faraday cup
13 beam dumper shield

Fig. 2-3

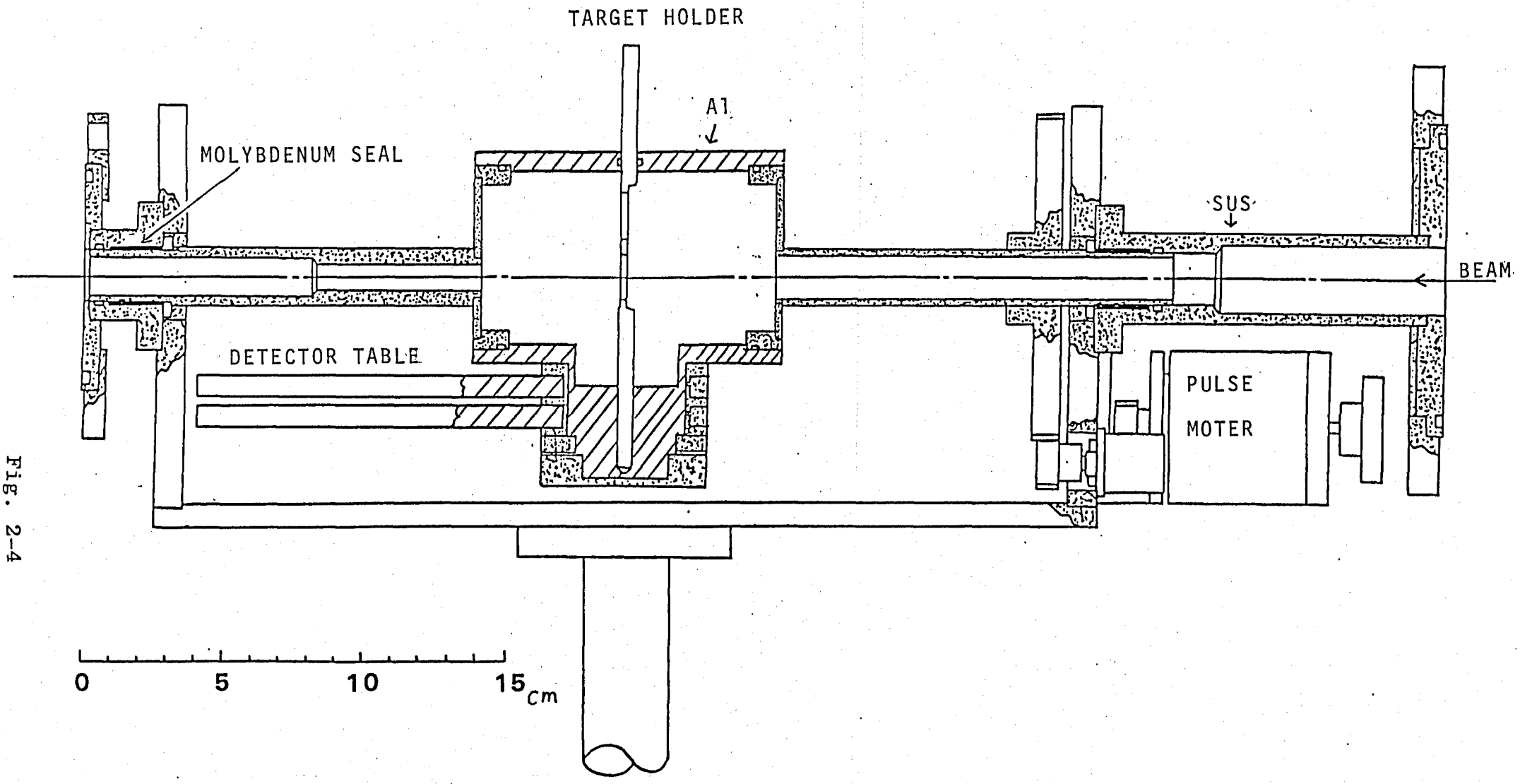
TARGET HOLDER
Al
MOLYBDENUM SEAL
SUS
BEAM
DETECTOR TABLE
PULSE
MOTER
0
5
10
15 cm
GONIOMETER

Fig. 2-4

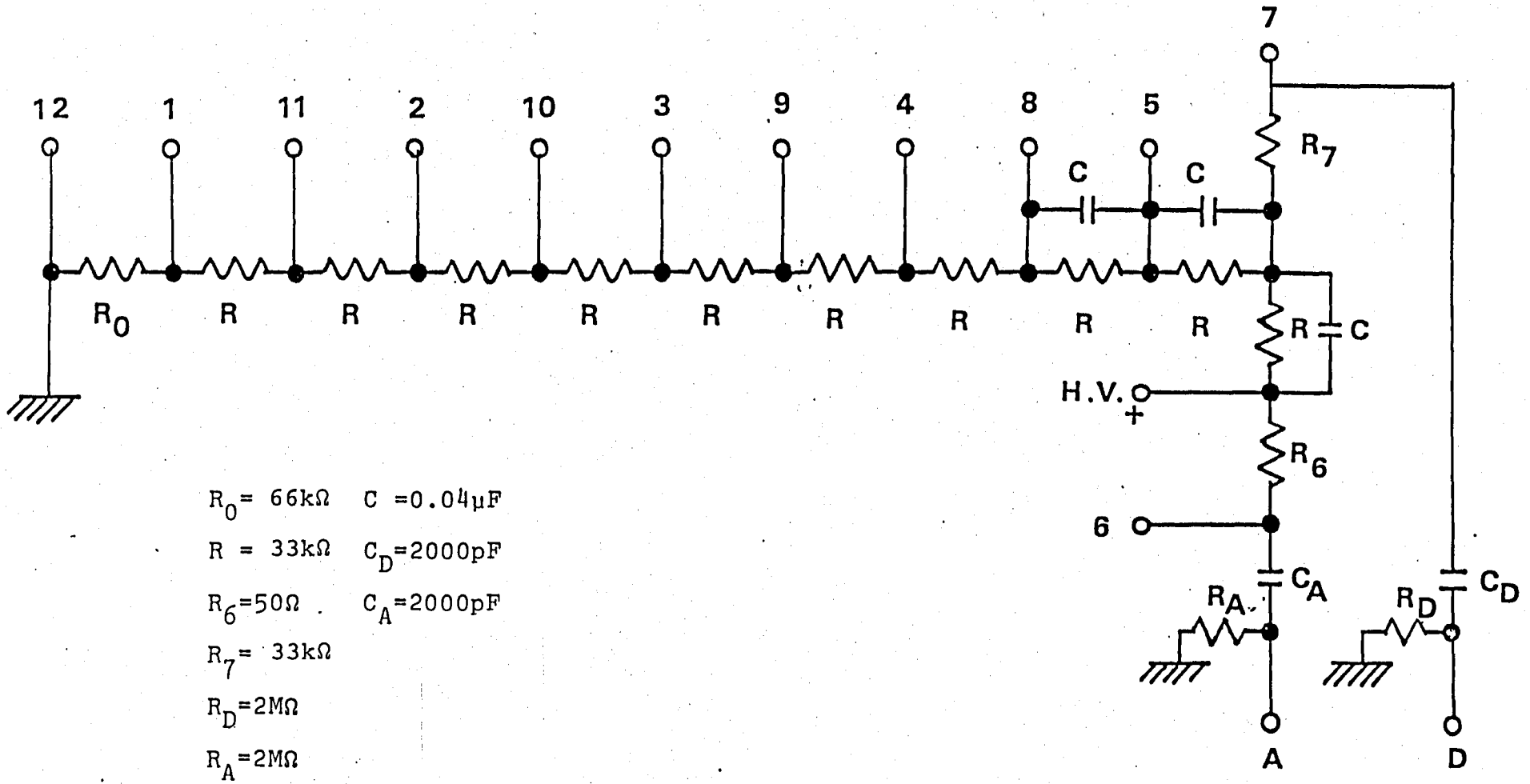

R_0= 66kΩ C =0.04μF

R = 33kΩ C_D=2000pF

R_6=50Ω C_A=2000pF

R_7= 33kΩ

R_D=2MΩ

R_A=2MΩ

Fig. 2-5

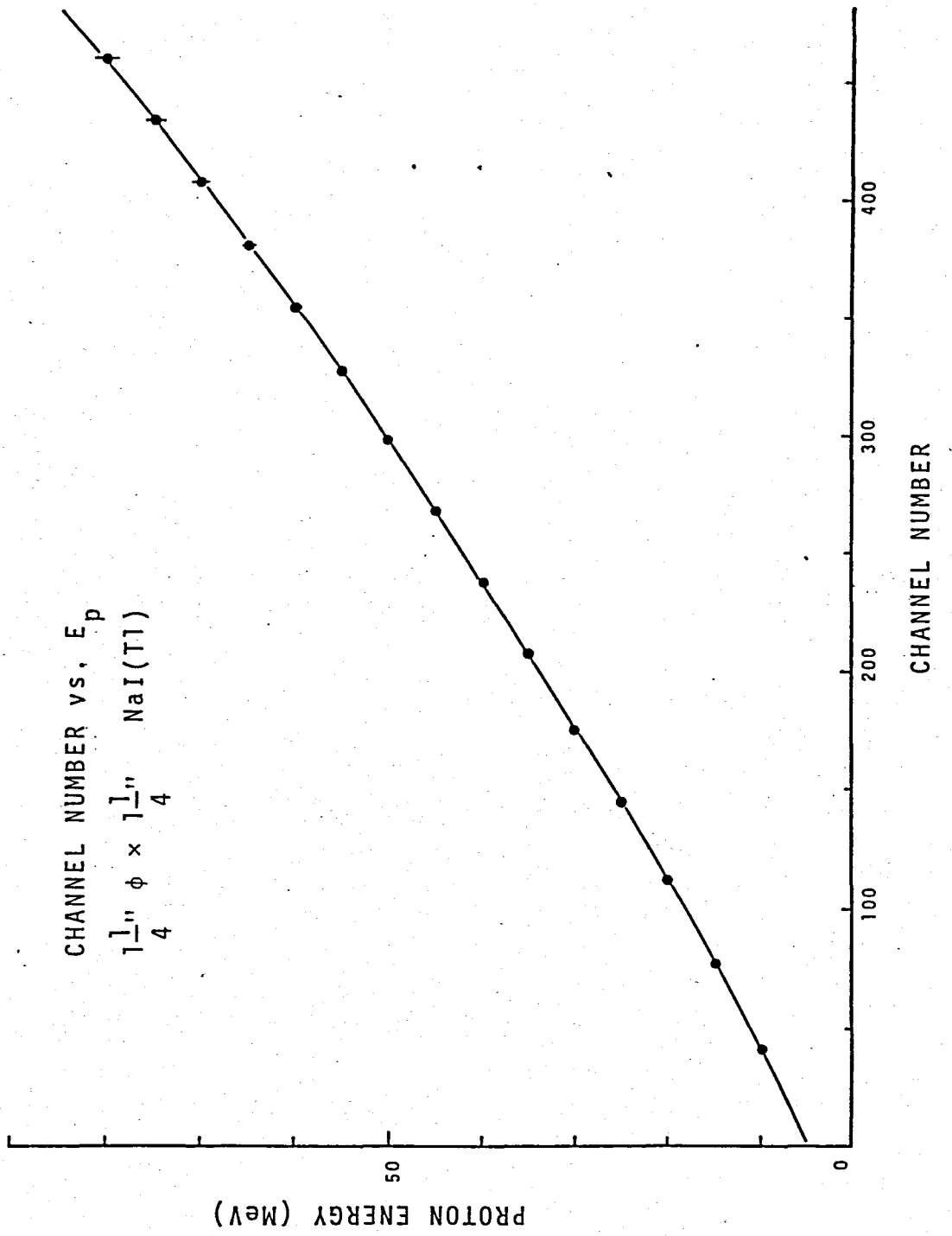
CHANNEL NUMBER vs. E_p
$1\frac{1}{4}$" ϕ × $1\frac{1}{4}$" NaI(Tl)
PROTON ENERGY (MeV)
0
50
100
200
300
400
CHANNEL NUMBER

Fig. 2-6

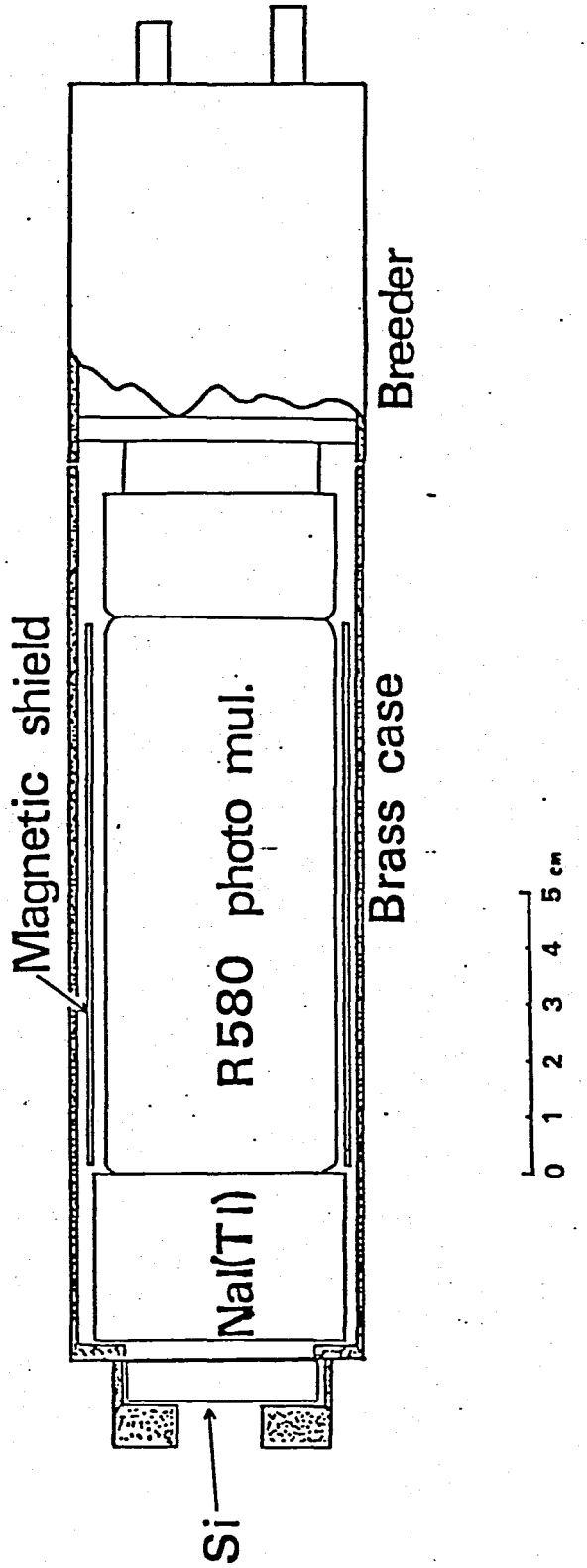
Breeder
Brass case
R580 photo mul.
NaI(Tl)
Magnetic shield
Si
0 1 2 3 4 5 cm

Fig. 2-7

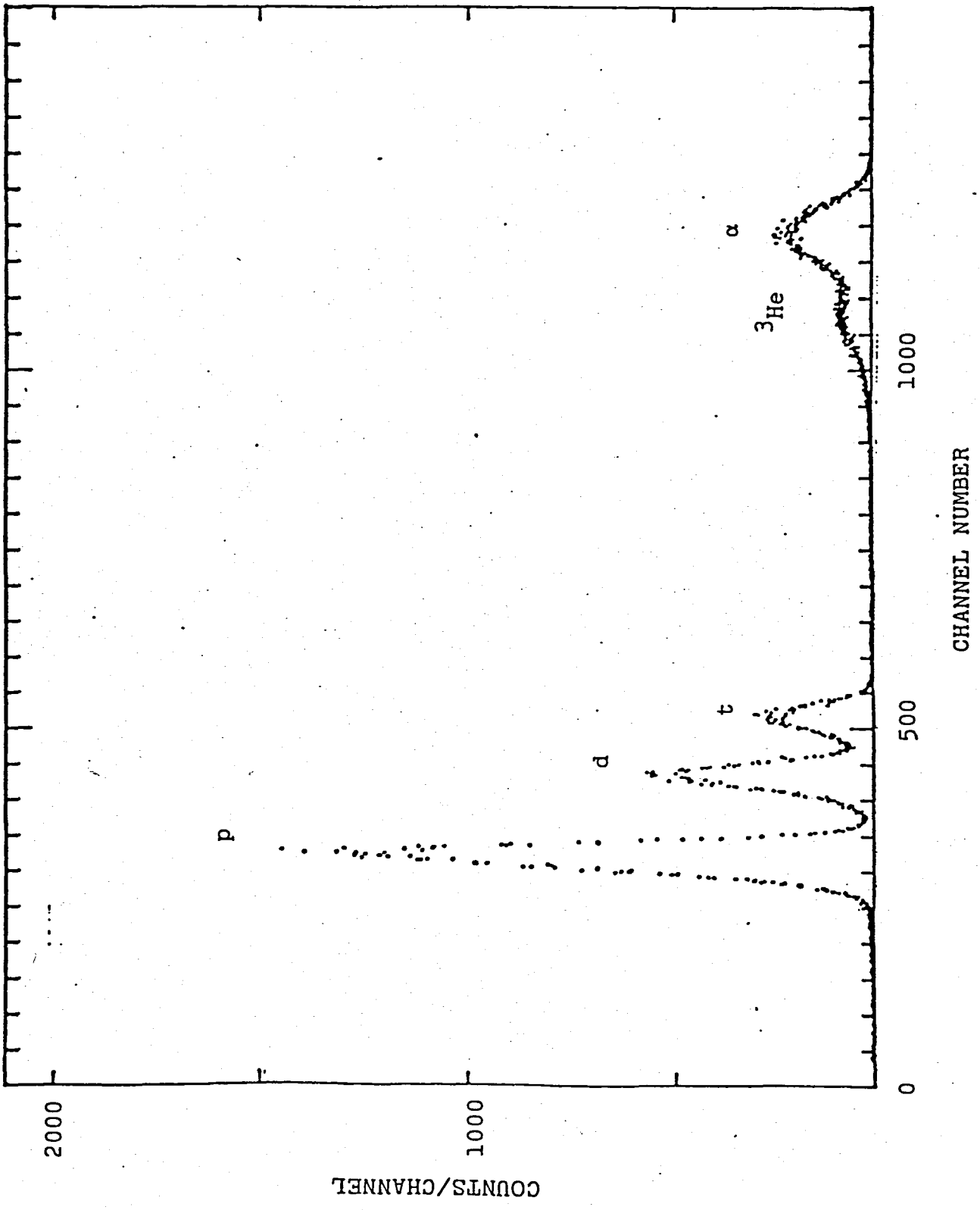

Fig. 2-8

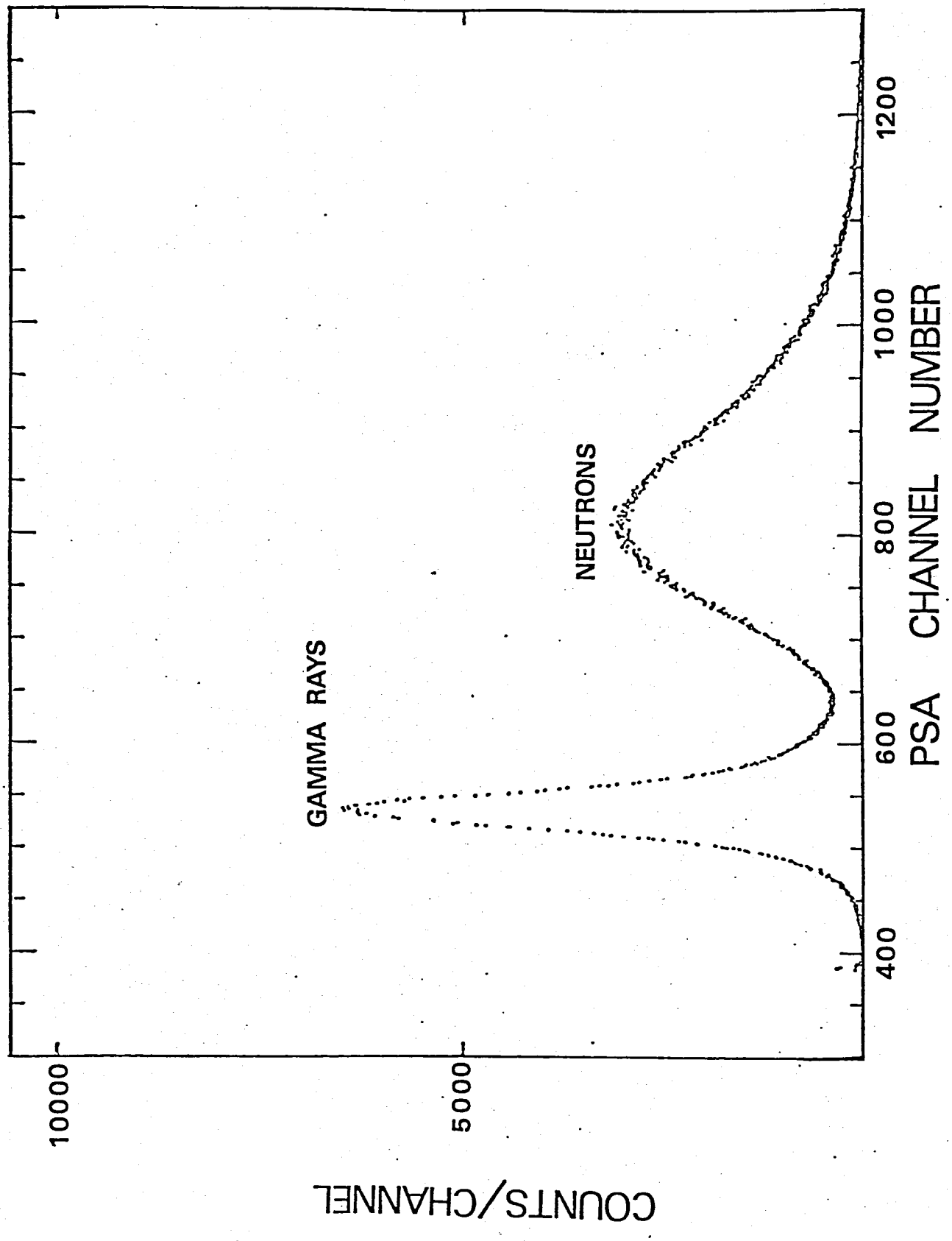
COUNTS/CHANNEL
10000
5000
400
600
800
1000
1200
PSA CHANNEL NUMBER
NEUTRONS
GAMMA RAYS

Fig. 2-9-a

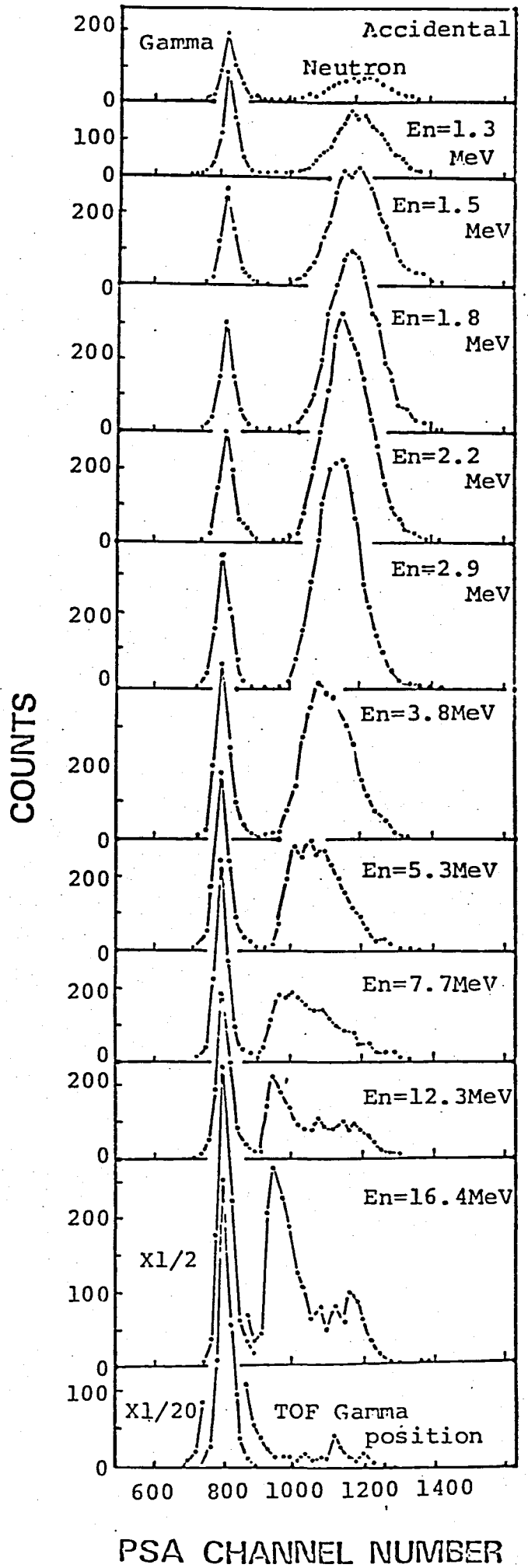

Fig. 2-9-b

NEUTRON GAMMA DISCRIMINATION

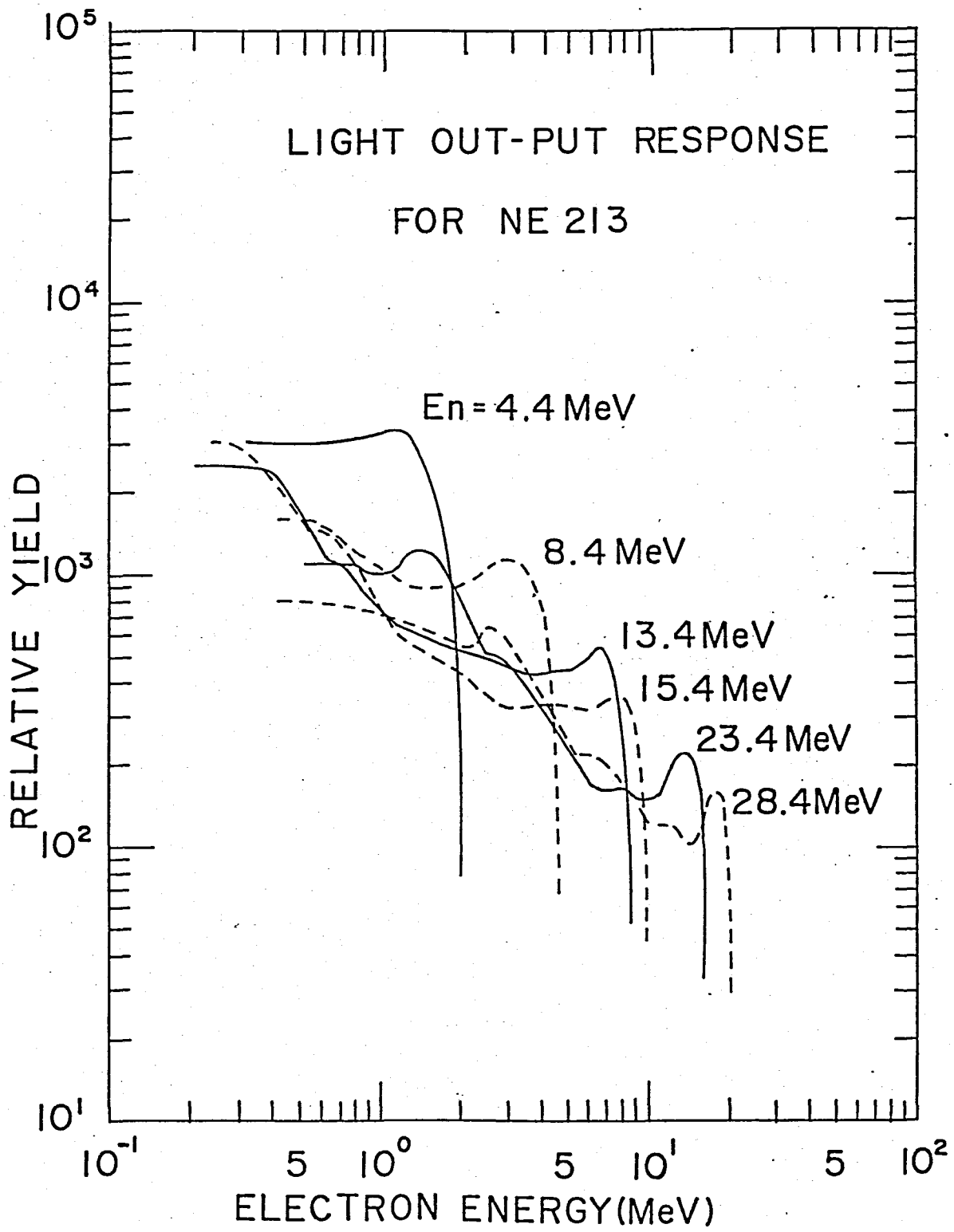
LIGHT OUT-PUT RESPONSE
FOR NE 213
En = 4.4 MeV
8.4 MeV
13.4 MeV
15.4 MeV
23.4 MeV
28.4 MeV
RELATIVE YIELD
ELECTRON ENERGY(MeV)

Fig. 2-10-a

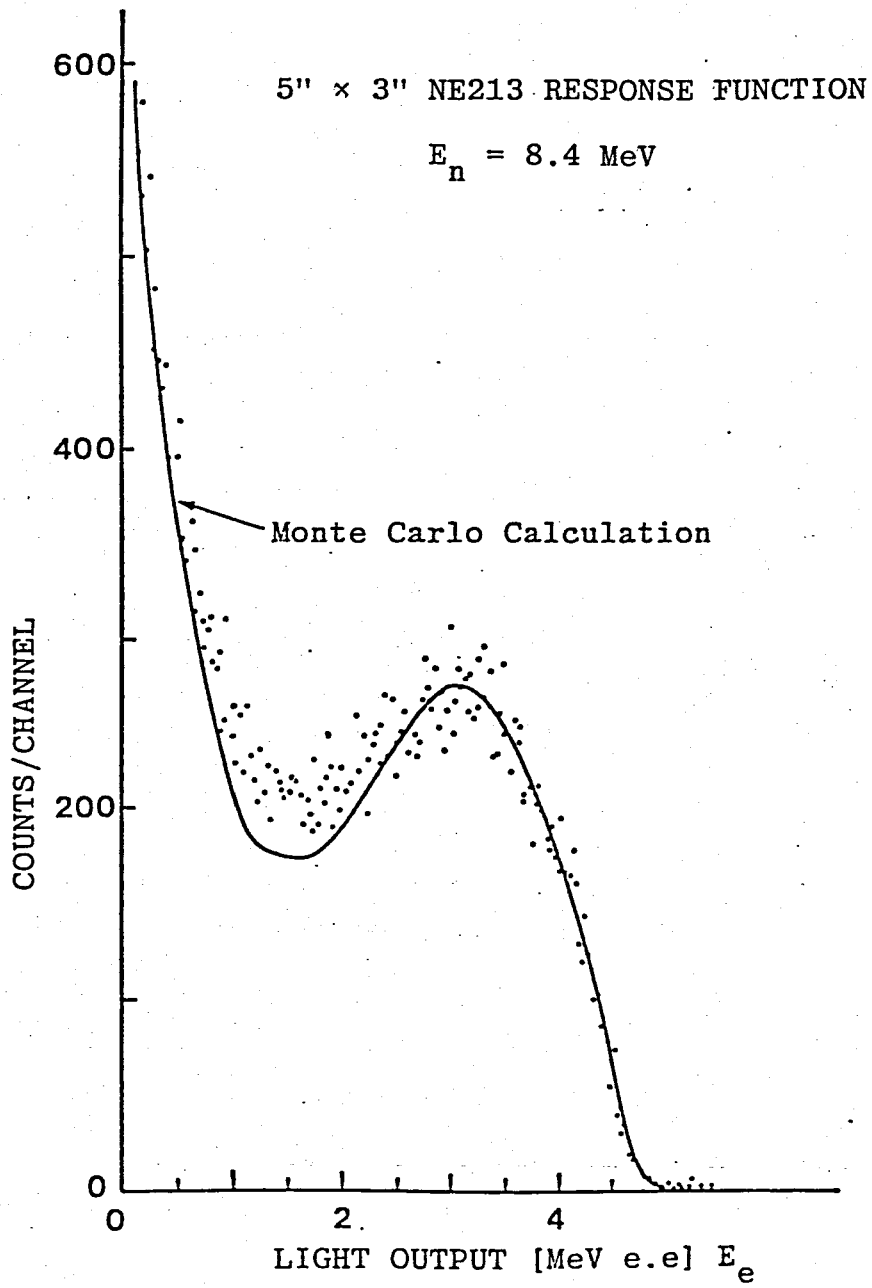
5" × 3" NE213 RESPONSE FUNCTION
E_n = 8.4 MeV
Monte Carlo Calculation
COUNTS/CHANNEL
600
400
200
0
0
2
4
LIGHT OUTPUT [MeV e.e] E_e

Fig. 2-10-b

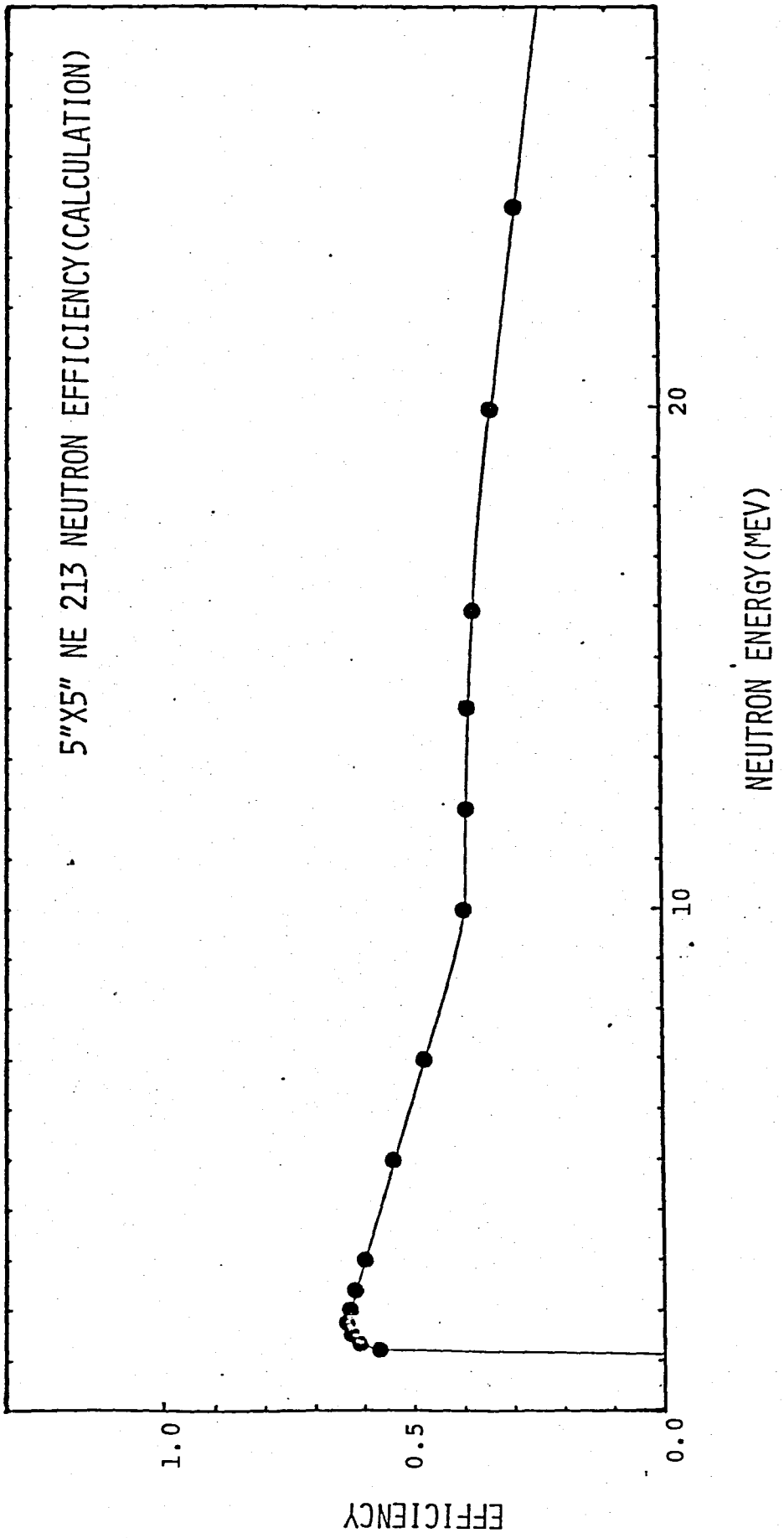
5"X5" NE 213 NEUTRON EFFICIENCY(CALCULATION)
EFFICIENCY
1.0
0.5
0.0
10
20
NEUTRON ENERGY(MEV)

Fig. 2-11

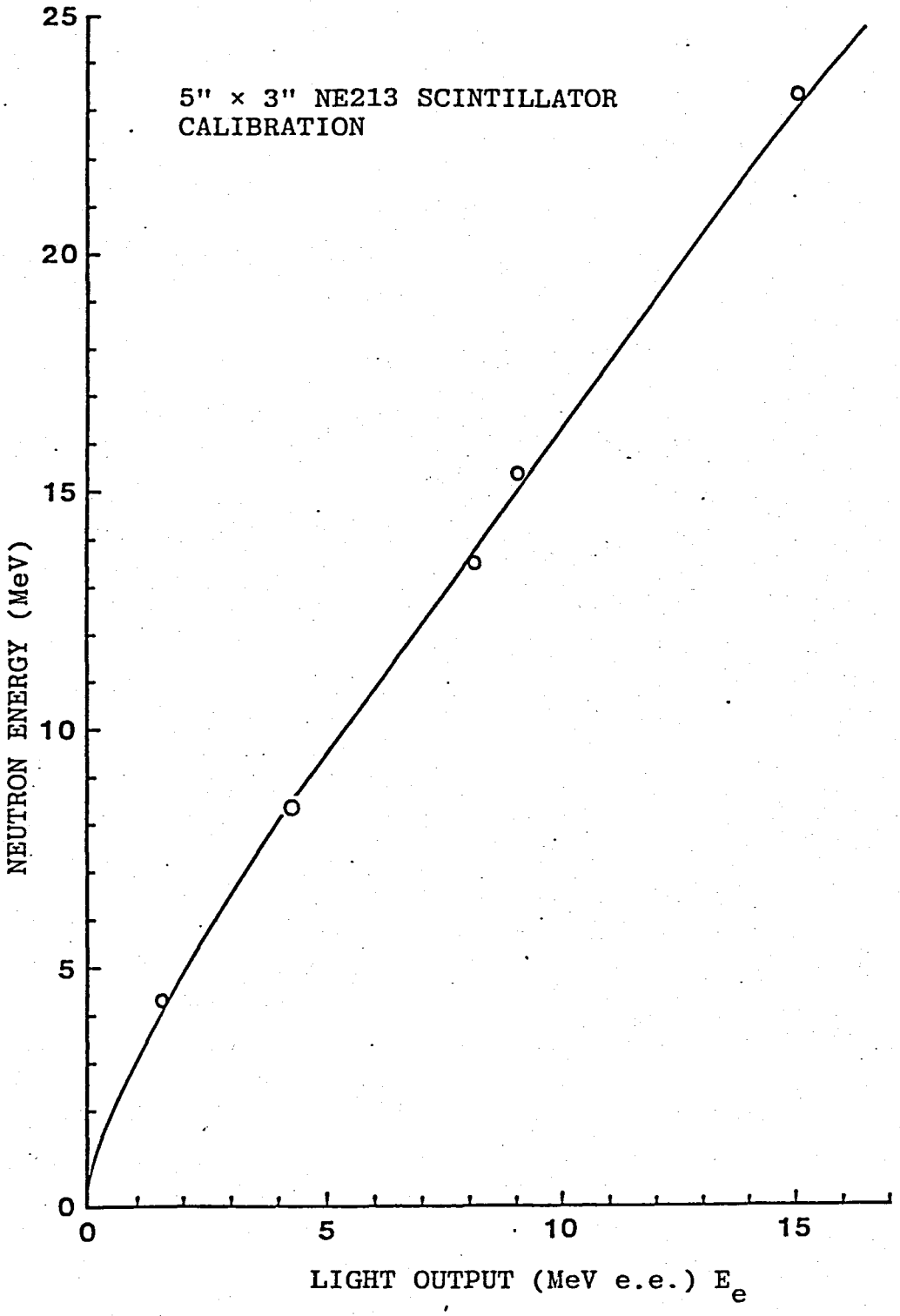
5" × 3" NE213 SCINTILLATOR
CALIBRATION
NEUTRON ENERGY (MeV)
LIGHT OUTPUT (MeV e.e.) E_e
0
5
10
15
20
25

Fig. 2-12

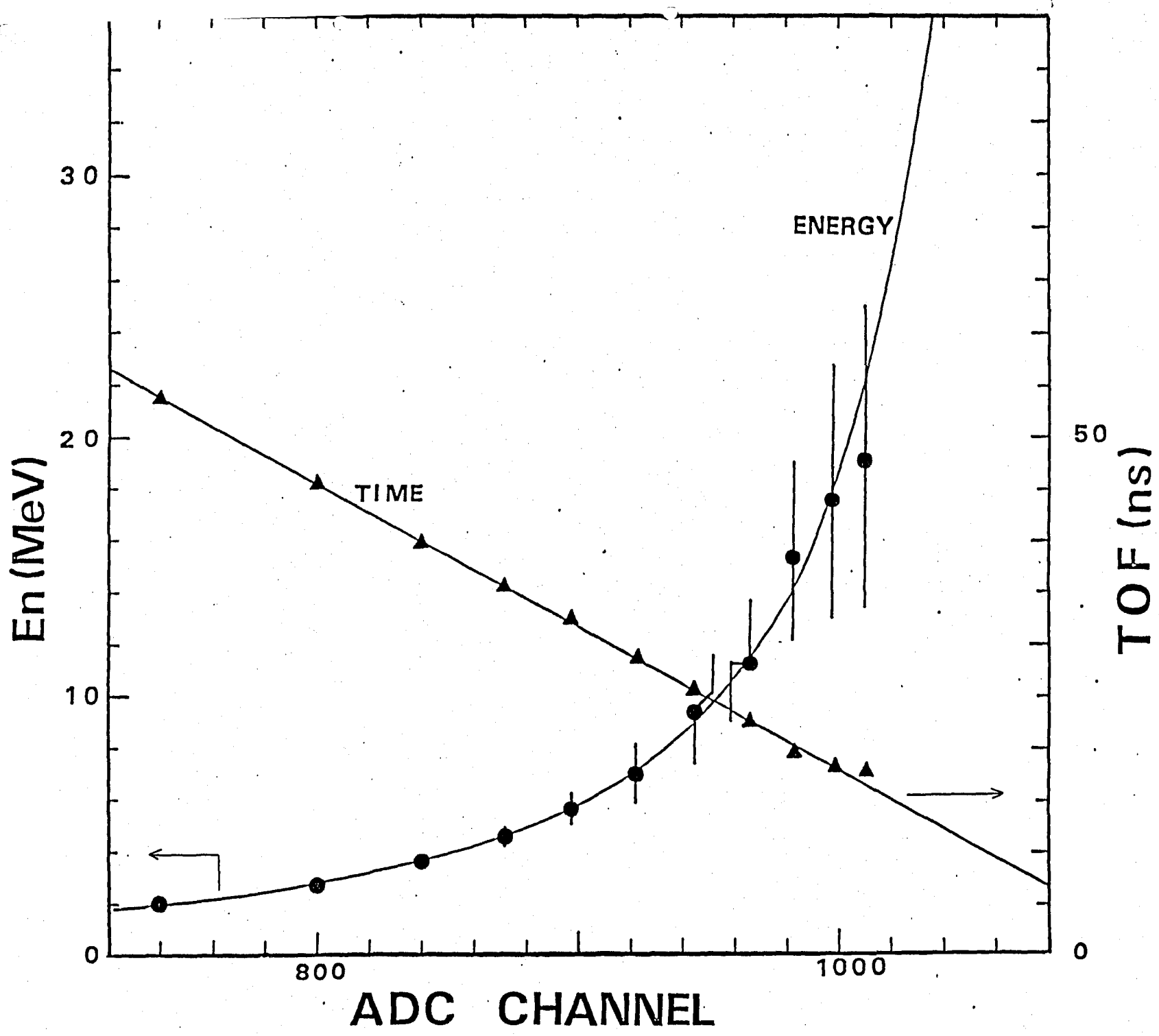

Fig. 2-13

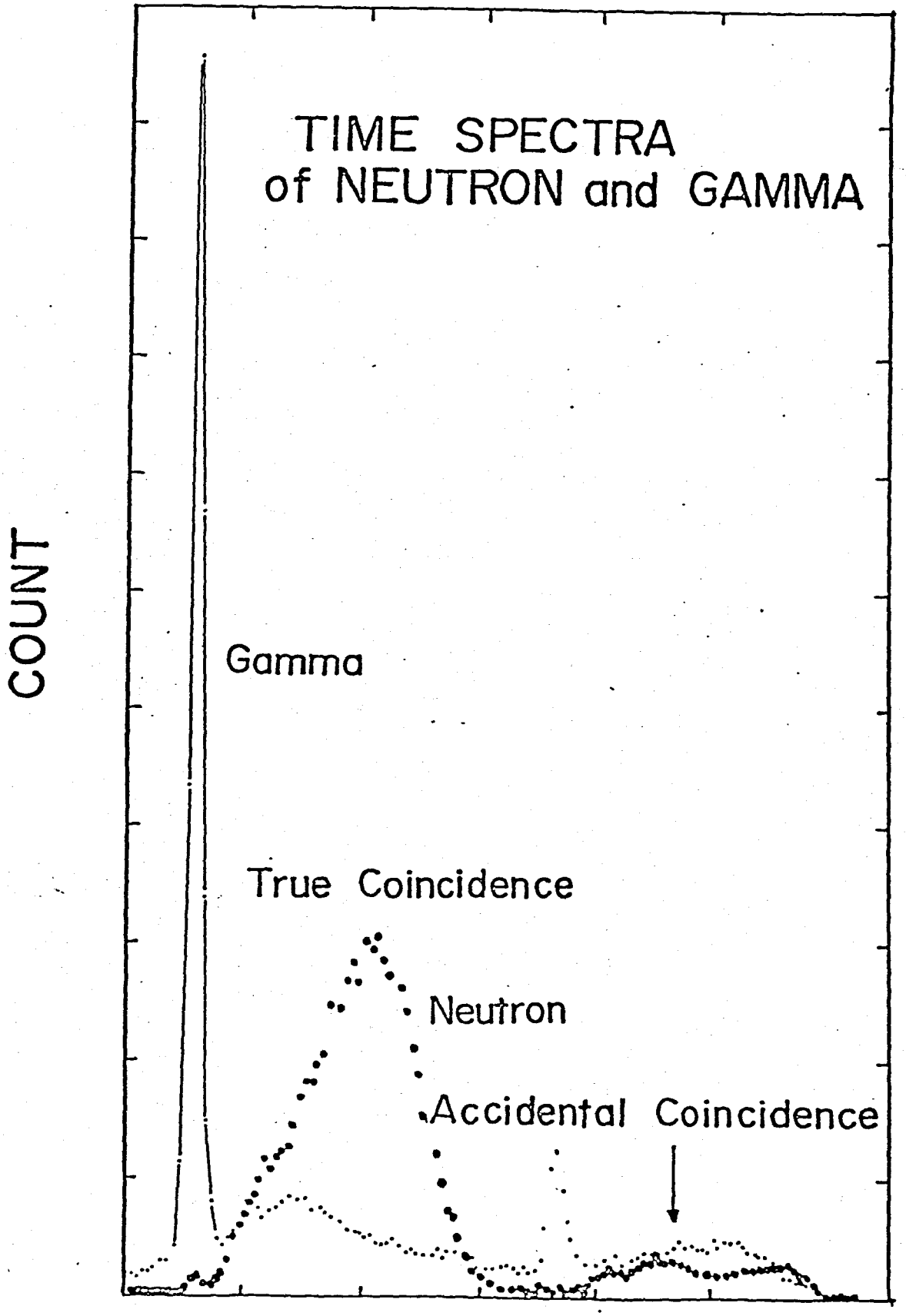
TIME SPECTRA
of NEUTRON and GAMMA
COUNT
Gamma
True Coincidence
Neutron
Accidental Coincidence
ADC6 CHANNEL NUMBER

Fig. 2-14

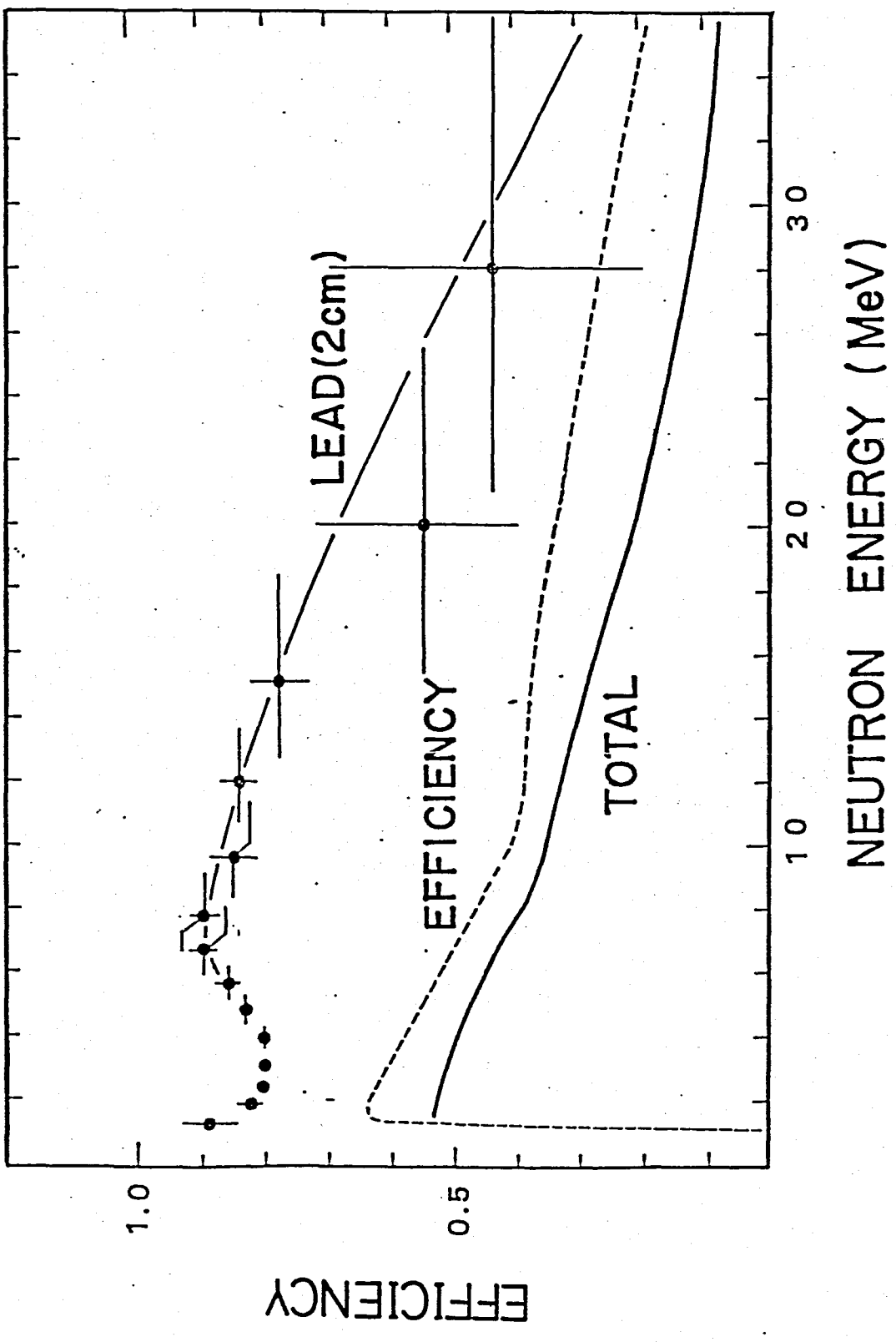
LEAD(2cm)
EFFICIENCY
TOTAL
NEUTRON ENERGY (MeV)
10
20
30
1.0
0.5
EFFICIENCY

Fig. 2-15

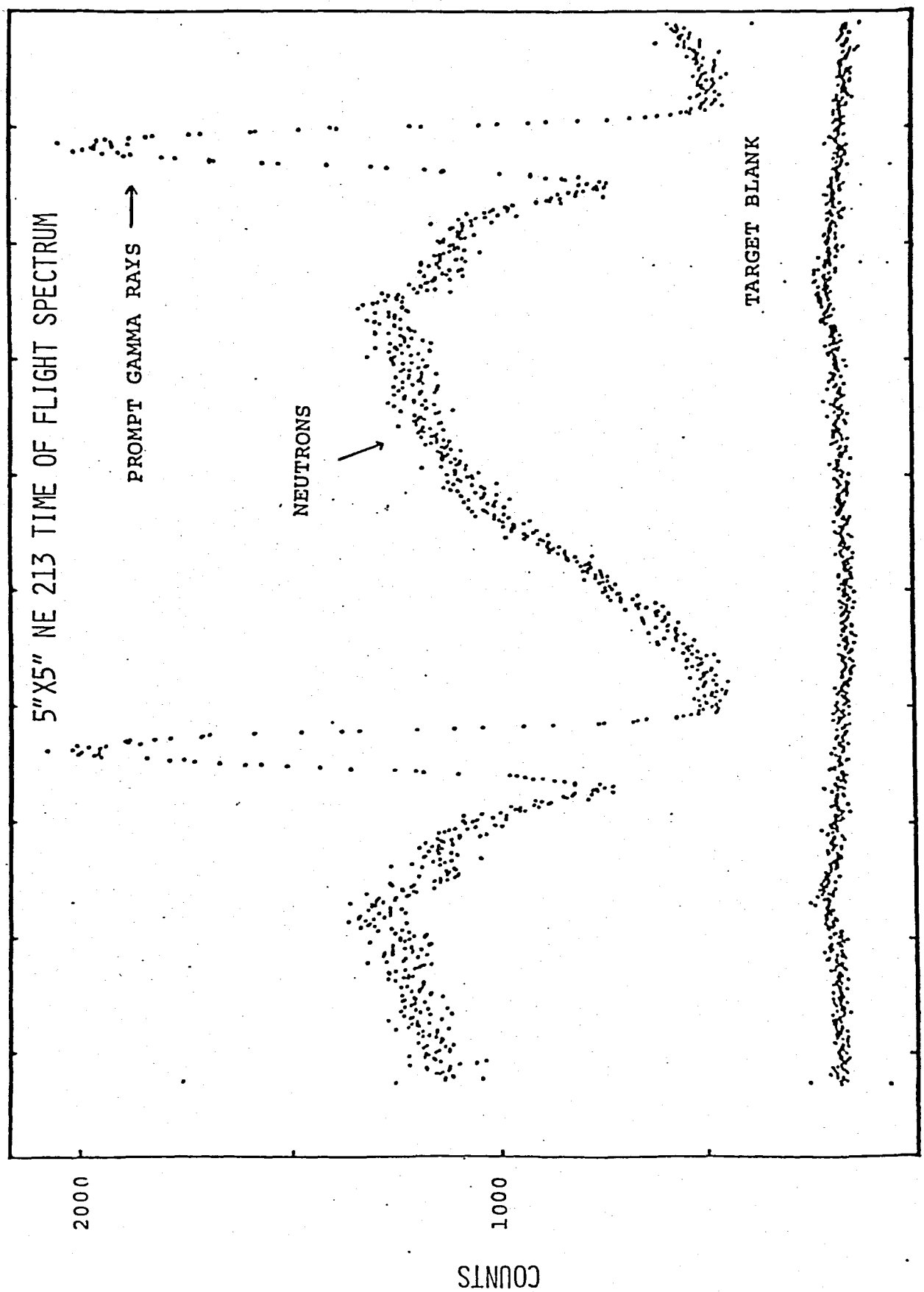
5"X5" NE 213 TIME OF FLIGHT SPECTRUM
PROMPT GAMMA RAYS
NEUTRONS
TARGET BLANK
COUNTS
2000
1000
200
400
600
800
TAC CHANNEL

Fig. 2-16

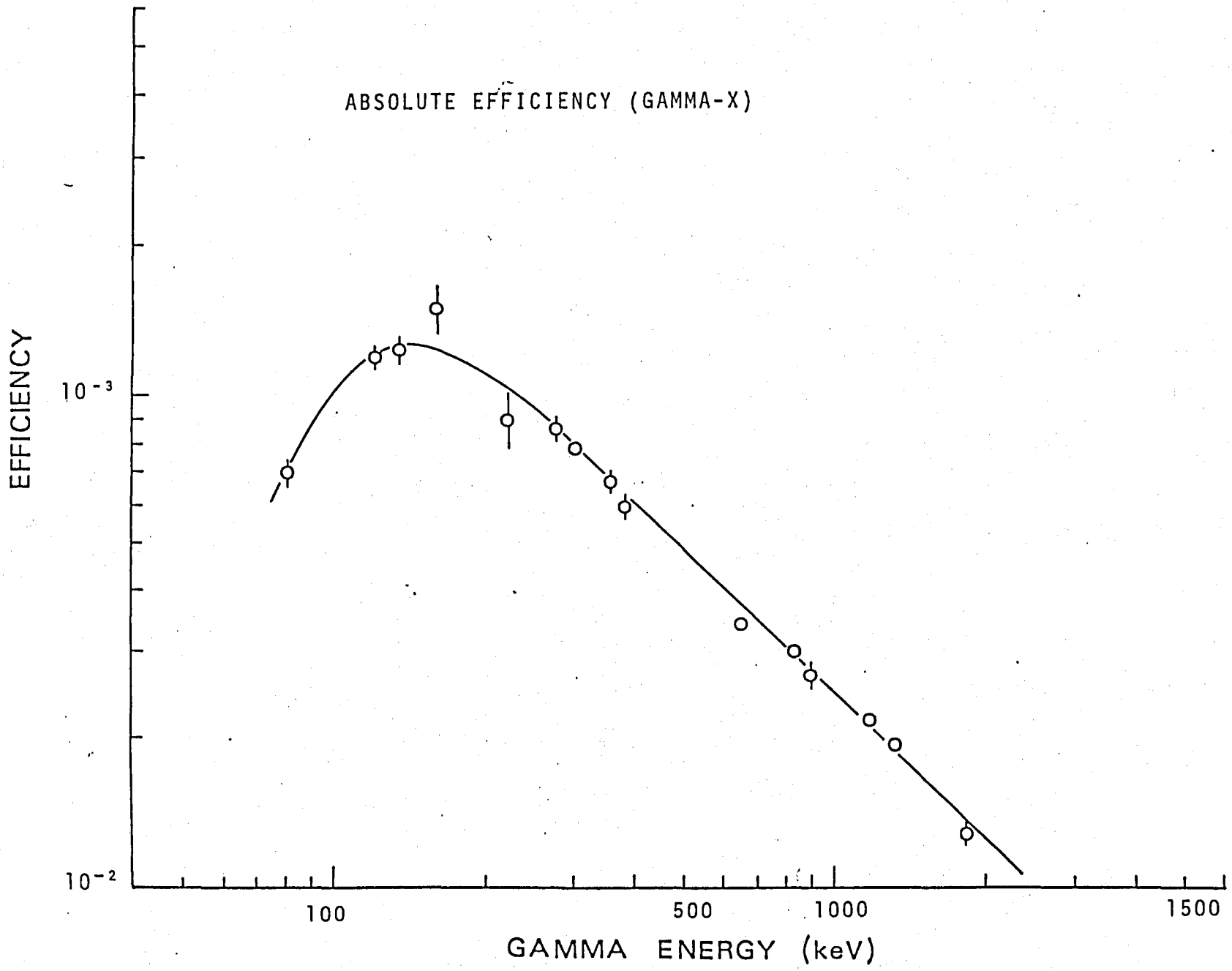
ABSOLUTE EFFICIENCY (GAMMA-X)
EFFICIENCY
10^{-3}
10^{-2}
100
500
1000
1500
GAMMA ENERGY (keV)

Fig. 2-17-a

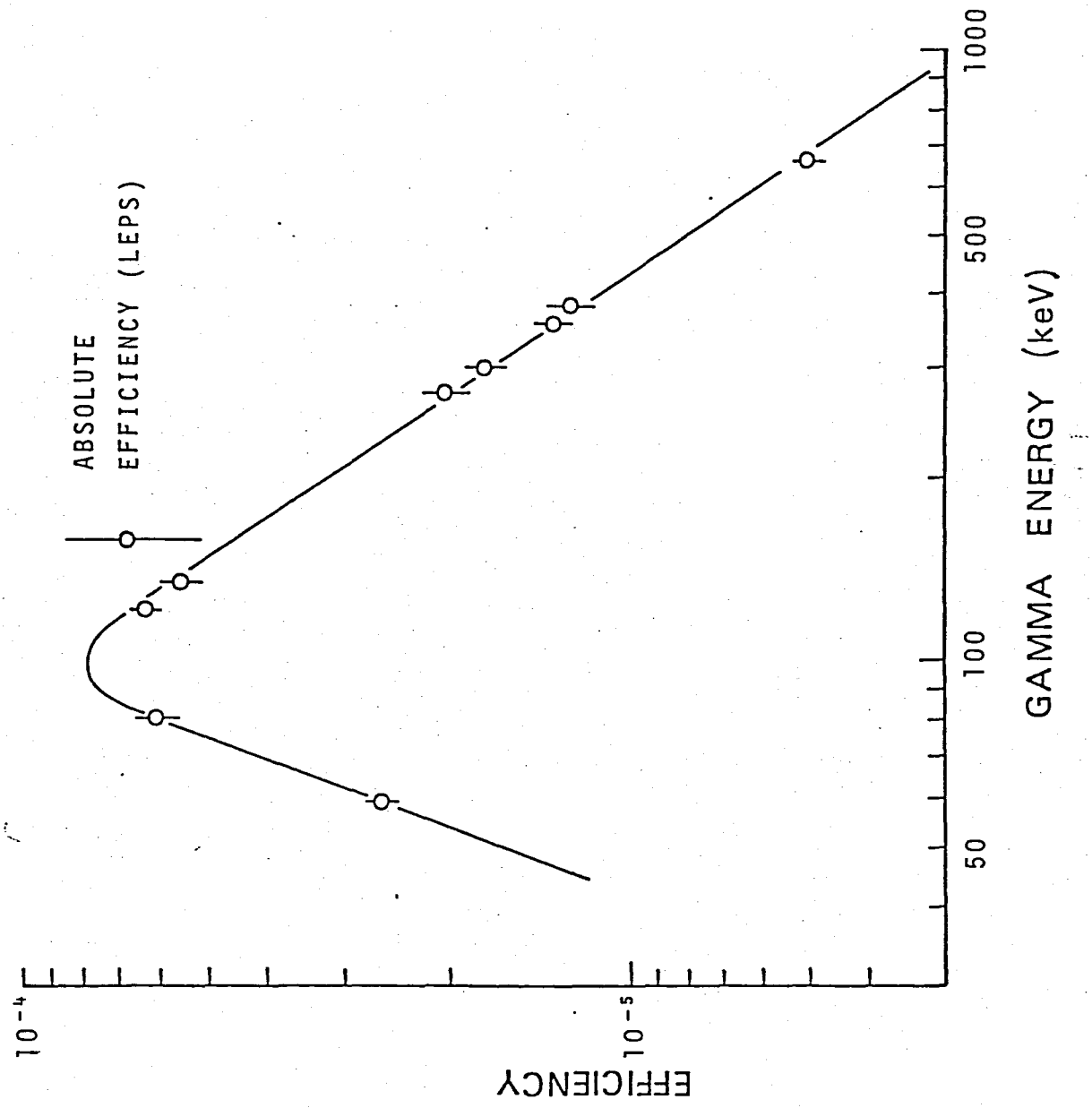
ABSOLUTE
EFFICIENCY (LEPS)
EFFICIENCY
10-4
10-5
50
100
500
1000
GAMMA ENERGY (keV)

Fig. 2-17-b

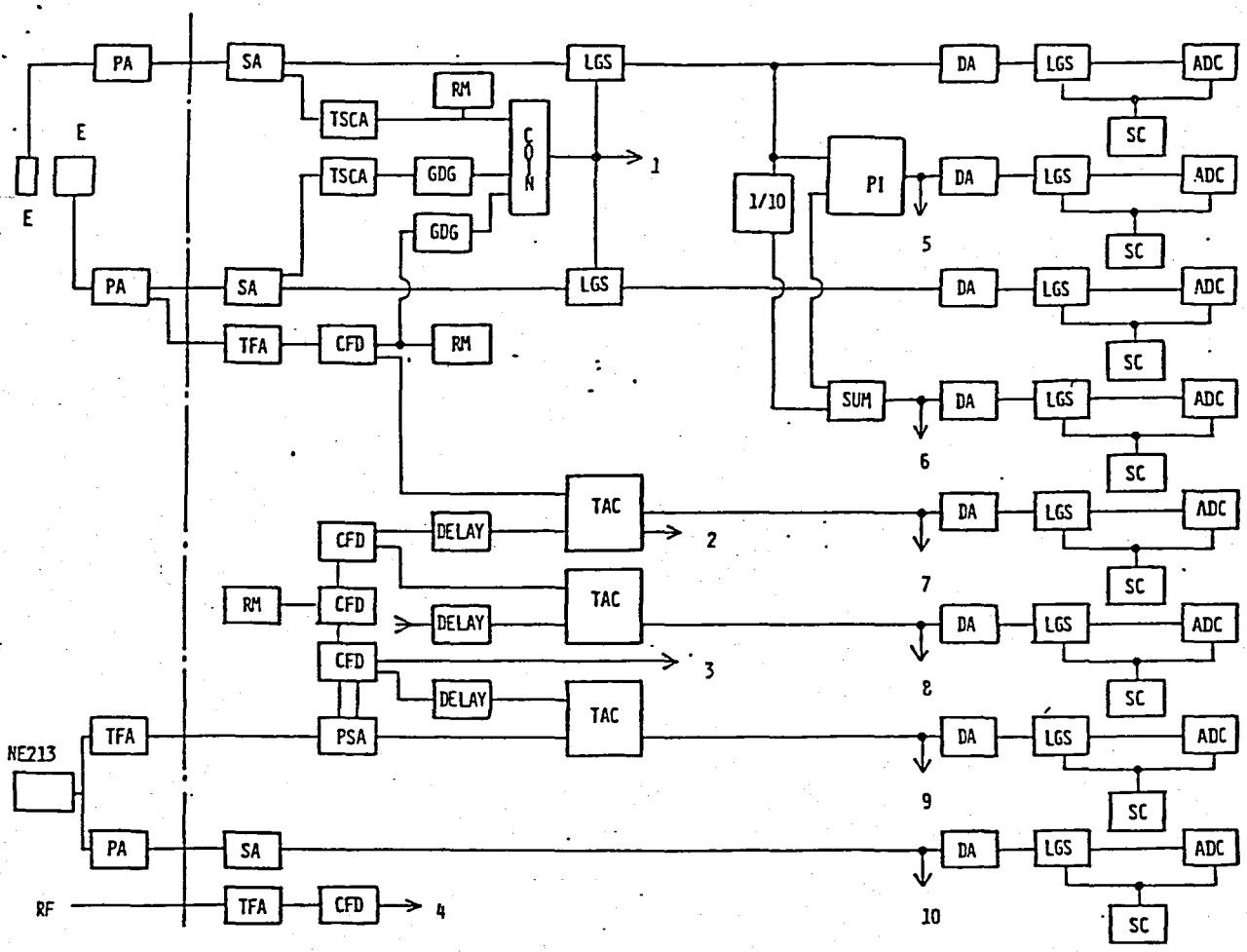
PA
SA
LGS
RM
TSCA
COIN
GDG
E
1
1/10
PI
DA
LGS
ADC
SC
5
6
SUM
TFA
CFD
TAC
DELAY
2
7
3
8
9
10
NE213
PSA
RF
4

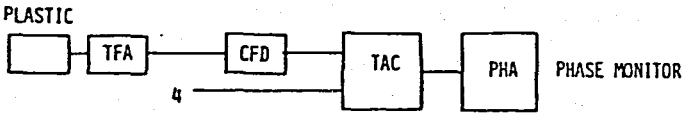
PLASTIC
TFA
CFD
TAC
PHA
PHASE MONITOR
4

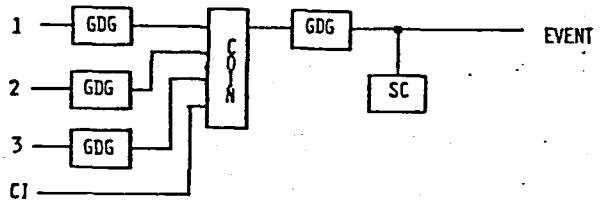
1
2
3
CJ
GDG
COIN
EVENT
SC

Fig. 2-18

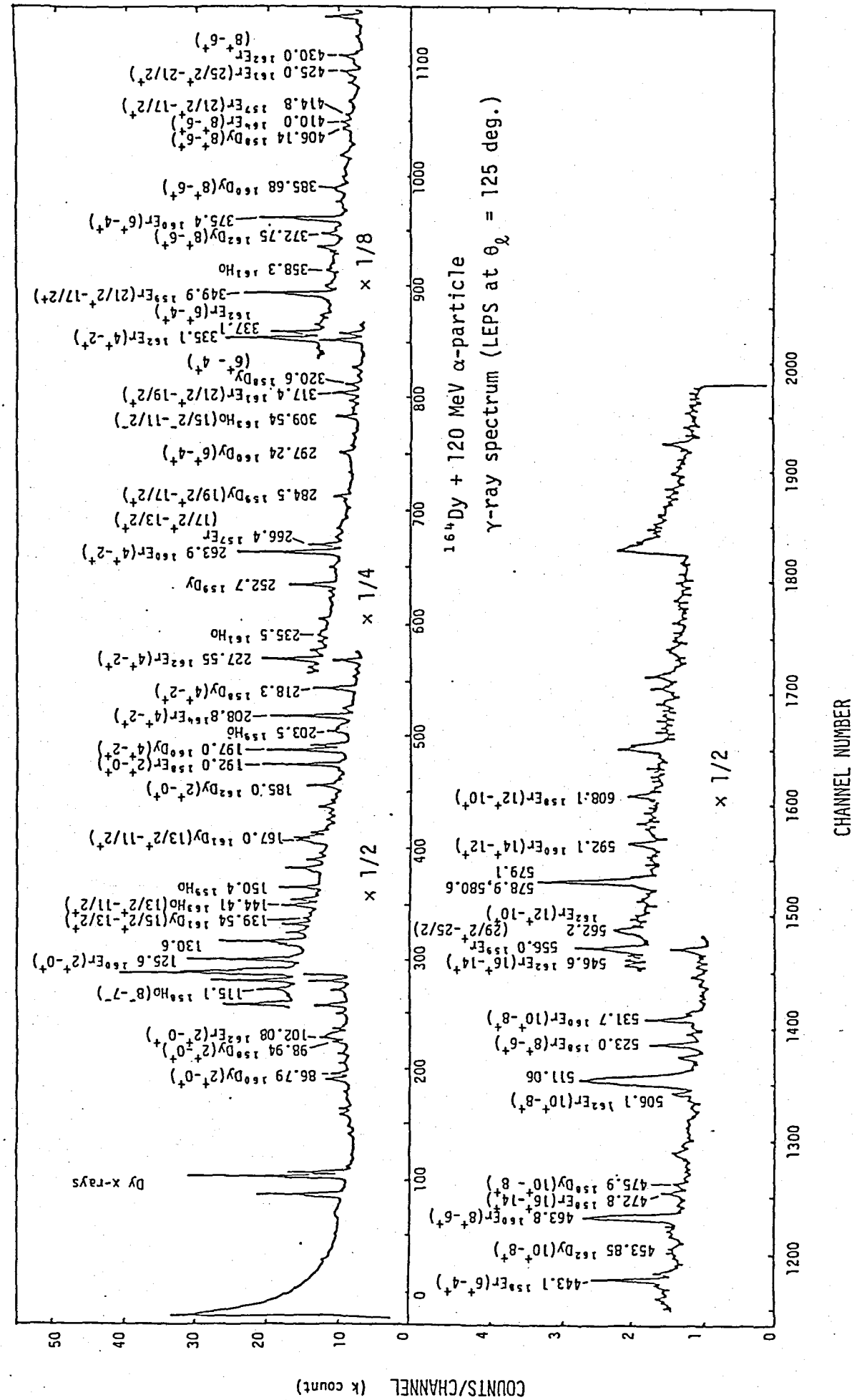
^{164}Dy + 120 MeV α-particle
γ-ray spectrum (LEPS at θ_γ = 125 deg.)
COUNTS/CHANNEL (k count)
CHANNEL NUMBER
Dy x-rays
× 1/2
× 1/4
× 1/8
× 1/2
86.79 ^{160}Dy(2$^+$-0$^+$)
98.94 ^{158}Dy(2$^+$-0$^+$)
102.08 ^{162}Er(2$^+$-0$^+$)
115.1 ^{156}Ho(8$^-$-7$^-$)
125.6 ^{160}Er(2$^+$-0$^+$)
130.6
139.54 ^{161}Dy(15/2$^+$-13/2$^+$)
144.41 ^{163}Ho(13/2$^+$-11/2$^+$)
150.4 ^{159}Ho
167.0 ^{161}Dy(13/2$^+$-11/2$^+$)
185.0 ^{162}Dy(2$^+$-0$^+$)
192.0 ^{158}Er(2$^+$-0$^+$)
197.0 ^{160}Dy(4$^+$-2$^+$)
203.5 ^{159}Ho
208.8 ^{164}Er(4$^+$-2$^+$)
218.3 ^{158}Dy(4$^+$-2$^+$)
227.55 ^{162}Er(4$^+$-2$^+$)
235.5 ^{161}Ho
252.7 ^{159}Dy
263.9 ^{160}Er(4$^+$-2$^+$)
266.4 ^{157}Er (17/2$^+$-13/2$^+$)
284.5 ^{159}Dy(19/2$^+$-17/2$^+$)
297.24 ^{160}Dy(6$^+$-4$^+$)
309.54 ^{163}Ho(15/2$^-$-11/2$^-$)
317.4 ^{161}Er(21/2$^+$-19/2$^+$)
320.6 ^{158}Dy (6$^+$- 4$^+$)
335.1 ^{162}Er(4$^+$-2$^+$)
337.1 ^{162}Er(6$^+$-4$^+$)
349.9 ^{159}Er(21/2$^+$-17/2+)
358.3 ^{161}Ho
372.75 ^{162}Dy(8$^+$-6$^+$)
375.4 ^{160}Er(6$^+$-4$^+$)
385.68 ^{160}Dy(8$^+$-6$^+$)
406.14 ^{158}Dy(8$^+$-6$^+$)
410.0 ^{164}Er(8$^+$-6$^+$)
414.8 ^{157}Er(21/2$^+$-17/2$^+$)
425.0 ^{161}Er(25/2$^+$-21/2$^+$)
430.0 ^{162}Er (8$^+$-6$^+$)
443.1 ^{158}Er(6$^+$-4$^+$)
453.85 ^{162}Dy(10$^+$-8$^+$)
463.8 ^{160}Er(8$^+$-6$^+$)
472.8 ^{158}Er(16$^+$-14$^+$)
475.9 ^{158}Dy(10$^+$- 8$^+$)
506.1 ^{162}Er(10$^+$-8$^+$)
511.06
523.0 ^{158}Er(8$^+$-6$^+$)
531.7 ^{160}Er(10$^+$-8$^+$)
546.6 ^{162}Er(16$^+$-14$^+$)
556.0 ^{159}Er
562.2 (29/2$^+$-25/2)
^{162}Er(12$^+$-10$^+$)
578.9,580.6
579.1
592.1 ^{160}Er(14$^+$-12$^+$)
608.1 ^{158}Er(12$^+$-10$^+$)

Fig. 3-1

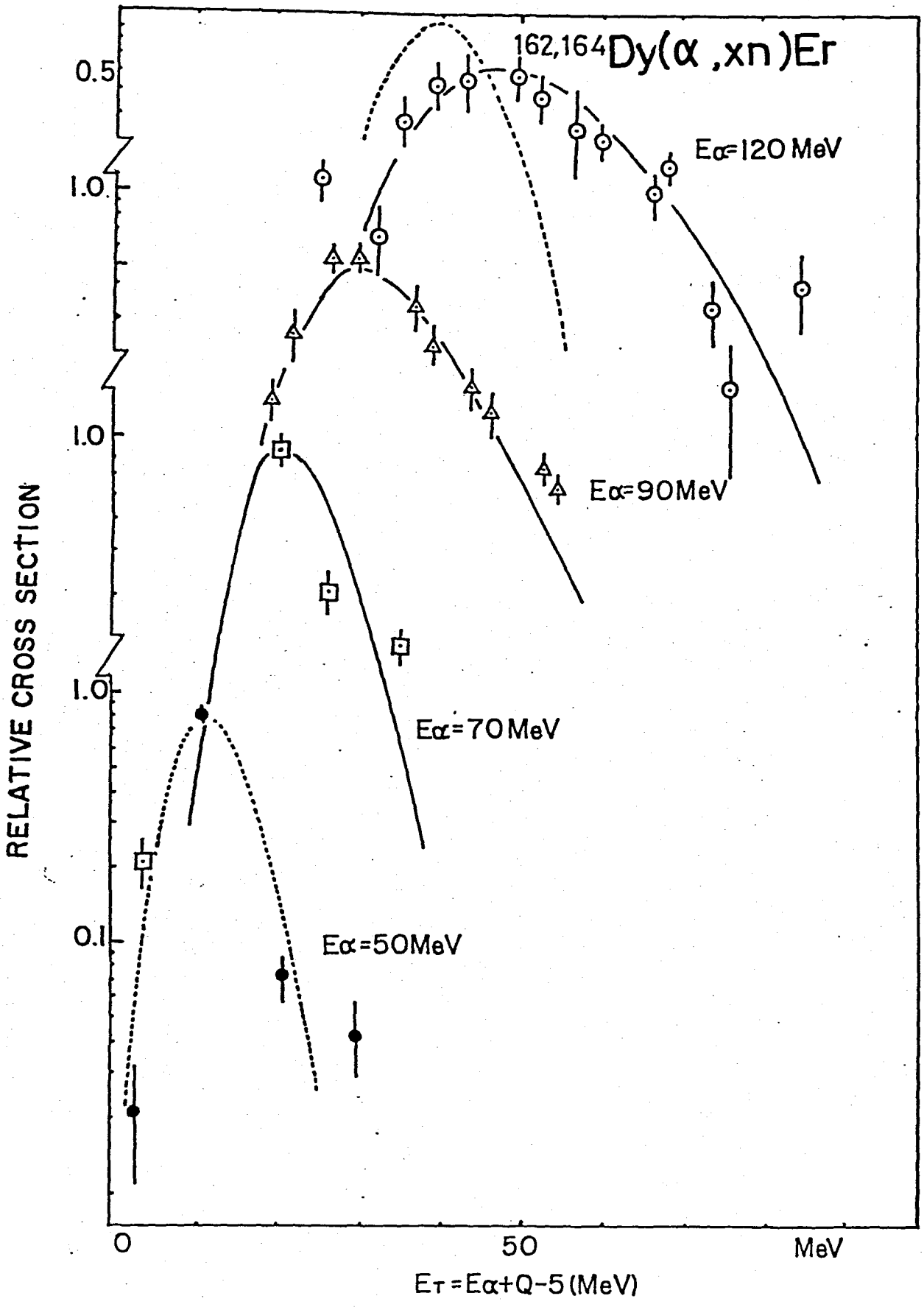
162,164Dy(α ,xn)Er
Eα=120 MeV
Eα=90MeV
Eα=70MeV
Eα=50MeV
RELATIVE CROSS SECTION
0.5
1.0
1.0
1.0
0.1
0
50
MeV
ET=Eα+Q-5(MeV)

Fig. 3-2

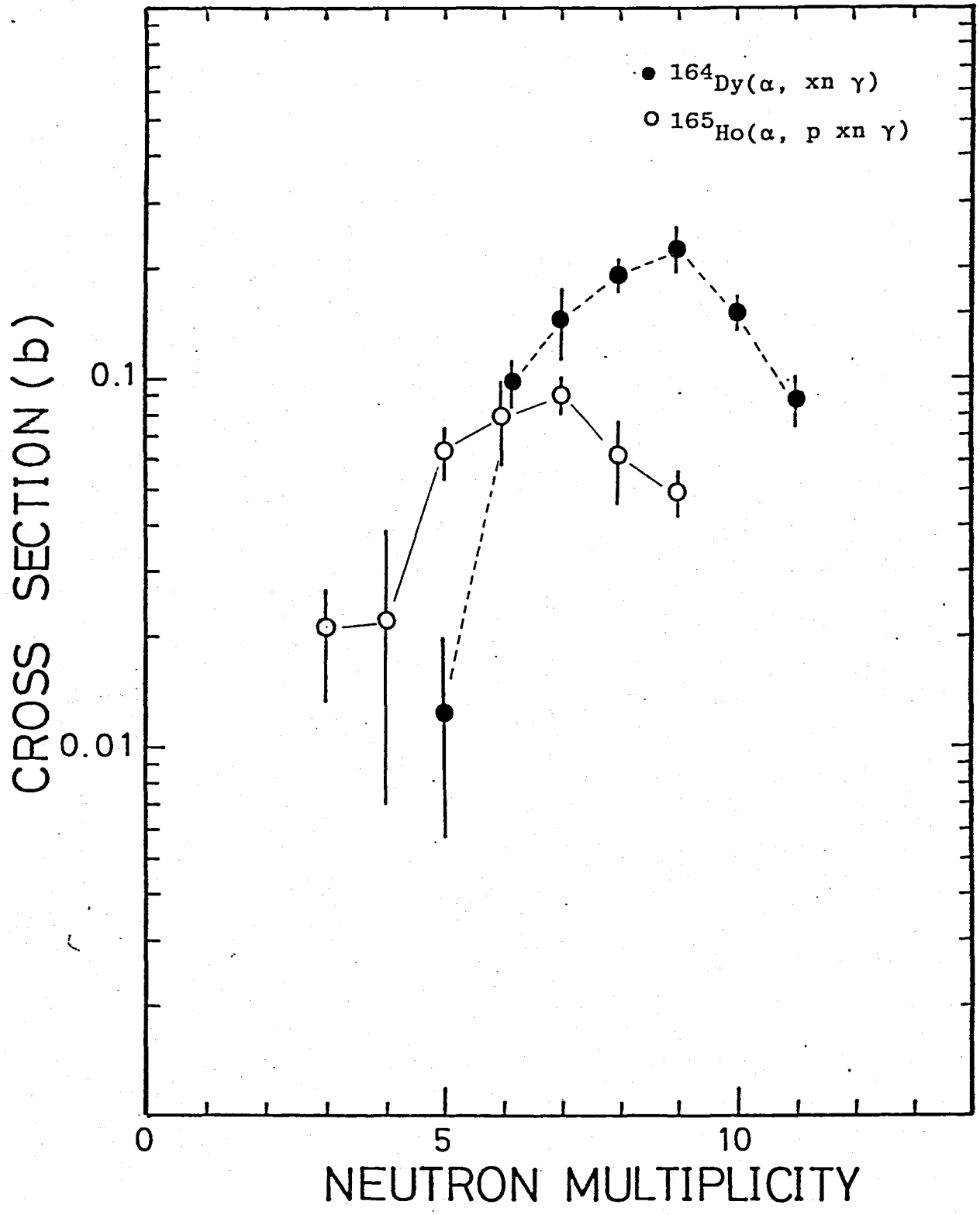
● 164Dy(α, xn γ)
○ 165Ho(α, p xn γ)
CROSS SECTION (b)
0.1
0.01
0
5
10
NEUTRON MULTIPLICITY

Fig. 3-3

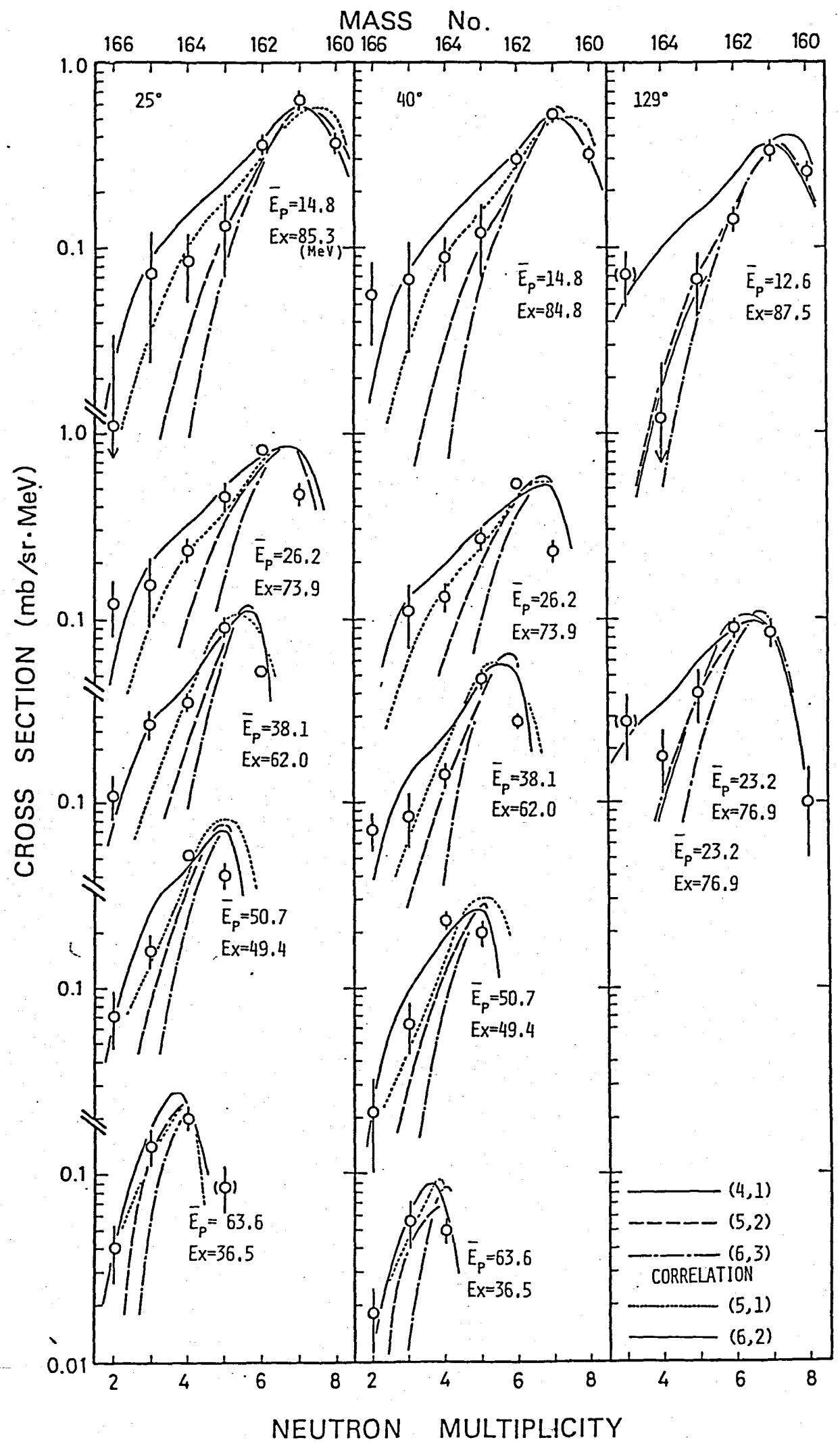
MASS No.
166
164
162
160
25°
40°
129°
$\bar{E}_p$=14.8
Ex=85.3
(MeV)
$\bar{E}_p$=14.8
Ex=84.8
$\bar{E}_p$=12.6
Ex=87.5
$\bar{E}_p$=26.2
Ex=73.9
$\bar{E}_p$=26.2
Ex=73.9
$\bar{E}_p$=38.1
Ex=62.0
$\bar{E}_p$=38.1
Ex=62.0
$\bar{E}_p$=23.2
Ex=76.9
$\bar{E}_p$=23.2
Ex=76.9
$\bar{E}_p$=50.7
Ex=49.4
$\bar{E}_p$=50.7
Ex=49.4
$\bar{E}_p$= 63.6
Ex=36.5
$\bar{E}_p$=63.6
Ex=36.5
(4,1)
(5,2)
(6,3)
CORRELATION
(5,1)
(6,2)
CROSS SECTION (mb/sr·MeV)
1.0
0.1
0.01
2
4
6
8
NEUTRON MULTIPLICITY

Fig. 3-4

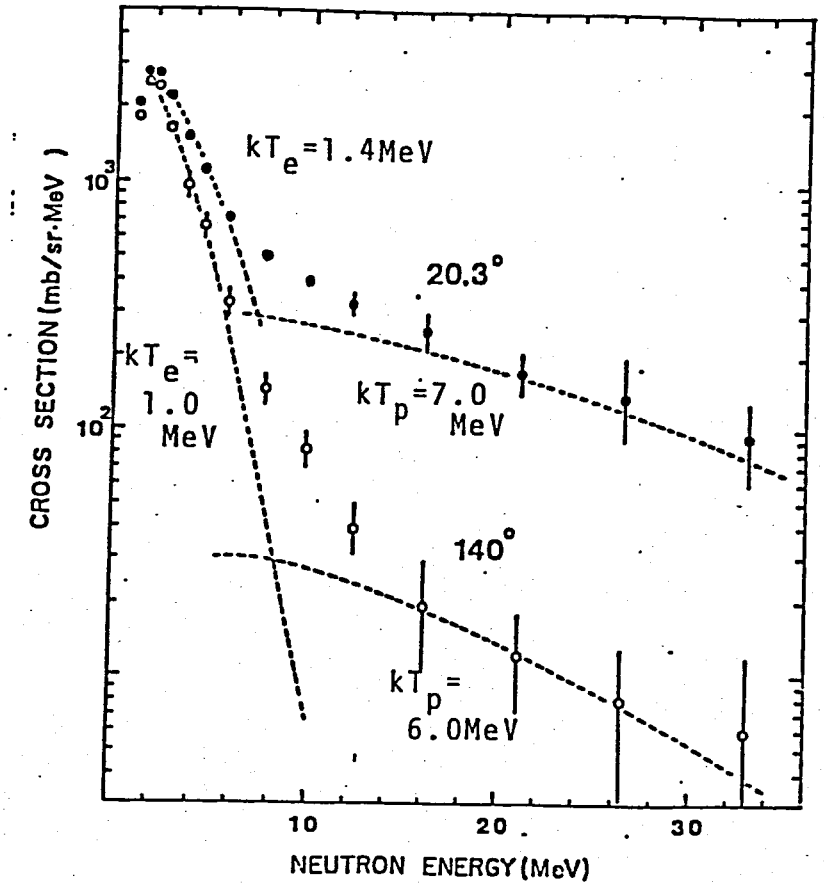
CROSS SECTION (mb/sr·MeV)
kT_e=1.4MeV
20.3°
kT_e= 1.0 MeV
kT_p=7.0 MeV
140°
kT_p= 6.0MeV
10
20
30
NEUTRON ENERGY(MeV)

Fig. 3-5

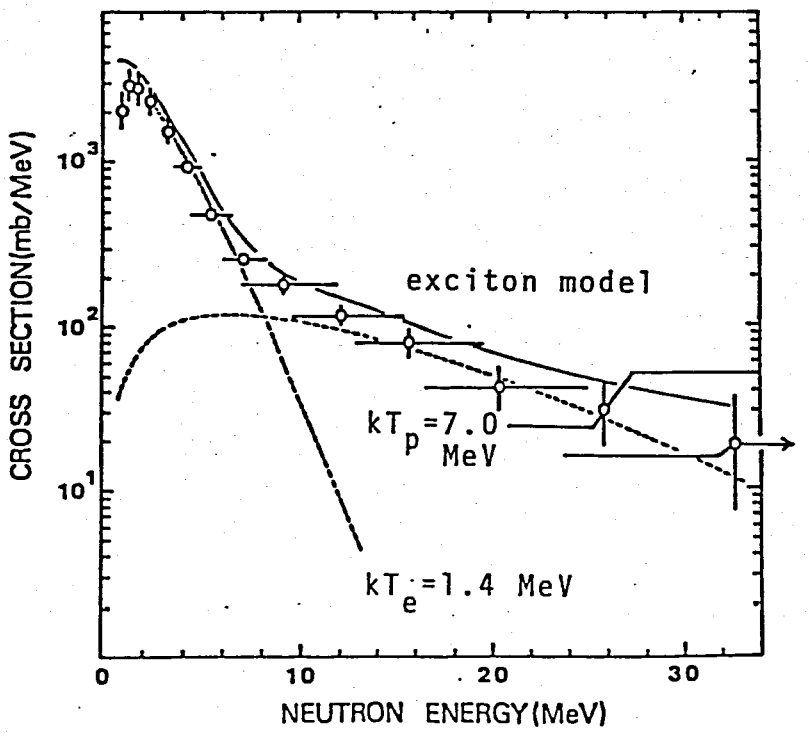
CROSS SECTION(mb/MeV)
exciton model
kT_p=7.0 MeV
kT_e=1.4 MeV
0
10
20
30
NEUTRON ENERGY(MeV)

Fig. 3-6

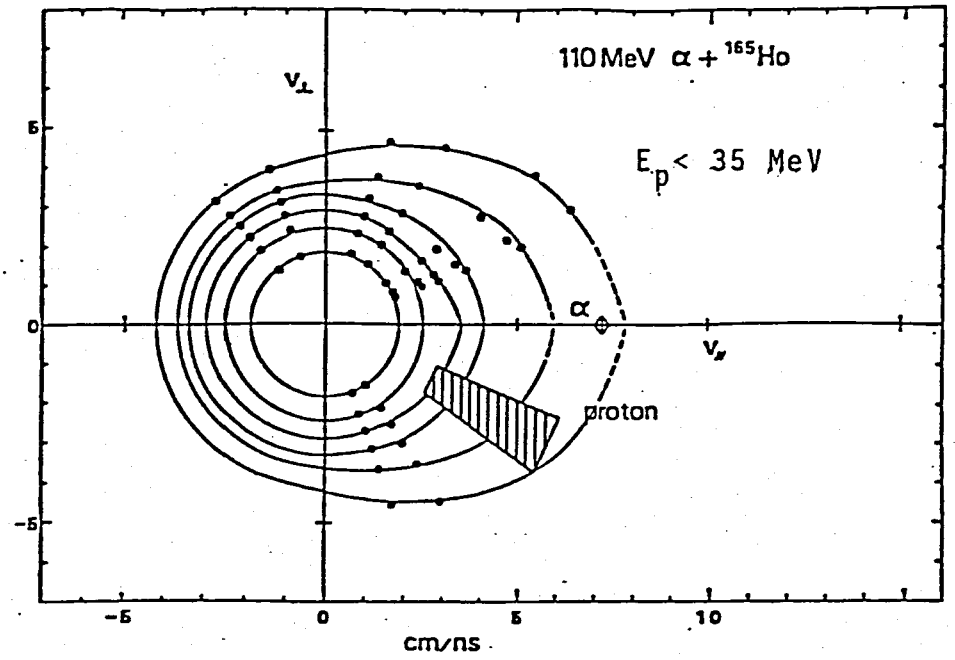
110 MeV α + 165Ho
E_p < 35 MeV
V⊥
V∥
α
proton
cm/ns

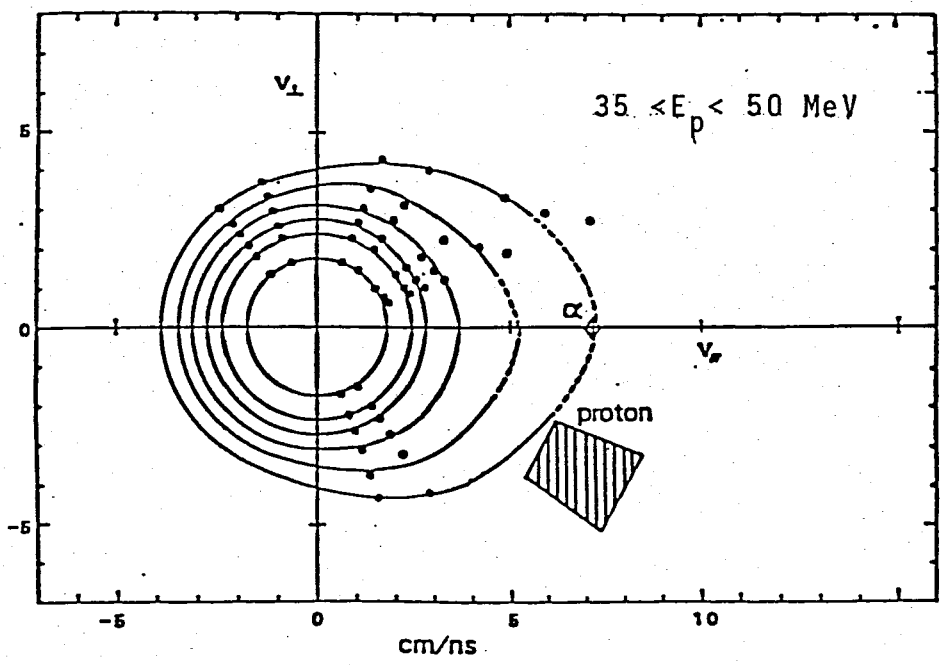
35 < E_p < 50 MeV
V⊥
V∥
α
proton
cm/ns

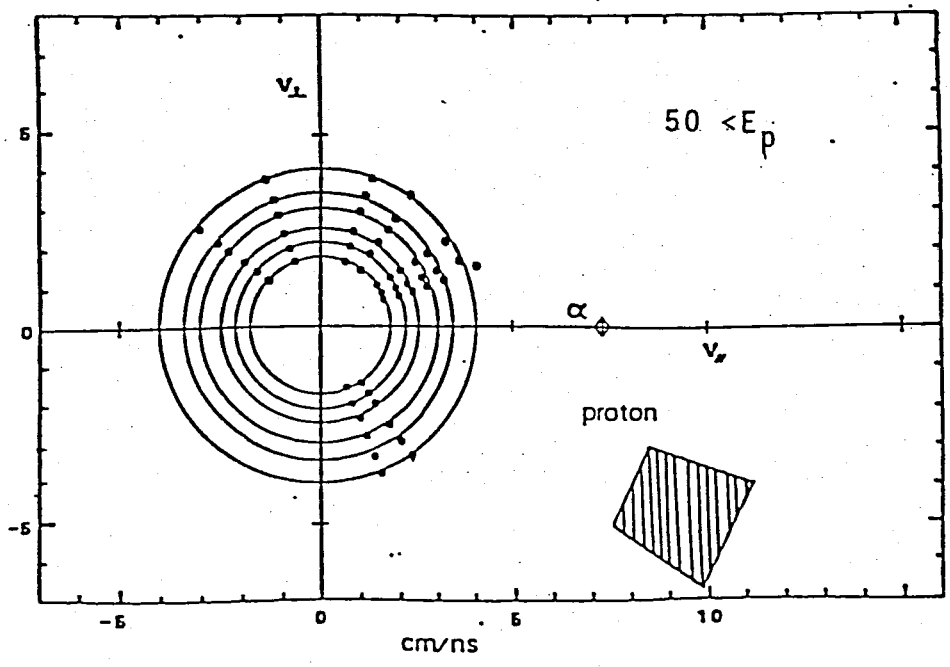
50 < E_p
V⊥
V∥
α
proton
cm/ns

Fig. 3-7

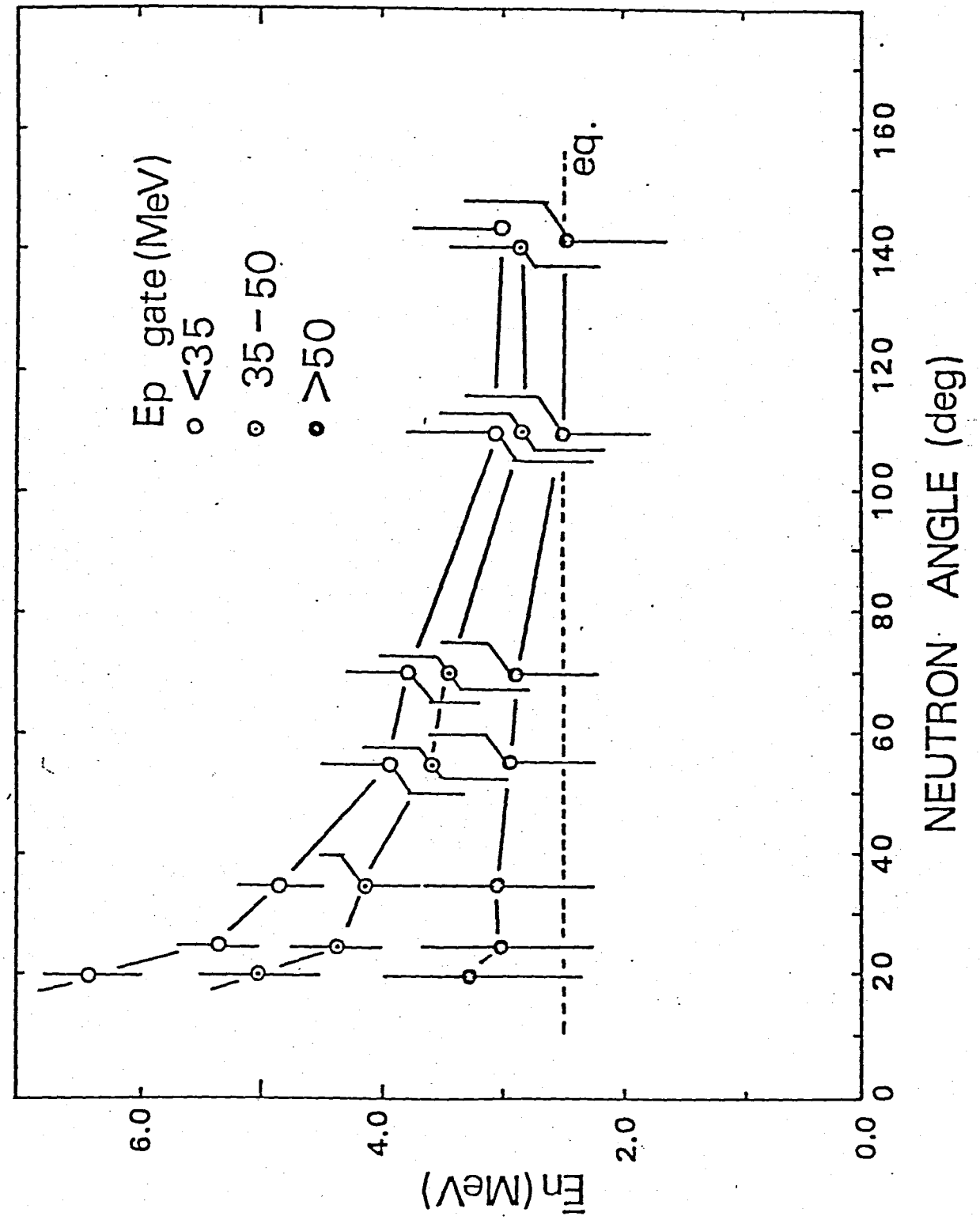
Ep gate (MeV)
o <35
o 35-50
o >50
eq.
En (MeV)
6.0
4.0
2.0
0.0
0
20
40
60
80
100
120
140
160
NEUTRON ANGLE (deg)

Fig. 3-8

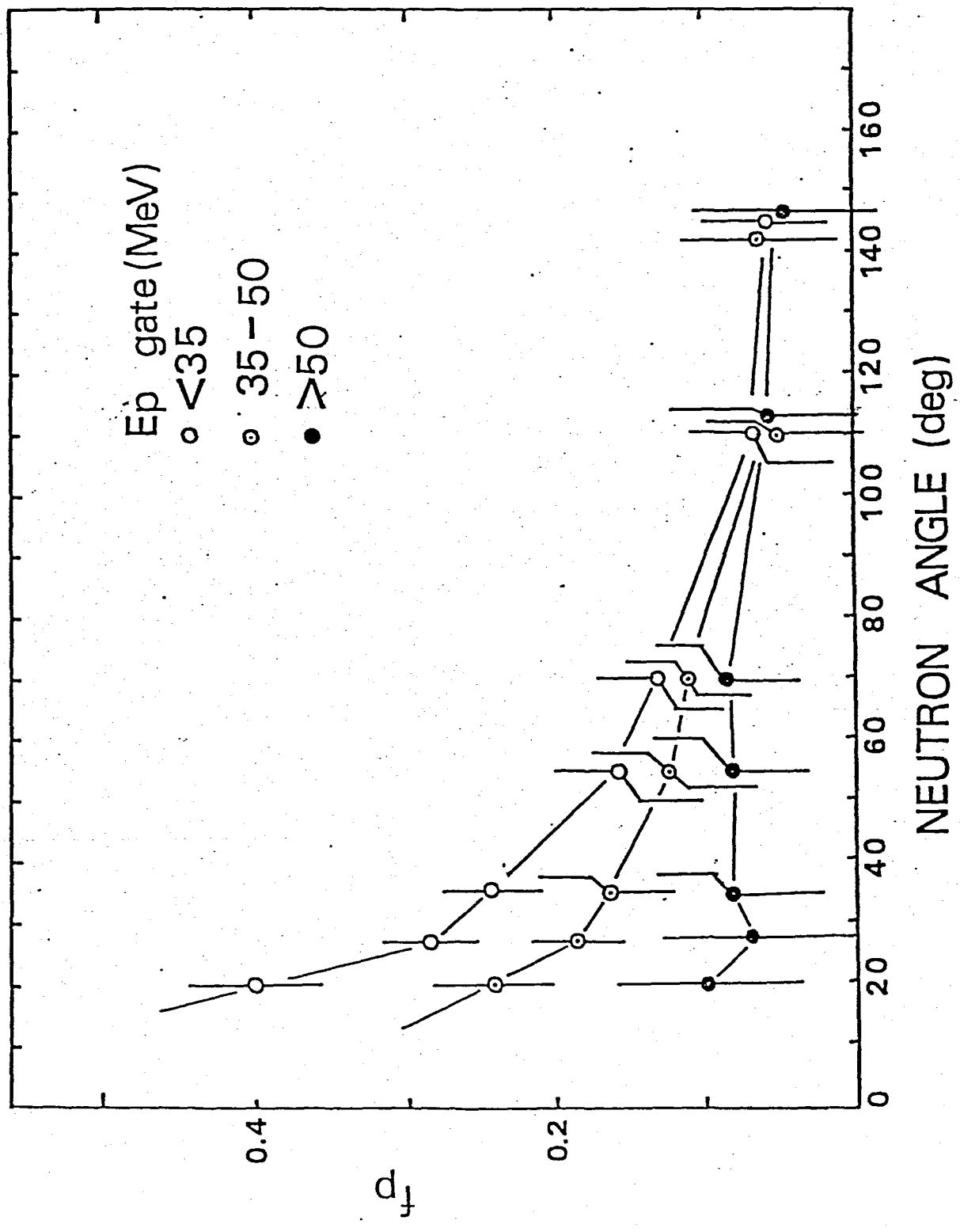
Ep gate (MeV)
○ <35
⊙ 35 - 50
● ≥50
NEUTRON ANGLE (deg)
0
20
40
60
80
100
120
140
160
0.4
0.2
d_f

Fig. 3-9

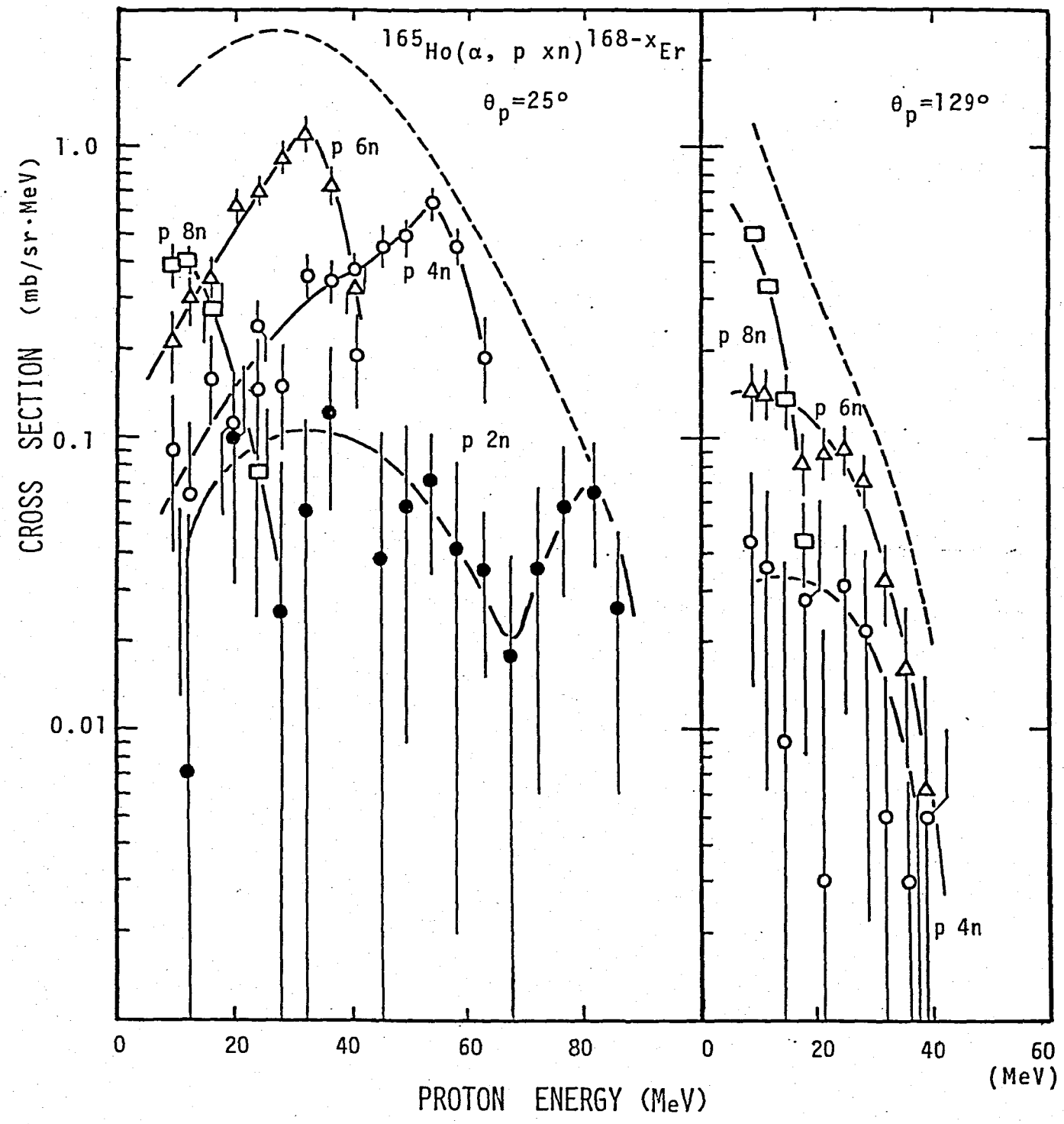
^{165}Ho(α, p xn)$^{168-x}$Er
θp=25°
θp=129°
p 8n
p 6n
p 4n
p 2n
CROSS SECTION (mb/sr·MeV)
1.0
0.1
0.01
0
20
40
60
80
0
20
40
60
(MeV)
PROTON ENERGY (MeV)

Fig. 3-10-a

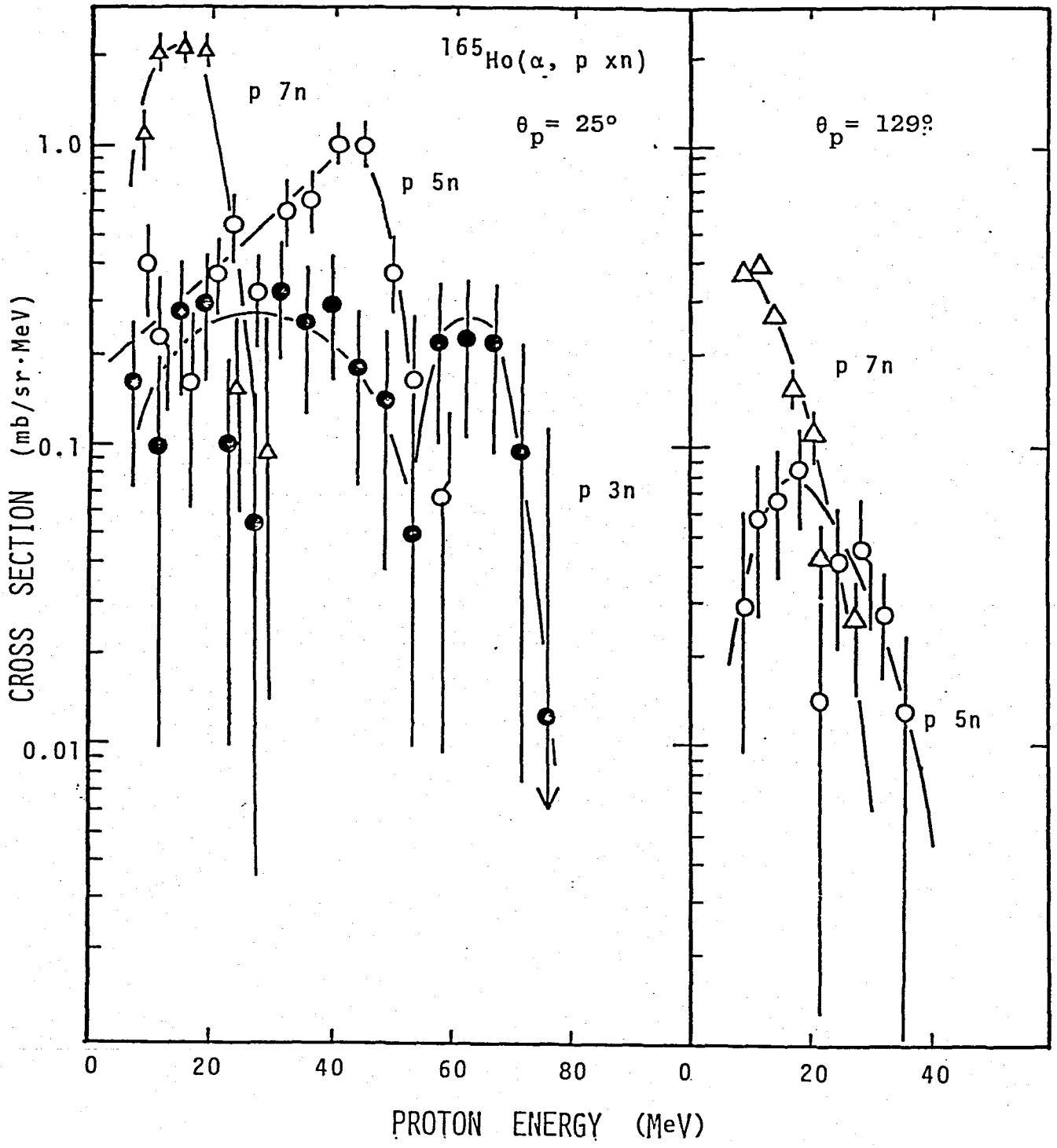
^{165}Ho(α, p xn)
p 7n
p 5n
p 3n
θ_p= 25°
θ_p= 129°
p 7n
p 5n
1.0
0.1
0.01
CROSS SECTION (mb/sr·MeV)
0
20
40
60
80
0
20
40
PROTON ENERGY (MeV)

Fig. 3-10-b

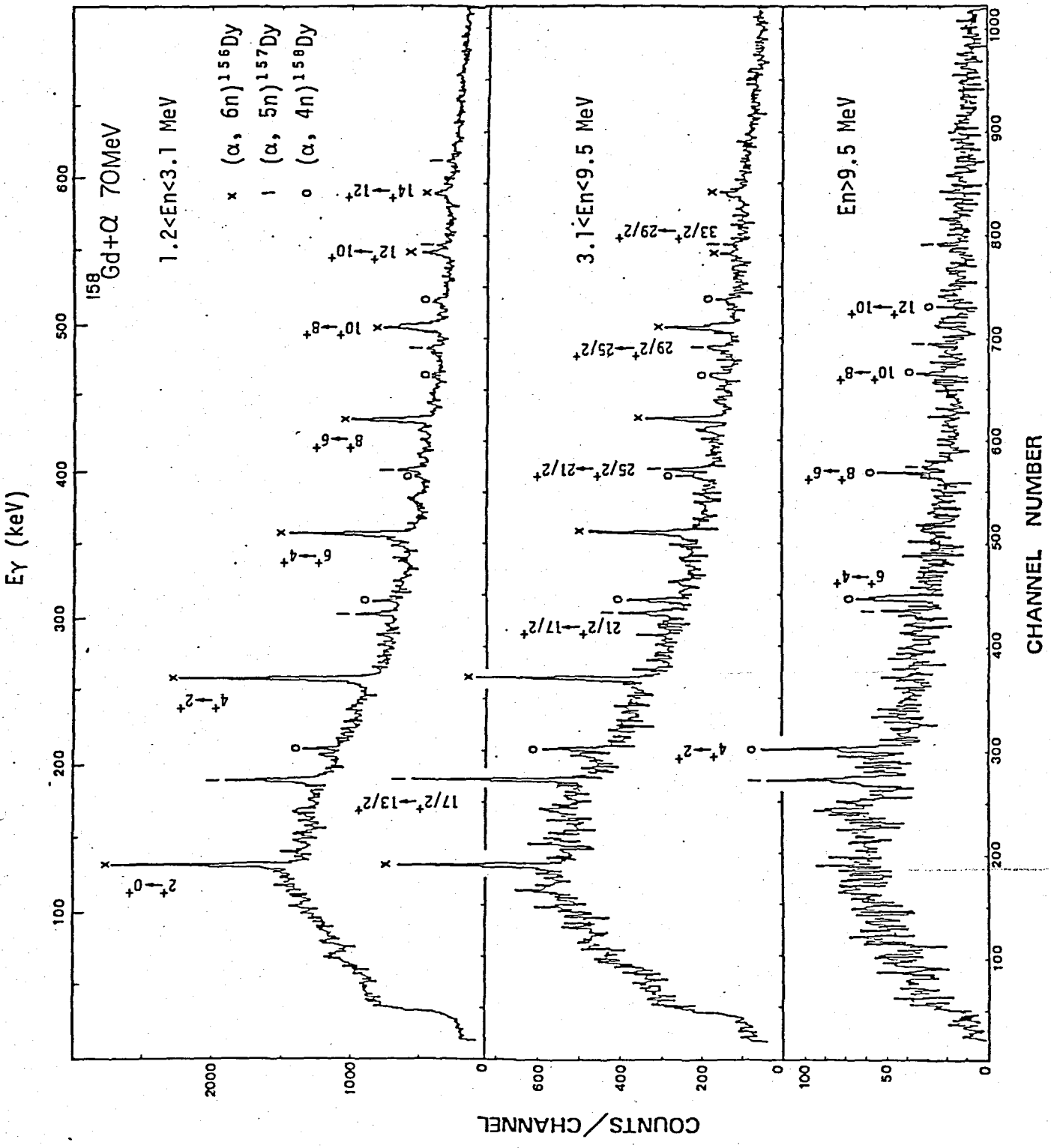
158Gd+α 70MeV
1.2<En<3.1 MeV
3.1<En<9.5 MeV
En>9.5 MeV
× (α, 6n)156Dy
| (α, 5n)157Dy
○ (α, 4n)158Dy
Eγ (keV)
COUNTS/CHANNEL
CHANNEL NUMBER

Fig. 3-11

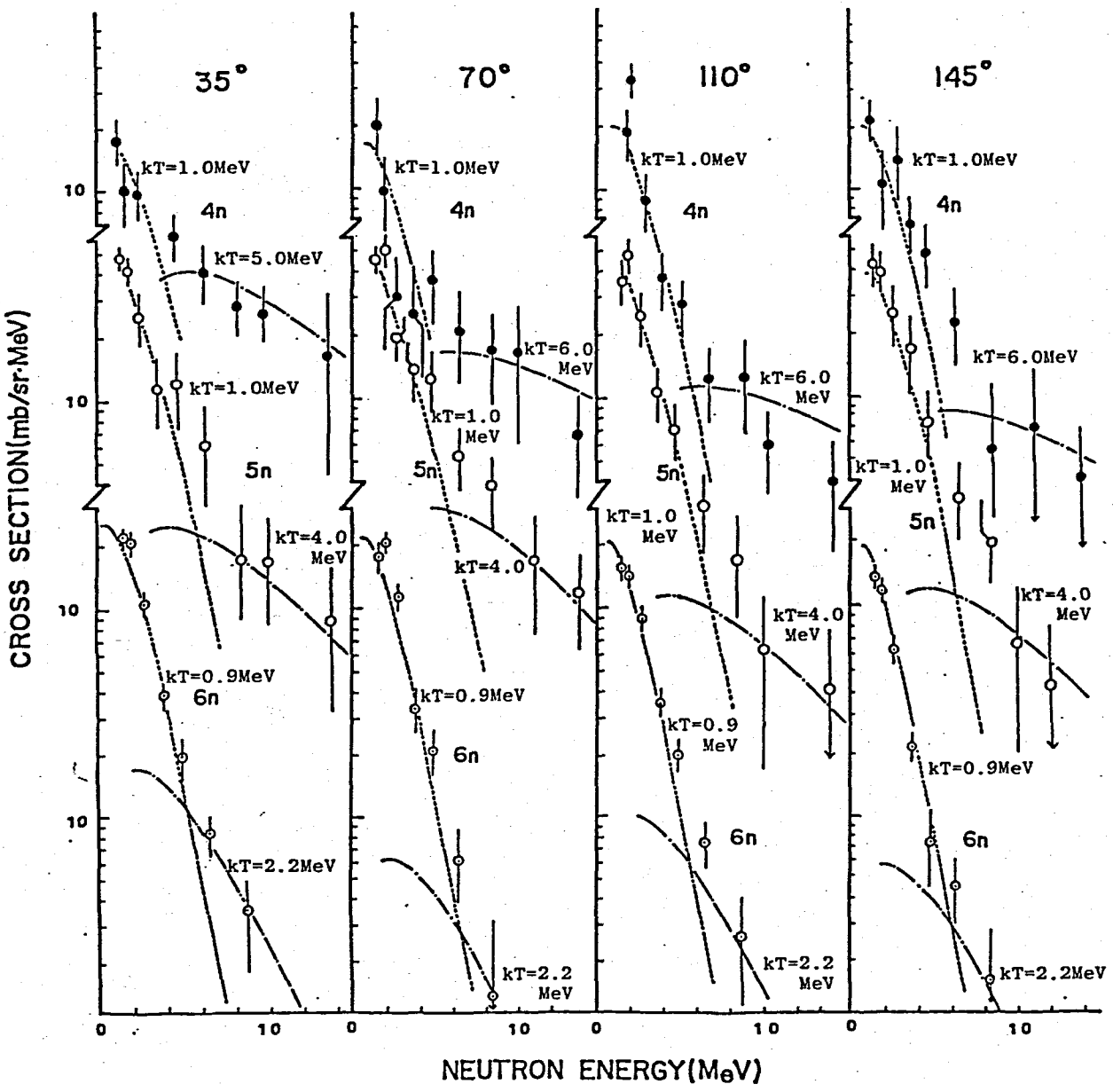
35°
70°
110°
145°
kT=1.0MeV
4n
kT=5.0MeV
kT=1.0MeV
5n
kT=4.0 MeV
kT=0.9MeV
6n
kT=2.2MeV
kT=6.0 MeV
kT=1.0 MeV
kT=4.0
kT=0.9MeV
kT=2.2 MeV
kT=6.0MeV
kT=0.9 MeV
CROSS SECTION(mb/sr·MeV)
NEUTRON ENERGY(MeV)

Fig. 3-12

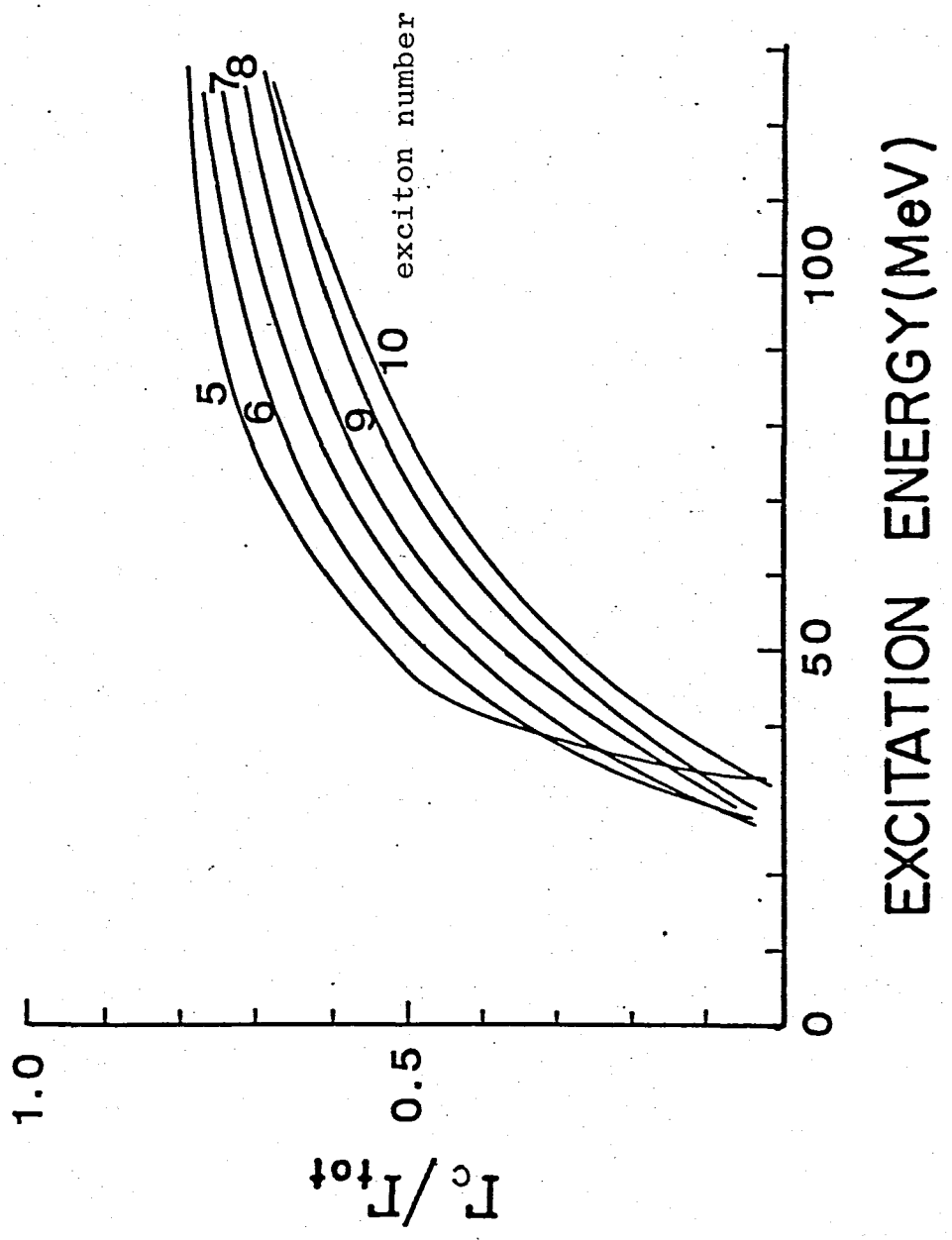
Γ_c/Γ_{tot}
1.0
0.5
0
50
100
EXCITATION ENERGY(MeV)
exciton number
5
6
7
8
9
10

Fig. 4-1

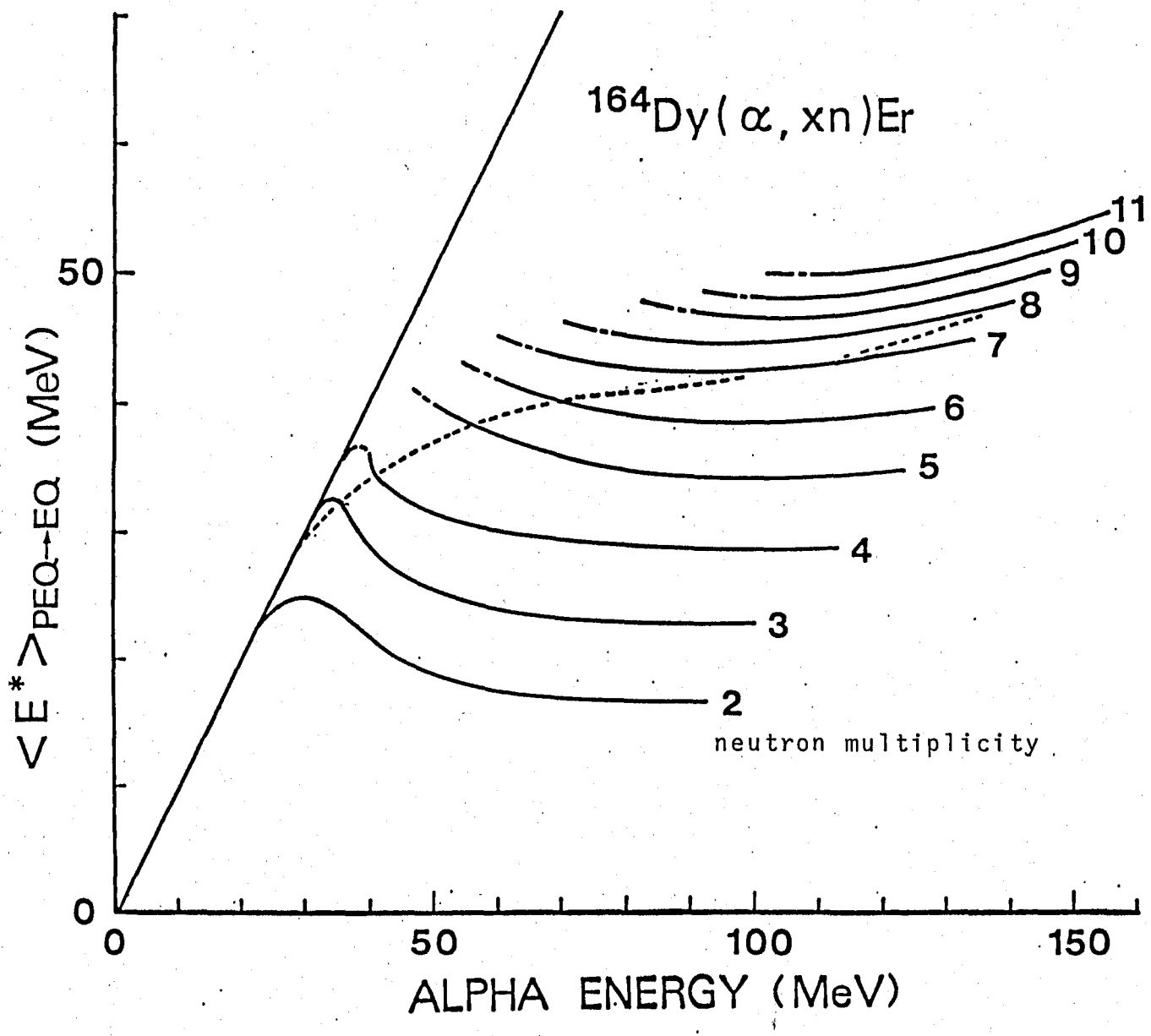
^{164}Dy(α, xn)Er
11
10
9
8
7
6
5
4
3
2
neutron multiplicity
50
0
$\langle E^* \rangle_{PEQ \to EQ}$ (MeV)
0
50
100
150
ALPHA ENERGY (MeV)

Fig. 4-2

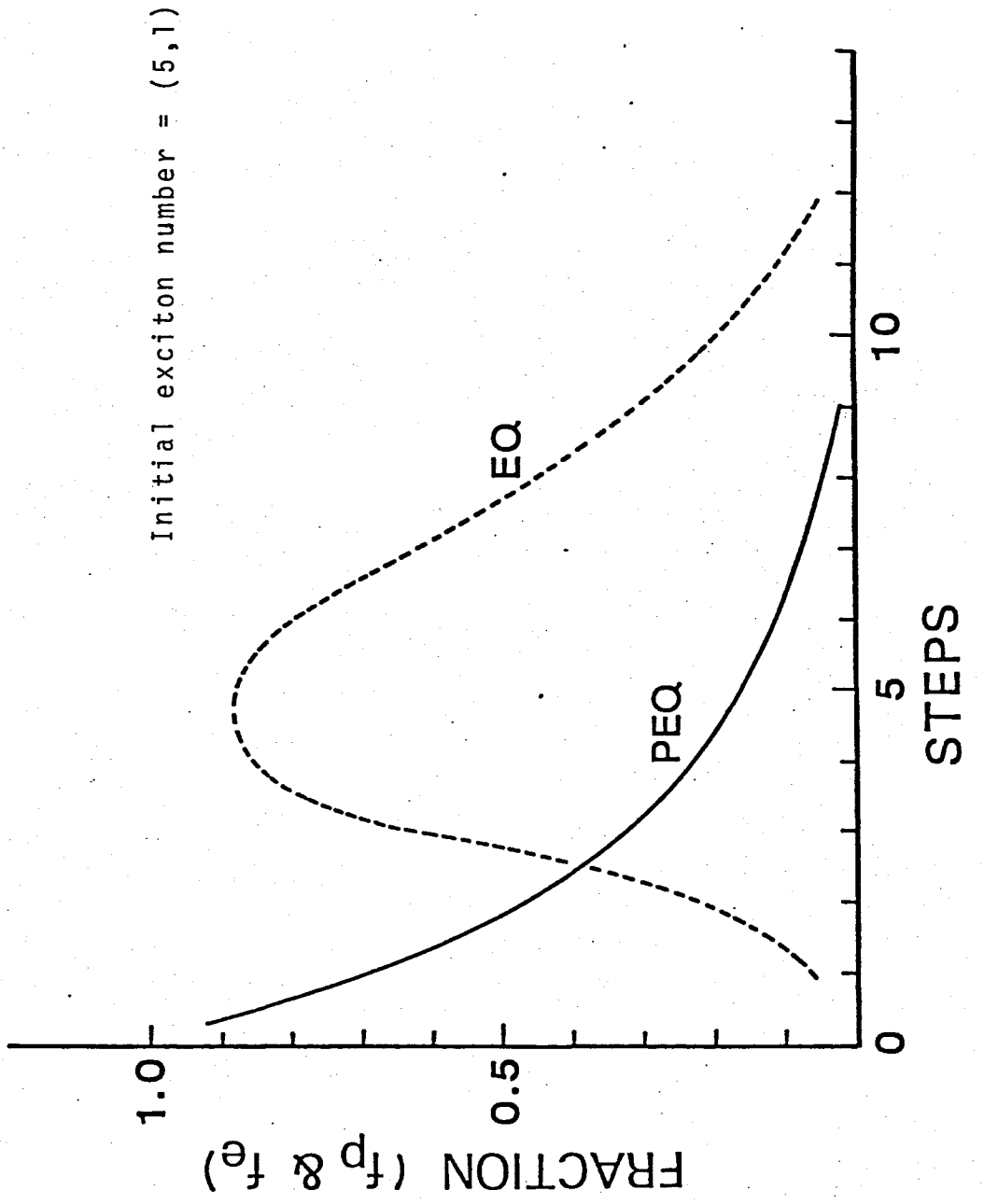
Initial exciton number = (5,1)
EQ
PEQ
1.0
0.5
0
5
10
STEPS
FRACTION (fp & fe)

Fig. 4-3

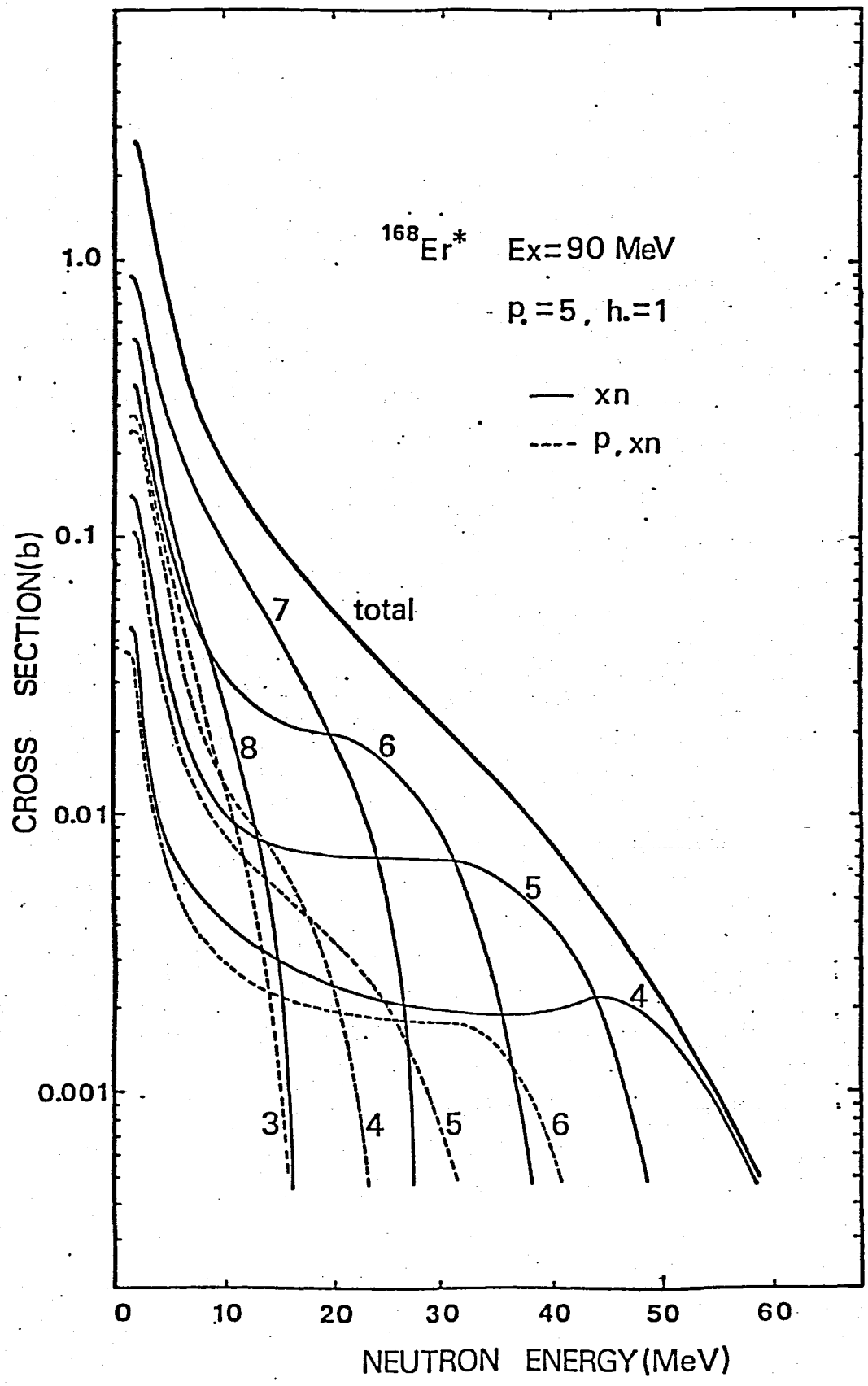
^{168}Er* Ex=90 MeV
p.=5, h.=1
xn
p, xn
total
7
8
6
5
4
3
4
5
6
1.0
0.1
0.01
0.001
CROSS SECTION(b)
0
10
20
30
40
50
60
NEUTRON ENERGY(MeV)

Fig. 4-4

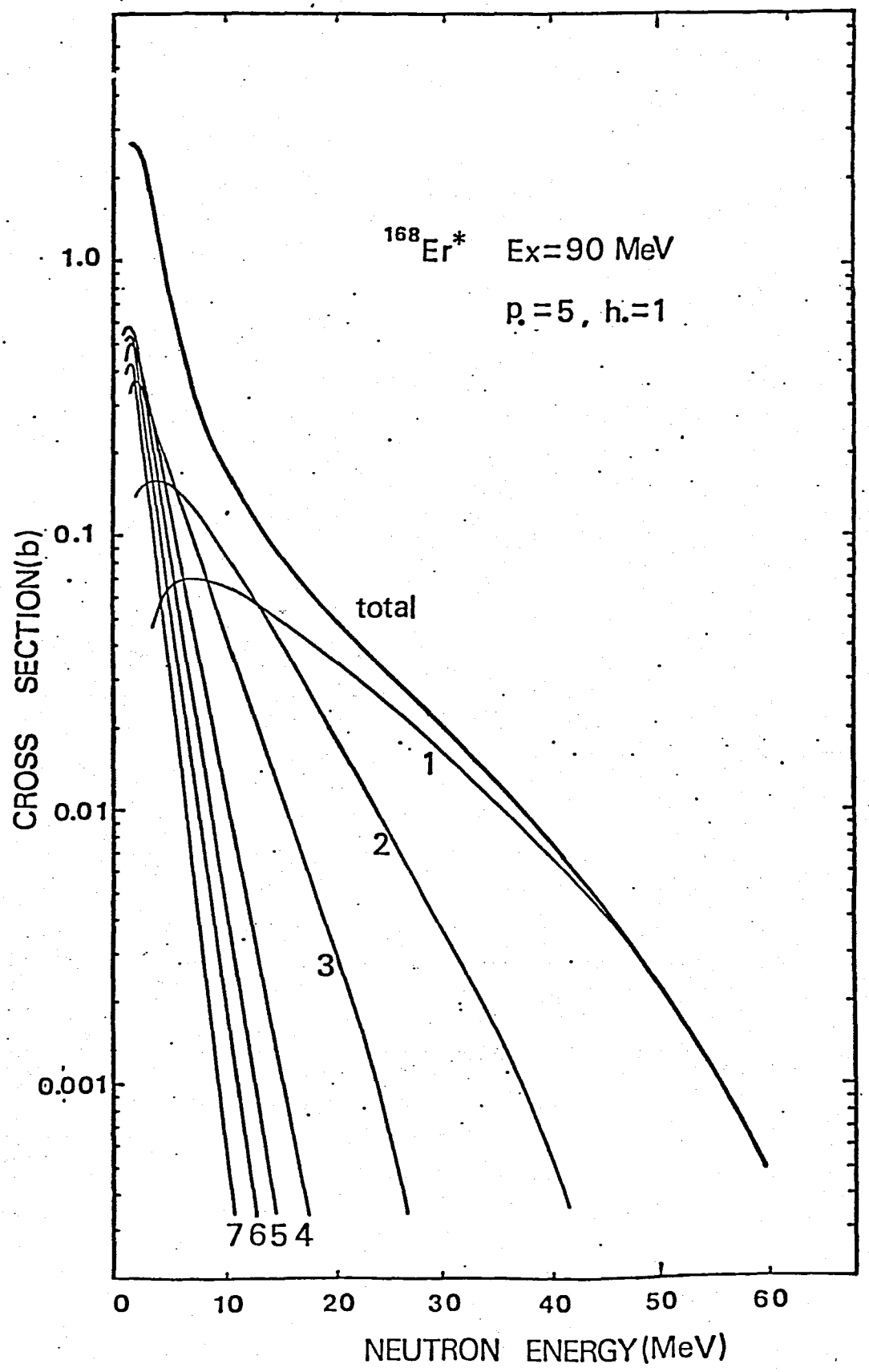
^{168}Er* Ex=90 MeV
p.=5, h.=1
1.0
0.1
0.01
0.001
CROSS SECTION(b)
total
1
2
3
7 6 5 4
0
10
20
30
40
50
60
NEUTRON ENERGY(MeV)

Fig. 4-5

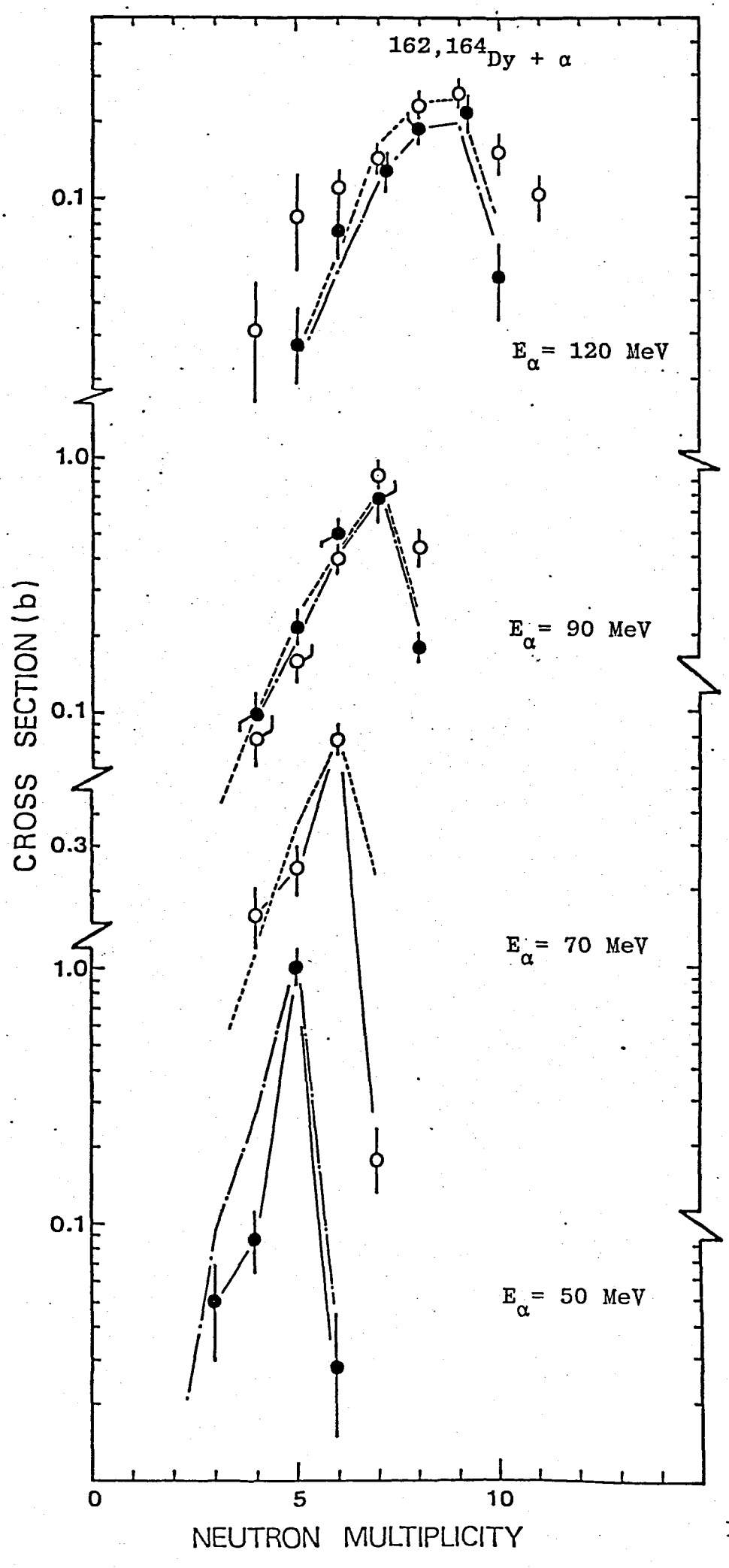
162,164Dy + α
Eα= 120 MeV
Eα= 90 MeV
Eα= 70 MeV
Eα= 50 MeV
CROSS SECTION (b)
NEUTRON MULTIPLICITY
0.1
1.0
0.1
0.3
1.0
0.1
0
5
10

Fig. 4-6-a

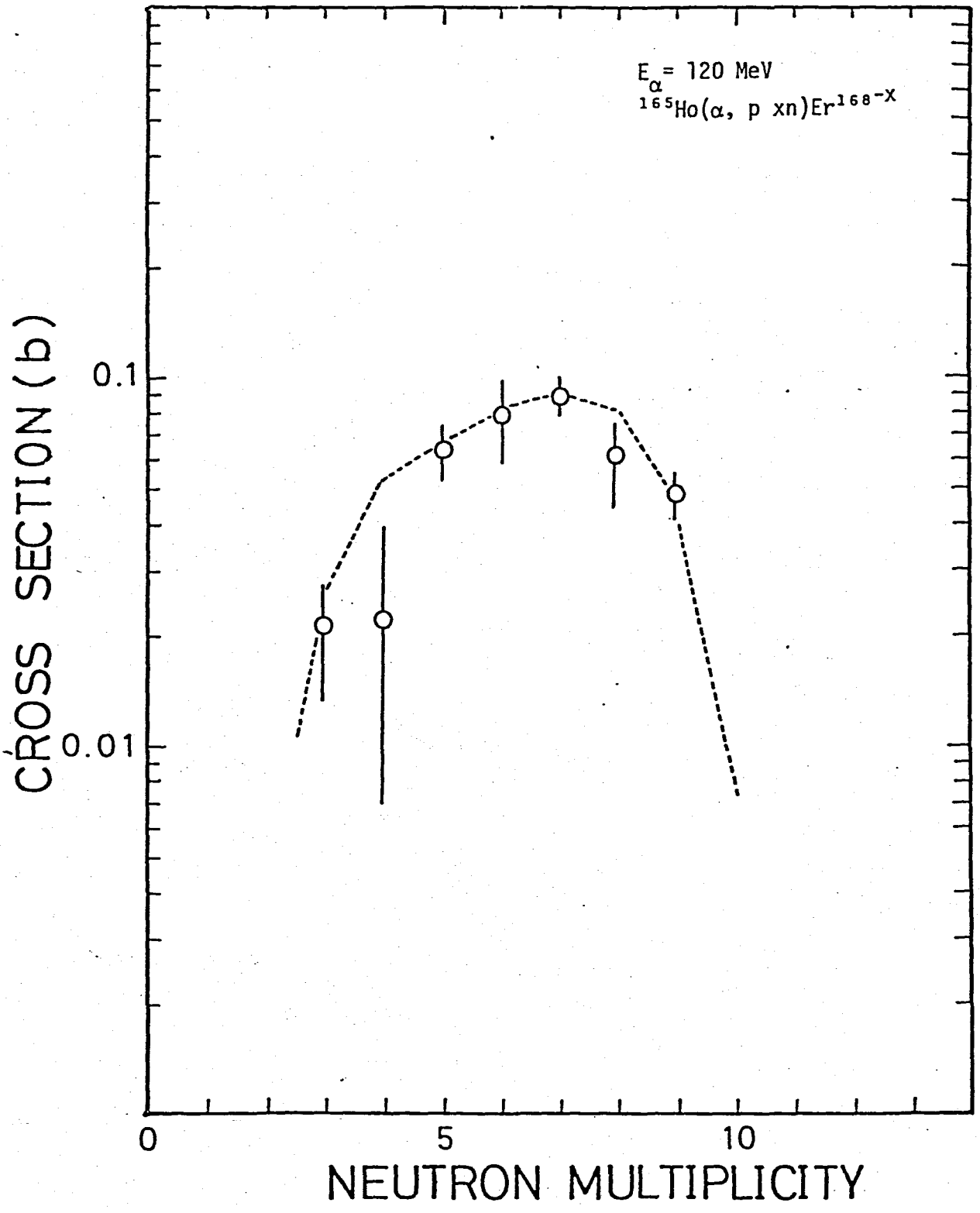
E_α = 120 MeV
^{165}Ho(α, p xn)Er^{168-x}
CROSS SECTION (b)
0.1
0.01
0
5
10
NEUTRON MULTIPLICITY

Fig. 4-6-b

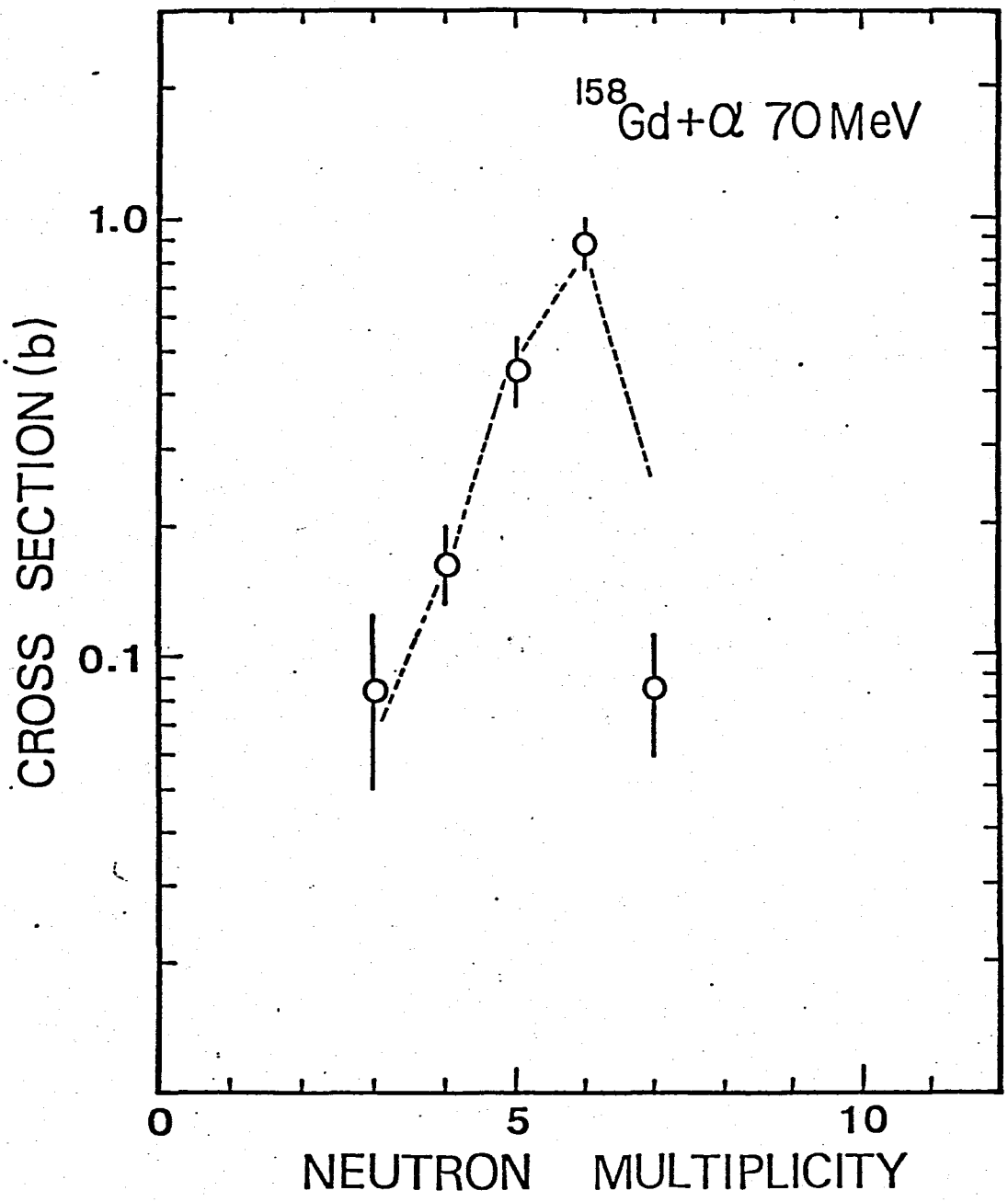
158Gd+α 70MeV
1.0
0.1
CROSS SECTION (b)
0
5
10
NEUTRON MULTIPLICITY

Fig. 4-6-c

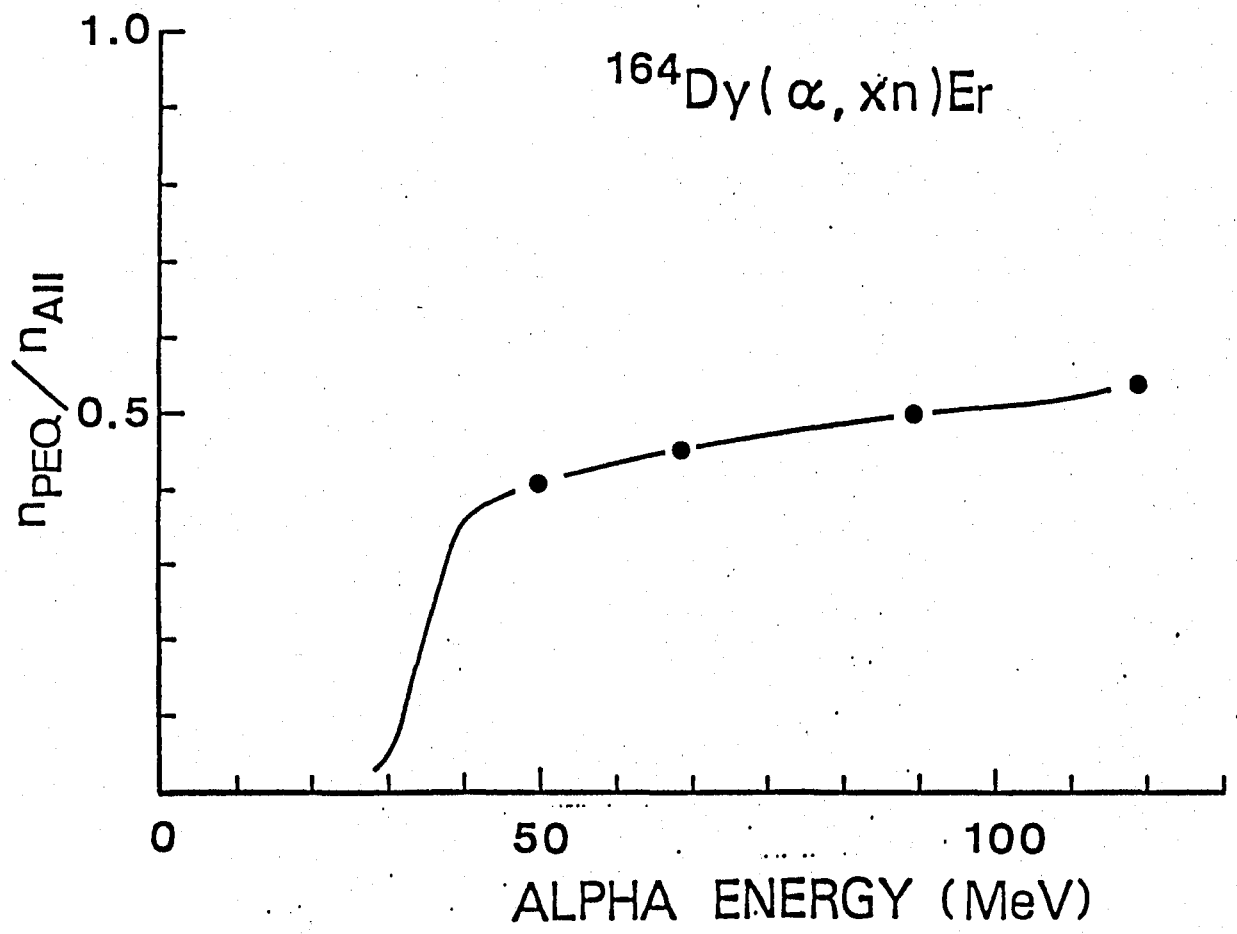

Fig. 4-8

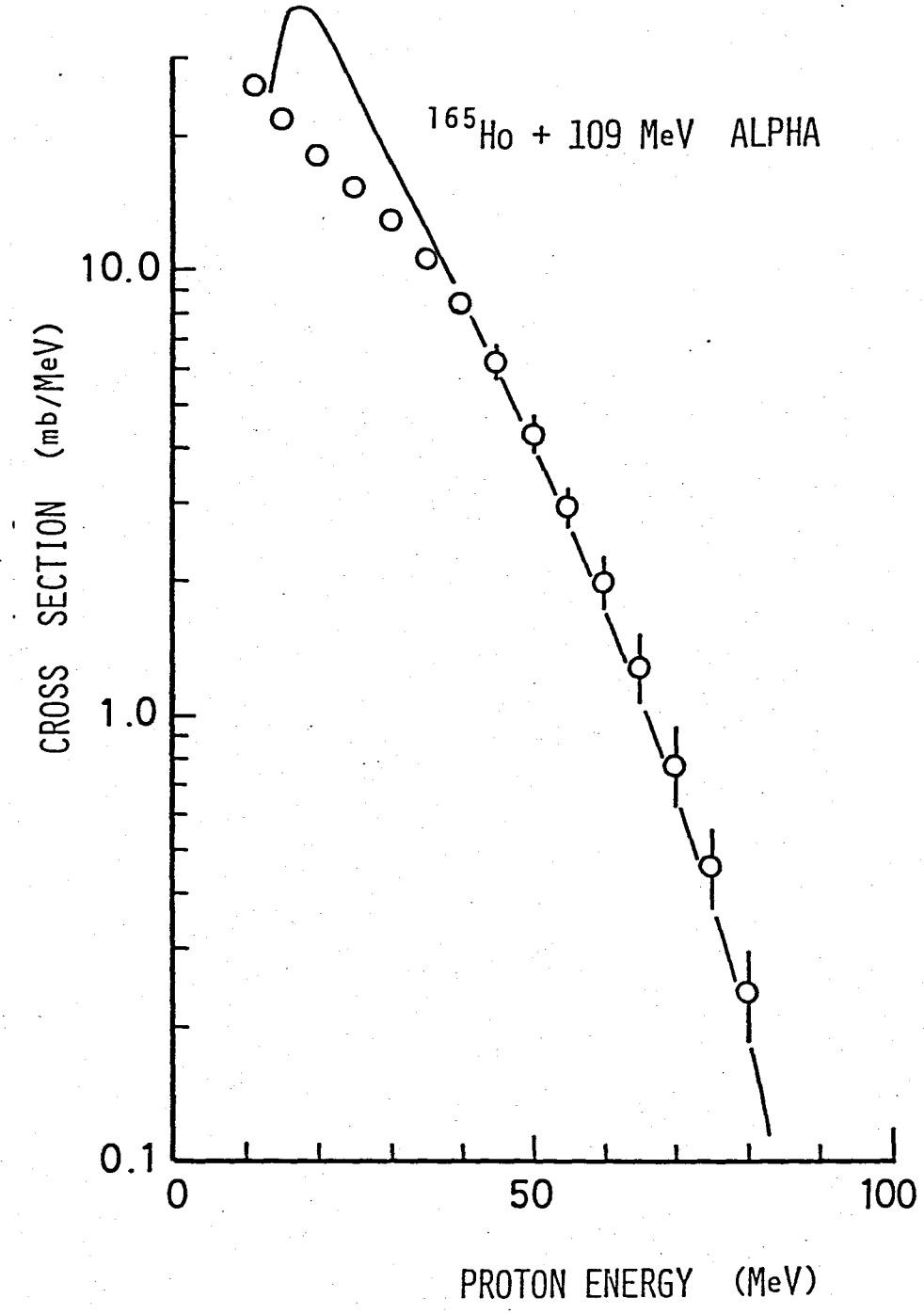
^{165}Ho + 109 MeV ALPHA
CROSS SECTION (mb/MeV)
10.0
1.0
0.1
0
50
100
PROTON ENERGY (MeV)

Fig. 4-9

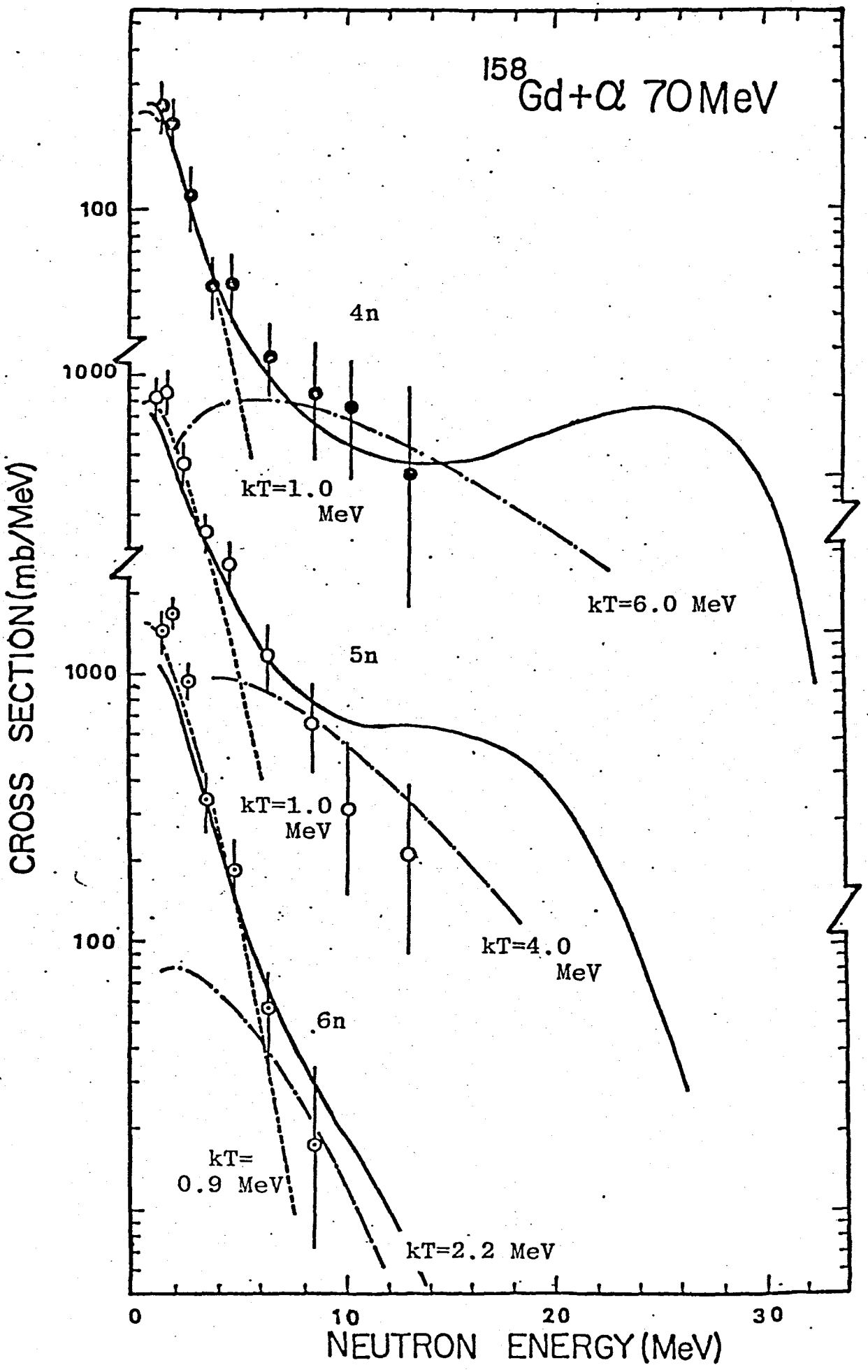
158Gd+α 70MeV
4n
5n
6n
kT=1.0 MeV
kT=6.0 MeV
kT=1.0 MeV
kT=4.0 MeV
kT= 0.9 MeV
kT=2.2 MeV
CROSS SECTION(mb/MeV)
NEUTRON ENERGY(MeV)
100
1000
1000
100
0
10
20
30

Fig. 4-10

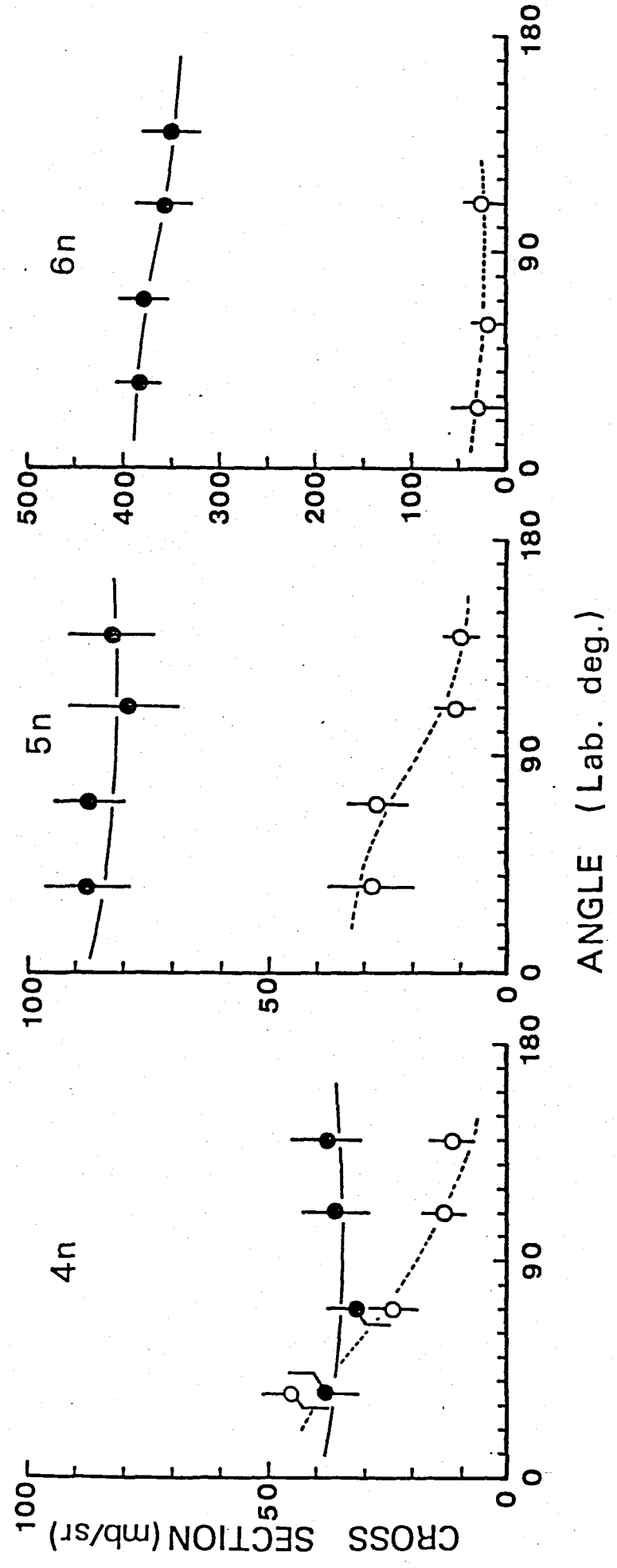
CROSS SECTION (mb/sr)
ANGLE (Lab. deg.)
4n
5n
6n
100
50
0
500
400
300
200
100
0
90
180

Fig. 4-11

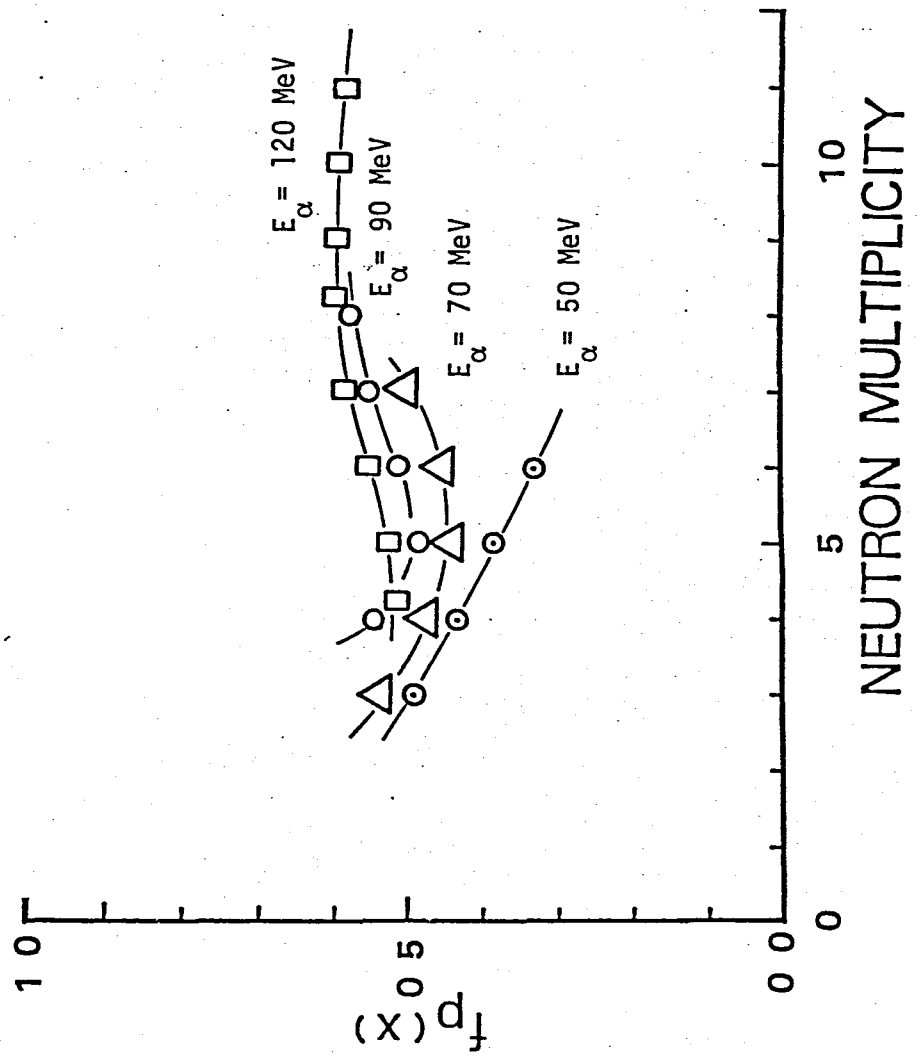
E_α = 120 MeV
E_α = 90 MeV
E_α = 70 MeV
E_α = 50 MeV
$f_D(x)$
1.0
0.5
0.0
0
5
10
NEUTRON MULTIPLICITY

Fig. 4-7

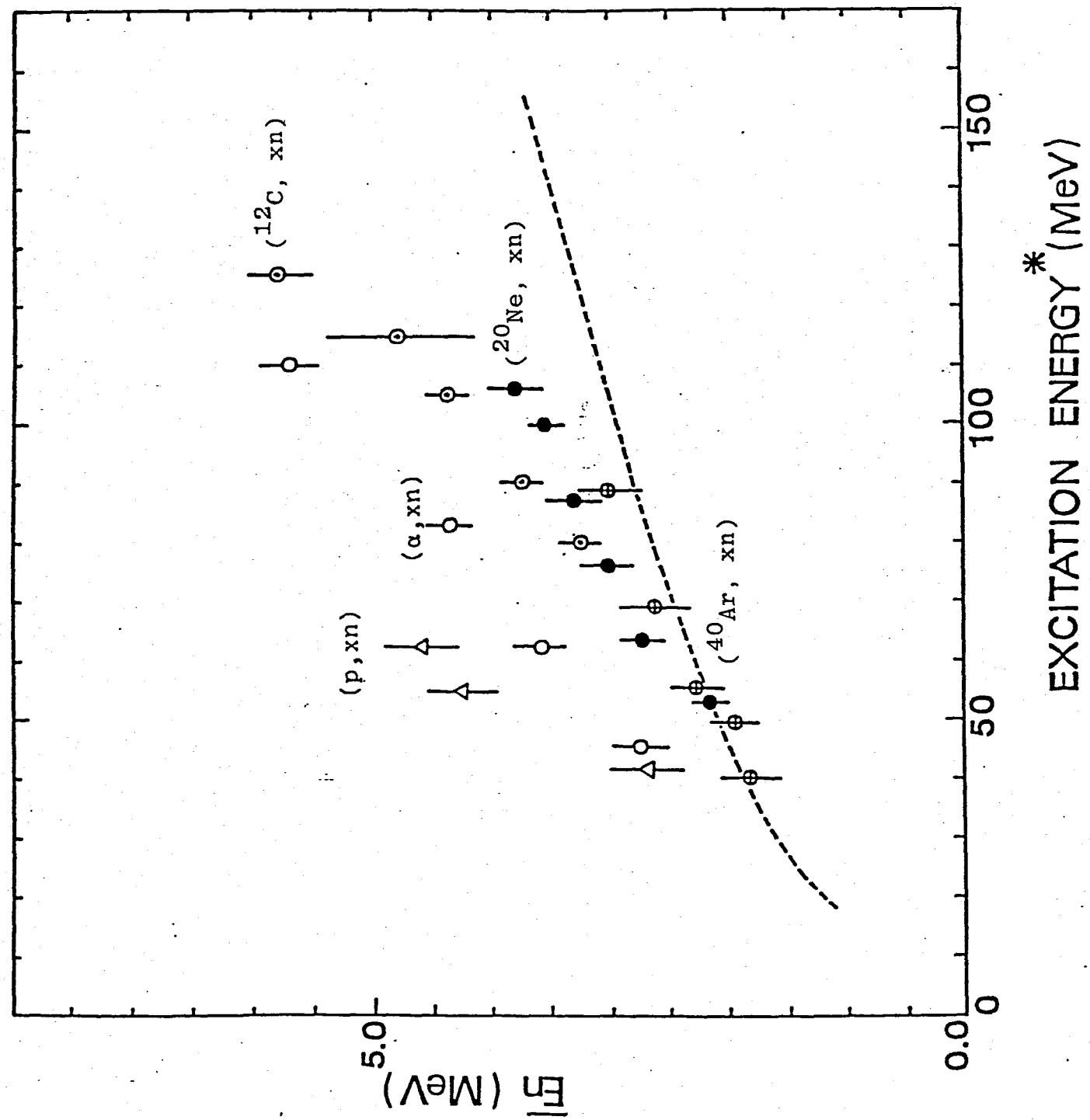
$\bar{E}_n$ (MeV)
5.0
0.0
0
50
100
150
EXCITATION ENERGY E^* (MeV)
(^{12}C, xn)
(^{20}Ne, xn)
(^{40}Ar, xn)
(α,xn)
(p,xn)

Fig. 5-1-a

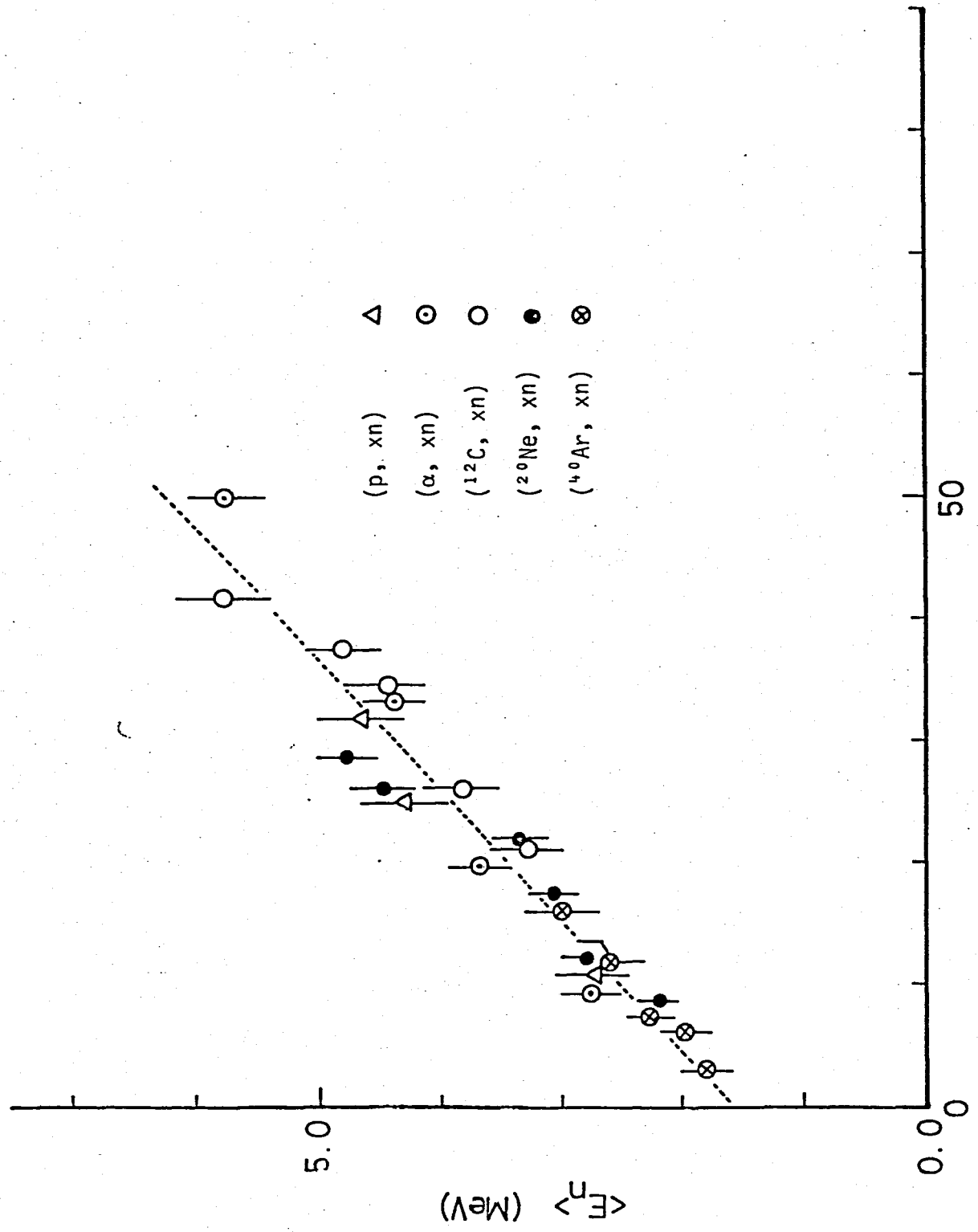

Fig. 5-1-b

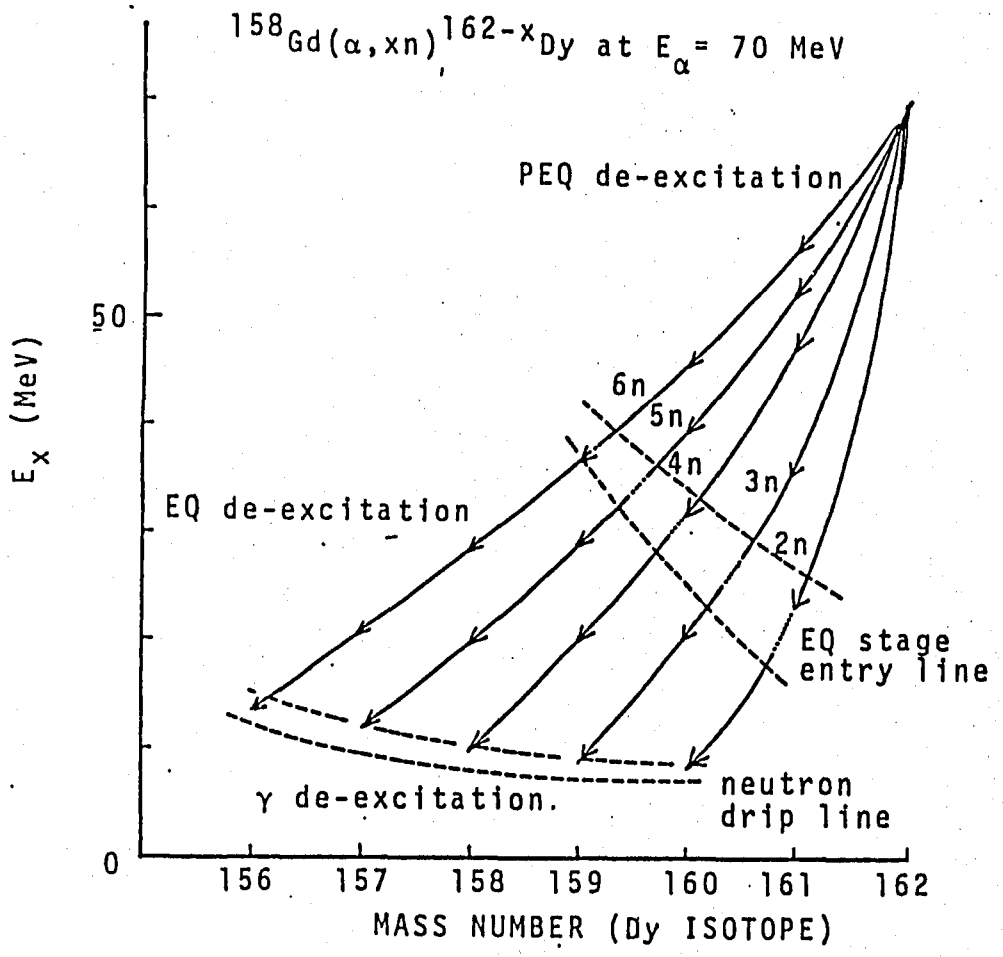
$^{158}Gd(\alpha,xn)^{162-x}Dy$ at E_α= 70 MeV
PEQ de-excitation
6n
5n
4n
3n
2n
EQ de-excitation
EQ stage entry line
γ de-excitation.
neutron drip line
E_x (MeV)
50
0
156
157
158
159
160
161
162
MASS NUMBER (Dy ISOTOPE)

Fig. 5-2

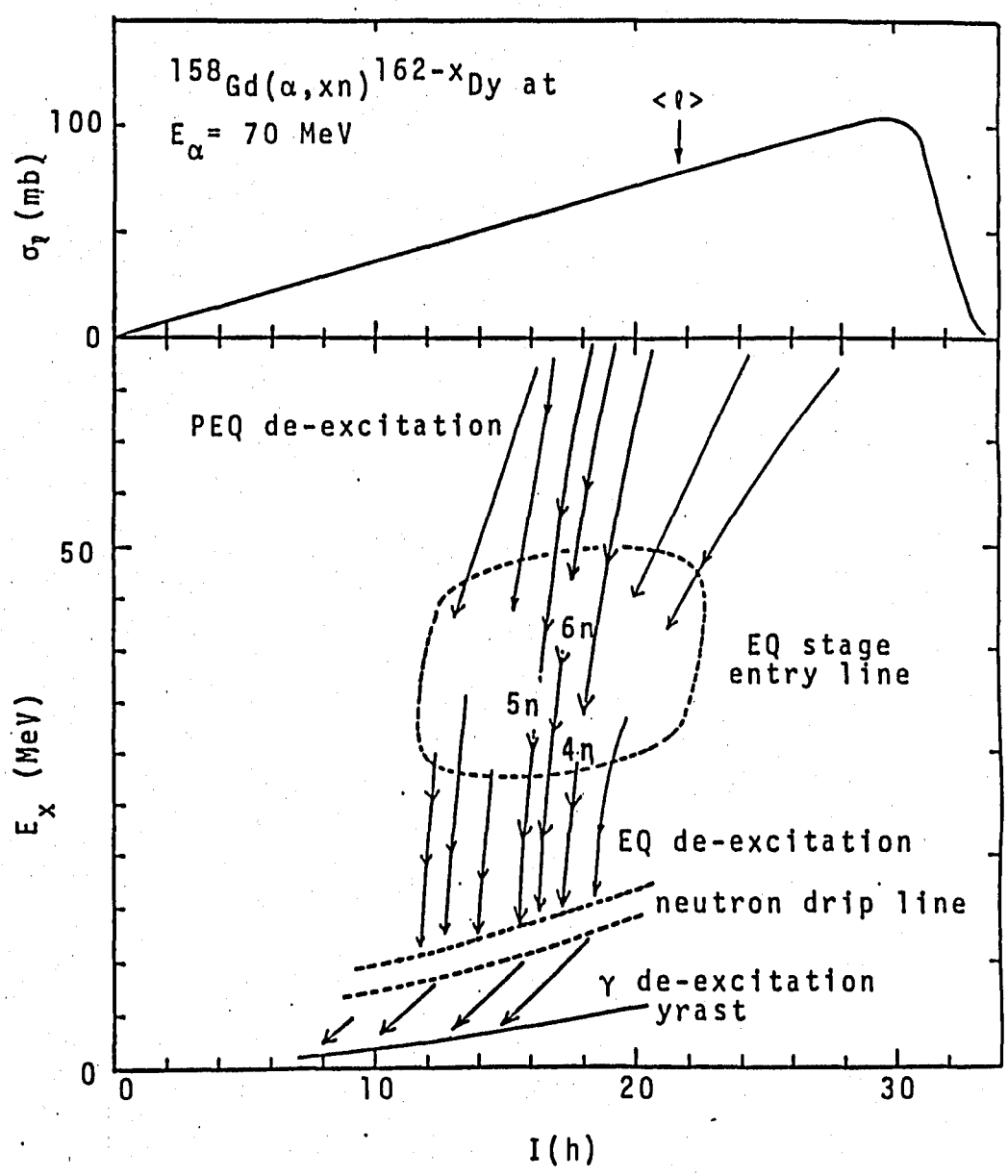
$^{158}Gd(\alpha,xn)^{162-x}Dy$ at
E_α= 70 MeV
<ℓ>
σ_ℓ (mb)
100
0
PEQ de-excitation
6n
5n
4n
EQ stage entry line
EQ de-excitation
neutron drip line
γ de-excitation
yrast
E_x (MeV)
50
0
0
10
20
30
I(h)

Fig. 5-3

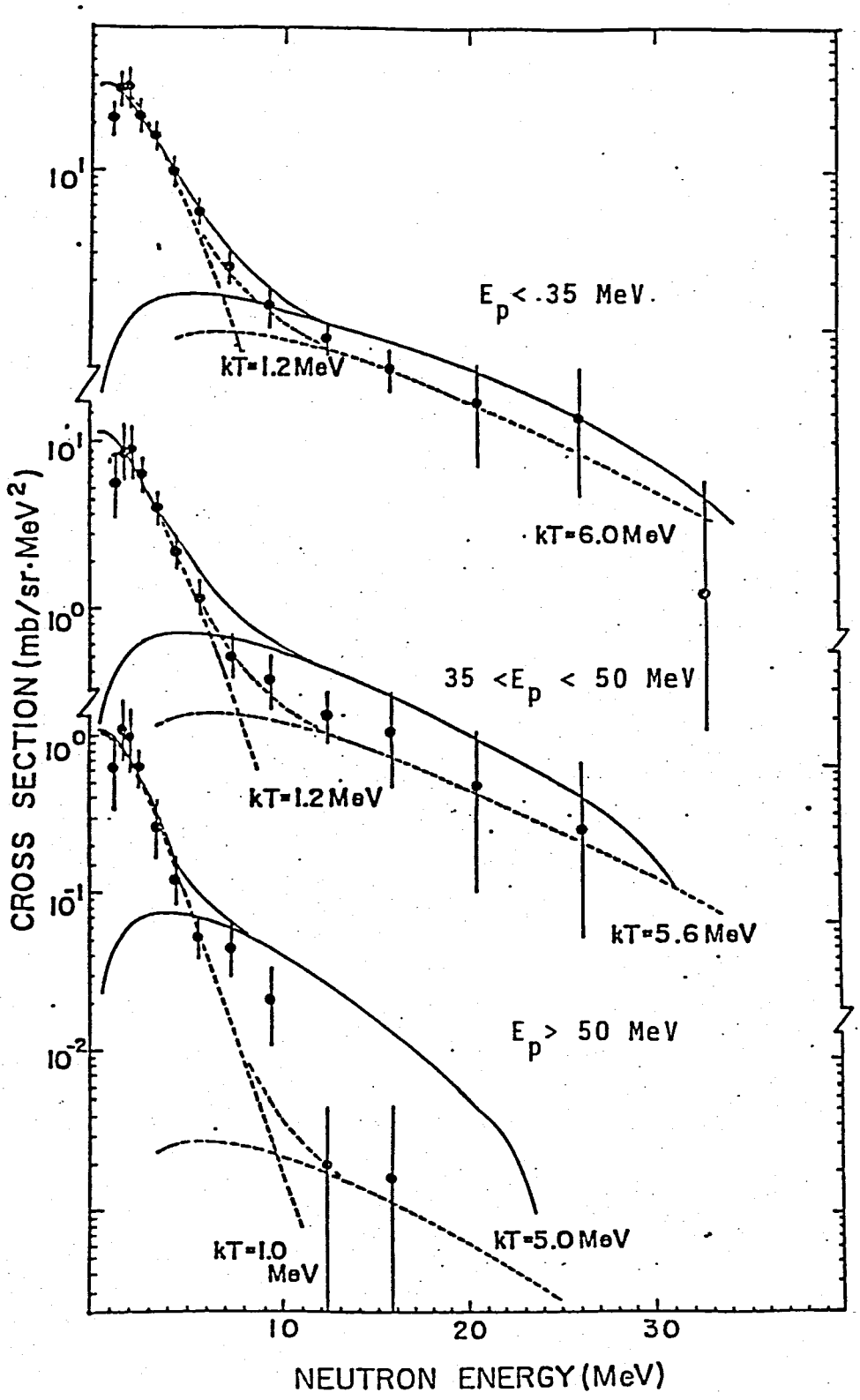
CROSS SECTION (mb/sr·MeV²)
NEUTRON ENERGY (MeV)
E_p < .35 MeV
kT=1.2MeV
kT=6.0MeV
35 < E_p < 50 MeV
kT=1.2MeV
kT=5.6MeV
E_p > 50 MeV
kT=1.0 MeV
kT=5.0MeV
10
20
30

Fig. 5-4

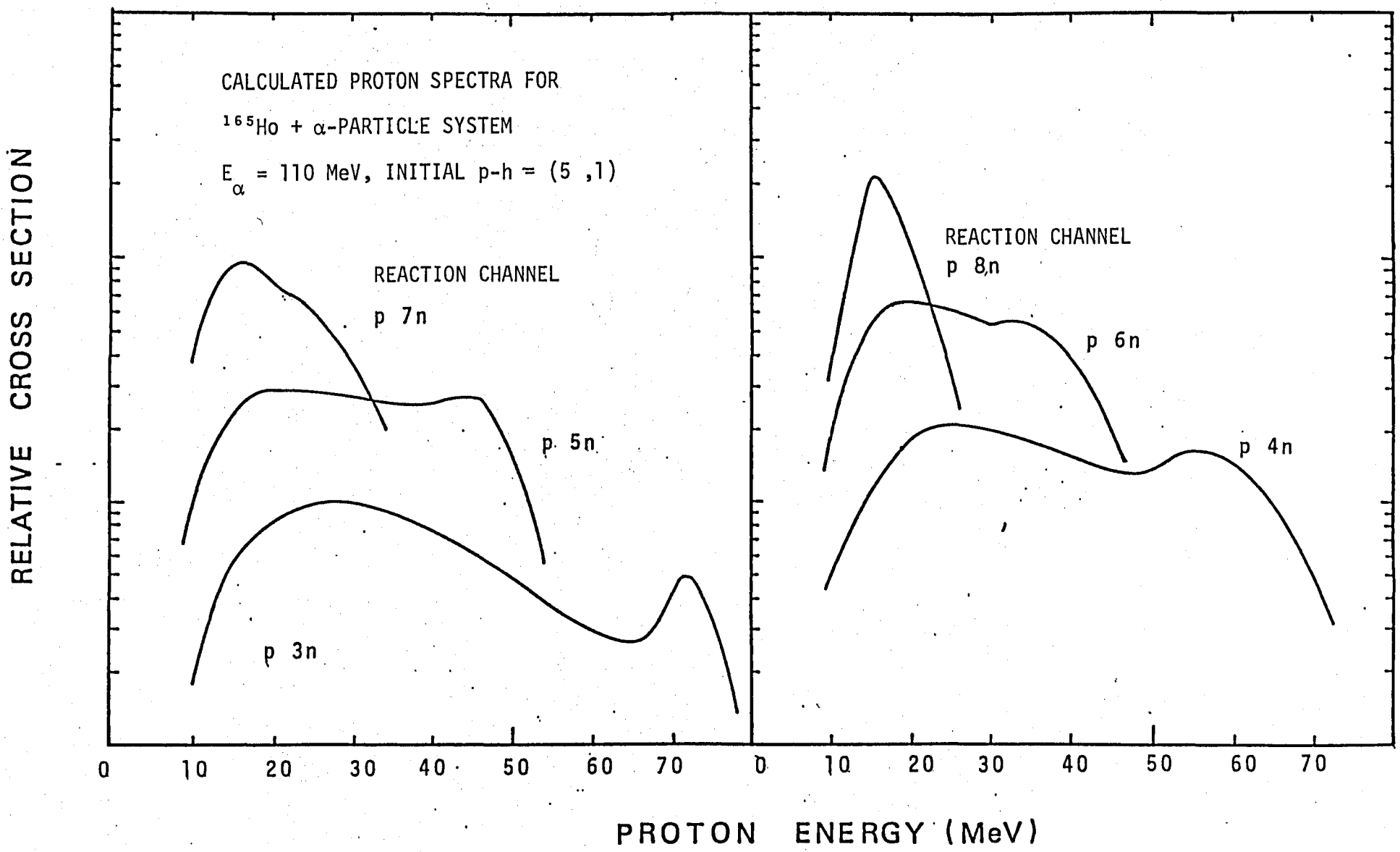
CALCULATED PROTON SPECTRA FOR
^{165}Ho + α-PARTICLE SYSTEM
E_α = 110 MeV, INITIAL p-h = (5 ,1)
REACTION CHANNEL
p 7n
p 5n
p 3n
REACTION CHANNEL
p 8n
p 6n
p 4n
RELATIVE CROSS SECTION
0
10
20
30
40
50
60
70
PROTON ENERGY (MeV)

Fig. 5-5

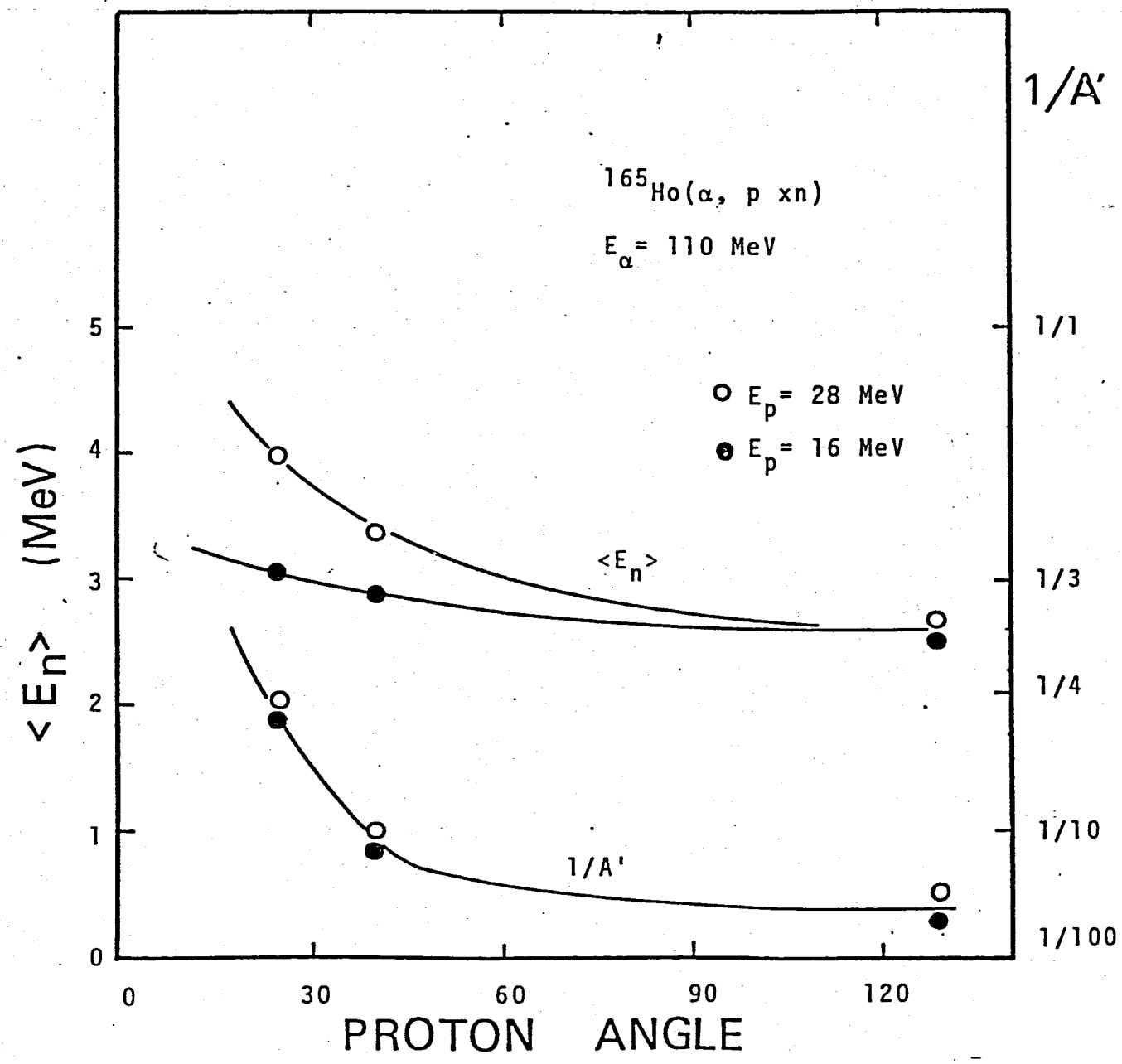
^{165}Ho(α, p xn)
E_α= 110 MeV
E_p= 28 MeV
E_p= 16 MeV
<E_n>
1/A'
<E_n> (MeV)
1/A'
1/1
1/3
1/4
1/10
1/100
0
1
2
3
4
5
0
30
60
90
120
PROTON ANGLE

Fig. 5-6

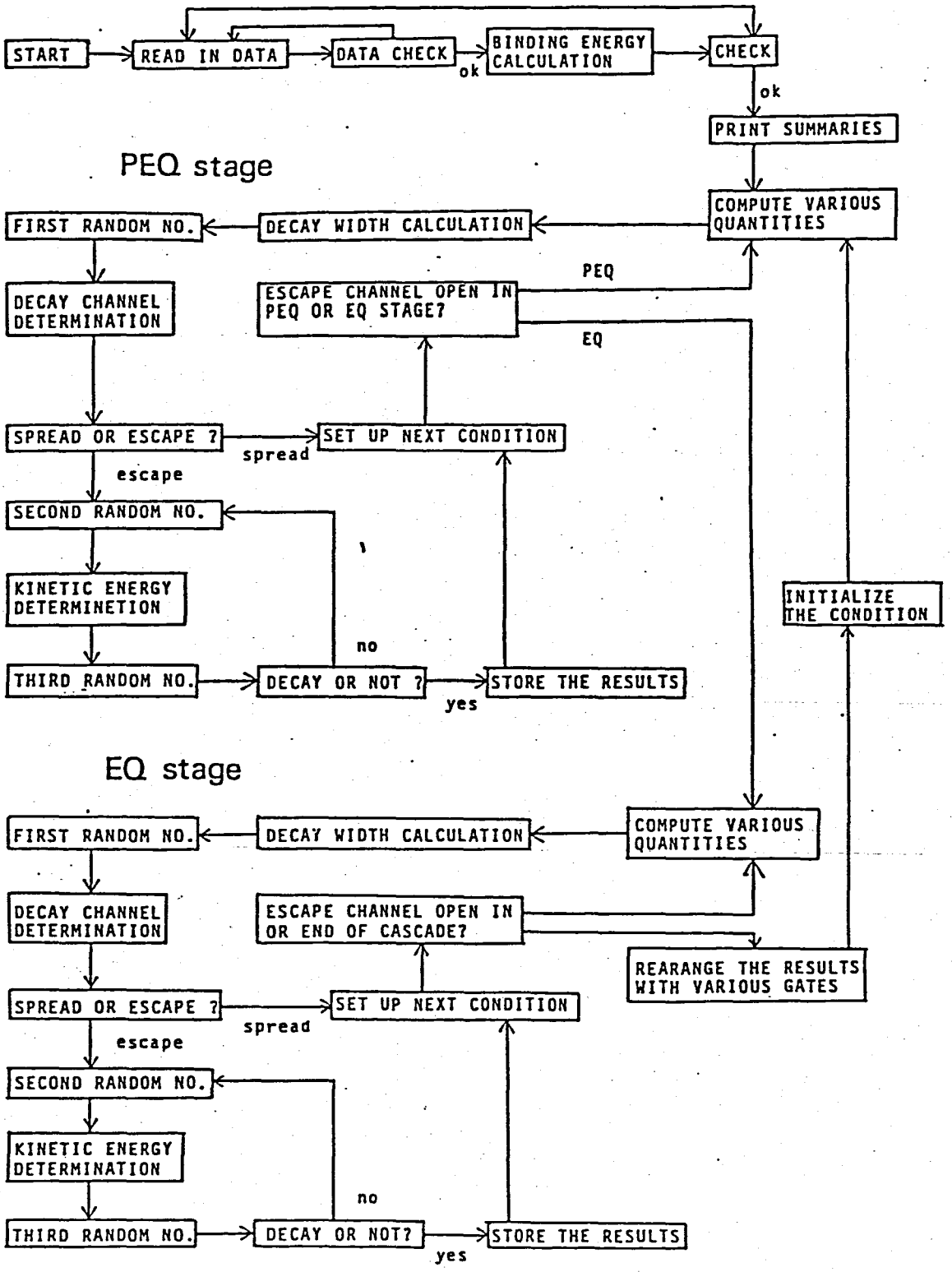
START
READ IN DATA
DATA CHECK
ok
BINDING ENERGY CALCULATION
CHECK
ok
PRINT SUMMARIES
PEQ stage
COMPUTE VARIOUS QUANTITIES
FIRST RANDOM NO.
DECAY WIDTH CALCULATION
DECAY CHANNEL DETERMINATION
ESCAPE CHANNEL OPEN IN PEQ OR EQ STAGE?
PEQ
EQ
SPREAD OR ESCAPE ?
spread
SET UP NEXT CONDITION
escape
SECOND RANDOM NO.
KINETIC ENERGY DETERMINETION
INITIALIZE THE CONDITION
no
THIRD RANDOM NO.
DECAY OR NOT ?
STORE THE RESULTS
yes
EQ stage
FIRST RANDOM NO.
DECAY WIDTH CALCULATION
COMPUTE VARIOUS QUANTITIES
DECAY CHANNEL DETERMINATION
ESCAPE CHANNEL OPEN IN OR END OF CASCADE?
REARANGE THE RESULTS WITH VARIOUS GATES
SPREAD OR ESCAPE ?
spread
SET UP NEXT CONDITION
escape
SECOND RANDOM NO.
KINETIC ENERGY DETERMINATION
no
THIRD RANDOM NO.
DECAY OR NOT?
STORE THE RESULTS
yes

Fig. A-1

```
      **** MAIN PROGRAM ***********************************************
C     ***** MAIN PROGRAM ***********************************************
C     *                                                                 *
C     *    CALCULATION FOR EQILIBLIUM AND PREEQUILIBLIUM DEEXCITATION   *
C     *    PROCESSES BY MONTE CARLO METHOD                              *
C     *    EXCITON MODEL AND EVAPOLATION MODEL WERE USED                *
C     *                                                                 *
C     *                                                                 *
C     *    PROGRAMMED BY KAZUSHIGE MAEDA                                *
C     *                                                                 *
C     *    SEPTEMBER  '79                                               *
C     *    MAY        '79                                               *
C     *                                                                 *
C     *******************************************************************
C
C     ***** PARAMETER LIST FOR PRE-EQUILIBLIUM CALCULATION **********
C     AEQB     EXCITON NO OF PHASE TRANSITION BETWEEN PRE-EQ AND EQ STAGE
C     APX      NO OF EXCITED PARTICLE IN A STATE
C     AHEX     NO OF EXCITED  HOLES   IN A STATE
C     AHEX     APEX+AHEX
C     APEX0, AHEX0,AMEX0,    INITIAL PARTICLE HOLE AND EXCITON NO
C     SYMBOL OF CHANNELS ----------------------------------------------
C     1 : PROTON, 2 : DEUTRON, 3 : TRITON, 4 : 3HE, 5 : ALPHA, 6 : NEUTR
C     ON
C      PARTICLE NO =3, SPREAD+, =4 SPREAD-
C     -----------------------------------------------------------------
C     INPUT CARDS -----------------------------------------------------
C     CARD0 (20A2) : REACTION NAME OR COMMENT
C
C     CARD1 (8F10.5)
C     AP,AT,ZP,ZT : MASS AND CHARGE OF PROJECTILE AND TARGET
C     AX : LEVELDENCITY PARAMETER (A/AX), AY : RADII PARAMETER
C
C     CARD2 (A10,7F10.5)
C     EXCITON CARD
C     INITIAL NO, 1 PARTICLE, 2 HOLE
C     3 TWO BODY MATRIX ELEMENT, 4 EXCITON NO LIMIT OF PREEQUILIBLIUN
C
C     CARD3 (A10,7F10.5)
C     CALCULATION CONTROL CARD
C     1 NO OF TRY, 2 NO OF TRY (FINAL),3 INITIALIZATION OF RANDOM NO
C
C     CARD4 (A10,7F10.5)
C
C     ESCAPE AND SPREADING WIDTH  MULTIPLYING PARAMETER
C
C     CARD5 (A10,7F10.5)
C
C     EVAPOLATION LIMIT
C     1
C     2 GAMMA DECAY STARTING LINE (MEV)C
C
C     CARD6 (A10,7F10.5)
C     KEYWORD -------
C     1. 'GATE MODE ' ; GATED BY ENERGY WITH SPECIFIC PARTICLE
C                       READ NEXT CARD
C      2. 'FINAL    .' ; GATED BY FINAL NUCLEI
C     IOUTMO=0    NORMAL MODE    =1    PROTON  SPECTRA GATED BY FINAL NU
C
C
C
C
C
C
C
C
C
C
C
C
C     IF GATE MODE IS SELECTED,MORE THAN TWO CARD
C     IF GATE MODE IS SELECTED, SORT CARD AND GATE CARD IS NESSESARY
C     SORT 1 GATED PARTICLE
C     SORT 1 GATE PARTICLE SYMBOL, 2 GATED PARTICLE SYMBOL
C     3 NO OF GATE ( MAX=10)
C     GATE    1 LOWER 2
C     GATE    1 LOWER AND 2 UPPER WINDOW IN MEV
C
C     ----------------------------------------------------------------
C
      CHARACTER KEY*10
C
C
C
C
C
C
    1 CONTINUE
C
      CALL PREEQ
C
      READ(5,1000) KEY
      IF(KEY.EQ.'NEXT      ') WRITE(6,2005)
      IF(KEY.EQ.'NEXT      ') GO TO 1
C
      WRITE(6,2000)
C
C     FORMAT STATEMENTS
 1000 FORMAT(A10)
 2000 FORMAT(//,' ***** END OF THE CALCULATION **********')
 2005 FORMAT(//,' ***** NEXT JOB START **********')
C
      STOP
      END
```

```
      SUBROUTINE OUTPUT(AMEVP,AMEVE,ISEP,IOUTMO,ITRY)
      DIMENSION IIJ(20)
      COMMON /INFBK1/ NORAND,IPART,ISTOP,IESCAP,IRAND,ISET
      COMMON /INFBK2/ ALPHA,BETA,AX
      COMMON /GAMWID/ GAM(10),PGAM(10)
      COMMON /LEVEL2/ AK(10),AZET(10),AQVAL(10),DELTA(10)
      COMMON /LEVEL1/ ALEV(10),VCOUL(10),AMASS(10),RENERG(10),AC(10)
      COMMON /EXDATA/ CMEXDA(100,6),CBEXDA(20,100,6)
      COMMON /DATABK/ CMDATA(100,6),CBDATA(20,100,6),ANUCL(20,10)
      COMMON /INF2/ IAZ,IAM,NSTEP,ASTEP
      COMMON /INIT/ AP,AT,ZP,ZT,EQ,AU,AY,AB,ANP,ANT
      COMMON /AUCBK/ AUCBUF(9,20),BUCBUF(5,5,5,12),ICOMT
C
      WRITE(6,2000)
      WRITE(6,2005) ITRY,NORAND
      SIGTOT=3.141592*(1.5*AMASS(R)**0.3333)**2.0
      IF(ISEP.EQ.1) GO TO 6
      DO 7 I=1,100
      DO 7 J=1,6
      CMDATA(I,J)=CMDATA(I,J)+CMEXDA(I,J)
    7 CONTINUE
      WRITE(6,2008)
      WRITE(6,2010)
      GO TO 8
    6 CONTINUE
      WRITE(6,2007)
      WRITE(6,2010)
    8 CONTINUE
      ATOTAL=0.0
      DO 5 I=1,20
      DO 5 J=1,10
      ATOTAL=ATOTAL+ANUCL(I,J)
    5 CONTINUE
      AS=SIGTOT/ATOTAL
      DO 10 J=1,100
      JJ=J
      WRITE(6,2015)JJ,(CMDATA(J,I),I=1,6)
   10 CONTINUE
      WRITE(6,2006)
      WRITE(6,2010)
      DO 15 J=1,100
      JJ=J
      WRITE(6,2015) JJ,(CMEXDA(J,I),I=1,6)
   15 CONTINUE
      WRITE(6,2020)
      DO 20 I=1,20
      IIJ(I)=IAM+1-I
   20 CONTINUE
      WRITE(6,2021)
      WRITE(6,2025) (IIJ(I),I=1,20)
```

```
      DO 25 J=1,10
      JJZ=IAZ-J+1
      WRITE(6,2030) JJZ,(ANUCL(K,J),K=1,20)
   25 CONTINUE
 2000 FORMAT(1H1,'  = SPECTRA AND ANGULAR DISTRIBUTION =')
 2005 FORMAT(/,5X,'TRYAL REACTION = ',I8,'   NO OF RANDOM NO =',I8)
 2010 FORMAT(//,5X,'     MEV   PROTON   DEUTERON    TRITON       3HE ',
     1'      4HE   NEUTRON',/)
 2015 FORMAT(5X,I7,6F10.0)
 2020 FORMAT(//,5X,' FINAL NUCLEUS',/)
 2021 FORMAT(/5X,' Z NO',',   ',30X,' MASS NO',/)
 2025 FORMAT(6X,20I6/)
 2030 FORMAT(I6,20F6.0)
 2006 FORMAT(' *** PRE-EQUILIBLIUM DISTRIBUTUON')
 2007 FORMAT(' *** EQUILIBLIUM DISTRIBUTION')
 2008 FORMAT('    *** TOTAL ENERGY SPECTRUM')
      RETURN
      END
      SUBROUTINE PREEQ
C
      CHARACTER KEY*10
      COMMON /NANZ/ NA,NZ
      COMMON /INFBK1/ NORAND,IPART,ISTOP,IESCAP,IRAND,ISET
      COMMON /INFBK2/ ALPHA,BETA,AX
      COMMON /LEVEL1/ ALEV(10),VCOUL(10),AMASS(10),RENERG(10),AC(10)
      COMMON /LEVEL2/ AK(10),AZET(10),AQVAL(10),DELTA(10)
      COMMON /EXTON1/ GAMP(10),ACPH(5),APH(5),ARCOMP(10)
      COMMON /EXTON2/ AKA,APEX,AHEX,AMEX,AG,AGA,AMAT
      COMMON /LYM1/ BE(10,20,6)
      COMMON /INIT/ AP,AT,ZP,ZT,EQ,AU,AY,AB,ANP,ANT
      COMMON /INF2/ IAZ,IAM,NSTEP,ASTEP
      COMMON /NUCLEI/ ARZERO
      COMMON /GAMWID/ GAM(10),PGAM(10)
      COMMON /IC1/ ICO(20)
      COMMON /ASBK1/ ASUP(8)
      COMMON /GATE2/ ANUGAT(20,10,10)
C
      COMMON /GATE1/ IGPAG,IGPAS,IGNO,AGPOS(10,2)
      COMMON /EM/ PR1,PR2,PR3,PR4,PR5,PR6,PR7,PR8
      COMMON /AUCBK/ AUCBUF(9,20),BUCBUF(5,5,5,12),ICOMT
      COMMON /EXDATA/ CMEXDA(100,6),CBEXDA(20,100,6)
      COMMON /EN/ ANESCA,ENESCA,ANBSCA,ENBSCA
      COMMON /DATABK/ CMDATA(100,6),CBDATA(20,100,6),ANUCL(20,10)
C
      DIMENSION RNAME(20)
      DATA DELTA/0.,0.,0.,0.,0.,0.,0.,0.,0.,0./
      NORAND=0
      ITRY=0
      WRITE(6,2065)
      READ(5,1000) (RNAME(I),I=1,20)
```

```
      READ(5,1005) AP,AT,ZP,ZT,EQ,AX,AY,AU
      IPRINT=AU
      ARZERO=AY
      READ(5,1010) KEY,AA1,AA2,AA3,AA4,AA5,AA6,AA7
      WRITE(6,2060) KEY,AA1,AA2,AA3,AA4,AA5,AA6,AA7
      APEX=AA1
      AHEX=AA2
      AMEX=APEX+AHEX
      APEXO=APEX
      AHEXO=AHEX
      AMEXO=AMEX
      AKA=AA3
      AEQB=AA4
      IROC=AA5
      READ(5,1010) KEY,AA1,AA2,AA3,AA4,AA5,AA6,AA7
      WRITE(6,2060) KEY,AA1,AA2,AA3,AA4,AA5,AA6,AA7
      IMOD=AA1
      IRAN=AA2
      IRAND=AA3
C
      READ(5,1010) KEY,(ASUP(I),I=1,7)
      WRITE(6,2060) KEY,(ASUP(I),I=1,7)
      READ(5,1010) KEY,AA1,AA2,AA3,AA4,AA5,AA6,AA7
      WRITE(6,2060) KEY,AA1,AA2,AA3,AA4,AA5,AA6,AA7
      PR1=AA1
      PR2=AA2
      READ(5,1010) KEY,AA1,AA2,AA3,AA4,AA5,AA6,AA7
      WRITE(6,2060) KEY,AA1,AA2,AA3,AA4,AA5,AA6,AA7
      IF(KEY.EQ.!GATE MODE !) IOUTMO=10
      IF(KEY.EQ.!GATE MODE !) CALL READAN(IOUTMO)
      IF(KEY.EQ.!GATE MODE !) GO TO 4
      IF(KEY.NE.!FINAL     !) GO TO 9999
    4 CONTINUE
      WRITE(6,2000)
      WRITE(6,2005) (RNAME(I),I=1,20)
      WRITE(6,2010)
      WRITE(6,2015)
      WRITE(6,2020) AP,AT,ZP,ZT
      WRITE(6,2025) EQ
      WRITE(6,2030) AX,AY,AU
      WRITE(6,2035) IRAND,IRAN,IROC,IMOD
      WRITE(6,2040) APEXO,AHEXO,AEQB,AKA
      WRITE(6,2045) PR1,PR2,PR3,PR4,PR5,PR6,PR7,PR8
      WRITE(6,2050) (ASUP(I),I=1,6)
      IF (IOUTMO.GE.10) GO TO 3
C
      AMEVP=AA1
      AMEVE=AA2
      ISEP=AA3
      IOUTMO=AA4
    3 CONTINUE
      IF(AMEVP.LT.0.1) AMEVP=1.0
      IF(AMEVE.LT.0.1) AMEVE=1.0
      IF(AEQB.LT.0.1) CALL EXNO(AEQB)
      AGCROS=(AT+AP)**0.66667*ARZERO*ARZERO*31.4159265
C
C     DATA BUFFER INITIALIZE
C
      DO 1 I=1,20
      DO 1 J=1,100
      DO 1 K=1,6
      CMDATA(J,K)=0.0
      CBDATA(I,J,K)=0.0
      CMEXDA(J,K)=0.0
      CBEXDA(I,J,K)=0.0
    1 CONTINUE
      DO 2 I=1,20
      DO 2 J=1,10
      DO 2 K=1,10
      ICO(I)=0
      ANUCL(I,J)=0.0
      ANUGAT(I,J,K)=0.0
C
    2 CONTINUE
C
C     INITIAL CONDITION SETTING
C
      AZET(8)=ZP+ZT
      AMASS(8)=AT+AP
      ANP=AP-ZP
      ANT=AT-ZT
C
    5 CONTINUE
      AZEE=ZP+ZT
      AAMA=AP+AT
      IAZ=AZEE
      IAM=AAMA
      NNZZ=10
      NNAA=20
      MMCC=0
      MMPP=1
      AQA=0.0
      NA=1
      NZ=1
C
C     Q-VALUE TABLE CALCULATION
C
      CALL LYMASS(AZEE,AAMA,NNZZ,NNAA,MMCC,MMPP,AP,AT,ZP,ZT,AQA,IPRINT)
C
      IF(AEQB.LT.0.0) GO TO 36
```

```
C
C     MONTE CARLO START
C
   10 CONTINUE
C
C     REINITIARIZE THE CONDITION
C
      NSTEP=0
      DO 16 I=1,9
      DO 17 J=1,20
      AUCBUF(I,J)=0.0
   17 CONTINUE
   16 CONTINUE
      ICOMT=0
      AHEX=AHEX0
      APEX=APEX0
      NA=1
      NZ=1
C
      AMASS(7)=AT+AP
      AZET(7)=ZP+ZT
      RENERG(7)=EQ-AQA
C
   15 CONTINUE
      AMEX=APEX+AHEX
      IF(IPART.EQ.10) GO TO 19
      IF(AMEX.GT.AEQB) GO TO 19
      GO TO 18
   19 CONTINUE
      CALL EQBLIM(IRAN,ITRY,IMOD)
      GO TO 40
   18 CONTINUE
      IF(IROC.NE.0) CALL ROCMAS
      AMASS(1)=AMASS(7)-1.0
      AMASS(2)=AMASS(7)-2.0
      AMASS(3)=AMASS(7)-3.0
      AMASS(4)=AMASS(7)-3.0
      AMASS(5)=AMASS(7)-4.0
      AMASS(6)=AMASS(7)-1.0
      AZET(1)=AZET(7)-1.0
      AZET(2)=AZET(7)-1.0
      AZET(3)=AZET(7)-1.0
      AZET(4)=AZET(7)-2.0
      AZET(5)=AZET(7)-2.0
      AZET(6)=AZET(7)
   20 CONTINUE
      DO 25 I=1,6
      AQVAL(I)=+BE(NZ,NA,I)
   25 CONTINUE
      CALL KCPARA
      CALL STAPARA
      CALL EXPARA
      CALL RCOMP
   30 CONTINUE
      CALL ESCWID
      CALL SPREDS
   35 CONTINUE
      IF(RENERG(6).LT.0.1) GO TO 40
      CALL EXFPAR
      CALL DKEXM
C
      IF(IPART.EQ.10) GO TO 15
      IF(RENERG(6).LT.0.1) GO TO 40
      IF(IPART.EQ.7) GO TO 15
      IF(IESCAP.EQ.0) GO TO 35
      IF(ISTOP.EQ.0) GO TO 40
      CALL TRANS
C
      II=IPART
      IF(II.EQ.1) NZ=NZ+1
      IF(II.EQ.1) APEX=APEX-1.0
      IF(II.EQ.1) NA=NA+1
      IF(II.EQ.2) NZ=NZ+1
      IF(II.EQ.2) NA=NA+2
      IF(II.EQ.2) APEX=APEX-2.0
      IF(II.EQ.3) APEX=APEX+1.0
      IF(II.EQ.3) AHEX=AHEX+1.0
      IF(II.EQ.4) APEX=APEX-1.0
      IF(II.EQ.4) AHEX=AHEX-1.0
      IF(II.EQ.5) NZ=NZ+2
      IF(II.EQ.5) APEX=APEX-4.0
      IF(II.EQ.5) NA=NA+4
      IF(II.EQ.6) APEX=APEX-1.0
      IF(II.EQ.6) NA=NA+1
      IF(II.EQ.3) IPART=7
      IF(II.EQ.4) IPART=7
      AMASS(7)=AMASS(8)-FLOAT(NA-1)
      AZET(7)=AZET(8)-FLOAT(NZ-1)
      IF(IPART.LE.6) ICOMT=ICOMT+1
      IF(IPART.GE.7) GO TO 36
      IENE=ENESCA+1.0
      IF(IENE.LT.1) IENE=1
      IF(IENE.GE.99) IENE=99
      CMEXDA(IENE,IPART)=CMEXDA(IENE,IPART)+1.0
      CMEXDA(100,IPART)=CMEXDA(100,IPART)+1.0
      ASTEP=NSTEP
      AM=ICOMT
      AI=IPART
      AUCBUF(1,ICOMT)=AM
      AUCBUF(2,ICOMT)=AI
```

```
      RETURN
      END
      SUBROUTINE ADDMO2(AMEVP,AMEVE,ISEP,IOUTMO)
C
C     GATE MODE SORTING
C
      COMMON /DATABK/ CMDATA(100,6),CRDATA(20,100,6),ANUCL(20,10)
      COMMON /EN/ ANESCA,ENESCA,ANBSCA,ENBSCA
      COMMON /EXDATA/ CMEXDA(100,6),CREXDA(20,100,6)
      COMMON /AUCBK/ AUCBUF(9,20),BUCBUF(5,5,5,12),ICOMT
      COMMON /EM/ PR1,PR2,PR3,PR4,PR5,PR6,PR7,PR8
      COMMON /GATE2/ ANUGAT(20,10,10)
      COMMON /GATE1/ IGPAG,IGPAS,IGNO,AGPOS(10,2)
      COMMON /NANI/ NA,NI
C
      DIMENSION ISET(15)
      DATA ISET/0,0,0,0,0,0,0,0,0,0,0,0,0,0,0/
C
      IF(IOUTMO.LT.10) GO TO 999
      IPG=1
      IPS=1
      IF(IOUTMO.GE.10) GO TO 100
      IF(IOUTMO.LT.10) GO TO 999
      GO TO 999
C
C     GATED SPECTRA ACUMLATION TO BUFFER "CBEXDA" AND "CBDATA"
C
  100 CONTINUE
      DO 120 I=1,ICOMT
C
C     BUFFER ADDRESS SETTING
C     ISET IS GATE ADDRESS
C
      IP=AUCBUF(2,I)
      AENE=AUCBUF(3,I)
      IF(IP.EQ.IGPAS) IPS=IPS+1
      IF(IP.EQ.IGPAG) IPG=IPG+1
      IF(IP.NE.IGPAG) GO TO 105
C
C     POSITIONED BY THE GATE?
C
      DO 110 J=1,IGNO
      IF(AENE.GT.AGPOS(J,1).AND.AENE.LT.AGPOS(J,2)) ISET(IPG)=J
  110 CONTINUE
  105 CONTINUE
  115 CONTINUE
  120 CONTINUE
      IF(IPS+IPG.LE.3) GO TO 999
C
      DO 135 J=1,IPG
      AUCBUF(3,ICOMT)=ENESCA
      AUCBUF(4,ICOMT)=ANESCA
      AUCBUF(5,ICOMT)=ENBSCA
      AUCBUF(6,ICOMT)=ANBSCA
      AUCBUF(7,ICOMT)=APEX
      AUCBUF(8,ICOMT)=AHEX
      AUCBUF(9,ICOMT)=ASTEP
   36 CONTINUE
C
C
      IF(NA.GT.20) GO TO 40
      IF(NZ.GT.10) GO TO 40
      GO TO 15
   40 CONTINUE
      ITRY=ITRY+1
      IF(IOUTMO.LT.10) CALL ADDMOD(AMEVP,AMEVE,ISEP,IOUTMO)
      IF(IOUTMO.GE.10) CALL ADDMO2(AMEVP,AMEVE,ISEP,IOUTMO)
      ANUCL(NA,NZ)=ANUCL(NA,NZ)+1.0
      IF(ITRY.GT.IRAN) GO TO 999
      ISEP=1
      IF(MOD(ITRY,IMOD).EQ.0) CALL OUTPUT(AMEVP,AMEVE,ISEP,IOUTM
      IF(MOD(ITRY,IMOD).EQ.0) CALL OUT2(AMEVP,AMEVE,ISEP,IOUTMO,
      GO TO 10
  999 CONTINUE
      ISEP=0
      CALL OUTPUT(AMEVP,AMEVE,ISEP,IOUTMO,ITRY)
      CALL OUT2(AMEVP,AMEVE,ISEP,IOUTMO,ITRY)
 9999 CONTINUE
 1000 FORMAT(20A2)
 2000 FORMAT(1H1,110('*')/'  M O N T E  C A R L O  C A L C U L
     1  F O R  T H E  D E E X C I T A T I O N  P R O C E S S
     2110('*'))
 1005 FORMAT(8F10.5)
 2005 FORMAT(//,15X,20A2)
 2010 FORMAT(1H0,10X,'PROJECTILE     TARGET  PROJECTILE      TAR
 2015 FORMAT(8X,4(8X,'MASS'))
 2020 FORMAT(/8X,4(2X,F10.3))
 2025 FORMAT(/,10X,' INCIDENT ENERGY(LAB) = ',F9.3,'MEV')
 2030 FORMAT(/,8X,'   AX = ',F8.3,' RO = ',F8.3,' AU = ',F8.3)
 2035 FORMAT(/,7X,'    IRAND = ',I10,' IRAN = ',I10,'  IROC =',I
     10D = ',I10)
 2040 FORMAT(11X,'INITIAL EXCITED PARTICLE =',F6.1,' INITIAL EXC
     1E = ',F6.1,' AEQB= ',F6.1/10X,' MATRIXELEMENT PARAMETER =
 2060 FORMAT(' DATA ',A10,7F10.3)
 2045 FORMAT(11X,'PARAMETERS ---',8F10.4)
 1010 FORMAT(A10,7F10.5)
 2050 FORMAT(11X,'SUPRESSION FACTOR ---',6F8.3)
 2070 FORMAT(//,20('-'),' CALCULATION STOP ---')
      WRITE(6,2070)
 2065 FORMAT(1H1,20('-'),' INPUT DATA ',70('-'))
```

```
      DO 130 I=1,ICOMT
      IENE=AUCBUF(3,I)+1.0
      IF(IENE.LT.1) IENE=1
      IF(IENE.GT.99) IENE=99
      AME=AUCBUF(7,I)+AUCBUF(8,I)
      IP=AUCBUF(2,I)
      IF(AME.LT.0.5) GO TO 125
      IF(IP.EQ.IGPAS) CBEXDA(ISET(J),IENE,IGPAS)=CBEXDA(ISET(J),IENE,
     *IGPAS)+1.0
  125 CONTINUE
      IF(IP.EQ.IGPAS) CBDATA(ISET(J),IENE,IGPAS)=CBDATA(ISET(J),IENE,
     *IGPAS)+1.0
  126 CONTINUE
C
  130 CONTINUE
  135 CONTINUE
      DO 145 I=1,IPG
      IPI=I
      IF(ISET(IPI).EQ.0) GO TO 140
      IF(ISET(IPI).GT.10) GO TO 140
      ANUGAT(NA,NZ,ISET(IPI))=ANUGAT(NA,NZ,ISET(IPI))+1.0
  140 CONTINUE
  145 CONTINUE
  999 CONTINUE
C
      RETURN
      END
      SUBROUTINE OUT3(AMEVP,AMEVE,ISEP,IOUTMO,ITRY)
C
C
      COMMON /DATABK/ CMDATA(100,6),CBDATA(20,100,6),ANUCL(20,10)
      COMMON /EN/ ANESCA,ENESCA,ANBSCA,ENBSCA
      COMMON /EXDATA/ CMEXDA(100,6),CBEXDA(20,100,6)
      COMMON /AUCBK/ AUCBUF(9,20),BUCBUF(5,5,5,12),ICOMT
      COMMON /EM/ PR1,PR2,PR3,PR4,PR5,PR6,PR7,PR8
      COMMON /GATE2/ ANUGAT(20,10,10)
      COMMON /GATE1/ IGPAG,IGPAS,IGNO,AGPOS(10,2)
      COMMON /NANI/ NA,NZ
      COMMON /INF2/ IAZ,IAM,NSTEP,ASTEP
      DIMENSION IIJ(20)
      DIMENSION IMEC(10)
      COMMON /NUCLEI/ ARZERO
      COMMON /INIT/ AP,AT,ZP,ZT,EQ,AU,AY,AB,ANP,ANT
      COMMON /INFBK1/ NORAND,IPART,ISTOP,IESCAP,IRAND,ISET
      CHARACTER NAME*8(6)
      DATA NAME/'PROTON  ','DEUTERON','TRITON  ','  3HE   ','ALPHA   ',
     *'NEUTRON'/
      DO 106 I=1,10
      AI=I
      IMEC(I)=AI*AMEVP
  106 CONTINUE
      WRITE(6,2000)
      WRITE(6,2003)
      WRITE(6,2005) ITRY,NORAND
      WRITE(6,2010) NAME(IGPAS),NAME(IGPAG)
      IP=IGPAS
      DO 10 I=1,IGNO
      IX=I
C
C     SPECTRUM SUM
C
      ASUMP=0.0
      ASUMT=0.0
C
      DO 120 ISUM=1,89
      ASUMP=ASUMP+CBEXDA(IX,ISUM,IP)
      ASUMT=ASUMT+CBDATA(IX,ISUM,IP)
  120 CONTINUE
C
      WRITE(6,2020) ASUMP
      WRITE(6,2015) I,AGPOS(I,1),AGPOS(I,2)
      WRITE(6,2040) (IMEC(L),L=1,10)
      DO 210 J=1,9
      IY=10*(J-1)+1
      AJ=J
      AY=10.0*(AJ-1.0)
      IZ=AY
      AS1=0.0
      AS2=0.0
      DO 150 IS=IY,IY+9
      AS2=CBEXDA(I,IS,IP)+AS2
      IF(IS.EQ.IY+4) AS1=AS2
  150 CONTINUE
      AS2=AS2-AS1
      WRITE(6,2035) IZ,(CBEXDA(I,K,IP),K=IY,IY+9),AS1,AS2
  210 CONTINUE
  211 CONTINUE
      WRITE(6,2025) ASUMT
      WRITE(6,2040) (IMEC(L),L=1,10)
      DO 215 J=1,9
      IY=10*(J-1)+1
      AJ=J
      AY=10.0*(AJ-1.0)
      IZ=AY
C
      AS1=0.0
      AS2=0.0
      DO 151 IS=IY,IY+9
      AS2=CBDATA(I,IS,IP)+AS2
      IF(IS.EQ.IY+4) AS1=AS2
```

```
  151 CONTINUE
      AS2=AS2-AS1
C
      WRITE(6,2035) IZ,(CBDATA(I,K,IP),K=IY,IY+9),AS1,AS2
  215 CONTINUE
      WRITE(6,2050)
      DO 20 IF=1,20
      IIJ(IF)=IAM+1-IF
   20 CONTINUE
      WRITE(6,2051)
      WRITE(6,2055) (IIJ(IJK),IJK=1,20)
      DO 25 JF=1,10
      JJZ=IAZ-JF+1
      WRITE(6,2060) JJZ,(ANUGAT(IF,JF,IX),IF=1,20)
   25 CONTINUE
   10 CONTINUE
  216 CONTINUE
  205 CONTINUE
  217 CONTINUE
 2000 FORMAT(1H1,'  M O N T E C A R L O   C A L C U L A T I O N   F O R
     1   T H E    D E E X C I T A T I O N   P R O C E S S !)
 2003 FORMAT(/,'** GATE MODE **')
 2005 FORMAT(//'  NO OF TRYAL =',I10,' NO OF RANDOM =',I10)
 2010 FORMAT(/' - ',A8,' SPECTRUM GATED BY ',A8,' -')
 2015 FORMAT(I2,'  GATE POSITION --- ',F8.2,'MEV TO ',F8.2,'MEV')
 2025 FORMAT(/,'    --- TOTAL ENERGY DISTRIBUTION ---    TOTAL =',F10.0)
 2020 FORMAT(/,'    --- PRE- EQUILIBLIUM DISTRIBUTION --- TOTAL =',F10.0)
 2030 FORMAT(9X,10(8X,I3),2X,'MEV')
 2035 FORMAT(1X,I3,2X,10F10.0,2F8.0)
 2040 FORMAT(5X,10(7X,I3),5X,'2.5',5X,'7.5 MEV')
 2050 FORMAT(/,5X,' ** FINAL NUCLEOUS DISTRIBUTION')
 2051 FORMAT(/5X,' Z NO',' ',30X,' MASS NO',/)
 2055 FORMAT(6X,20I6/)
 2060 FORMAT(I6,20F6.0)
      RETURN
      END
      SUBROUTINE EXNO(AEQB)
      RETURN
      END
      SUBROUTINE ROCMAS
C     DETERMINATION OF ROCAL MASS AND VELOCITY
C
      RETURN
      END
      SUBROUTINE TRANS
      COMMON /DATABK/ CMDATA(100,6),CBDATA(20,100,6),ANUCL(20,10)
C     CM LAB TRANSFORMATION
C
      RETURN
      END
```

```
      SUBROUTINE READAN(IOUTMO)
C     READ THE DATA FOR GATE MODE
      COMMON /GATE1/ IGPAG,IGPAS,IGNO,AGPOS(10,2)
C
C     IGPAG --- GATED PARTICLE SYMBOL
C     IGPAS --- GARE PARTICLE SYMBOL.
C
C     IGNO ---- NO. OF GATES.
C     AGPOS --- GATE POSITION (IN MEV)  START AND STOP
C
C     ***************************************************
C
      CHARACTER KEY*10
C
      READ(5,1000) KEY,AGPAG,AGPAS,AGNO
      WRITE(6,2060) KEY,AGPAG,AGPAS,AGNO,IOUTMO
C
      IF(KEY.NE.'SORT      ') GO TO 100
      IGPAG=AGPAG
      IGPAS=AGPAS
      IGNO=AGNO
      IOUTMO=IOUTMO+IGPAS
C
      IF(IGNO.GE.10) GO TO 990
C
      DO 5 I=1,IGNO
C
      READ(5,1000) KEY,AST,ASP,ADUMMY
      WRITE(6,2060) KEY,AST,ASP,ADUMMY,IOUTMO
C
      IF(KEY.NE.'GATE      ') GO TO 990
C
      IN=I
      AGPOS(IN,1)=AST
      AGPOS(IN,2)=ASP
C
    5 CONTINUE
C
  100 CONTINUE
  200 CONTINUE
C
C
  990 CONTINUE
 1000 FORMAT(A10,3F10.5)
 2060 FORMAT(' DATA ',A10,3F10.3,I10)
C
      RETURN
      END
      SUBROUTINE OUT2(AMEVP,AMEVE,ISEP,IOUTMO,ITRY)
      COMMON /INF2/ IAZ,IAM,NSTEP,ASTEP
```

```
      COMMON /DATABK/ CMDATA(100,6),CBDATA(20,100,6),ANUCL(20,10)
      COMMON /EXDATA/ CMEXDA(100,6),CBEXDA(20,100,6)
      COMMON /AUCBK/ AUCBUF(9,20),BUCBUF(5,5,5,12),ICOMT
      COMMON /EM/ PR1,PR2,PR3,PR4,PR5,PR6,PR7,PR8
      COMMON /IC1/ ICQ(20)
      DIMENSION IMEC(10)
      COMMON /NUCLEI/ ARZERO
      COMMON /INIT/ AP,AT,ZP,ZT,EQ,AU,AY,AB,ANP,ANT
      COMMON /INFBK1/ NORAND,IPART,ISTOP,IESCAP,IRAND,ISET
      COMMON /GATE2/ ANUGAT(20,10,10)
      ATRY=ITRY
      IF(IOUTMO.GE.10) GO TO 990
      WRITE(6,2000)
      WRITE(6,2005) ITRY,NORAND
      DO 106 I=1,10
      AI=I
      IMEC(I)=AI*AMEVP
  106 CONTINUE
C
      IF(IOUTMO.EQ.0) GO TO 100
      IF(IOUTMO.EQ.1) GO TO 200
      IF(IOUTMO.EQ.6) GO TO 200
      GO TO 99
C
  100 CONTINUE
      IP=1
      GO TO 104
  102 CONTINUE
      IP=2
      GO TO 104
  103 CONTINUE
      IP=6
      GO TO 104
  104 CONTINUE
      A=0.0
C
      DO 105 I=1,20
C
C     TOTAL NO
C
      ATRY=CBEXDA(I,100,IP)
      ATRE=CBDATA(I,100,IP)
      IF(ATRY.LT.0.1) AII=0.0
      IF(ATRY.LT.0.1) GO TO 114
      AII=CBEXDA(I,99,IP)/ATRY
      AISP=CBEXDA(I,98,IP)/ATRY
      IF(ATRE.LT.0.1) ATRE=1.0
      AISE=CBDATA(I,98,IP)/ATRE
C
C
C
  114 CONTINUE
      IF(IP.EQ.1) WRITE(6,2051) I,AII
      IF(IP.EQ.2) WRITE(6,2052) I,AII
      IF(IP.EQ.6) WRITE(6,2056) I,AII
      IF(ATRY.LT.0.1) GO TO 111
      WRITE(6,2020) ATRY,AISP
      WRITE(6,2030) (IMEC(L),L=1,10)
C
      DO 110 J=1,9
      IY=10*(J-1)+1
      AJ=J
      AY=10.0*(AJ-1.0)
      IZ=AY
C
      IF(ANUGAT(3,J,IP).LE.0.) ANUGAT(3,J,IP)=1.0
      AISPS=ANUGAT(1,J,IP)/ANUGAT(3,J,IP)
      AISPE=ANUGAT(2,J,IP)/ANUGAT(3,J,IP)
C
      WRITE(6,2015) IZ,(CBEXDA(I,K,IP),K=IY,IY+9),AISPS,AISPE
  110 CONTINUE
  111 CONTINUE
      IF(ATRE.LT.0.1) GO TO 116
      WRITE(6,2025) ATRE,AISE
      WRITE(6,2030) (IMEC(L),L=1,10)
      DO 115 J=1,9
      IY=10*(J-1)+1
      AJ=J
      AY=10.0*(AJ-1.0)
      IZ=AY
C
      IF(ANUGAT(6,J,IP).LE.0.) ANUGAT(6,J,IP)=1.0
      AISPS=ANUGAT(4,J,IP)/ANUGAT(6,J,IP)
      AISPS=ANUGAT(5,J,IP)/ANUGAT(6,J,IP)
C
      WRITE(6,2015) IZ,(CBDATA(I,K,IP),K=IY,IY+9),AISPS,AISPE
  115 CONTINUE
  116 CONTINUE
  105 CONTINUE
      IF(IP.EQ.1) GO TO 102
      IF(IP.EQ.2) GO TO 103
      IF(IP.EQ.6) GO TO 999
      GO TO 99
C
  200 CONTINUE
      IF(IOUTMO.EQ.1) WRITE(6,2100)
      IF(IOUTMO.EQ.6) WRITE(6,2110)
C
      DO 217 IP=1,6
      DO 205 I=1,20
```

```
      IQ=IP-1
      IR=I-1
      ATRY=CBEXDA(I,100,IP)
      ATRE=CBDATA(I,100,IP)
      IF(ATRY.LT.0.1) GO TO 211
      WRITE(6,2105) IQ,IR
      WRITE(6,2020) ATRY
      WRITE(6,2040) (IMEC(L),L=1,10)
      DO 210 J=1,9
      IY=10*(J-1)+1
      AJ=J
      AY=10.0*(AJ-1.0)
      IZ=AY
C
      AS1=0.0
      AS2=0.0
      DO 150 IS=IY,IY+9
      AS2=CBEXDA(I,IS,IP)+AS2
      IF(IS.EQ.IY+4) AS1=AS2
  150 CONTINUE
      AS2=AS2-AS1
C
      WRITE(6,2035) IZ,(CBEXDA(I,K,IP),K=IY,IY+9),AS1,AS2
  210 CONTINUE
  211 CONTINUE
      IF(ATRE.LT.0.1) GO TO 216
      WRITE(6,2105) IQ,IR
      WRITE(6,2025) ATRE
      WRITE(6,2040) (IMEC(L),L=1,10)
      DO 215 J=1,9
      IY=10*(J-1)+1
      AJ=J
      AY=10.0*(AJ-1.0)
      IZ=AY
C
      AS1=0.0
      AS2=0.0
      DO 151 IS=IY,IY+9
      AS2=CBDATA(I,IS,IP)+AS2
      IF(IS.EQ.IY+4) AS1=AS2
  151 CONTINUE
      AS2=AS2-AS1
C
      WRITE(6,2035) IZ,(CBDATA(I,K,IP),K=IY,IY+9),AS1,AS2
  215 CONTINUE
  216 CONTINUE
  205 CONTINUE
  217 CONTINUE
      GO TO 999
  990 CONTINUE
      CALL OUT3(AMEVP,AMEVE,ISEP,IOUTMO,ITRY)
   99 CONTINUE
      RETURN
  999 CONTINUE
 2000 FORMAT(1H1,'  M O N T E C A R L O   C A L C U L A T I O N   F O I
     1    T H E    D E E X C I T A T I O N   P R O C E S S ')
 2005 FORMAT(//'  NO OF TRYAL =',I10,' NO OF RANDOM =',I10)
 2052 FORMAT(/' - DEUTERON DISTRIBUTION- NO OF STEP = ',I2,'  MEAN EXCI
     1ON NO = ',F8.3)
 2056 FORMAT(/' - NEUTRON DISTRIBUTION - NO OF STEP = ',I2,'  MEAN EXCI
     1ON NO = ',F8.3)
 2015 FORMAT(5X,I3,2X,10F9.0,2F9.2)
 2020 FORMAT(/,'   --- PRE- EQUILIBLIUM DISTRIBUTION --- TOTAL =',F10.0,
     *'   NO OF STEPS =',F10.2)
 2025 FORMAT(/,'   --- TOTAL ENERGY DISTRIBUTION ---      TOTAL =',F10.0,
     *'   NO OF STEPS =',F10.2)
 2030 FORMAT(9X,10(6X,I3),2X,'MEV',5X,'STEP NO',2X,'EXCITON')
 2035 FORMAT(1X,I3,2X,10F10.0,2F8.0)
 2040 FORMAT(5X,10(7X,I3),5X,'2.5',5X,'7.5 MEV')
 2051 FORMAT(/' - PROTON DISTRIBUTION -  NO OF STEP = ',I2,'  MEAN EXCIT
     1ON NO = ',F8.3)
 2100 FORMAT(/'  -  PROTON DISTRIBUTION GATED BY FINAL NUCLEI  -')
 2105 FORMAT('   GATED BY ',I2,'PROTON ',I2,'NEUTRON')
 2110 FORMAT(/'  -  NEUTRON DISTRIBUTION GATED BY FINAL NUCLEI  -')
      RETURN
      END
      SUBROUTINE ADDMOD(AMEVP,AMEVE,ISEP,IOUTMO)
C
      COMMON /GATE2/ ANUGAT(20,10,10)
      COMMON /IC1/ ICO(20)
      COMMON /AUCBK/ AUCBUF(9,20),BUCBUF(5,5,5,12),ICOMT
      COMMON /NUCLEI/ ARZERO
      COMMON /EXDATA/ CMEXDA(100,6),CBEXDA(20,100,6)
      COMMON /DATABK/ CMDATA(100,6),CBDATA(20,100,6),ANUCL(20,10)
      IF(IOUTMO.GE.10) GO TO 99
      IF(IOUTMO.EQ.0) GO TO 100
      IF(IOUTMO.EQ.1) GO TO 200
      IF(IOUTMO.EQ.6) GO TO 200
      GO TO 99
C
  100 CONTINUE
      DO 105 I=1,ICOMT
      IENE=AUCBUF(3,I)+1.0
      IF(IENE.LT.1) IENE=1
      IF(IENE.GE.89) IENE=89
      AME=AUCBUF(7,I)+AUCBUF(8,I)
      II=AUCBUF(2,I)
C
      IENEX=AUCBUF(3,I)/10.0+1.0
      IF(IENEX.LT.1) IENEX=1
```

```
      IF(IENEX.GT.9) IENEX=9
C
      IF(AUCBUF(7,I).LT.0.5) GO TO 101
      IF(AME.LT.0.5) GO TO 101
      CBEXDA(I,IENE,II)=CBEXDA(I,IENE,II)+1.0
      CBEXDA(I,100,II)=CBEXDA(I,100,II)+1.0
      CBEXDA(I,99,II)=CBEXDA(I,99,II)+AME
      CBEXDA(I,98,II)=CBEXDA(I,98,II)+AUCBUF(9,II)
C
      ANUGAT(3,IENEX,II)=ANUGAT(3,IENEX,II)+1.0
      ANUGAT(1,IENEX,II)=ANUGAT(1,IENEX,II)+AME
      ANUGAT(2,IENEX,II)=ANUGAT(2,IENEX,II)+AUCBUF(9,II)
C
  101 CONTINUE
      ICO(I)=ICO(I)+1
      CBDATA(I,IENE,II)=CBDATA(I,IENE,II)+1.0
      CBDATA(I,100,II)=CBDATA(I,100,II)+1.0
      CBDATA(I,98,II)=CBDATA(I,98,II)+AUCBUF(9,II)
C
      ANUGAT(4,IENEX,II)=ANUGAT(4,IENEX,II)+AME
      ANUGAT(5,IENEX,II)=ANUGAT(5,IENEX,II)+AUCBUF(9,II)
      ANUGAT(6,IENEX,II)=ANUGAT(6,IENEX,II)+1.0
C
  102 CONTINUE
  105 CONTINUE
      GO TO 99
C
  200 CONTINUE
      IPRO=1
      INEU=1
      DO 205 I=1,ICOMT
      II=AUCBUF(2,I)
      IF(II.EQ.1) IPRO=IPRO+1
      IF(II.EQ.2) GO TO 99
      IF(II.EQ.5) GO TO 99
      IF(II.EQ.6) INEU=INEU+1
  205 CONTINUE
      IF(IPRO.EQ.0) GO TO 99
C
      DO 210 I=1,ICOMT
      IENE=AUCBUF(3,I)+1.0
      IF(IENE.LT.1) IENE=1
      IF(IENE.GE.89) IENE=89
      II=AUCBUF(2,I)
      AME=AUCBUF(7,I)+AUCBUF(8,I)
      IF(IOUTMO.EQ.1) GO TO 204
      IF(IOUTMO.EQ.6) GO TO 206
  204 CONTINUE
      IF(AUCBUF(7,I).LT.0.5) GO TO 201
      IF(AME.LT.0.5) GO TO 201
C
      IF(II.EQ.1) CBEXDA(INEU,IENE,IPRO)=CBEXDA(INEU,IENE,IPRO)+1.0
      IF(II.EQ.1) CBEXDA(INEU,100,IPRO)=CBEXDA(INEU,100,IPRO)+1.0
  201 CONTINUE
      IF(II.EQ.1) CBDATA(INEU,IENE,IPRO)=CBDATA(INEU,IENE,IPRO)+1.0
      IF(II.EQ.1) CBDATA(INEU,100,IPRO)=CBDATA(INEU,100,IPRO)+1.0
      GO TO 202
  206 CONTINUE
      IF(AUCBUF(7,I).LT.0.5) GO TO 207
      IF(AME.LT.0.5) GO TO 207
      IF(II.EQ.6) CBEXDA(INEU,IENE,IPRO)=CBEXDA(INEU,IENE,IPRO)+1.0
      IF(II.EQ.6) CBEXDA(INEU,100,IPRO)=CBEXDA(INEU,100,IPRO)+1.0
  207 CONTINUE
      IF(II.EQ.6) CBDATA(INEU,IENE,IPRO)=CBDATA(INEU,IENE,IPRO)+1.0
      IF(II.EQ.6) CBDATA(INEU,100,IPRO)=CBDATA(INEU,100,IPRO)+1.0
  202 CONTINUE
C
  210 CONTINUE
      GO TO 99
C
   99 CONTINUE
      RETURN
      END
      SUBROUTINE DKEXM
C     DETERMINATION OF KINETIC ENERGY USED EXCITON MODEL
C
      COMMON /INIT/ AP,AT,ZP,ZT,EQ,AU,AY,AB,ANP,ANT
      COMMON /INFBK1/ NORAND,IPART,ISTOP,IESCAP,IRAND,ISET
      COMMON /EN/ ANESCA,ENESCA,ANBSCA,ENBSCA
      COMMON /INFBK2/ ALPHA,BETA,AX
      COMMON /LEVEL1/ ALEV(10),VCOUL(10),AMASS(10),RENERG(10),AC(10)
      COMMON /LEVEL2/ AK(10),AZET(10),AQVAL(10),DELTA(10)
      COMMON /EXTON1/ GAMP(10),ACPH(5),APH(5),ARCOMP(10)
      COMMON /EXTON2/ AKA,APEX,AHEX,AMEX,AG,AGA,AMAT
      COMMON /EXDATA/ CMEXDA(100,6),CBEXDA(20,100,6)
      COMMON /EM/ PR1,PR2,PR3,PR4,PR5,PR6,PR7,PR8
      ISTOP=1
      IESCAP=0
      PART=IPART
      IF(RENERG(7).LT.PR2) GO TO 45
      IF(IPART.EQ.3) GO TO 99
      IF(IPART.EQ.4) GO TO 99
      IF(IPART.EQ.10) GO TO 99
      IF(RENERG(IPART).GT.0.1) GO TO 6
C
      DO 5 I=1,6
      IF(RENERG(I).GT.0.1) GO TO 50
    5 CONTINUE
      GO TO 45
    6 CONTINUE
```

```
      7 CONTINUE
        IF(AMEX.LT.0.0) AMEX=0.0
        XMAX=RENERG(IPART)/(AMEX+1.0)
        CALL S9UNI1(IR,R)
        RANSU=R
        NORAND=NORAND+1
        XEN=RANSU*RENERG(IPART)
        IF(XEN.LT.0.1) GO TO 999
C
        CALL PREX(PART,XEN,PRBEX)
        IF(PRBEX.LT.0.001) GO TO 999
C
        CALL S9UNI1(IR,R)
        RANSU=R
        NORAND=NORAND+1
        IF(PRBEX.GT.RANSU) GO TO 10
        IESCAP=0
        GO TO 7
C
     10 CONTINUE
        IESCAP=1
        ENESCA=XEN+VCOUL(IPART)
        RANSU=RAND20(IRAND)
        NORAND=NORAND+1
        ANESCA=RANSU*180
        REN=RENERG(7)
        RENERG(7)=REN-AQVAL(IPART)-ENESCA
        IF(RENERG(7).LT.0.1) RENERG(7)=0.0
        GO TO 99
     45 CONTINUE
        IESCAP=1
        ISTOP=0
        RETURN
     50 CONTINUE
        ISTOP=1
     99 CONTINUE
        IESCAP=1
        RETURN
    999 CONTINUE
        IESCAP=0
        RETURN
        END
        SUBROUTINE ESCWID
C       THE ESCAPE WIDTH IS CALCULATED BY INTEGRATING THE PROBABILITY
C       PER UNIT TIME AND UNIT ENERGY FOR EMISSION OF A VARIOUS PARTICLE
C       WITH KINETIC ENERGY AND BINDING ENERGY FROM M-EXCITON STATE
C
        COMMON /INIT/ AP,AT,ZP,ZT,EQ,AU,AY,AB,ANP,ANT
        COMMON /INFBK1/ NORAND,IPART,ISTOP,IESCAP,IRAND,ISET
        COMMON /INFBK2/ ALPHA,BETA,AX
```

```
      COMMON /LEVEL1/ ALEV(10),VCOUL(10),AMASS(10),RENERG(10),AC(10)
      COMMON /LEVEL2/ AK(10),AZET(10),AQVAL(10),DELTA(10)
      COMMON /NUCLEI/ ARZERO
      COMMON /EXTON1/ GAMP(10),ACPH(5),APH(5),ARCOMP(10)
      COMMON /EXTON2/ AKA,APEX,AHEX,AMEX,AG,AGA,AMAT
      COMMON /ASBK1/ ASUP(8)
      RER=RENERG(7)
   20 CONTINUE
   25 CONTINUE
      IF(AGA*AMEX.LT.0.0) GAL=0.0
      IF(AGA*AMEX.LT.0.0) GO TO 26
      GAL=(RER-APH(1))*APEX/(AGA*AMEX)
   26 CONTINUE
      IF(RER.LT.APH(1)) GAL=0.0
      GP=ARCOMP(1)*GAL*0.01539108/2.0
      GN=ARCOMP(6)*GAL*0.01539946/2.0
      GD=ARCOMP(2)*APEX*(APEX-1.)*0.023081452/(AGA*AGA)
      IF(RER.LT.APH(1)) GAO=0.0
      IF(RER.LT.APH(1)) GO TO 1
      GAO=APEX*(APEX-1.0)/((RER-APH(1))**2.0)
    1 CONTINUE
      GA1=GAO*(APEX-2.0)*(APEX-3.)*(AMEX-1.)*(AMEX-2.)/(AGA**4.0)
      GA=ARCOMP(5)*GA1*0.0152898375
C
      MEX=AMEX
      CPO=1.
      CNO=1.
      CDO=1.
      CAO=1.
      AA=(AMASS(7)-1.)/AMASS(7)
C
      IF(RER-APH(1).LT.0.1) GO TO 6
      DO 5 I=1,MEX
      IF(RER.LE.APH(1)) APH(1)=RER-0.1
      CPO=CPO*(RENERG(1)-APH(2))*AA/(RER-APH(1))
      CNO=CNO*(RENERG(6)-APH(2))*AA/(RER-APH(1))
      CDO=CDO*(RENERG(2)-APH(3))*AA/(RER-APH(1))
      CAO=CAO*(RENERG(5)-APH(5))*AA/(RER-APH(1))
      IF(I.EQ.MEX-1) CD=CDO
      IF(I.EQ.MEX-3) CA=CAO
    5 CONTINUE
      GO TO 7
    6 CONTINUE
      CPO=0.0
      CNO=0.0
      CA=0.0
      CA=0.0
    7 CONTINUE
C
      CP=CPO
```

```
      CN=CND
      IF(RENERG(1)-APH(2).LT.0.01) CP=0.0
      IF(RENERG(6)-APH(2).LT.0.01) CN=0.0
      IF(RENERG(2)-APH(3).LT.0.01) CD=0.0
      IF(RENERG(5)-APH(5).LT.0.01) CN=0.0
      ARR=ARZERO*(AMASS(7)**0.333333)
      IF(AA.LE.0.0) AA=1.0
      GAMP(1)=GP*CP/AA
      GAMP(2)=GD*CD/AA
      GAMP(5)=GA*CA/AA
      GAMP(6)=GN*CN/AA
C
C     ESCAPE WIDTH
C
      GAMP(1)=GAMP(1)*ARR*ARR*ASUP(1)*2.0
      GAMP(2)=GAMP(2)*ARR*ARR*ASUP(2)*2.0
      GAMP(5)=GAMP(5)*ARR*ARR*ASUP(5)*2.0
      GAMP(6)=GAMP(6)*ARR*ARR*ASUP(6)*2.0
C
C     SPREADING WIDTH
      IF(AGA*RER.LT.ACPH(1)) GAMP3=0.0
      IF(AGA*RER.LT.ACPH(1)) GO TO 10
      GAMP3=(AGA*RENERG(7)-ACPH(1))**2.*AGA/(AMEX+1.0)
   10 CONTINUE
      GAMP(3)=3.14159*(AMAT*GAMP3)*2.0*ASUP(3)
      GAMP4=APEX*AHEX*(APEX+AHEX-2.)*AGA
      GAMP(4)=3.14159*(AMAT*GAMP4)*2.0*ASUP(4)
C
      DO 15 I=1,6
      IF(GAMP(I).LE.0.0) GAMP(I)=0.0
   15 CONTINUE
   99 CONTINUE
      RETURN
      END
      SUBROUTINE PREX(AI,XE,PRBEX)
C
      COMMON /INFBK1/ NORAND,IPART,ISTOP,IESCAP,IRAND,ISET
      COMMON /INFBK2/ ALPHA,BETA,AX
      COMMON /LEVEL1/ ALEV(10),VCOUL(10),AMASS(10),RENERG(10)
      COMMON /LEVEL2/ AK(10),AZET(10),AQVAL(10),DELTA(10)
      COMMON /EXTON1/ GAMP(10),ACPH(5),APH(5),ARCOMP(10)
      COMMON /EXTON2/ AKA,APEX,AHEX,AMEX,AG,AGA,AMAT
      COMMON /INIT/ AP,AT,ZP,ZT,EQ,AU,AY,AB,ANP,ANT
      IA=AI
      IME=AMEX
      IF(IA.EQ.1) RERE=RENERG(IA)-APH(2)
      IF(IA.EQ.2) RERE=RENERG(IA)-APH(3)
      IF(IA.EQ.5) RERE=RENERG(IA)-APH(5)
      IF(IA.EQ.6) RERE=RENERG(IA)-APH(2)
      IF(IA.EQ.1) MEX=AMEX-2.0
      IF(IA.EQ.2) MEX=AMEX-3.0
      IF(IA.EQ.6) MEX=AMEX-2.0
      IF(IA.EQ.5) MEX=AMEX-5.0
      IF(IME.EQ.MEX) GO TO 99
      IF(MEX.EQ.0) GO TO 999
      IF(RERE.LT.0.0001) GO TO 999
      PMEX=MEX
      P1=1.0
C
      DO 5 I=1,MEX
      IF(RERE.LE.0.0) RERE=0.1
      P1=((PMEX+1.0)/PMEX)*((RERE-XE)/RERE)*P1
    5 CONTINUE
      PRBEX=XE*(PMEX+1.0)*P1/RERE
      RETURN
   99 CONTINUE
      RETURN
  999 CONTINUE
      PRBEX=0.0
      RETURN
      END
      SUBROUTINE RCOMP
C     CALCULATION OF PARTICLE DISTINGUSHABILITY
C     PROBABILITY OF GETTING THE RIGHT CONFIGURATION IN THE OUTGOING
C     PARTICLE
      COMMON /INIT/ AP,AT,ZP,ZT,EQ,AU,AY,AB,ANP,ANT
      COMMON /INFBK1/ NORAND,IPART,ISTOP,IESCAP,IRAND,ISET
      COMMON /INFBK2/ ALPHA,BETA,AX
      COMMON /LEVEL1/ ALEV(10),VCOUL(10),AMASS(10),RENERG(10),AC(10)
      COMMON /LEVEL2/ AK(10),AZET(10),AQVAL(10),DELTA(10)
      COMMON /EXTON1/ GAMP(10),ACPH(5),APH(5),ARCOMP(10)
      COMMON /EXTON2/ AKA,APEX,AHEX,AMEX,AG,AGA,AMAT
C
      DO 1 I=1,10
      ARCOMP(I)=0.0
    1 CONTINUE
C
      ICOM=APEX-AP
      AICOM=ICOM
      A=1.
      DO 5 I=1,ICOM
      AI=I
      DO 10 J=1,I-1
      AJ=J
      IF(AI-AJ+1.0.LT.0.1) GO TO 9
      A=((APEX-AP-AJ+1.)*A/(AI-AJ+1.))
      IF(A.LT.0.1) A=1.0
    9 CONTINUE
      IF(APEX.LT.0.1) GO TO 99
   10 CONTINUE
```

```
      W1=(AZET(7)/AMASS(7))**AI
      W2=((AMASS(7)-AZET(7))/AMASS(7))**(AICOM-AI)
      W=A*W1*W2
C
      IF(APEX.LE.0.1) APEX=1.0
C
      ARCOMP(1)=ARCOMP(1)+W*(ZP+AI)/APEX
      IF(APEX.LT.1.1) GO TO 25
      ARCOMP(2)=ARCOMP(2)+2.*W*(ZP+AI)*(APEX-ZP-AI)/(APEX*(APEX-1.0)
   25 CONTINUE
      AR51=(ZP+AI)*(ZP+AI-1.)*(APEX-ZP-AI)*(APEX-ZP-AI-1.)
      AR52=(APEX-3.)*(APEX-2.)*(APEX-1.)*APEX
      IF(AR52.LE.0.0) GO TO 30
      ARCOMP(5)=ARCOMP(5)+6.*W*AR51/AR52
   30 CONTINUE
      ARCOMP(6)=ARCOMP(6)+W*(APEX-ZP-AI)/APEX
C
    5 CONTINUE
      W1=(AZET(7)/AMASS(7))**AICOM
      ANW=W1
      ARCOMP(1)=ARCOMP(1)+ANW*ZP/APEX
      ARCOMP(2)=ARCOMP(2)+2.*ANW*(ZP*(APEX-ZP)/(APEX*(APEX-1.0)))
      IF(APEX.LT.2.1) GO TO 35
      AR53=(ZP/APEX)*((ZP-1.)/(APEX-1.))*((APEX-ZP)/(APEX-2.))
      AR54=(APEX-ZP-1.)/(APEX-3.)
      ARCOMP(5)=ARCOMP(5)+6.*ANW*AR53*AR54
   35 CONTINUE
      ARCOMP(6)=ARCOMP(6)+ANW*(APEX-ZP)/APEX
C
C
C
C
C
      DO 15 I=1,10
      IF(ARCOMP(I).LT.0.00001) ARCOMP(I)=0.0
   15 CONTINUE
   99 CONTINUE
      RETURN
      END
      SUBROUTINE EXPARA
C     DETERMINATION OF THE PARAMETER TO CALCULATE
      COMMON /INFBK1/ NORAND,IPART,ISTOP,IESCAP,IRAND,ISET
      COMMON /INFBK2/ ALPHA,BETA,AX
      COMMON /LEVEL1/ ALEV(10),VCOUL(10),AMASS(10),RENERG(10),AC(10)
      COMMON /LEVEL2/ AK(10),AZET(10),AQVAL(10),DELTA(10)
      COMMON /EXTON1/ GAMP(10),ACPH(5),APH(5),ARCOMP(10)
      COMMON /EXTON2/ AKA,APEX,AHEX,AMEX,AG,AGA,AMAT
      COMMON /INIT/ AP,AT,ZP,ZT,EQ,AU,AY,AB,ANP,ANT
C
      AG=AMASS(7)/AX
      AGA=6.0*AX/9.8696
C
C
      IF(RENERG(7).LE.0.0) RENERG(7)=0.1
C
      AMAT=AKA/(AMASS(7)**3.*RENEPG(7))
C
      DO 5 I=1,5
      A=I
      AI=APEX-A+1.0
      ACPH(I)=0.5*(AI*AI+AHEX*AHEX)
      APH(I)=(2.*(ACPH(I)+AI-3.*AHEX))/(4.0*AGA)
    5 CONTINUE
      AI=APEX+1.
      AJ=AHEX+1.
      ACPH(1)=0.5*(AI*AI+AJ*AJ)
   99 CONTINUE
      RETURN
      END
      SUBROUTINE EXFPAR
      COMMON NSTEP,ASTEP
      COMMON /INFBK1/ NORAND,IPART,ISTOP,IESCAP,IRAND,ISET
      COMMON /EXTON1/ GAMP(10),ACPH(5),APH(5),ARCOMP(10)
      COMMON /GAMWID/ GAM(10),PGAM(10)
      COMMON /EM/ PR1,PR2,PR3,PR4,PR5,PR6,PR7,PR8
C
C      DETERMINATION OF ESCAPE PARTCLE OR SPREAD
C     IN PRE-EQUILIBLIUM PHASE
C
      GAMTOT=GAMP(1)+GAMP(2)+GAMP(3)+GAMP(4)+GAMP(5)+GAMP(6
      IF(GAMTOT.LT.0.00001) GO TO 99
      PGAM(1)=GAMP(1)/GAMTOT
      PGAM(2)=GAMP(2)/GAMTOT+PGAM(1)
      PGAM(3)=GAMP(3)/GAMTOT+PGAM(2)
      PGAM(4)=GAMP(4)/GAMTOT+PGAM(3)
      PGAM(5)=GAMP(5)/GAMTOT+PGAM(4)
      PGAM(6)=GAMP(6)/GAMTOT+PGAM(5)
      GAMES=(GAMP(3)+GAMP(4))/GAMTOT
      IF(GAMES.GT.PR1)  GO TO 999
C
      CALL S9UNI1(IR,R)
      RANSU=R
      NORAND=NORAND+1
C
      DO 10 I=1,6
      II=I
      IF(PGAM(I).GT.RANSU) GO TO 20
   10 CONTINUE
C
   20 CONTINUE
```

```
      IPART=II
      NSTEP=NSTEP+1
      RETURN
   99 CONTINUE
      IPART=7
      RETURN
  999 CONTINUE
      IPART=10
      RETURN
      END
      SUBROUTINE EQBLIM(IRAN,ITRY,IMOD)
C
      COMMON /NANZ/ NA,NZ
      COMMON /INFBK1/ NORAND,IPART,ISTOP,IESCAP,IRAND,ISET
      COMMON /INFBK2/ ALPHA,BETA,AX
      COMMON /LEVEL1/ ALEV(10),VCOUL(10),AMASS(10),RENERG(10),AC(10)
      COMMON /LEVEL2/ AK(10),AZET(10),AQVAL(10),DELTA(10)
      COMMON /EXTON1/ GAMP(10),ACPH(5),APH(5),ARCOMP(10)
      COMMON /EXTON2/ AKA,APEX,AHEX,AMEX,AG,AGA,AMAT
      COMMON /LYM1/ BE(10,20,6)
      COMMON /DATABK/ CMDATA(100,6),CBDATA(20,100,6),ANUCL(20,10)
      COMMON /INIT/ AP,AT,ZP,ZT,EQ,AU,AY,AB,ANP,ANT
      COMMON /EXDATA/ CMEXDA(100,6),CBEXDA(20,100,6)
      COMMON /INF2/ IAZ,IAM,NSTEP,ASTEP
      COMMON /EN/ ANESCA,ENESCA,ANBSCA,ENBSCA
      COMMON /NUCLEI/ ARZERO
      COMMON /GAMWID/ GAM(10),PGAM(10)
      COMMON /AUCBK/ AUCBUF(9,20),BUCBUF(5,5,5,12),ICOMT
    6 CONTINUE
   10 CONTINUE
   15 CONTINUE
      AMASS(1)=AMASS(7)-1.0
      AMASS(2)=AMASS(7)-2.0
      AMASS(3)=AMASS(7)-3.0
      AMASS(4)=AMASS(7)-3.0
      AMASS(5)=AMASS(7)-4.0
      AMASS(6)=AMASS(7)-1.0
      AZET(1)=AZET(7)-1.0
      AZET(2)=AZET(7)-1.0
      AZET(3)=AZET(7)-1.0
      AZET(4)=AZET(7)-2.0
      AZET(5)=AZET(7)-2.0
      AZET(6)=AZET(7)
   20 CONTINUE
      DO 25 I=1,6
      AQVAL(I)=+BE(NZ,NA,I)
   25 CONTINUE
C
      CALL KCPARA
      CALL STAPARA
   30 CONTINUE
      CALL GAMMAD
      CALL SPREDS
   35 CONTINUE
      IF(RENERG(6).LT.0.1) GO TO 40
      CALL DEFPAR
      CALL DEFKIN
      IF(RENERG(6).LT.0.1) GO TO 40
      IF(IPART.EQ.7) GO TO 15
      IF(IESCAP.EQ.0) GO TO 35
      IF(ISTOP.EQ.0) GO TO 40
      CALL TRANS
      II=IPART
      IF(II.EQ.1) NZ=NZ+1
      IF(II.EQ.2) NZ=NZ+1
      IF(II.EQ.3) NZ=NZ+1
      IF(II.EQ.4) NZ=NZ+2
      IF(II.EQ.5) NZ=NZ+2
      IF(II.EQ.1) NA=NA+1
      IF(II.EQ.6) NA=NA+1
      IF(II.EQ.2) NA=NA+2
      IF(II.EQ.3) NA=NA+3
      IF(II.EQ.4) NA=NA+3
      IF(II.EQ.5) NA=NA+4
      AMASS(7)=AMASS(8)-FLOAT(NA-1)
      AZET(7)=AZET(8)-FLOAT(NZ-1)
      IF(IPART.LE.6) ICOMT=ICOMT+1
      IF(IPART.GE.7) GO TO 36
      IENE=ENESCA+1.0
C
      IF(IENE.GE.99) IENE=99
      CMDATA(100,IPART)=CMDATA(100,IPART)+1.0
      IF(IENE.LT.1) IENE=1
      CMDATA(IENE,IPART)=CMDATA(IENE,IPART)+1.0
C
      AM=ICOMT
      ASTEP=NSTEP
      AI=IPART
      AUCBUF(1,ICOMT)=AM
      AUCBUF(2,ICOMT)=AI
      AUCBUF(3,ICOMT)=ENESCA
      AUCBUF(4,ICOMT)=ANESCA
      AUCBUF(5,ICOMT)=ENBSCA
      AUCBUF(6,ICOMT)=ANBSCA
      AUCBUF(9,ICOMT)=ASTEP
   36 CONTINUE
      IF(NA.GT.20) GO TO 40
      IF(NZ.GT.10) GO TO 40
      GO TO 15
   40 CONTINUE
```

```
  999 CONTINUE
      RETURN
      END
      SUBROUTINE KCPARA
C     DETERMINATION OF KC AND CC FOR COUROMB BARRIOR PENETRATION EFFECT
      COMMON /GAMWID/ GAM(10),PGAM(10)
      COMMON /INFBK1/ NORAND,IPART,ISTOP,IESCAP,IRAND,ISET
      COMMON /INFBK2/ ALPHA,BETA,AX
      COMMON /LEVEL1/ ALEV(10),VCOUL(10),AMASS(10),RENERG(10),AC(10)
      COMMON /LEVEL2/ AK(10),AZET(10),AQVAL(10),DELTA(10)
      DIMENSION AKPDAT(5),AKADAT(5),ACPDAT(5),ACADAT(5)
      DATA AKPDAT/0.42,0.58,0.68,0.77,0.80/
      DATA AKADAT/0.68,0.82,0.91,0.97,0.98/
      DATA ACPDAT/0.50,0.28,0.20,0.15,0.10/
      DATA ACADAT/0.10,0.10,0.10,0.08,0.06/
C
      ISET=5
      IENE=AZET(7)
      IF(IENE.LT.10) ISET=1
      IF(IENE.LT.20) ISET=1
      IF(IENE.LT.30) ISET=2
      IF(IENE.LT.50) ISET=3
      IF(IENE.LT.70) ISET=4
C     K PARAMETER
      AK(1)=AKPDAT(ISET)
      AK(2)=AKPDAT(ISET)+0.06
      AK(3)=AKPDAT(ISET)+0.12
      AK(4)=AKADAT(ISET)-0.06
      AK(5)=AKADAT(ISET)
C     C PARAMETER
      AC(1)=ACPDAT(ISET)
      AC(2)=ACPDAT(ISET)/2.0
      AC(3)=ACPDAT(ISET)/3.0
      AC(4)=ACADAT(ISET)+1.3333333333
      AC(5)=ACADAT(ISET)
      RETURN
      END
      SUBROUTINE SPREDS
      COMMON /GAMWID/ GAM(10),PGAM(10)
      COMMON /INFBK1/ NORAND,IPART,ISTOP,IESCAP,IRAND,ISET
      COMMON /INFBK2/ ALPHA,BETA,AX
      COMMON /LEVEL1/ ALEV(10),VCOUL(10),AMASS(10),RENERG(10),AC(10)
      COMMON /LEVEL2/ AK(10),AZET(10),AQVAL(10),DELTA(10)
C     CALCURATION OF SPREADING WIDTH
      RETURN
      END
      SUBROUTINE GAMMAD
      COMMON /INFBK2/ ALPHA,BETA,AX
      COMMON /GAMWID/ GAM(10),PGAM(10)
      COMMON /LEVEL1/ ALEV(10),VCOUL(10),AMASS(10),RENERG(10),AC(10)
```

```
      COMMON /LEVEL2/ AK(10),AZET(10),AQVAL(10),DELTA(10)
C     CALCURATION OF ESCAPE WIDTH
      IF(RENERG(7).LT.0.001) RENERG(7)=0.
C     NEUTRON ESCAPE WIDTH
      IF(RENERG(6).LT.0.00001) RENERG(6)=0.0
C     NEUTRON
      GAM(6)=1.0
      ARN=SQRT(ALEV(6)*RENERG(6))
C
C     CHARGED PARTICLES
C
      DO 10 I=1,5
      IF(RENERG(I).LT.0.0001) RENERG(I)=0.0
      ARI=SQRT(ALEV(I)*RENERG(I))
      RIN=2.0*(ARI-ARN)
      RIM=EXP(RIN)
      AIN=(AMASS(I)/AMASS(6))**0.6666667
      SAI=((ALEV(6)/ALEV(I))**2.0)*((1.0+AC(I))/ALPHA)
      A1R=2.0*(ARI**2.0)-1.5*(2.0*ARI-1.0)
C
      IF(A2R.LE.0.0) A2R=0.1
C
      A2R=2.0*(ARN**2.0)-(1.5-ALEV(6)*BETA)*(2.0*ARN-1.0)
      GAM(I)=3.0*RIM*AIN*SAI*A1R/A2R
   10 CONTINUE
      GAM(1)=GAM(1)/3.0
      GAM(5)=2.0*GAM(5)/3.0
C
      DO 15 I=1,6
      IF(GAM(I).LE.0.0) GAM(I)=0.0
   15 CONTINUE
      RETURN
      END
      SUBROUTINE STAPARA
C     PARAMETER DETERMINATION
C     1 LEVEL DENCITY, 2 COULOMB BARRIOR, 3 RESIDUAL ENERGY
C     4 ALPHA AND BETA FOR INVERSE CROSS SECTION
      COMMON /GAMWID/ GAM(10),PGAM(10)
      COMMON /NUCLEI/ ARZERO
      COMMON /INFBK1/ NORAND,IPART,ISTOP,IESCAP,IRAND,ISET
      COMMON /INFBK2/ ALPHA,BETA,AX
      COMMON /LEVEL1/ ALEV(10),VCOUL(10),AMASS(10),RENERG(10),AC(10)
      COMMON /LEVEL2/ AK(10),AZET(10),AQVAL(10),DELTA(10)
      ALEV(7)=AMASS(7)/AX
      ATHT=(AMASS(7)-2.0*AZET(7))/AMASS(7)
      ALEV(1)=ALEV(7)*((1.0+1.3*ATHT/AMASS(7))**2.)
      ALEV(2)=ALEV(7)*((1.0-0.5/AMASS(7))**2.0)
      ALEV(3)=ALEV(7)*((1.0-1.0/AMASS(7)-1.3*ATHT/AMASS(7))**2.)
      ALEV(4)=ALEV(7)*((1.0-1.0/AMASS(7)+1.3*ATHT/AMASS(7))**2.)
      ALEV(5)=ALEV(7)*((1.0-1.5/AMASS(7))**2.0)
```

```
      ALEV(6)=ALEV(7)*((1.0-1.3/AMASS(7))**2.0)
C
      DO 10 I=1,5
      VCOUL(I)=1.43987*AK(I)*AZET(I)/(ARZERO*(AMASS(I)**0.33333))
   10 CONTINUE
      VCOUL(4)=2.0*VCOUL(4)
      VCOUL(5)=2.0*VCOUL(5)
C
      RENERG(6)=RENERG(7)-AQVAL(6)-DELTA(6)
      DO 20 I=1,5
      RENERG(I)=RENERG(7)-AQVAL(I)-VCOUL(I)-DELTA(I)
      IF(RENERG(I).LT.0.01) RENERG(I)=0.0
   20 CONTINUE
C
      AENE=AMASS(7)
      ALPHA=0.76+2.2*(AENE**(-0.33333))
      BETA=2.12*(AENE**(-0.66666))/ALPHA
      VCOUL(6)=-BETA
      RETURN
      END
      SUBROUTINE DEFPAR
      COMMON /INF2/ IAZ,IAM,NSTEP,ASTEP
      COMMON /DATABK/ CMDATA(100,6),CBDATA(20,100,6),ANUCL(20,10)
      COMMON /GAMMID/ GAM(10),PGAM(10)
      COMMON /INFBK1/ NORAND,IPART,ISTOP,IESCAP,IRAND,ISET
      COMMON /INFBK2/ ALPHA,BETA,AX
      COMMON /LEVEL1/ ALEV(10),VCOUL(10),AMASS(10),RENERG(10),AC(10)
      COMMON /LEVEL2/ AK(10),AZET(10),AQVAL(10),DELTA(10)
C     DETERMINATION OF ESCAPE PARTICLE OR SPREAD
      GAMTOT=GAM(1)+GAM(2)+GAM(3)+GAM(4)+GAM(5)+GAM(6)+GAM(7)
C
      IF(GAMTOT.LE.0.01) GAMTOT=0.1
C
      PGAM(1)=GAM(1)/GAMTOT
      PGAM(2)=GAM(2)/GAMTOT+PGAM(1)
      PGAM(3)=GAM(3)/GAMTOT+PGAM(2)
      PGAM(4)=GAM(4)/GAMTOT+PGAM(3)
      PGAM(5)=GAM(5)/GAMTOT+PGAM(4)
      PGAM(6)=GAM(6)/GAMTOT+PGAM(5)
      PGAM(7)=GAM(7)/GAMTOT+PGAM(6)
    5 CONTINUE
      CALL S9UNI1(IR,R)
      RANSU=R
      NORAND=NORAND+1
      NSTEP=NSTEP+1
      DO 10 I=1,7
      II=I
      IF(PGAM(I).GT.RANSU) GO TO 20
   10 CONTINUE
   20 CONTINUE
```

```
      IF(PGAM(5).GT.0.999) II=6
      IPART=II
      RETURN
      END
      SUBROUTINE DEPKIN
      COMMON /INF2/ IAZ,IAM,NSTEP,ASTEP
      COMMON /DATABK/ CMDATA(100,6),CBDATA(20,100,6),ANUCL(20,10)
      COMMON /GAMWID/ GAM(10),PGAM(10)
      COMMON /INFBK1/ NORAND,IPART,ISTOP,IESCAP,IRAND,ISET
      COMMON /INFBK2/ ALPHA,BETA,AX
      COMMON /EN/ ANESCA,ENESCA,ANBSCA,ENBSCA
      COMMON /LEVEL1/ ALEV(10),VCOUL(10),AMASS(10),RENERG(10),AC(10)
      COMMON /LEVEL2/ AK(10),AZET(10),AQVAL(10),DELTA(10)
      COMMON /EM/ PR1,PR2,PR3,PR4,PR5,PR6,PR7,PR8
C     DETERMINATION OF KINETIC ENERGY
      ISTOP=1
      IESCAP=0
      IF(IPART.EQ.7) GO TO 99
      IF(RENERG(7).LT.PR2) GO TO 20
      IF(RENERG(IPART).GT.0.10) GO TO 6
      DO 5 I=1,6
      IF(RENERG(I).GT.0.10) GO TO 30
    5 CONTINUE
      GO TO 20
    7 CONTINUE
    6 CONTINUE
C
      IF(ALEV(IPART).LE.0.0) ALEV(IPART)=0.1
C
      XMAX=((ALEV(IPART)*RENERG(IPART)+0.25)**0.5-0.5)/ALEV(IPART)
      CALL S9UNI1(IR,R)
      RANSU=R
      NORAND=NORAND+1
      XEN=RANSU*RENERG(IPART)
      IF(XEN.LT.0.01) GO TO 999
      PX1=SQRT(ALEV(IPART)*(RENERG(IPART)-XEN))
C     USED MAXWELLIAN DISTRIBUTION
      PX=(XEN/XMAX)*EXP(1.0-XEN/XMAX)
      IF(PX.LT.0.001) GO TO 999
      CALL S9UNI1(IR,R)
      RANSU=R
      NORAND=NORAND+1
C
      IF(PX.GT.RANSU) GO TO 10
      IESCAP=0
      GO TO 7
   10 CONTINUE
      IESCAP=1
      ENESCA=XEN+VCOUL(IPART)
      CALL S9UNI1(IR,R)
```

```
      RANSU=R
      NORAND=NORAND+1
      ANESCA=RANSU*180.
      REN=RENERG(7)
      RENERG(7)=RENERG(7)-AQVAL(IPART)-ENESCA
      IF(RENERG(7).LT.0.00001) RENERG(7)=0.0
      GO TO 99
   20 CONTINUE
      IESCAP=1
      ISTOP=0
      RETURN
   30 CONTINUE
      ISTOP=1
   99 CONTINUE
 5000 FORMAT(1 @@@@@ ',9F9.4,I10)
 5005 FORMAT(1 NOTES ',9F9.4,I10)
      RETURN
  999 CONTINUE
      IESCAP=0
      RETURN
      END
      SUBROUTINE LYMASS(ZEE,AMASS,NZ,NA,MC,MP,AP,AT,ZP,ZT,QVAL,IPRINT)
C     W.MYERS AND W.SWIATECKI: N.P. 81 1 (1966)
C     MASS FORMULA
C     CALCURATION OF GRAND Q-VALUE
C
      DIMENSION EM(10),XK(10),Y(10),F(10),XMS(20,20),EMP(10),XQ(20)
      COMMON /LYM1/ BE(10,20,6)
      COMMON /SF/ M3
      DATA EM/0.0,2.0,8.0,14.0,28.0,50.0,82.0,126.0,184.0,258.0/
      DATA A1,A2,A3/15.4941,17.9439,0.7053/
      DATA D,C,SMALC,GAMMA/0.444,5.8,0.325,1.7826/
      M3=6
      MMA=AMASS
      MZE=ZEE
      IF(NZ.GE.MZE) NZ=MZE-1
      IF(NA.GE.MMA) NA=MMA-1
      CAY1=1.15303
      CAY3=200.
      CAY4=11.0
      CAY5=8.07144
      CAY6=7.28899
      IF(MP) 5,5,10
    5 CAY4=0.0
   10 CONTINUE
      DO 15 I=1,10
      EMP(I)=EM(I)**(5.0/3.0)
   15 CONTINUE
      DO 20 I=1,9
      XK(I)=0.6*(EMP(I+1)-EMP(I))/(EM(I+1)-EM(I))
   20 CONTINUE
      RZ=0.863987/A3
      L=0
      Z=1.0
   25 KZ=ZEE
      KA=AMASS
      IF(MC.EQ.2.AND.QVAL.NE.0.) GO TO 250
      IF(QVAL)35,30,35
   30 NNZ=3
      NNA=1
      GO TO 90
   35 NNZ=NZ+2
      NNA=NA+2
      WRITE(6,2085)
      IF(MC)45,45,40
   40 WRITE(6,2065)
      GO TO 50
   45 WRITE(6,2070)
   50 IF(MP)55,55,60
   55 WRITE(6,2075)
      GO TO 90
   60 WRITE(6,2080)
   90 DO 215 JZ=1,NNZ
      DO 215 JA=1,NNA
      IF(QVAL)115,95,115
   95 IF(JZ-2)100,105,110
  100 Z=ZEE
      A=AMASS
      IA=A
      IZ=Z
      N=IA-IZ
      UN=AMASS-ZEE
      GO TO 125
  105 Z=ZT
      A=AT
      IA=A
      IZ=Z
      N=IA-IZ
      UN=AT-ZT
      GO TO 125
  110 Z=ZP
      A=AP
      IZ=Z
      IA=A
      N=IA-IZ
      UN=AP-ZP
      GO TO 125
  115 IA=KA+2-JA-JZ
      IZ=KZ+1-JZ
      N=IA-IZ
```

```
      120 Z=IZ
          UN=N
          A=IA
      125 A3RT=A**(1./3.)
          A2RT=SQRT(A)
          A3RT2=A3RT**2.0
          ZSQ=Z**2.0
          SYM=((UN-Z)/A)**2
          ACOR=1.0-GAMMA*SYM
          PARMAS=CAY5*UN+CAY6*Z
          VOLNUC=-1.0*A1*ACOR*A
          SUFNUC=A2*ACOR*A3RT2
          COULOMB=A3*ZSQ/A3RT
          FUZSUR=-1.0*CAY1*ZSQ/A
          ODDEV=-1.0*(1.0+2.0*(N/2)-UN+2.*(IZ/2)-Z)/SQRT(A)*CAY4
          IF(SYM.GT.0.4) WTERM=0.
      130 WTERM=0.
          WOTNUC=PARMAS+COULOMB+FUZSUR+ODDEV+WTERM
          SMASS=WOTNUC+VOLNUC+SUFNUC
          XMS(JA,JZ)=SMASS
          XQ(JZ)=SMASS
          IF(MC)135,135,215
      135 CONTINUE
          C2=(SUFNUC+WTERM)/(A**(2.0/3.0))
          X=COULOMB/(2.0*(SUFNUC+WTERM))
      140 BARR=0.0
      145 Y(1)=UN
          Y(2)=Z
          DO 165 J=1,2
          DO 150 I=1,9
          IF(Y(J)-EM(I+1)) 160,160,150
      150 CONTINUE
      155 STOP
      160 F(J)=XK(I)*(Y(J)-EM(I))-0.6*(Y(J)**(5./3.)-EMP(I))
      165 CONTINUE
          S=(2.0/A)**(2.0/3.0)*(F(1)+F(2))-SMALC*A**(1./3.)
          EE=2.*C2*D**2*(1.-X)
          FF=0.42591771*C2*D**3*(1.+2.*X)/A3RT
          SSHELL=C*S
          V=SSHELL/EE
          EPS=1.5*FF/EE
          IF(EE*(1.-3.*V).LE.0.0) GO TO 170
          QCALC=0.0
          THETA=0.0
          SHLL=SSHELL
          GO TO 210
      170 T0=1.0
      175 DO 180 IPQ=1,10
          T=T0-(1.-EPS*T0-V*(3.-2.*T0**2)*EXP(-T0**2))/(-EPS+V*(10.*T0-4.
         1 *T0**3)*EXP(-T0**2))
```

```
      IF(T.LE.0.0) GO TO 190
      IF(ABS(T-T0).LT.0.0001) GO TO 185
      T0=T
  180 CONTINUE
      GO TO 200
  185 IF(2.*EE*(1.-2.*EPS*T-V*(3.-12.*T**2+4.*T**4)*EXP(-T**2))
     1.GT.0.0) GO TO 205
  190 CONTINUE
      DO 195 I=1,20
      T0=FLOAT(I)/10.0
      GL=EE*(1.0-EPS*T0-V*(3.-2.*T0**2)*EXP(-T0**2))
      IF(GL.GE.0.0) GO TO 175
  195 CONTINUE
  200 CONTINUE
      GO TO 215
  205 THETA=T
      ALPHA0=0.*SQRT(5.)/A**(1./3.)
      ALPHA=ALPHA0*THETA
      SIGMA=ALPHA*(1.+ALPHA/14.)
      QCALC=0.004*Z*(RZ*AJRT)**2*(EXP(2.*SIGMA)-EXP(-SIGMA))
      SHLL=EE*T**2-FF*T**3+SSHELL*(1.-2.*T**2)*EXP(-T**2)
  210 CMASS=SMASS+SHLL
      XMS(JA,JZ)=CMASS
      XQ(JZ)=CMASS
  215 CONTINUE
      IF(QVAL)240,220,240
  220 IF(ZP-20.)225,225,230
  225 IF(AP.EQ.01..AND.ZP.EQ.01.)XQ(3)=7.29
      IF(AP.EQ.01..AND.ZP.EQ.00.)XQ(3)=8.07
      IF(AP.EQ.02..AND.ZP.EQ.01.)XQ(3)=13.14
      IF(AP.EQ.03..AND.ZP.EQ.01.)XQ(3)=14.95
      IF(AP.EQ.03..AND.ZP.EQ.02.)XQ(3)=14.93
      IF(AP.EQ.04..AND.ZP.EQ.02.)XQ(3)=2.43
      IF(AP.EQ.06..AND.ZP.EQ.03.)XQ(3)=14.09
  230 QVAL=XQ(2)+XQ(3)-XQ(1)
      WRITE(6,2234)
      WRITE(6,2235) QVAL
      GO TO 25
  240 DO 245 JZ=1,NZ
      DO 245 JA=1,NA
      BE(JZ,JA,6)=8.07+XMS(JA+1,JZ)-XMS(JA,JZ)
      BE(JZ,JA,1)=7.29+XMS(JA,JZ+1)-XMS(JA,JZ)
      BE(JZ,JA,2)=13.3+XMS(JA+1,JZ+1)-XMS(JA,JZ)
      BE(JZ,JA,3)=14.95+XMS(JA+2,JZ+1)-XMS(JA,JZ)
      BE(JZ,JA,4)=14.93+XMS(JA+1,JZ+2)-XMS(JA,JZ)
  245 BE(JZ,JA,5)=2.420+XMS(JA+2,JZ+2)-XMS(JA,JZ)
      GO TO 260
  250 DO 255 IZ=1,NZ
  255 READ(5,1270)((BE(IZ,IA,K),K=1,6),IA=1,NA)
      WRITE(6,2275)
```

```
1701              260 WRITE(6,2280)
1702                  WRITE(6,2300)
1703            C
1704                  IF(IPRINT.EQ.1) GO TO 270
1705                  WRITE(6,2281)
1706                  WRITE(6,2282)
1707                  IZEE=ZEE
1708                  IAMAS=AMASS
1709                  DO 265 IZ=1,NZ
1710                  DO 265 IA=1,NA
1711                  MZ=MZE+1-IZ
1712                  MA=MMA+1-IA
1713               265 WRITE(6,2285)MA,MZ,(BE(IZ,IA,K),K=1,M3)
1714                  WRITE(6,2300)
1715               270 CONTINUE
1716              1270 FORMAT(6F10.5)
1717              2065 FORMAT(10X,' LIQUID DROP MASSES')
1718              2070 FORMAT(10X,' SHELL CORRECTED MASSES')
1719              2075 FORMAT(10X,' ZERO PAIRING')
1720              2080 FORMAT(10X,' WITH PAIRING')
1721              2085 FORMAT(5X,' --- MYERS SWIATESKI LYEKIL AMSSES ---')
1722              2234 FORMAT(1H1)
1723              2235 FORMAT(5X,' *** QVAL(MYERS SWIATECKI MASS FORMULA) = ',F7.3,'MEV')
1724              2275 FORMAT(5X,' --- BINDING ENERGIES WERE PROVIDED BY USER --->')
1725              2280 FORMAT(5X,' --- BINDING ENERGIES USED --->',40X,'IN MEV')
1726              2281 FORMAT(10X,' IZ=ZINDEX OF NUCLEUS, IA=A-INDEX OF NUCLEUS IN ISOTOP
1727                 1E TABLE OF THIS PROGRAM')
1728              2282 FORMAT(/8X,' A     Z      PROTON          DEUTERON        TRITON',
1729                 19X,'3HE',12X,'4HE             NEUTRON'/)
1730              2285 FORMAT(5X,2I5,2X,6(F10.5,5X))
1731              2300 FORMAT(/,6X,100('*'))
1732                  RETURN
1733                  END
1734       ******  END OF FILE ON OUTPUT (OT).  ******
```